The stability of a glass facetted shell structure

Jaap Aanhaanen

Members of the graduation committee:

Prof.dipl.-ing. J.N.J.A. Vamberský	Delft University of Technology, president
Prof.dr.ir. J.G. Rots	Delft University of Technology, vice-president
A. Bagger MSc.	Technical University of Denmark, member
Ir. A. Borgart	Delft University of Technology, member
Dr.ir P.C.J. Hoogenboom	Delft University of Technology, member

This Master's Thesis is a part of the *Structural Design Lab* (SDL) of the Delft University of Technology. The SDL is a educational and research body that deals with subjects of innovative structures, the relating (structural) design process and related technolgies. By tracking and researching innovative structureal types, knowledge is gained on the challenges that are emphasised by special structures.

More information on the SDL can be found on www.structuraldesignlab.citg.tudelft.nl.

Author: J.A.M. (Jaap) Aanhaanen
E-mail: j.aanhaanen@gmail.com
Telephone: +31 (0)618684504/+45 61665663

Keywords: facetted structures, plate structure, structural glass, shell structures, stability, buckling

Printed in The Netherlands

Preface

This report contains the results of a research into the stability of facetted glass structures. This research is a Master's Thesis project at the Delft University of Technology. At the same time it also contributes to a comprehensive Ph.D. research at the Danish Technical University (DTU) in Lyngby, Denmark. At the DTU an overall research is conducted by Anne Bagger MSc, into the possibilities to create facetted glass shell structures.

I would like to take this opportunity to thank a number of people. First, my graduation committee, consisting of Prof. Vamberský, Prof. Rots, Andrew Borgart, Anne Bagger and Pierre Hoogenboom, for their support. Without their inspiring comments and ideas this report would not be here today. Especially I would like to thank Anne Bagger for being so hospitable in providing me with a workplace and fantastic traditional Danish lunches whenever I visited the DTU in Denmark.

Secondly I would like to thank my fellow students at the graduation room for the many very welcome, and often slightly too long, coffee and lunch breaks. I am still sorry for the times I was (or felt) too busy to join you.

Last but not least I would like to thank my girlfriend and my family for being that stable factor whenever I needed that.

Delft, May 2008,

Jaap Aanhaanen

Summary

The stability of a glass facetted shell structure

A Ph.D. research on the possibilities to create a facetted shell structure in glass is currently undertaken by Anne Bagger at the Technical University of Denmark (DTU). This Master's thesis contributes to this research by attaining the structural stability of a facetted glass shell structure.

History

The idea of the facetted glass shell structure was first put forward by Ture Wester in one of his papers on the behaviour of plate structures:

> "[...] if a reliable structural joint method, i.e. gluing is available, then eliminate the metal muntins as well, and leave the glass itself to carry and transfer all the forces.
>
> Such a plate dome challenges the vision for a dome design with forces distributed so evenly, that it can be made so 'thin' that it becomes totally transparent and nearly disappears - a structure as clear as air, only made visible by mirroring the clouds and the sky." (Wester 1990)

Combining flat glass with a plate structure is a very effective way to use the in-plane strength of glass panels in an efficient structural system. In addition, production of flat (or float) glass is very cheap compared to bent glass.

Placement of the Master's thesis

The Ph.D. thesis by Anne Bagger at the DTU aims at investigating the possibilities to create such a facetted shell structure in glass. One of the crucial aspects of designing a shell structure is the (buckling) stability. Shell structures are highly slender structures that are loaded in compression. Consequently, they are highly sensitive to failure through buckling. However, for a facetted shell shape it is not clear how the structure behaves

in stability. Therefore, an investigation is made in this Master's thesis into the stability behaviour of a glass facetted shell structure.

Design and model of the structure

A relatively straightforward design is chosen for analysis; a dome structure. This way it is easier to see the influence of varying properties of the structure on the behaviour.

The dome structure is developed from a geodesic dome, based on the duality between plate and lattice structures (Wester 1984). This way an efficient and straight forward facetted structure is created.

In order to analyse the structure it is modelled in a finite element programme (DIANA). In this model the glass panels are all given the material properties of glass with a thickness of 16mm. The joints in between the panels are modelled with the same finite elements. However, different material properties are used which represent early expectations. The relation between the bending stiffness and normal/shear stiffness of the joint can be controlled by changing the material stiffness and thickness of the joint. This way the influence of the joint stiffness on the structural behaviour can be investigated.

Influence of the plate behaviour

A linear buckling analysis of the structure results in local buckling behaviour of the glass panels, see Figure 1. This behaviour is, however, not found in an incremental buckling analysis. In the incremental results, see Figure 2, the joints turn out to be decisive. The difference is explained by the behaviour of a single plate loaded by an in-plane load. After the theoretical linear buckling load is reached the plate can internally redistribute the stresses and start acting like a stiff hexagonal frame.

This stiffening effect can be translated to the behaviour of the dome, which explains that the buckling load found with the incremental calculation is higher than that of the linear calculation. The result is that the panels are no longer governing, but the joints in the structure.

Influence of the joint stiffness

Because of the fact that the joint is governing for the structural behaviour of the dome it is interesting to look at the influence of the joint itself.

A joint design has been proposed by Anne Bagger, see Figure 3. The stiffness properties of this joint have been incorporated in the model. The joint design has been largely based on the bending stiffness of the joint and the prevention of stress concentrations. However, the joint lacked the stiffness to support the dome structure. It turns out that the normal and shear stiffness of the joint have a strong influence on the structure , while the

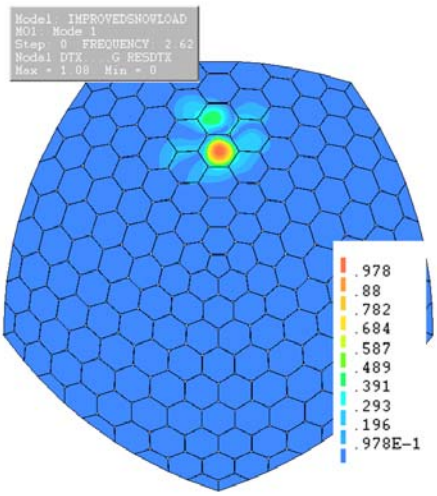

Figure 1: The result of the linear buckling analysis; $\lambda \approx 2,9$. Note the local buckling of the plate (absolute deformations).

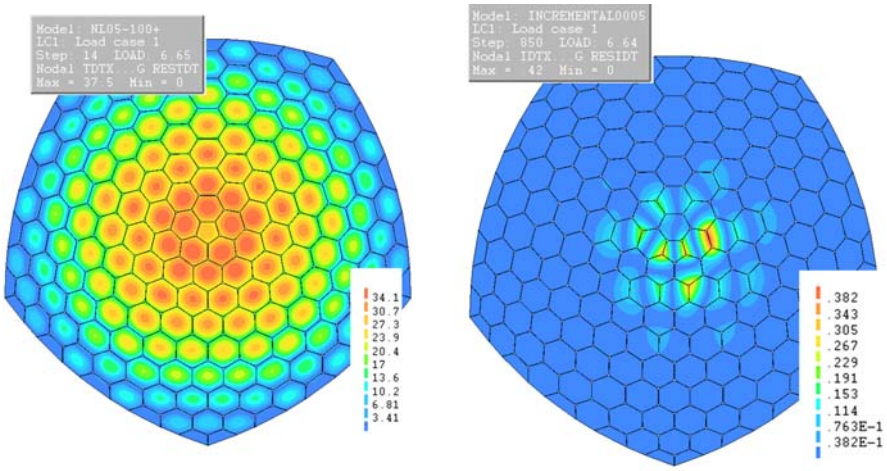

Figure 2: The result of the incremental buckling analysis; $\lambda \approx 6,64$. Note the influence of the joints on the buckling shape (absolute deformations). NB the left image shows the total deformations and the right image the deformations due to the last incremental load. Therefore the right image shows the (asymmetric) buckling deformation shape.

bending stiffness is less important, see Figure 4. Therefore the current joint design will need to be improved or revised to increase the normal and shear stiffness.

Unfortunately it was not possible to de-couple the normal and shear stress in the current modelling of the joint. Therefore the separate influence of changing these properties could not be assessed.

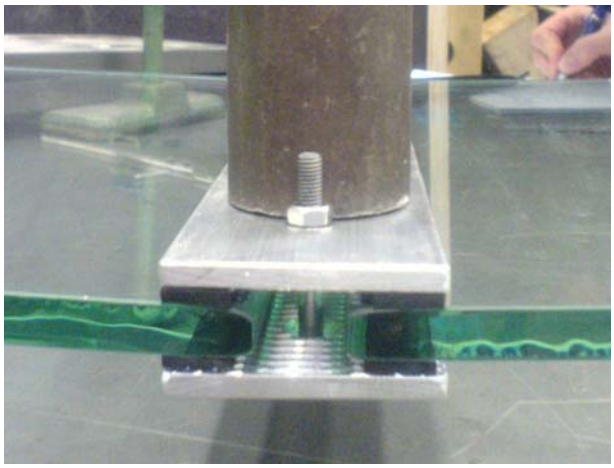

Figure 3: A physical model of the proposed joint design by Anne Bagger.

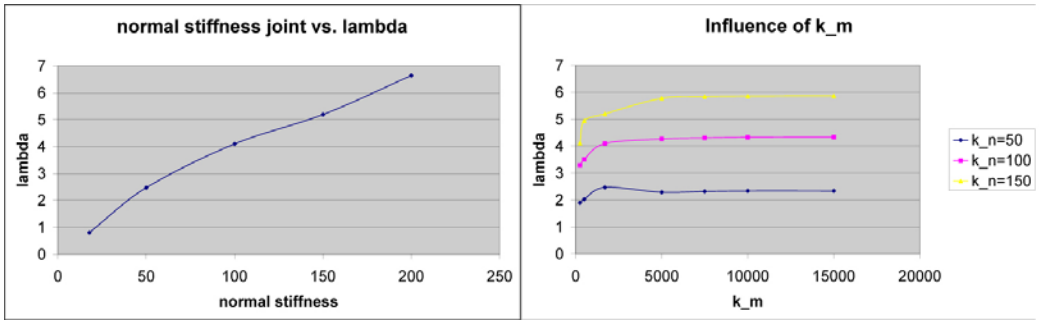

Figure 4: The influence of the normal stiffness (k_n) and the bending stiffness (k_m) on the buckling factor of the structure.

Imperfection sensitivity

Smooth shell structures are very sensitive to deviations in the structure. One can think of misalignments, local forces, material deviations, etc. The facetted structure for a large part acts like a shell structure and therefore might also be sensitive to imperfections.

The imperfection sensitivity is investigated using an imperfect geometry of the structure. The largest applied dislocation in the geometry is based on the order of magnitude of the thickness of the glass. This is realistic when considering that two glass panels will need to be connected. As an imperfection shape the buckling shape of the perfect geometry is used. This is the shape of the first failure mode of the structure, which makes it a very unfavourable imperfection shape.

The result of the analysis shows that the structure is indeed sensitive to imperfections of this magnitude. The load factor drops with approximately 55%. This shows that the magnitude of the imperfections should be very well considered. It is also shown that other

imperfection patterns yield a higher load factor. The load factor will, however, be in the same order of magnitude.

Robustness of the structure

Since glass is a brittle material and safety is an important issue in designing and building glass load bearing structures, the structure needs to be capable of redistributing the loads when a glass panel breaks.

The structure is analysed with one facet taken out completely. Even though the loads have been reduced according to the standards for an accidental load case, a safety factor of 3.6 is found. This shows that the structure is capable of resisting a reasonable load even, when a facet is taken out.

Material properties of the glass

Laminated glass will need to be used for the structure. One of the properties of laminated glass, however, is creeping of the interlayer under long term loads. This results in a lower cooperation between the glass layers in the laminate. An investigation is carried out to see the influence of a reduction of the stiffness of the glass. The result is shown in Figure 5. The three points in the graph refer to three different cases, from left to right: no cooperation for all loads, only cooperation for the live loads (snow) and full cooperation for all loads.

The true behaviour of the glass lies in between the first and the second case. The result shows that it will be very interesting to investigate the creep behaviour of the laminate and therefore the cooperation behaviour of the glass layers.

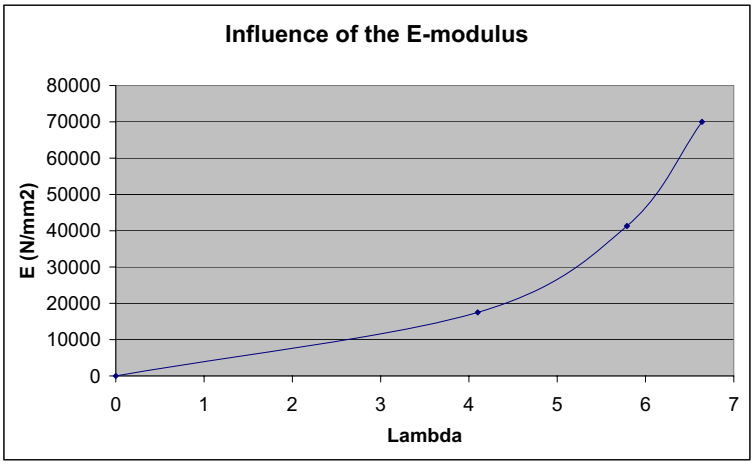

Figure 5: The influence of the glass stiffness; the true behaviour of the material due to creep lies between the two middle points.

Conclusions

The most important conclusion that can be drawn from the research is that the structural concept is very promising. Sufficiently high safety factors are found even when introducing large imperfections. However, some aspects still need to be taken into consideration. One might think of the support conditions, different load conditions, etc. Furthermore, a suitable joint needs to be developed.

Other interesting conclusions can be drawn from the different investigations. The fact that the normal and shear stiffness of the joint are crucial in the design is very important, as well as the imperfection sensitivity and glass stiffness. No real problems are found even though the influence of some factors is quite large. These aspects will need to be combined in future studies; also with the realistic support and load conditions.

Contents

Chapter 1

Introduction

The thought to create incredibly slender structures with the capability to cover large areas has for a long time inspired architects and engineers to push the boundaries of technology, of their knowledge. The concrete used in the Pantheon, the masonry domes of the Hagia Sophia, the gothic European churches, all the way down to Candelas concrete shells and modern membrane structures; ever more slender, ever more efficient, ever more clever.

The shell is one of the most efficient load carrying structures nature ever invented and mankind has copied. It is found in many of natures creations, like eggs, cochleae and some dwellers of the sea; a shape that is made to protect and resist, exactly what a roof is meant to do for us.

Light in buildings is an important aspect of feeling safe in a building, to be able to live and work in a building. Bringing light into buildings has been a difficult matter for architects, but the invention of glass has created more and more possibilities over the centuries.

In the last century the possibilities of transparency have been explored by architects in buildings like the Crystal Palace, but also in many glass-clad office buildings and transparent roofs like the German Reichstag and British Museums courtyard. There is one aspect these transparent structures have in common: a supporting (steel-) structure. This structure interferes with the transparency of the building as a whole and damages the idea(l) of the architect. But what if truly transparent roofing could be created? What if the transparency could be brought again one step closer?

Of course this is the dream, the idea, the ideal to strive for. But how will this be achieved? By combining the strength of structural glass with the effectiveness of a shell, it is in theory possible to create transparency and lightness of unprecedented efficiency. However, as the Dutch saying goes, there are many bears on the road; many problems need to be solved before a glass shell can become reality.

This Master's thesis contributes to a research into the possibility to create facetted shell

structures in glass. The stability of shell structures is often an important issue and the slenderness that can be reached when using glass makes it vulnurable for buckling.

This report is the final report of the Master's thesis. It contains the research that has been caried out and tries to give more insight into the stability behaviour of the facetted glass shell structure.

1.1 Problem definition

As has been stated in the Introduction, many problems need to be solved to be able to build a glass shell structure. An investigation into these problems is being executed at the Technical University of Denmark (DTU) in Copenhagen by Anne Bagger. A short overview of the general problems of designing a glass shell structure will be given in Paragraph 1.1.1. After this the positioning of this Master's thesis project into the total research will be put down in Paragraph 1.1.2. Finally in Paragraph 2.3 the problem definition and objectives for this Master's project will be stated.

1.1.1 Designing a glass shell structure

A number of problems are encountered when starting to design a glass shell structure. First of all, it will not be possible to create a continuous shell on a suitable scale, so the structure will in every case need to be subdivided in smaller elements. These elements will then preferably be plane, for economic reasons. This creates a vast array of possibilities of subdividing and shaping the structure, each with its own structural behaviour. Also important is the shape of the building as a whole, what are the possibilities for creating more free-form structures? What are the limiting factors? Secondly, the behaviour of the shell as a segmented structure in general; segmenting a shell creates a deviation from the ideal smooth shell which might have an enormous impact on the structural behaviour of the shell. Will it still act as a shell or will concentrations of forces or movement occur? Will the stability of the shell still be ensured? What about the slenderness and edge conditions?

A third very important aspect of a glass shell will be the connections between the glass panels. When the behaviour of the shell as a whole can be satisfactorily predicted, will it be possible to find a joint design to also satisfy the presumptions made in modelling the shell? Or will it be necessary to backtrack and change the modelling of the shell?

The last challenge to be mentioned here is the glass itself. The brittle behaviour will need to be controlled, the possibility of failure of one pane needs to be considered in the design, high localized stresses will need to be avoided, production will need to be standardized and of high quality, and more.

1.1.2 Positioning of the Master's thesis project

In a Master's thesis project only a small part of this research can be carried out with sufficient depth. At the time of writing the Ph.D.-research has already been going on for approximately two years. Another year is available in which the final goal is to build a full scale model of the facetted glass shell. Preliminary studies leading up to this Ph.D.-research have already been going on for many years, mainly by Ture Wester who has performed extensive studies into the structural morphology of triangulated structural shapes and their duals. The reader is especially referred to his book *'Structural order in space: the plate lattice dualism'* (Wester 1984), which has been an important inspiration for the development of a facetted glass shell structure.

At this moment one of the important fields of study is the stability of the facetted glass structure. It is difficult to predict the influence of the faceting on this stability. The joints are relatively flexible elements in a structure that is preferably as uniform as possible and might therefore be weakening the system. However, the structural morphology of the system ensures a stable unity. What is then the effect of the edges on buckling lengths? What is the effect on local buckling? What about the sensitivity to imperfections that continuous shells show?

In this Master's thesis project it is aimed to find an answer to these and other questions concerning the stability of the facetted shell structure.

1.1.3 Problem definition and objectives for the Master's thesis

Problem definition;

> *'A facetted glass shell has a structural behaviour that deviates from regular shell structures due to the use of material and, perhaps more importantly, due to the facetted shape. It is of great importance to assess the stability of such a shell structure.'*

Aim of the Master's thesis; in the research at the DTU in Copenhagen the possibilities for designing and building a facetted glass shell are investigated. This Master's Thesis will be a contribution to this research by attaining the structural behaviour of the facetted shell, to understand the facetted system. The final goal is to find a way to describe the behaviour of the facetted shell with a focus on buckling behaviour and stability.

> *'By attaining the structural behaviour of a facetted glass shell, including the impact of shape deviations and an assumed behaviour of the joints, the stability of a facetted glass shell will be judged.'*

1.2 Deciding on the general shape for the shell

It is important to decide on a general shape for the shell in a very early stage of the project. This way it will be possible to find more specific information regarding the shape of the shell. This will be especially useful for the method of facetting and the theories on smooth shells. These are extensive fields with many options and they are not supposed to be a substantial part of this research.

To be able to decide on a general shape for the shell a number of factors are considered.

- Direction of curvature
  Glass is generally weak in tension due to microscopically small cracks in the surface. The joints between the glass facets are preferably loaded in compression too. This is why it is important to have a shell shape which leads to compression in the largest part of the load cases. On of the demands for compression is for the shell to have positive Gaussian curvature.

- Magnitude of curvature
  In order to create a shell with an efficient load bearing behaviour it is necessary to refrain from having areas of low curvature in the shell. These areas are more ductile and it will therefore be tried to create a relatively high curvature for the entire shell. These areas can also invoke bending stresses in the shell, which is a very inefficient load carrying mechanism. Of course this also depends on the angle of the flat areas with the load and support.

- Characteristic shape
  It is the aim of this thesis to investigate the buckling behaviour of facetted glass shell structures. To be able to sufficiently assess this behaviour it will be necessary to choose a straight forward, but realistic, design as a starting point. To be able to make the step to free-form facetted structures, which in theory seems very well possible, it is important to understand the behaviour of a ‘simple’ shell first. This shell can easily be judged and compared to for instance its smooth counterpart. Furthermore it can serve as a basis to say something about more elaborate shell structures.

- Openings
  In first instance there will be no openings in the shell structure. After evaluating a fully closed shell it will be interesting to look into the safety and stability when holes are made, either for entering or due to the failure of a glass panel. It should be noted that failure of a glass panel does not necessary lead to a structural hole since a laminated panel will still have some load bearing capacity after one of the layers breaks.

- Free edges
  A shell can also be cut off. This will in the future definitely be an interesting field of study. An option is also to couple a number of shells with a positive Gaussian curvature to create more free-form structures. However, in this stage it is again decided to investigate a fairly simple shell structure. Large openings or chamfers might require stiffening the edges which will give a more elaborate behaviour; this could cloud the results.

The spherical shell of revolution complies with the previously mentioned characteristics in the way that it is a shell shape that is fairly well known. It is also very well possible to create a facetted shape that is convex and sufficiently curved. The characteristics of the spherical shell of revolution will be further defined in Paragraph 4.

Chapter 2

Project references

Introduction

In this Chapter a number of projects will be presented which are in some way related to the glass facetted shells structure. The projects will be shortly described and the relationship with the glass facetted shell will be explained.

2.1 The Eden project, 2001, Cornwall UK

The Eden project was built in 2001 in England as one of the millennium projects in the United Kingdom. The project consists of outdoor areas and two large greenhouses where gardens are situated. Especially the two greenhouses are the eye catching element of the project, see Figure 2.1.

*Figure 2.1: One of the domes of the Eden project in Cornwall UK, from (2007*a*).*

The greenhouses are giant geodesic domes built up from steel structures which are

filled in with EFTE foil air cushions. The architectural concept was based on a single layer hexagonal division, this way more light could enter the greenhouse than in a rectangular structure. Furthermore it would be easier to fit the hexagonal based structure to the ground plan, in contradiction to earlier designs that were rectangular. Structurally, however, the hexagonal pattern is a strange choice. The hexagonal structure is principally not stable as a lattice structure and therefore moments will need to be transferred in the corners of the hexagons. This is why the deformations of the structure soon became too large and to maintain a high transparency of the structure it was decided to add a second structural layer. The combination of the two structural layer can be compared to placing a dodecahedron and an icosahedron together, so creating a dodeca-ico network (Knebel, Sanchez-Alvarez & Zimmerman 2003), see Figure 2.2 and 2.3. This combination makes the structure very efficient.

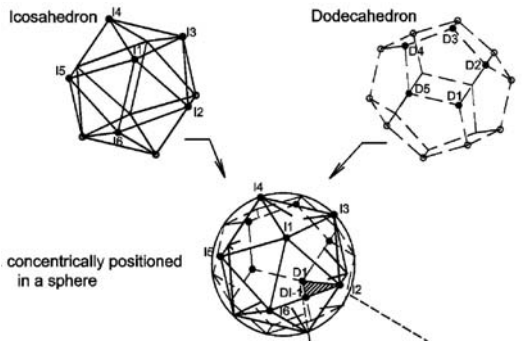

Figure 2.2: The principle of combining the icosahedron and the dodecahedron, creating a dodeca-ico network. From (Knebel et al. 2003)

Figure 2.3: The dodeca-ico network as it was built. From (Knebel et al. 2003)

The outside appearance of the Eden domes is similar to the glass facetted dome that is researched in this thesis. However, the structural system is different. The choice to

create hexagonal faces is made on architectural and functional wishes and not at all on structural efficiency. By creating a second structural layer the stability was ensured and the system still turned out to be structurally efficient. Considering the size of the facets at the Eden project it could never have been realized in glass and it would be difficult to create the same transparency in a triangulated structure. This is why it is an impressive feat of engineering to have realized such a light weight and transparent dome structure

2.2 A glass facetted dome, 2002, Delft NL

At the Delft University of Technology in 2002 a glass facetted dome has been designed and built, see Figure 2.4. The dome is based on rectangular plates of glass and the glass is the load carrying element.

Figure 2.4: The facetted glass dome developed at the Delft University of Technology, from (Veer et al. 2003).

The structural system of the glass dome is not principally stable for all load cases, since the rectangular panels result in four-way vertices. The effect is that (small) bending moments will need to be transferred in the joints and that tension rings are necessary at the top and bottom of the dome. The joint design was an important part of the dome. In the end it was chosen to use a linear joint, but to keep the corners free, see Figure 2.5. The reason for this was mainly to avoid tolerance problems while building the dome. At the end result it was also commented to be aesthetically pleasing by some viewers. The linear joint was made by gluing aluminium strips onto the edges of the glass using a thick and flexible polymer. During erection these strips were clamped by two outside strips to connect the glass panels.

The end result shows that it is very well possible to construct a facetted dome structure in glass. The structural principle of the facetted glass dome in this thesis will, however, have a different structural concept and will need to be water tight.

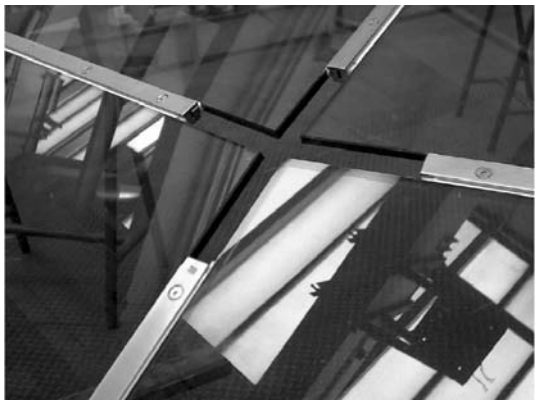

Figure 2.5: The connections in the facetted glass dome, from (Veer et al. 2003).

2.3 A pre-stressed glass dome with triangular panes, 1998, Düsseldorf G

In Germany a fully glazed spherical shell was developed by the Firm Seele GmbH & Co. The shell was exposed at the Glasstec 1998 in Düsseldorf. The full shell was built up from triangular glass panes to create the dome shape, see Figure 2.6.

Figure 2.6: The glass dome by Seele GmbH at the Glasstec 1998, from (Behling & Behling 1999).

The interesting aspect about this dome is that the glass panes are the actual load carrying elements. The triangular elements are six-wise situated around steel cast nodes. The structural system is solid for the static load (in compression) and for stability and pre-stressing a steel wire mesh, following the edges of the glass panes, is connected to all steel nodes. The dome consists of 282 triangular panes in 27 different sizes with edge lengths of up to 1,10m. The forces are transferred from the glass to the nodes by prefabricated connecting shoes in the nodes, see Figure 2.7.

There are two main differences between this dome and the proposed facetted dome

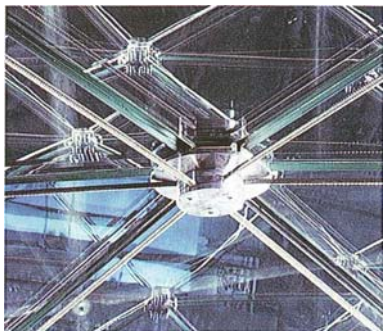

Figure 2.7: Detail of the nodes in the glass dome by Seele GmbH at the Glasstec 1998, from (Behling & Behling 1999).

in the Ph.D. research by Anne Bagger (Bagger, Jönsson & Wester 2007*a*). The first is the inclusion of the steel wire mesh, which takes part in stabilizing the structure by pre-stressing. This steel mesh does guarantee that the structure is always loaded in compression and it might also serve as tension layer to relief the glass structure of tension forces. The proposed facetted glass dome has to ensure its stability from the structural lay-out and tension needs to be taken up by the glass as well.

The second important difference is the shape of the glass panels. The triangular system, as chosen in the Seele dome, results in concentrated nodal forces. This is a result of the fact that the system can not act as a plate structure due to the six-way vertices; more on this subject can be found in Appendix C.3. The flow of force therefore has to travel from the corners in the glass panes through the connectors to the next glass panes. This leads to fairly concentrated stresses. The structural concept of the proposed dome is based on plate action, which results in distributed stresses along the edges of the joints between the panels. The stresses are therefore likely to be lower.

2.4 A frameless glass dome, 2003, Stuttgart G

In the early 2000's a research was undertaken by Lucio Blandini at the ILEK institute of the University of Stuttgart, Germany. The starting point of his research was the fact that more and more glazed domes and roofs were being built, but still the possibility of using the glass as a structural element was overlooked. A supporting steel structure is usually in place to provide stiffness and stability. Blandini had the idea that it might be possible to build a frameless glass dome while using adhesives as the joint between the different glass panes. The end result of the research was a built prototype of a frameless glass dome, see Figure 2.8

The research was started with finding a suitable adhesive. This adhesive was found

Figure 2.8: The frameless glass dome at the ILEK in Stuttgart, from (Blandini & Sobek 2005).

after submitting a number of different adhesives to, amongst others, tensile and bending stress tests, see Figure 2.9. It turned out that the joint could be made and the step to designing the glass dome was made.

Figure 2.9: One of the tensile tests on the adhesive joints, from (Blandini & Sobek 2005).

Finite element models were made to find the stress distributions and strength of the shell in combination with imperfections. Then a fairly high safety factor was applied for the adhesive to incorporate long term effects. The structure was built in three months, using an advanced movable scaffolding system. This was needed to precisely position every glass pane before the adhesive was put in place. After the connections were made the scaffolding could be lowered all at once to make sure to start loading the entire shell simultaneously. A snowy winter showed the strength of the shell structure. It did not give at all even though the adhesive is considered weaker in low temperatures. The structure itself proved the aesthetic quality of a glass dome, in this case made out of double curved

glass panes, see Figure 2.10.

Figure 2.10: A view from the inside of the shell structure, from (Blandini & Sobek 2005).

2.5 The USA Pavilion at the World Fair, 1967, Montreal C

For the 1967 World Fair in Montreal, Canada, Buckminster Fuller designed the USA pavilion see Figure 2.11. The pavilion was a giant geodesic dome, also referred to as 'Fuller domes', and it reproduces almost 97% of a full sphere. The dome enclosed a number of platforms which formed the heart of the USA Pavilion. The outside of the dome was clad with a transparent acrylic material and a complex system of solar powered shades to control the inner climate. This system did not work as well as Fuller had envisioned, partly because he was ahead of his time.

*Figure 2.11: The former USA pavilion for the 1967 World Fair in Montreal (2007*b*)*

In 1976 a fire broke out during repair works on the outer cladding. Within half an hour the fire destroyed all the acrylic cladding on the dome, leaving the steel structure underneath it bear to the sky but structurally intact. The site was abandoned for many years until in 1992 restoration works began to turn the dome into the 'Biosphere' as it is called today. The outer shell is left unclad even though the steelwork is protected against the influences of the environment by painting.

The structural system of this geodesic dome consists of a large number of steel bars that are configured as triangles, together forming a highly efficient and light weight system. More on the structural system of geodesic domes can be found in Appendix C. The triangles are situated in two different layers, again inter-connected by bars; this way a curved space frame is constructed, which forms the structural layer of the dome (Figure 2.12). In every node a large number of elements come together. This concentrates the forces in the nodes and transfers them between the bars lying directly opposite of each other. Figure 2.13 shows one of the nodes in the structure.

The relevance of this structure in relation with the facetted glass dome lies in the fact that the facetted dome can be very well based on the geodesic dome. The geodesic dome

Figure 2.12: A view on the space frame forming the structure (2007c)

Figure 2.13: A node in the dome structure (2007c)

will then be turned into a plate structure by finding its structural dual. This plate structure will have a similar efficiency in its structural behaviour as a geodesic lattice structure. This will result in the possibility of a low material use with a high span to thickness ratio.

2.6 A facetted shell structure, 1991, Hoersholm DK

In 1991 Henrik Almegaard developed a facetted shell structure to test his stringer theory; a theory on necessary support conditions for shell structures (Almegaard 2003). The structure has stood in an open field ever since its erection but is still in good condition. Due to the chosen geometry only membrane forces developed in the shell structure, except of course for local bending in the facets and some torsion near the free edges.

The entire shell is built from 2cm thick multiplex plates connected by especially made steel plate connectors. The steel connecters have to transfer the membrane forces from timber plate to timber plate, without developing concentrated forces. Local bending forces

Figure 2.14: A facetted shell structure in Hørsholm, Denmark. (Almegaard 2003)

are of course encountered in the timber plates since the loads act with a component perpendicular to the plane. The structure is a positively curved shell, based on a rotational paraboloid, with a triangular plan. The span of the shell is 9m and the height is 4m. It is supported at three points and therefore has three free edges. The facets are all hexagonal and thanks to the symmetrical build up there are only a few different dimensions for the facets since every facet is found three or six times, see Figure 2.15.

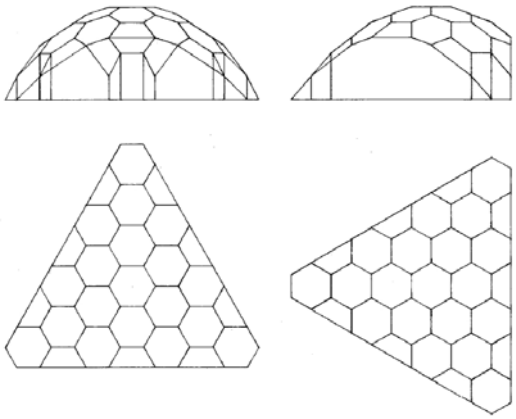

Figure 2.15: The faceting of the shell structure. (Almegaard 2003)

The erection of a plate shell structure was in the first place difficult because of the fabrication of the plate elements. It was time-consuming to get the timber to the right size and in this sense computer steered fabrication would be an interesting option when the number of elements (or shells built) will increase. The shell was designed in such way that the elements could be easily managed by two persons at the same time. This was very convenient. The elements were connected by bent steel plates that were screwed to the timber. The production of the steel plates was difficult, since they needed to be bent while checking the angle by hand and rechecking it in erection. Here also automation would be

very beneficial. The screwing of the joints was no problem at all. Because the structure was statically determined, the shell was flexible until the last piece was installed. This is why it was not very hard to position the shell, though a scaffolding that is capable of pulling the elements together during the erection will reduce erection time.

The most interesting thing about this shell is the experience that is gained with erecting a facetted shell structure. It is shown that it is fairly difficult to get all dimensions precise and that during erection especially getting the angles of the connections right was hard in the beginning. Especially the problems with the dimensions will be encountered when creating a facetted glass shell structure. Also it will be interesting to prevent the glass panels to become too large and unworkable by hand. Since the joining method will be different it is hard to conclude anything on that subject yet.

Chapter 3

Preceding and current research

Introduction

At the Technical University of Denmark (DTU) a research is undertaken into glass facetted shell structures. The Ph.D. research is carried out by Anne Bagger and it is partly based on earlier research by, amongst others, Ture Wester at the Royal Academy of Fine Arts in Copenhagen. Especially plate structures and the structural duality between plate and lattice structures has been an important field preceding the idea of the glass facetted shell structure. The possibility of such a structure was actually first mentioned by Ture Wester in an article written for the International Journal of Space Structure in 1990 (Wester 1990). Here he states:

> ”[...] if a reliable structural joint method, i.e. gluing is available, then eliminate the metal muntins as well, and leave the glass itself to carry and transfer all the forces.
>
> Such a plate dome challenges the vision for a dome design with forces distributed so evenly, that it can be made so ‘thin’ that it becomes totally transparent and nearly disappears - a structure as clear as air, only made visible by mirroring the clouds and the sky.” (Wester 1990)

In Paragraph 3.1 the work preceding the research of Anne Bagger is considered.

In Paragraph 3.2 the research of Anne Bagger herself and the ideas she developed during this research are discussed. Finally the Master’s thesis of Theis Isgreen will be discussed in Paragraph 3.3, who has modelled a facetted glass shell structure in order to find the stress distributions in the structure. From this work a number of conclusions were drawn that greatly influence the future design of glass facetted shell structures.

3.1 Discovering the plate structure

Introduction

The plate structure has been an underexposed field in structural mechanics for many years. Grid shells, lattice domes and such have been studied to a great extent and have been used in the field many times. From the mid seventies of the last century Ture Wester has researched the structural properties of plate structures and the duality between plate and lattice structures. The plate structure turned out to be a highly efficient structural system with many examples in nature. The field of plate structures has been developed over the years, amongst others by Henrik Almegaard at the DTU, who has investigated the demands for stably supporting shell structures, among which also facetted shell structures.

In this Paragraph a short introduction to the plate-based shell structure duality will be given and the stability requirements for plate-based shell structures will be discussed.

3.1.1 Duality

Structural dualism between plate and lattice structures has been developed by Ture Wester (Wester 1984) at the Royal Academy of Fine Arts in Copenhagen from the mid seventies. It has served as a basis to develop the possibilities of plate-based structures and has already led to a number of examples in the field, see Chapter 2.

The duality principle will be treated in more detail in Appendix C.3, but the main idea is as follows; the dualism between lattice and plate structures is based on the fact that from a lattice structure with concentrated normal forces in the line elements a translation can be made into a plate based structure with distributed in plane normal forces. This results in an efficient structural system with low stresses. The whole of differences and similarities in behaviour of the two different structural systems is called structural dualism.

3.1.2 The behaviour of a facetted shell structure

The definition of a facetted shell structure, as used in this thesis, is a shell built up from planar elements that mainly interact through in plane forces.

The loads on the shell, however, always have component perpendicular to the tangent of the shell. This load will be taken up by the planar elements (facets) locally by bending, see Figure 3.1.

The resulting normal forces that are transferred between two neighbouring facets can now be defined as the vector summation of the normal forces from the other neighbouring facets and the normal component of the vertical load on the specific facet.

The foregoing implies that the facets need to transfer forces in two ways: as a plate loaded perpendicular to the plane resulting in bending and as a plate loaded parallel to

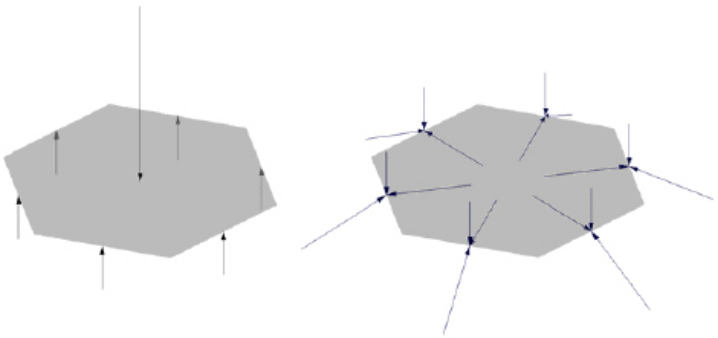

Figure 3.1: The mechanism of local bending of the facets, from (Bagger et al. 2007a).

the plane resulting in normal forces. Since their resistance against bending is much lower than their in-plane strength, it is feasible to minimise the bending action and maximize the membrane action. This means increasing the number of facets and/or decreasing their span.

In order to make the facetted shell work with membrane forces, it is necessary for it to transfer normal forces between the edges of the facets. This is only possible when the vertices of the system are forceless, because otherwise normal forces would develop in the edges between the vertices. The systems with concentrated normal forces between the nodes are more commonly known as grid structures. When three-way vertices are used, however, the vertices will become forceless and the system will be forced to transfer the forces through normal forces between the edges of the facets. This can be explained by a normal force through one of the three edges is considered. Because there are only two other edges connected to the vertex they will not be able to counter this force without being in the same plane. Since this does not hold, the concentrated forces in the vertices can not develop.

3.1.3 Supporting a facetted shell structure

The information for this Paragraph is largely based on 'Skalkonstruktioner; metoder til afklaring af sammenhaengede mellem form, stabilitet, og understoetninger.'; the Ph.D. thesis of Henrik Almegaard (Almegaard 2003).

It is very important for a (facetted) shell structure to be sufficiently supported. Since all elements are very thin, their bending resistance is very low and membrane action is of the utmost importance. However, membrane action can only be developed when the structure is sufficiently supported. The importance of the development of membrane action is emphasized by Figure 3.2. Here both shells are stably supported but in the right

image the membrane action cannot develop sufficiently.

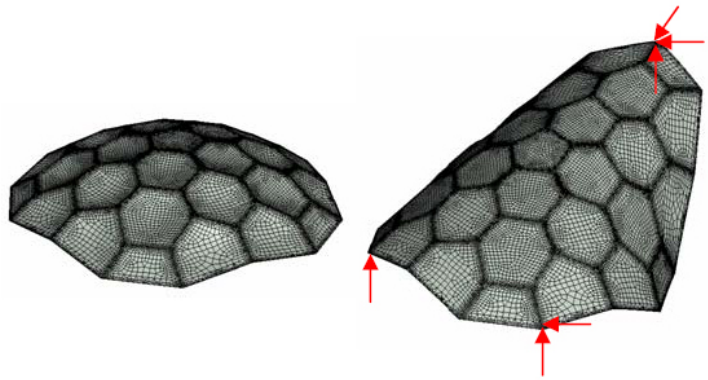

Figure 3.2: Two identical shell structures but differently supported, from (Bagger et al. 2007b). N.B. the deformations in the left image have been scaled up 4500x.

Since plane elements are the bases for the facetted shell, the stability demands for a plane element were investigated in (Almegaard 2003).

For out-of-plane loads there are three conditions to be fulfilled for stability (see Figure 3.3):

1. Three lines of support in the plane of the plate
2. the three lines of support can not be parallel all three of them and can not intersect in one point

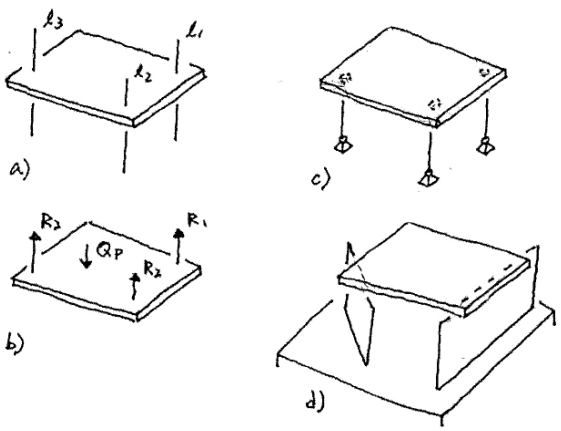

Figure 3.3: The conditions for stability of a plate loaded out-of-plane (Almegaard 2003).

For in-plane loads two additional requirements need to be fulfilled for stability (see Figure 3.4):

1. three lines of support necessary perpendicularly to the plane of the plate
2. the three supports can not be on one line

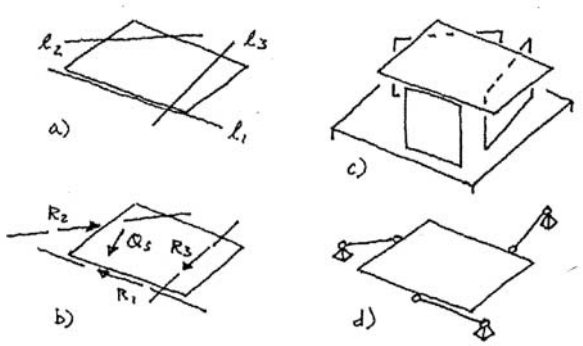

Figure 3.4: The conditions for stability of a plate loaded in-plane (Almegaard 2003).

In the facetted shell both behaviours are combined in one element, as was already stated before. This means that six supports directions will be necessary for the plates in the shell structure; three in the direction of the plate and three perpendicular to it. Often these six directions are represented as three supports, all three supporting in a direction perpendicular and a direction parallel to the element. None of the three supports may be in the same direction as one of the others, since this will reduce the number of support directions. When a facetted structure as a whole is considered, overall stability is ensured when every element in itself complies with the aforementioned conditions for stability.

In (Almegaard 2003) Almegaard developed the so-called 'Stringer-method', which provides a very direct way to consider the stability of shell structures due to their supports. The method considers the shell shape as a geometric system of bars by defined by a number of 'strings' which represent chains of bars, see Figure 3.5. The necessary support conditions for these strings will then define the required support conditions for the shell as a whole.

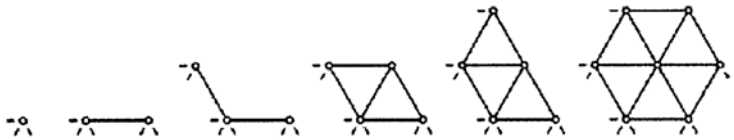

Figure 3.5: An example of the Stringer Method, from (Almegaard 2004).

As a result, the method defines the minimal necessary support conditions for *stability*. However, *stiffness* is not secured by this basic requirement, therefore it can not be

directly used for defining the supports of a shell structure. To be able to take stiffness into account the Stringer method can be complemented with physical models or computer calculations. It is thought, however, that the facetted shell structure is so vulnerable in its stiffness requirements, see Figure 3.2, that the minimal supports following from the Stringer Method will be too far from the practically necessary support conditions for the facetted shell structure. The interested reader is, however, highly recommended to read the article (Almegaard 2004) (in English), which discusses the Stringer Method.

For supporting a simple spherical dome, it will be enough to simply support the shell around its perimeter. For deviations of the sphere, like when making openings in the shell structure or when chamfering the shell, empirical methods can be used; for instance testing different boundary conditions in physical models and/or FE models.

3.2 Designing a facetted glass shell structure

The information in this Paragraph is taken from the papers (Bagger et al. 2007*a*) and (Bagger et al. 2007*b*) as well as from discussions with Anne Bagger.

Introduction

Typically, triangular and quadrangular glass facets are used in curved glass structures. These facets can together form a wide variety of shapes; however, structurally the system always has to rely on a structural subsystem which is triangular based. This system leads to concentrated normal forces in the subsystem with the glass merely serving as a separation to the outside or as a stabilizing element.

In the research for a facetted glass shell structure, a system is proposed with three way vertices. A plate structure with three edges joining in every vertex has a load carrying capacity based on in plane stresses in the plates and distributed in plane stresses in the joints. Such a plate structure will therefore create the possibility of giving the glass both the separating as well as the load carrying function.

3.2.1 Overall structural behaviour of glass facetted shells

The geometry of the considered shell is created by a faceting process based on a geodesic dome, as is discussed in (Wester 1984). The system transfers all its forces (in the case of an evenly distributed load!) through in planes stresses, except for local bending of the plates themselves. The corners of the plates have the tendency to lift up, which leads to additional bending stress concentrations. This is discussed in Paragraph 3.3.

An important aspect of the facetted shell structure is the development of the membrane behaviour. This behaviour can only develop when the shell is adequately supported, just

as in triangulated structures. When a triangulated shell is insufficiently supported, the membrane action will not develop and it will be unstable as a mechanism. A facetted (plate-) structure on the other hand, has some extra capacity to improve stability. In the edges between the facets moments can develop which stabilize the structure by bending. These moments are directed parallel to the edge and will lift one corner while pushing the opposite corner down; they will therefore be referred to as torsional moments. This system is unfortunately not suitable for a safe behaviour of the facetted shell, since the deformations will increase rapidly, see Figure 3.2. In shell theory this behaviour is referred to as 'inextensional deformation', since the deformations take place due to bending and hardly any in-plane stresses develop.

There is one important lesson that can be derived from this behaviour and that is that torsional bending moments can and will develop in a facetted shell structure. Even when the structure is stable as a membrane, a low stiffness can still result in torsional moments.

3.2.2 Singularities in the corners of the plates

In the research of Theis Isgreen (Isgreen 2007), see also Paragraph 3.3, stress singularities were found in the corners of the plates. These singularities are caused by a geometrical and structural contradiction in the corner that arises because of the fact that the angles of the corners are between 90 and 180 degrees. The directions of the principle stresses need to be at a 90 degree angle to the edge, while at the same time the deformed plate has zero curvature in the direction of and perpendicular to the edge. In the corner the 90 degree angle is impossible, leading to a singularity. This is made visible in Figure 3.6. An analytical explanation can be found in (McGee, Kim & Leisa 2005).

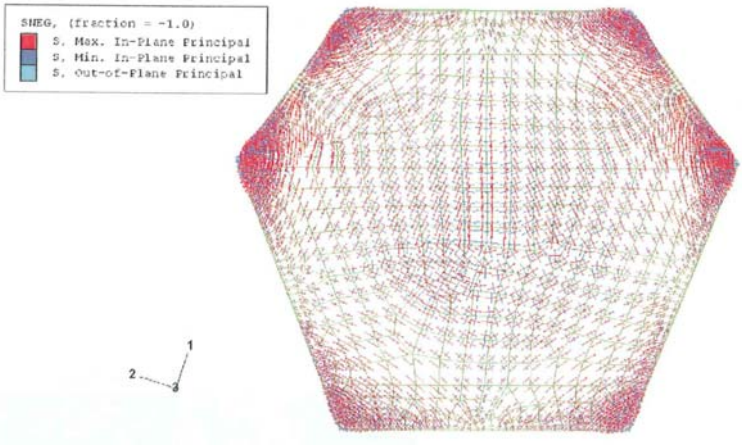

Figure 3.6: The stresses in a corner of a plate; simply supported plate with a evenly distributed load of $1,0kN/m^2$ *perpendicular to the plane. From (Isgreen 2007).*

The singularities can be avoided by giving the joints a finite stiffness. However, large stress concentrations will still occur when the stiffness of the joint is high. The stress concentrations are a result of the uplift of the corners. When the vertices are released, however, the corners can move freely and the stress concentrations will be diminished. At the same time this has little influence on the stability and stiffness of the structure, since the forces are transferred distributed over the entire length of the edges. If the connected edge becomes a little bit shorter the increase of these stresses is negligible. It will still need to be assessed whether stress concentrations will occur around the transition in the joint, see Figure 3.7, but this is not expected to be a large problem. Another reason to refrain from transferring forces in the vertices is to prevent over-stressing of the joint material.

Another interesting way of dealing with the stress concentrations is to round off the corners. This will prevent peak stresses as well and will at the same time give good possibilities for a nice finishing with a soft polymer, where the corners of the glass no longer protrude out. Since the rounding off can be fairly small the visual effect in combination with the joining material might be negligible.

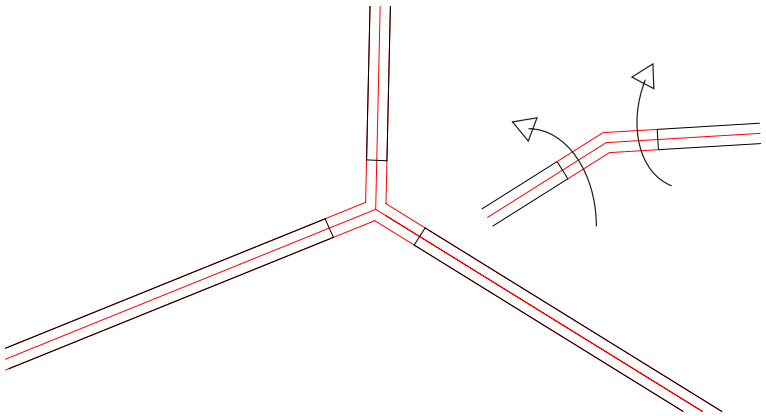

Figure 3.7: The result of releasing the corner.

3.2.3 Connections between the facets

Currently a research is undertaken into the connections between the facets. The current results are an overview of the different stresses that need to be transferred by the joint and a number of solution directions. The stresses in the joint are five-fold:

1. bending moments resulting from the clamping effect due to the stiffness of the joint

2. out of plane shear forces (which are transformed into in-plane forces)

3. in plane normal and shear forces

4. forces resulting from the up lift of the corners

5. out of plane shear force from the transfer of torsional moments

ad. 5 is only applicable when the structure is not shaped and supported to be efficient as a membrane structure, for more on this subject see Paragraph 3.1.3.

The research will need to be extended to find suitable solutions for the joints.

3.2.4 Future topics

For the future a number of important topics are defined in (Bagger et al. 2007*b*).

- faceting of the shell
- free edges/openings and their stiffness
- a comparison to smooth shells to be able to make estimations
- stability (buckling behaviour) of the facetted shell
- parameter studies of the stability behaviour

The fourth mentioned subject will be treated in this Master's thesis and a start will be made on the fifth mentioned subject.

3.3 Stress distribution in an arbitrary facetted glass shell structure

Introduction

At the DTU, Theis Isgreen has performed a study into the stress distributions of a facetted glass shell structure. The research has been carried out in a MSc. thesis and has stood under the supervision of Prof. Jeppe Jönsson and Anne Bagger. All the information in this Paragraph is based on the thesis report 'FEM-modellering af facetterede skaller I glas' (lit. 'FEM-modelling of facetted shells in glass') by Theis Isgreen (Isgreen 2007).

3.3.1 Geometry of the shell

In the thesis a facetted dome has been studied with a span of 10,9m. It is shown in Figures 3.8 to 3.10. The dome is based on a rotated paraboloid and based on hexagons and one pentagon. The top of the dome is formed by a pentagon, leading to a five way radial symmetry. This symmetry has been used in the modelling of the dome. The pentagon also shows that it is actually an approximation of a smooth dome that is a development of the dual of a subdivided icosahedron (see Paragraph 3.1 and C.3).

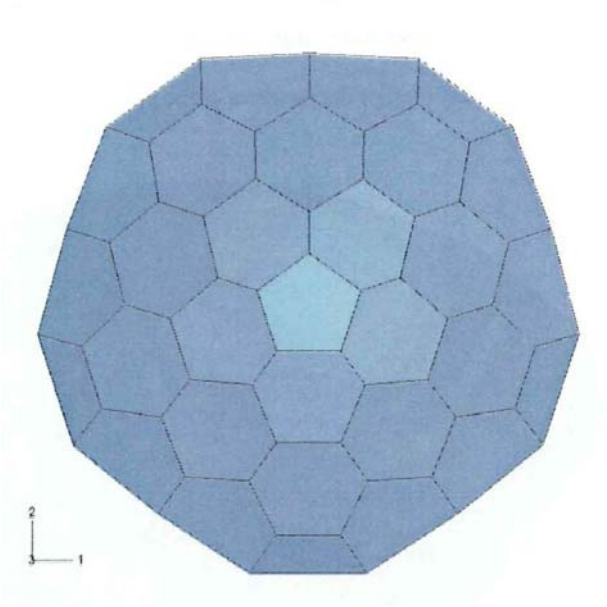

Figure 3.8: Top view of the dome in the research by T. Isgreen, from (Isgreen 2007).

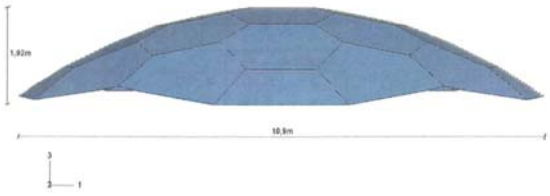

Figure 3.9: Side elevation of the dome in the research by Teis Isgreen, from (Isgreen 2007).

The subdivision is kept fairly coarse and the facets are therefore larger (approximately 2m diameter) than they are likely to be in reality. This is an approximation that will lead to greater bending stresses in the facets; however, it will be shown that the bending stresses

Figure 3.10: Bird's eye view of the dome in the research by T. Isgreen, from (Isgreen 2007).

in the centres of the plates are not governing even with the coarse faceting. A problem that does arise in a coarse faceting is edge rotations and deformations of the individual facets. This will induce stresses on the joint.

3.3.2 Modelling of the shell

The facetted shell has been analyzed in the FEM-program AbaQus. This section will deal with the main parameters used in the modelling.

Loads; The loads on the dome have been based on the Danish standards (DS410, Dansk Standard (*Dansk Standard* 1998)) as well as the Eurocodes (*Eurocode 1: Actions on structures-General actions-part 1-4* 2003), in order to find realistic stresses. The total loading has consisted of wind loads and vertical snow loads. Of course also the self weight of the structure has been incorporated in the model.

Materials; Glass has been chosen as the material for the total structure. In the model a material with a thickness of two times 10mm. This refers to the thickness of a laminated glass pane consisting of two 10mm layers. The material properties for glass that have been considered are:

- density: $\rho = 2550 kg/m^3$
- E-modulus: $E = 70,0 GPa$
- Poisson ratio: $\mu = 0,22$

The strength of the glass was not considered since only the stress distributions were sought.

The material of the connections was chosen as an epoxy with different stiffness. Three stiffnesses were defined as, 250MPa, 1,00GPa and 70,0Gpa. The last value here refers to the glass, so the joint will have the same stiffness as the glass.

3.3.3 Local bending in the facets

The principle of the facetted shell is that the main stress distribution is by normal stresses in the same plane as the facets. However, inherent to the structural build up is that locally the facets are always loaded perpendicular to their plane. The result is local bending in the plates and this is shown in Figure 3.11. This behaviour is automatically incorporated in the model by placing the distributed loads on the surface of the plates.

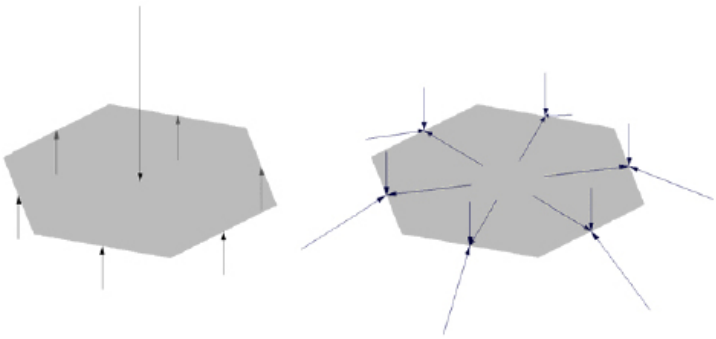

Figure 3.11: Local bending of the facets, from (Bagger et al. 2007a).

The important issue is whether the plates are capable of resisting the bending and shear stresses that develop due to the loads perpendicular to their plane. An investigation in the structural behaviour of a single facet shows that the bending stresses in the middle of the plate will not pose large problems for the material. However, when a fairly stiff joint material is used large stress concentrations arise at the edges of the facet. This is logically explicable, since a stiff joint will have a large clamping effect. The only way to reduce the stresses is to use a joint with a large rotational capacity. Figure 3.12 shows the relation between the stiffness of the joint and the bending moments in the field and the edges. This distribution is explicable with the analogy of a beam where the supports are able to transfer bending moments.

When the edges of the single plate are considered it becomes visible that the stress concentrations are even larger at the corners of the plate. In plates with 90 degree angles this effect would not arise, but since the angles are larger than 90 degrees, the stresses in the corners are significant when they are connected to other facets. See also Paragraph 3.2.2.

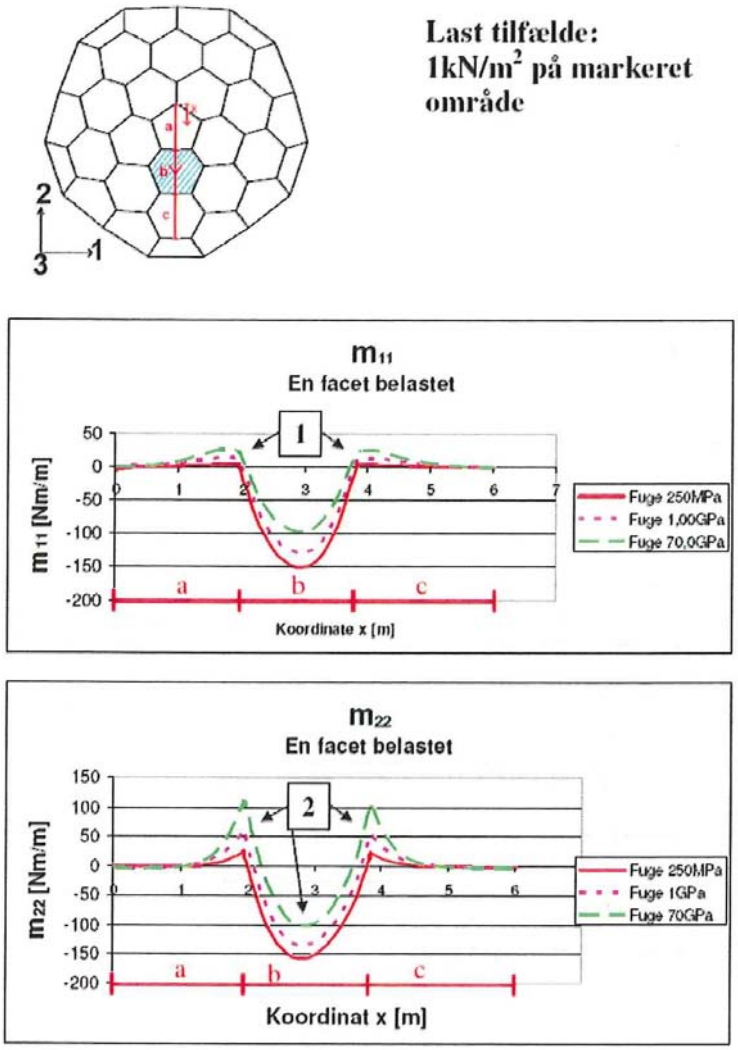

Figure 3.12: The influence of the stiffness in the joint; the diagrams are showing the bending moments in the two main directions for different joint stiffnesses. From (Isgreen 2007).

3.3.4 Stress distribution of the dome as a whole

When the step is made to analyzing the full structural system of the facetted dome, the same stress concentrations as in the local behaviour of the facets are found. However, the overall behaviour of the dome is indeed as a shell. The stresses are transferred from facet to facet by in plane forces and over the full length of the edges of each facet. This means that the stresses remain low and the system works as expected.

One of the problems still facing the dome is the local bending stresses arising in the corners of the plate. The stress concentrations are a result of the tendency of the corners of the plates to lift up. A proposed solution is to 'release' the corners of the facets by locally 'removing' the joint by introducing a very ductile material. It is expected that this will greatly reduce the stress concentrations (Bagger et al. 2007*b*).

3.3.5 Discussion

It can be concluded that the facets locally indeed transfer their loads by bending and into membrane forces at their edges. The stiffness of the joint has an influence on the degree of clamping on the edges of the facets. In these edges the bending moments that will need to be transferred by the joints will decrease when the joint stiffness decreases. In the corners of the plates stress concentrations arise due to the prevention of the uplift of the corners by a stiff joint.

Chapter 4

Definition of the shell structure

Introduction

Based on the information gathered on geometry and materials, see Appendices A and C, a considerate choice will be made for the geometry of the glass facetted shell structure for this research. The geometry that is defined here will be the basis from which it will be possible to deviate in parameter studies and such to find the most important characteristics of the buckling behaviour of a facetted shell structure in glass.

4.1 Definition of the geometry of the structure

4.1.1 The geodesic dome as a basis for a facetted dome structure

The facetted glass shell structure would ideally be a true plate structure. Since the geodesic dome is a very efficient lattice structure, it will be chosen as a basis. When the dual is created, the result is a very efficient plate structure.

The main reasons to choose a regular geodesic dome as a basis for the analysis of the stability of facetted glass shell structures are related to the goals of the study and are as follows:

- **Comparison to known structures**
  Because a dome shape has been analyzed many times before, it is expected that a comparison can be fairly easily made. It will be interesting to find the general deviations from regular dome structures and perhaps to implement these differences in a theory. When a more free-form shape is chosen it will be much more difficult to generalize the findings.

- **Changing dimensions**
  It will be interesting to look at the effects of the dimensions of both the plates them-

selves as well as the overall dimensions. In order to avoid local effects influencing the results, it is important to keep the shape as straight forward as possible. Again a dual geodesic dome would be a good option, since it is very symmetrical and with a fairly clear flow of forces. The stability can then be tested by changing the dimensions of the different parts.

- **Translation to general rules**
  To be able to come up with general rules for facetted glass shell structures, it is not very interesting to look at a free form shape which is very specially formed and unique. When using a more simple shape it will be easier to generate ideas about a larger number of deviations separately.

- **Shape effects**
  The overall shape of the shell structure of course has a large influence on the stability of the shell. When a free-form shape is chosen these influences will be more difficult to assess than with a dome shape.

It is of course architecturally more interesting to design a shape deviating from a dome. However, it is thought that by assessing the dome structure, in the future the step to free-from structures will be possible on basis of more general results.

Figure 4.1 shows a principle start for the dome structure. There are a number of aspects that still need to be decided on, which are the class, the frequency (see Appendix C.2) and the cutting angle for the sphere. These will also be some of the variables that can be adjusted in the future when the stability properties of the dome are assessed. The class and frequency depend, amongst others, on the type of glass and the size in which it can be (economically) produced, as well as on the cutting angle; this is the angle of the cutting plane when taking a section of a full sphere, see Figure 4.2.

Paragraph 4.1.2 will deal with the geometrical properties of the facetted shell structure.

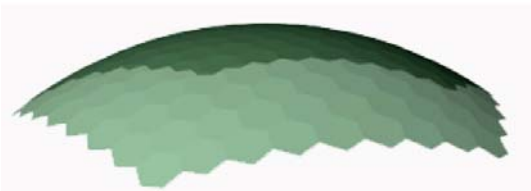

Figure 4.1: The basic idea for the dome structure, from (Bagger et al. 2007a).

4.1.2 Geometrical properties of the facetted shell structure

The geometry of the shell depends on different aspects. These aspects are treated in this Paragraph.

Cutting angle of the sphere; the cutting angle of the sphere is defined as the angle α that is made between the normal of the sphere and the edge of the spherical dome, see Figure 4.2. This cutting angle therefore defines which part of the total sphere will be the dome. Since bending stresses are undesirable in the facetted structure, it is beneficial to keep the hoop tensile stresses as low as possible.

Paragraph B.1 shows that for a smooth shell it holds that when the angle α is equal to $51^o50'$, the hoop tensile stress will not develop. When $\alpha > 51^o50'$, the hoop forces will become tensile and increase until the angle is zero degrees.

To minimise the tensile forces it will therefore be decided that the angle α should be approximately equal to $51^o50'$. The precise angle is hard to define right away, since this also depends on the faceting.

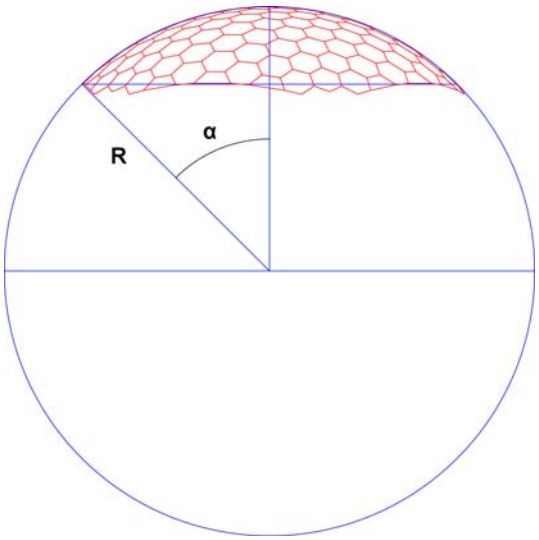

Figure 4.2: Definition of the cutting angle α.

Span of the sphere; the most important criterion for choosing a span for the sphere is the realism of the structure. It is of course also important to make sure that the buckling behaviour becomes an issue, since a shell structure with a span of 2m is not very likely to buckle.

Until this day only a small number of glass shell structures have been built, so little reliable information is available. This is why it is decided not to choose the diameter of the shell structure based on previously built structures, but on a wish for the future. A diameter of the shell of 20m is therefore proposed. It is of course an option for a parameter study to increase or decrease the span to see the influence on the buckling behaviour.

Dimensions of the facets; the size of the facets for a great deal depends on the production process. In Appendix A it is shown that the maximum width of normal float glass at the moment is 3m. However, three meters is quite large from an aesthetic point of view, because it will mean a mere 7 facets over the width of the shell. Structurally it might pose problems in the development of the membrane behaviour and local bending stresses, since the glass panes will need to span 3m by themselves. When the width of three meters is used to cut two glass panes, it will be possible to get a diameter of the glass panes of around 1,7m, as was shown in Appendix A.2. To be sure to have the possibility to get a high quality finishing it is decided to keep the diameter of the facets around 1,6m. However, since the dimensions of the facets change while going down the dome this is not enough. The sum of the maximum and minimum diameter also needs to be kept below approximately 3,2m to be able to cut two facets from one strip of glass. When considering the average of the largest and smallest diameter this will be fulfilled though.

A facet diameter of 1,6m will lead to approximately 14 facets over the diameter of the shell (20/1,6=12,5 and adding some for the curvature of the shell).

Cutting off the shell structure; The bottom of the shell structure is preferably flat. This will improve the possibilities for supporting the shell in a sufficient way and it will at the same time make a clearer ending of the shell. However, when cutting off a facetted shell with a horizontal plane, it will always cut through a number of the facets, see Figure 4.3. Structurally this should not pose any real problems as long as the facets are still sufficiently supported at their free edge, however, in a straight cut the dome will have the best approximation of a circle at its base. This is structurally interesting, especially when it is hard to sufficiently support the edges. For production reasons it will be feasible to have as many facets in the same size as possible which is only partly possible in the geodesic geometry.

For the buckling analysis the exact cut of the shell is not very important, since it is expected that local buckling will occur in the areas with low curvature. These areas are found near the top of the dome. Global buckling is influenced by the supports, but if

Table 4.1: Varying frequencies and classes to find a suitable approximation of the dome.

Variant	Class	Frequency	diameter dome (m)	average diameter facets (m)
Ideal	-	-	20	1,5
A	I	9	19,7	1,9
B	I	10	19,4	1,7
C	II	6	19,4	1,6
D	II	7	18,9	1,4
E	II	8	18,6	1,2

they are kept more or less in the same plane it will not pose a problem when sufficiently supported.

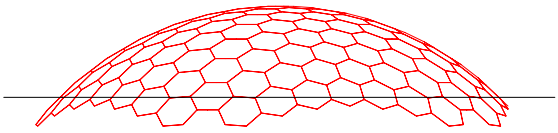

Figure 4.3: Cutting the dome using a horizontal plane will always cause cutting through a number of the facets.

4.1.3 The resulting geometry of the shell structure

By using the properties and demands for the shell as stated in the foregoing Paragraph, a geometry for the facetted shell structure can be defined. Several classes and frequencies have been investigated. The goal is to end up with an approximately 20m span of the dome and an average facet size of approximately 1,5m. Table 4.1 shows the results.

The table shows that the class II subdivision creates a more precise subdivision. The class II frequency 6 dome will be chosen for further development of the model. In a parameter study the frequency 7 and 8 could be used to see the influence of the facet size on the buckling behaviour. This geometry is shown in Figure 4.4-4.6.

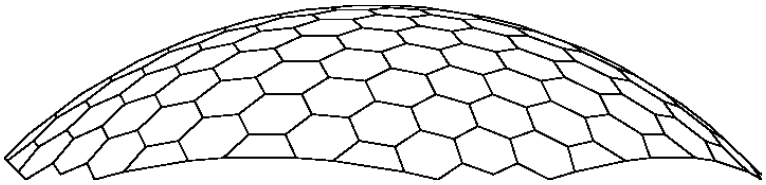

Figure 4.4: The chosen geometry for the facetted shell structure; side elevation.

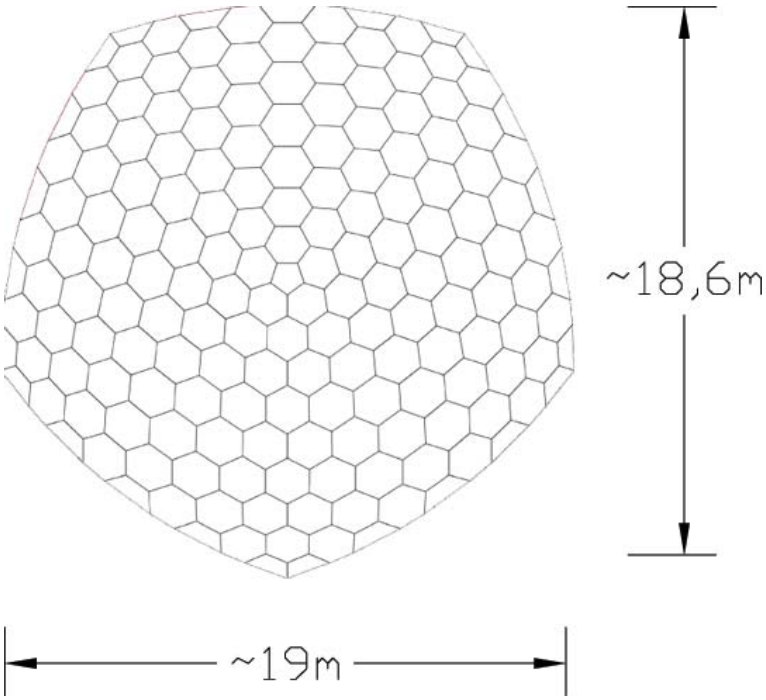

Figure 4.5: The chosen geometry for the facetted shell structure; top view.

4.2 Properties for the finite element model

Besides the geometry a number of other aspects are important to be able to build a finite element model of the facetted glass shell structure. These aspects are discussed in this Paragraph.

The material properties of the glass; The finite element model will be used to consider the bucking behaviour of a facetted glass shell structure. The main structural material is glass with the following significant properties, see Paragraph A.5:

$$Density \quad \rho = 2500 kg/m^3$$

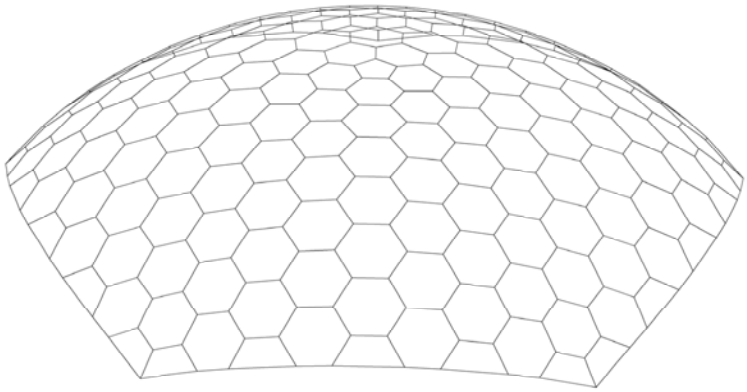

Figure 4.6: The chosen geometry for the facetted shell structure; bird's eye view.

$$\begin{aligned} Young's\ Modulus \quad & E = 7 * 10^{10} Pa \\ Poisson's\ ratio \quad & \mu = 0,2 \end{aligned}$$

The glass will be laminated glass, but will be modelled as a single glass pane with double thickness.

Connections between the glass facets; The joints between the facets will be represented by a strip of material with a different (lower) stiffness than the glass. This stiffness should correspond with the desired stiffness in the final joints.

As has been concluded in Theis Isgreen's thesis (Isgreen 2007), also see 3.3, the joints between the facets can not be continued in the vertices. Releasing theses joints will be done by assigning zero stiffness (no material) to the joint areas around the vertices and assigning the normal joint stiffness to the rest of the joint area, see Figure 4.7.

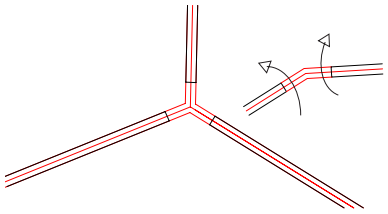

Figure 4.7: Releasing the vertices of the facetted shell will allow them to move.

The rotational stiffness of the joint is expected to be the most important characteristic for the overall buckling behaviour of the facetted shell. The rotational stiffness can be defined by combining the thickness of the joint with a stiffness (E-modulus) that is assigned

to the material, see Figure 4.8. Further elaborations on the joint can be found in Chapter 12

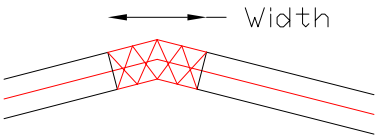

Figure 4.8: A vertical cut over a joint between facets.

Boundary conditions; The best way to connect the shell structure to the outside world without introducing high bending stresses is to simply support the entire edge of the shell. It is important to note that the shell will need to be horizontally supported as well, which will cause bending moments to develop, see Paragraph B.2. All edges of the shell will be supported in three directions, while all rotations are kept free.

Conclusion; with this information the first finite element model of the structure can be developed. Fine-tuning of the model and aspects like meshing and the type of elements will be treated in Appendix E.

4.3 Creating the detailed geometry

Introduction

In order to model the stability behaviour of the facetted shell structure, the geometry as found in Chapter 4 needs to be further developed. As was stated in Chapter 4.2 the joint will be modelled by creating a gap between the glass panels. This gap will be partially filled with a different material to model a different stiffness. The process of creating the geometry of the joints will be discussed in this Chapter. One of the starting points is the five-way radial symmetry of the dome, which can be used in DIANA. By addressing all properties to on-fifth of the geometry and copy and rotate it, the full shell can be generated.

4.3.1 Creating the gaps

The geometry of the shell that is defined in Paragraph 4.1 results in a dome with a large number of different size facets. The different dimensions of the facets of course also result

in different edge lengths. This complexity makes it very time consuming to develop an automatic system to generate the joints. This is the reason that it is chosen to create the geometry of the joints by hand, which requires a straight-forward system to develop the joints.

There are two principle ways of creating the gap from the current geometry.

1. off setting the edges inside
2. shrinking the hexagonal faces

Both methods create some inconsistency with the ideal situation, which will be shortly described here.

Off setting the edges; The hexagonals in the shell are not only different in size from each other, but the edges also have three different lengths, see Figure 4.9. When all the edges are off set inside the new shape will deviate a little from the original shape of the hexagonal; the skewness will increase (see Figure 4.10. All joints, however, will have exactly the same width. This shape deviation is structurally negligible, since the deviation lies within a couple of millimetres when the width of the joint is a couple of centimetres.

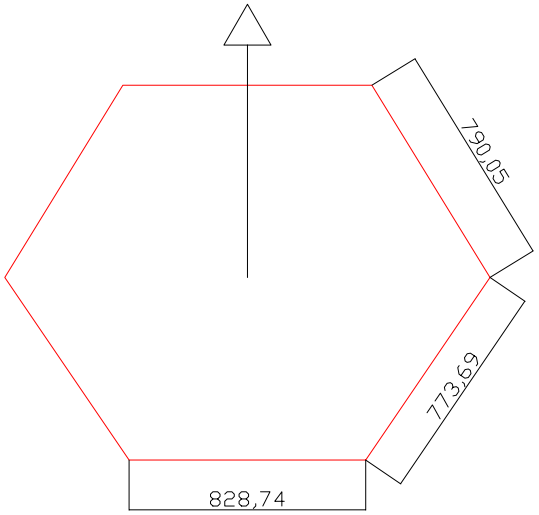

Figure 4.9: The different lengths of the edges in an arbitrary facet.

The steps that have to be taken are as follows:

1. offset edges 1 to 6
2. trim all new edges

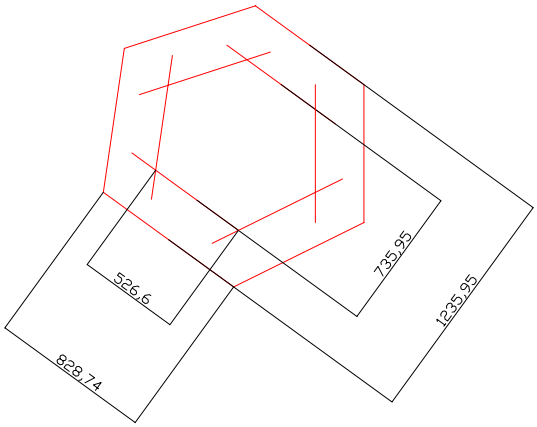

Figure 4.10: When the edges are offset, the shape changes slightly: $\frac{527}{826} > \frac{736}{1236}$.

3. draw the new (triangular) faces

4. define the points that describe the corners of the real joint

5. draw the joints in between the facets

The most important downside of the changing of the shape is that it will become more elaborate to create the joints in between the facets. The relation with the old edge is lost and it will be necessary to draw the edge directly to the adjoining facet. Especially at the edges of the one-fifth part of the shell this will be significant, since there is no adjoining facet to draw to. It is also fairly elaborate that it is necessary to offset all edges one by one, which requires setting the coordinate system to the plane of the facet, and the necessity to trim all these edges.

The most important upside to the off set method is that all joints will have exactly the same width.

Shrinking the facets; The facets are in principle built up out of six triangular planes, lying in the same general plane. When these six facets are scaled as a group on the centre point of the facet, a new facet will be found. The new facet will have exactly the same dimensional ratios. However, since the corner angles of the facets are unequal, the width of the joint will differ slightly per edge. This is important, since the (bending) stiffness of the joint depends on this width. This means this method can only be used when the deviations in the width of the joint are limited.

The steps that have to be taken are as follows:

1. calculate the scale factor per facet depending on the desired width of the joint

2. scale every facet

3. define the points that describe the corners of the real joint

4. draw the joints between the facets

It is obvious that this method is far less elaborate. The scale factor is easily defined by the following Equation:

$$\alpha = \frac{(D_{facet,average} - t_{joint})}{D_{facet,average}} \tag{4.1}$$

Where $D_{facet,average}$ stands for the average 'diameter' of the facet and t_{joint} for the desired thickness of the joint. Since the 'diameter' of the facet can have three different values, see Figure 4.11, it is important to take the average value to obtain a more equal thickness of the joint. To further improve the evenness of the thickness it is also possible to take the average radius of the facet.

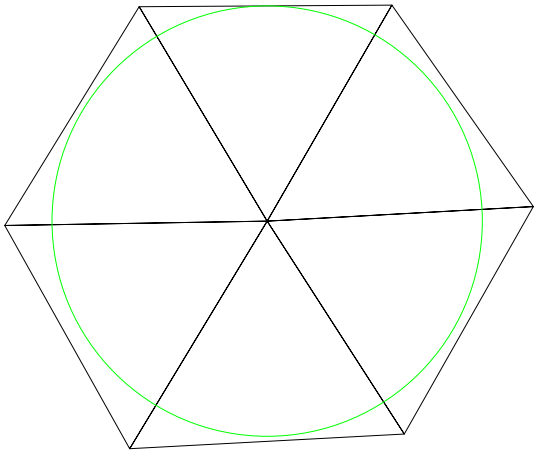

Figure 4.11: The three different 'diameters' of a facet are defined by the distance between the mid points of two opposing edges; the circle shows that all these distance can be all different due to distortions in the shape of the facet to fit the dome.

The differences between the diameters are largest for facets 4 and 8, see Figures 4.12 and 4.13. Since these two lie next to each other also the largest joint width deviation is found here. Furthermore, the facets are all slightly compressed in the meridional direction of the dome, so the measured distance between the two facets at the faces crossing the meridian is governing. This leads to a joint distance between facet 4 and 8 of 9,55mm, which is a deviation of 4,5% from the desired joint width (in this case 10mm).

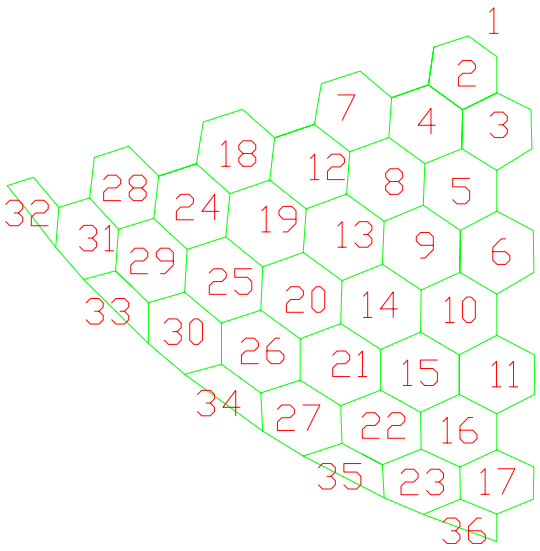

Figure 4.12: The facets of one-fifth of the dome numbered.

Conclusion; since the deviations that are found in the width of the joint are within reasonable margins, it is chosen to use the shrink method for creating the gaps between the facets. The main reasons for this choice are the speed of the method and the lack of deformation of the facets themselves.

Calculation shrink factor

width joint 0,01 (m)

element no.	D1 (m)	D2 (m)	D3 (m)	Daverage (m)	factor	**max dev.** (m)	(%)
1 *(pentagon)*	*0,4750*	-	-	*0,4750*	0,9895		
2	1,2405	1,2995	1,2995	1,2798	0,9922	0,0393	3,07%
3	1,3413	1,3579	1,3413	1,3468	0,9926	0,0111	0,82%
4	1,3128	1,4340	1,4340	1,3936	0,9928	0,0808	5,80%
5	1,3977	1,4326	1,4703	1,4335	0,9930	0,0368	2,56%
6	1,4878	1,4412	1,4878	1,4723	0,9932	0,0311	2,11%
7	1,3977	1,4703	1,4326	1,4335	0,9930	0,0368	2,56%
8	1,4420	1,5183	1,5183	1,4929	0,9933	0,0509	3,41%
9	1,4927	1,5191	1,5622	1,5247	0,9934	0,0375	2,46%
10	1,5300	1,4920	1,5566	1,5262	0,9934	0,0342	2,24%
11	1,5451	1,4725	1,5451	1,5209	0,9934	0,0484	3,18%
12	1,4927	1,5622	1,5191	1,5247	0,9934	0,0375	2,46%
13	1,5510	1,5880	1,5880	1,5757	0,9937	0,0247	1,57%
14	1,5843	1,5843	1,6123	1,5936	0,9937	0,0187	1,17%
15	1,5880	1,5510	1,5880	1,5757	0,9937	0,0247	1,57%
16	1,5566	1,4920	1,5300	1,5262	0,9934	0,0342	2,24%
17	1,4878	1,4412	1,4878	1,4723	0,9932	0,0311	2,11%
18	1,5300	1,5566	1,4920	1,5262	0,9934	0,0342	2,24%
19	1,5843	1,6123	1,5843	1,5936	0,9937	0,0187	1,17%
20	1,6246	1,6344	1,6344	1,6311	0,9939	0,0065	0,40%
21	1,6344	1,6246	1,6344	1,6311	0,9939	0,0065	0,40%
22	1,6123	1,5843	1,5843	1,5936	0,9937	0,0187	1,17%
23	1,5622	1,5191	1,4927	1,5247	0,9934	0,0375	2,46%
24	1,5880	1,5880	1,5510	1,5757	0,9937	0,0247	1,57%
25	1,6344	1,6344	1,6246	1,6311	0,9939	0,0065	0,40%
26	1,6507	1,6507	1,5421	1,6145	0,9938	0,0724	4,48%
27	1,6344	1,6344	1,6246	1,6311	0,9939	0,0065	0,40%
28	1,5566	1,5300	1,4920	1,5262	0,9934	0,0342	2,24%
29	1,5173	1,5843	1,5843	1,5620	0,9936	0,0447	2,86%
30	1,6344	1,6246	1,6344	1,6311	0,9939	0,0065	0,40%
31	1,5622	1,4927	1,5191	1,5247	0,9934	0,0375	2,46%
32 *radii!*	0,7115	0,7420	0,7070	0,7202	0,9931	0,0219	3,04%
33 *radii!*	0,7919	0,7961	0,7795	0,7892	0,9937	0,0097	1,22%
34 *radii!*	0,8183	0,8145	0,8183	0,8170	0,9939	0,0025	0,31%
35 *radii!*	0,7794	0,7961	0,7919	0,7891	0,9937	0,0097	1,23%
36 *radii!*	0,7070	0,7421	0,7112	0,7201	0,9931	0,0220	3,05%

Figure 4.13: A table showing the different 'diameters' of all facets, the average diameter and the resulting shrinkage factor.

4.3.2 Location of the joint

The joint itself can be either placed relative to the original vertex or the edge of the glass, see Figure 4.14 left. The main difference in the result is that when the original vertex is used, the distance from the corner of the glass facet to the start of the joint will not be the same on every glass edge, see Figure 4.14 right. This is caused by the fact that the widths of the joints influence the location of the joint. Since these widths have small deviations it is better to use the glass edge as a reference.

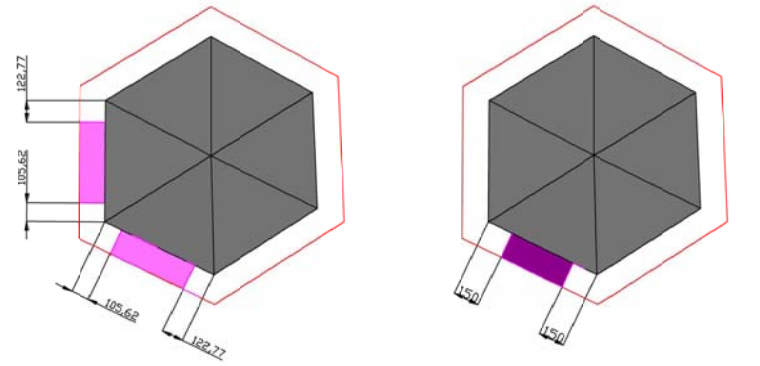

Figure 4.14: The resulting edge distances; left: original vertex as a basis, 200mm from vertex; right: corner of the facet as a basis, 150mm from corner. Different lengths arise when using the original vertex as a reference point.

4.3.3 Geometry of the modelled joint

Preferably the joint should be a plane element connecting two glass facets. In Paragraph 4.1 a model was proposed with a joint with a kink, see Figure 4.15. However, in the current geometry of the model it is actually easier to create the planar joints as shown in Figure 4.15 left. The only locations where it is more elaborate to use flat joints are at the edges of the one-fifth part of the shell. The differences are very small and structurally negligible when also the thickness of the joint will be taken into consideration. However, the kinked joints will not connect perfectly when the shell part is copied and rotated. This deviation is shown in Figure 4.16. The connectivity can be guaranteed by merging the nodes which are close together. However, when the model is run in a finite element model, stress peaks are found around the edges of the copied shell part, which might be a result of this geometrical inconsistency. To remove possible influences also the edges will get a precisely geometrized flat joint.

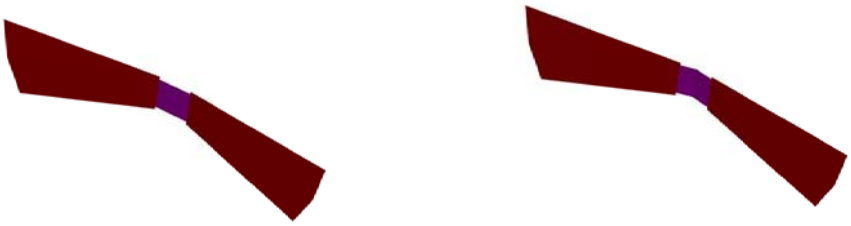

Figure 4.15: The shape of the joint in the model (exaggerated ratios!); left: the planar version; right: the 'kinked' version as proposed in Chapter 4.

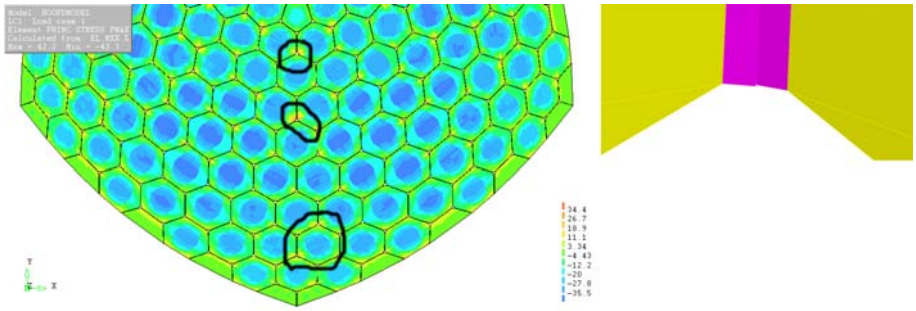

Figure 4.16: Left: Deviation in the connection of the kinked joint; also note the difference in the angles of the edges. Right: small deviations peaks in the stress distribution that are possibly arising from this geometry.

4.3.4 Properties of the modelled joint

Introduction; this shape of the joint will lead to a joint stiffness that is dependent on the material stiffness of the joint material. In this Paragraph the three different stiffnesses of this joint model will be discussed; the bending stiffness, the normal stiffness and the shear stiffness. They will be derived as functions of the width and thickness of the joint, to be able to see the influence of the geometry on the property of the joint.

Limitations; Creating a model of the joint to determine the interaction and behaviour of the joint is very important to be able to control the joint properties. In order to correctly implement a joint into the FEM model a translation will need to be made between the dimensions and material properties of the joint and its structural behaviour. By modelling the joint the influence of the interaction between the main variables on the structural behaviour, being the width, thickness and E-modulus of the material, will be known. The different joint stiffnesses can then be controlled by adjusting these variables.

In the model of the joint as it is proposed right now a number of limitations apply. Firstly, the joint is proposed with a linear elastic, isotropic material. In reality this is

not true since rubber, for instance, does not have a linear elastic behaviour. The materialization of the joint is, however, not finished. At the moment only a proposed joint is available, see Paragraph 4.3.5 and Chapter 12.

The second simplification is the 2D-analysis of the behaviour perpendicular to the joint direction. This simplification is thought to be justifiable because the joint has a very high length to width ratio. Deviating effects can be expected at the ends of the joints but these will damp out, leaving the largest part of the joint with the same behaviour perpendicular to the joint direction. A 2D-analysis will then be a suitable approximation. Local effects will need to be studied more thoroughly in a detailed stress analysis but are not expected to influence the overall behaviour to great extent.

The stiffnesses of the modelled joint will be discussed in Chapter 12.

4.3.5 The proposed joint

In reality the joint will most likely not be a (glued) butt joint. It is not yet totally clear which joint topology is going to be chosen, but the current proposal is shown in Figure 4.17. The idea for this joint has been developed by Anne Bagger and is currently being tested Anne Bagger and Helle Krogsgaard at the DTU in Denmark. This joint consists of two strips of material clamping on the outside of the glass. In between the glass and the clamps there will be a neoprene strip.

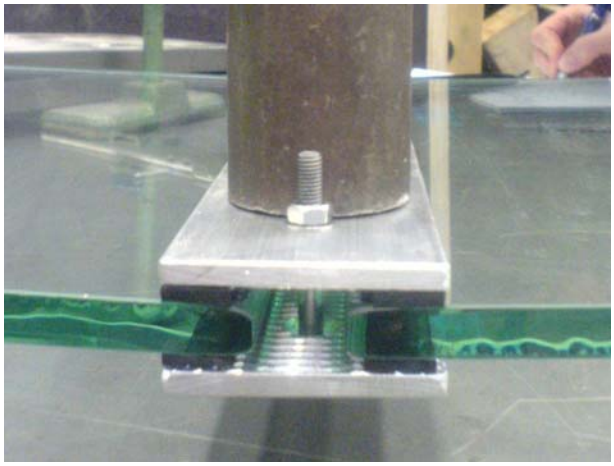

Figure 4.17: The likely configuration of the real joint; a test sample at the DTU by Anne Bagger and Helle Krogsgaard.

The main advantages of the joint are the possibility to transfer shear stresses along the length of the joint and a potential simplicity of erection. The latter refers to the fact that the joint allows for (some) deviations in the dimensions of the facets and joints as well as the placing of the facets. Furthermore the possibility exists to partially prefabricate the

joint by placing the rubber strips onto the glass facets before construction. Perhaps it will even be possible to attach one side of the joint to (half of) the panels. This will greatly increase the speed of erection.

The downside to the joint topology as is proposed is that the size of the clamping strips might be significant in the appearance of the structure. In order to retain the initial objective of a 'transparent dome' it will be necessary that the joint width will be as small as possible. However, the structural principle also implies that the joint width (or total joint area) will be significantly smaller than the dimensions of a supporting steel structure. As a reference the roof of the Great Courtyard of London's British Museum can be considered. This roof consists of triangular glass panes supported by a very slender steel structure, see Figure 4.18. The spans in this structure are smaller than the proposed span of the facetted dome, however, the shape is at the same time structurally much less feasible, because of the low curvature and small height. Considering these two aspects makes that the order of magnitude of the steel profiles is likely to be representative for a comparable structure used for a dome shape.

The detail to the right shows a hexagonal that is comparable to the dimensions of the hexagonal facets in the facetted dome. The width of the elements of the elements is very low and lies in the order of 2-3cm. The height of the elements, however, also has a large influence on the transparency of the structure, since, especially in a dome structure, a spectator will always be looking at the glass structure under an angle. A reasonable estimation of the total width of the joint is therefore approximately 5cm.

An additional factor in the transparency of the structure is the fact that a much lower area of the dome will be taken up by joints, since the edges of the hexagonal will have joints, in contrast to the edges of the triangular faces. This means that the facetted dome will have a much higher transparency. It should be noted, though, that a decrease in the size of the panels does not necessarily mean a proportional decrease in the width of the joint. Therefore a large transparency also requires fairly large facets. Increasing the size of the facets, however, decreases the smoothness of the dome and will result in larger local bending stresses in the facets.

The height of the proposed joint is not much more than the thickness of the plate and can be estimated around 3cm. This means that the increase in visible width is very small compared to the elements in the structure of the Great Courtyard. The width of the joints in the dome can therefore also be around 5cm without being considered as an important structural element or a disturbing element. Especially when it is considered that the hexagonals in the dome are considerably larger than the triangles in the Great Courtyard. A width of 5cm will likely be enough to create a clamping joint between the glass facets.

The stiffnesses of the proposed joint and its implications are evaluated in Chapter 12.

Figure 4.18: The Great Courtyard at the British Museum, London, UK; the right hand image shows a detail of the steel structure.

In Appendix E the geometry is translated into a finite element model for DIANA, the programme that is used for calculation.

Chapter 5

Testing the model

Introduction

Before the buckling analysis will be done, the model needs to be tested whether it fulfils the expectations. One aspect is of course the accuracy of the results, but other important aspects are visible distortions and possible connectivity issues. To test the model a linear elastic analysis will be carried out, since the results of this analysis can be estimated roughly. The results of the model will therefore be compared to reasonably expected results. NB. In this Chapter only the self weight of the shell is applied.

5.1 Distortions in the model

By looking at the overall stress distributions in the shell it can be determined whether strong deviations from the expected behaviour of the model arise. For the division of the bending stresses it must hold that negative bending stresses are found in the centre of the facets, which increase (become less negative/become positive) closer to the edges. This behaviour is also described in Paragraph 3.3.3. The joints in this model have a fairly low stiffness, so the bending stresses can only be low in these areas. The plot of the principal bending stresses as shown in Figure 5.1 shows exactly this expected behaviour.

Bending stresses in a smooth cylindrical shell are usually low when the shell is loaded by a uniformly distributed load. The dead weight complies to this load condition to a large extent. Therefore it is hard to recognize the overall bending behaviour, since the local bending stresses are much larger. Along the edges the constraints will introduce bending stresses, since they do not fully comply with the membrane behaviour, as is explained in Appendix B.1. When the deformations of the total shell are considered it does become clear that it behaves as expected, see Figure 5.2. There were a number of deviations found around the edges of the one-fifth part of the shell structure which have been resolved by

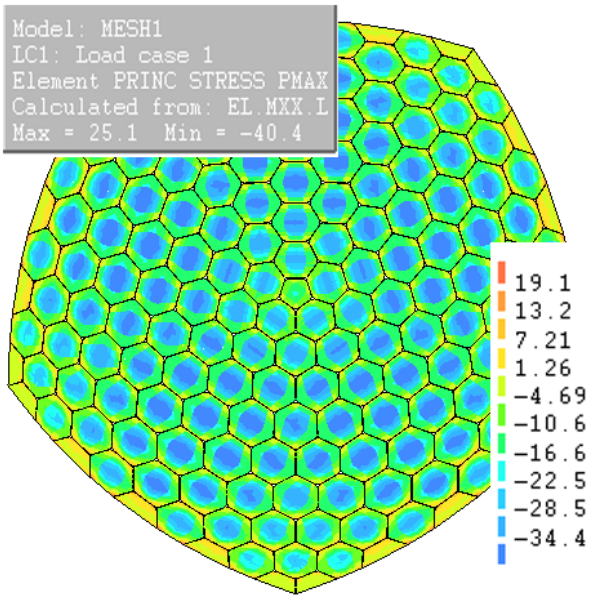

Figure 5.1: The principle bending stresses in the shell, according to the FEM-model.

changing the geometry of the joint, see Paragraph 4.3.3.

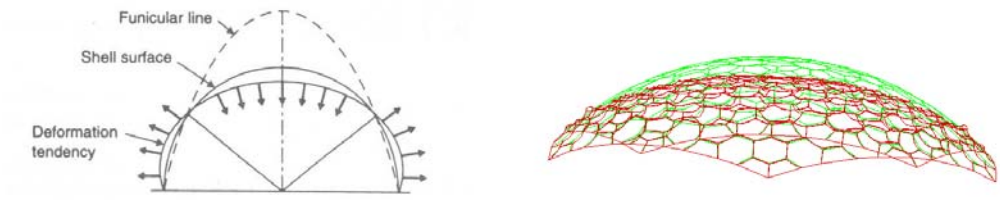

Figure 5.2: A comparison of the deformations of a smooth shell (Schodek 2004) and the results of the model for the facetted shell.

5.2 Accuracy of the model

5.2.1 Order of magnitude of the results

The accuracy of the model can be determined in two steps. First necessity is a check of the order of magnitude of the results. This can be most easily tested by looking at the

deflections. A very simple model can be used for the deflection of a single plate, which shows in what order the deflections should be. The model that will be used here is a combination of three simply supported beams which represent the three main lengths in the plate, see Figure 5.3. The simple support is chosen, since the joint can in this case only transfer small bending stresses. Each 'beam' should now support one-third of the load from the plate. When the resulting deflections are added, a rough approximation of the deflection is found.

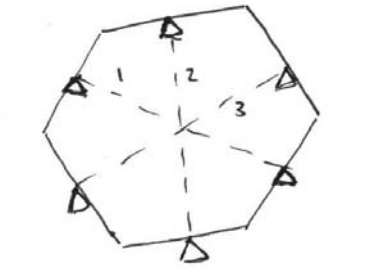

Figure 5.3: The three 'beams' in the plate.

The facet with the maximum deflection, according to the finite element model is shown in Figure 5.4. The dimensions of this facet will be taken for the approximative hand calculation of the deflection of a glass facet.

The following variables are used:

$$\begin{aligned} &b = 1mm \\ &t = 16mm \\ &\rho = 2,5 * 10^{-6} kg/mm^3 \\ &I = \tfrac{1}{12} * 1 * 16^2 = 341,33mm^3 \\ &E = 70000N/mm^2 \\ &Q = b * t * \rho * g = 1 * 16 * 2,5 * 10^{-6} * 10 = 4 * 10^{-4} N/mm \end{aligned} \tag{5.1}$$

The resulting deflections are therefore:

$$\begin{aligned} \delta_a &= \tfrac{5}{384} \tfrac{ql^4}{EI} = 0,9mm \\ \delta_b = \delta_c &= \tfrac{5}{384} \tfrac{ql^4}{EI} = 1,1mm \end{aligned} \tag{5.2}$$

The total deflection is then approximately equal to $\frac{1}{3} * (\delta_a + \delta_b + \delta_c) = 1mm$. This result shows that the order of magnitude of the deflections in the model ($\delta \approx 0,75mm$) is in accordance with the estimations of the hand calculation.

Another way to test the deflections is making the comparison with a simply supported

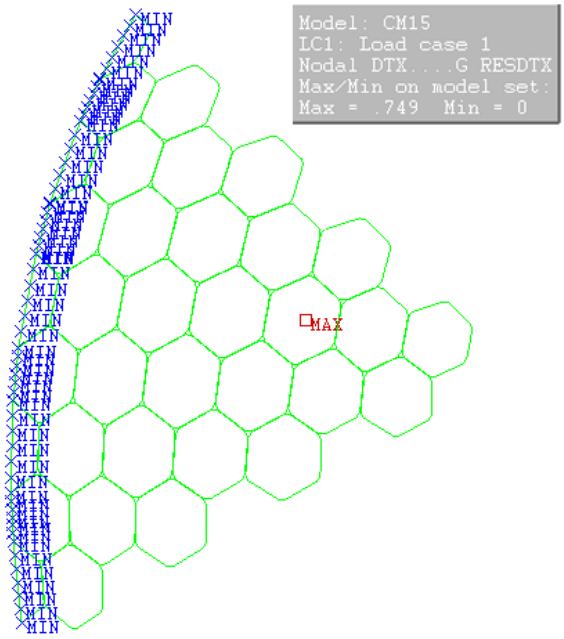

Figure 5.4: The facet with the maximum deflection according to the FEM model.

circular plate with a diameter similar to the diameter of the glass facets. All material and plate properties can be kept exactly the same. The deflection in the centre of a simply supported circular plate can be described by Equation 5.3.

$$w = \frac{pr_0(5+\mu)}{64D(1-\mu)} \tag{5.3}$$

Where,

$$\begin{aligned} p &= 4 * 10^{-4} N/mm^2 \\ r_0 &= 1500mm \\ \mu &= 0,2 \\ D &= \tfrac{1}{12}\tfrac{Et^3}{(1-\mu^2)} \\ t &= 16mm \\ E &= 7 * 10^4 N/mm^2 \end{aligned} \tag{5.4}$$

Using Equation 5.3, a maximum deflection of 5,5mm is found. This deflection is also in about the same order of magnitude as the earlier found deflections.

5.2.2 Accuracy and mesh refinement

The second step in determining the accuracy of the model is the checking of the necessary fineness of the mess. The mesh that has been developed in Paragraph E.9 will be refined using a scale factor for the mesh. The first scale factor will be 1,5, de second will be 2. The results will be compared for the deflections, bending stresses ($m_{1,2}$) and normal stresses ($n_{1,2}$).

The deflections; Figure 5.5 gives the deflections in the three different models. The absolute differences for the maximum deflections are respectively 0,01mm and 0,007mm. It is shown that the difference in results between the base model and the first refinement is fairly large. However, it is also visible that the differences between the next refinement step is smaller and that the solution is likely to converge. The finest mesh, MESH20, has a factor 2 in fineness compared to the original mesh, MESH1. The resulting error in MESH20 is shown in Equation 5.5. Since the elements have four nodes with a linear interpolation between the nodes the order of the difference in deflection, $\Delta u = O(h)$, this formula indeed holds.

$$\begin{aligned} u &= 2u_2 - u_1 = 2 * 0,753 - 0,736 = 0,770mm \\ E &= \frac{u-u_2}{u} = \frac{0,770-0,753}{0,770} = 2,2\% \end{aligned} \tag{5.5}$$

This is an acceptable error.

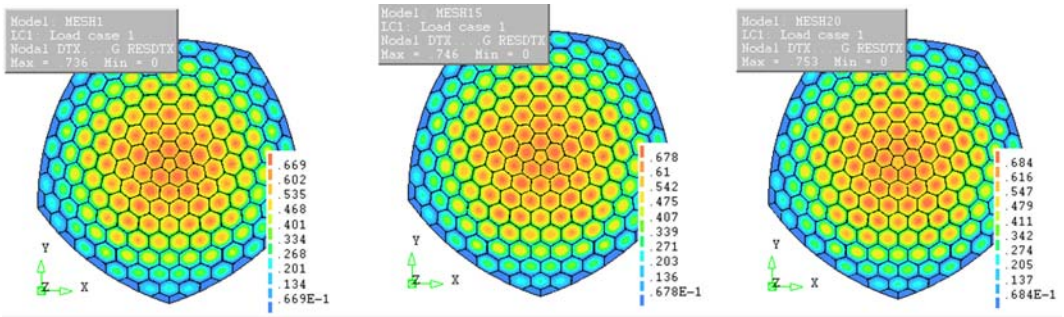

Figure 5.5: The deflections in the three different meshes.

The bending stresses; in Figure 5.6 the maximum bending stresses are shown and in Figure 5.7 the minimum bending stresses. In this image the differences between the meshes are even clearer. Again the differences between the two finer meshes are fairly small, pointing in the direction of convergence. The finest mesh, MESH20, has a factor 2

in fineness compared to the original mesh, MESH1. The resulting error in MESH20 for the maximum bending stress therefore is:

$$u = 2u_2 - u_1 = 2 * -43,7 - -40,4 = -47N/mm$$
$$E = \frac{u-u_2}{u} = \frac{47-43,7}{47} = 7\% \tag{5.6}$$

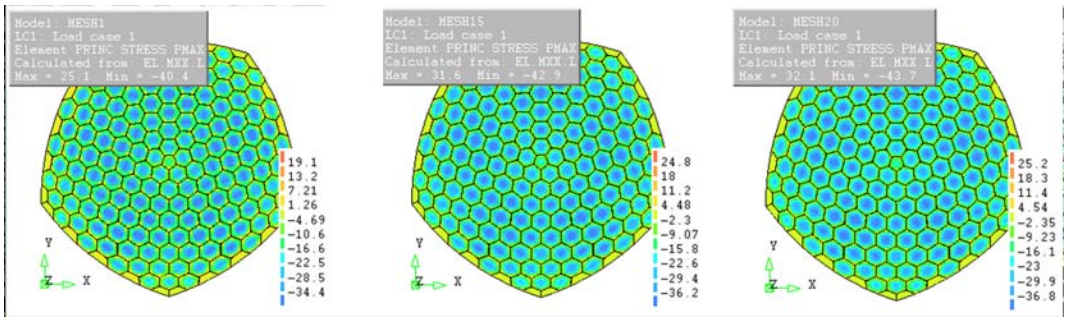

Figure 5.6: The maximum bending stresses in the three different meshes. NB note the sign

For the minimum bending stress:

$$u = 2u_2 - u_1 = 2 * -49,7 - -47,8 = -51,6N/mm$$
$$E = \frac{u-u_2}{u} = \frac{51,6-49,7}{47} = 3,7\% \tag{5.7}$$

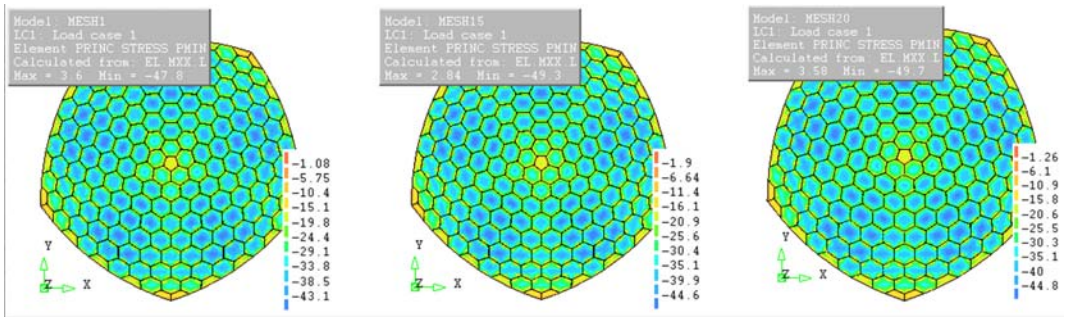

Figure 5.7: The minimum bending stresses in the three different meshes. NB note the sign

For the maximum bending stress and for the minimum bending stress the error is not very high and acceptable.

The normal stresses; In Figure 5.8 the maximum normal stresses are given and in Figure 5.9 the minimum normal stresses. The maximum stresses, which are mostly the

tensile stresses, seem to differ quite a lot. The maximum tensile stresses, however, are only found as peak stresses near the connection. These peak stresses are not interesting for the overall stability behaviour and will therefore be disregarded. When the total image is considered, the stresses do not deviate much at all between the three models and especially between the MESH15 and MESH20 models. The minimum stresses, representing the maximum compressive normal stresses, are very equal between the three models. It is also visible that the compressive stresses are nicely distributed over the dome, increasing to the bottom.

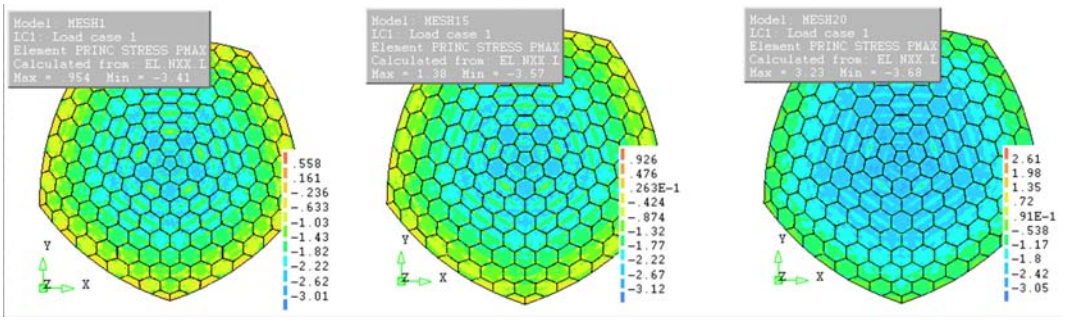

Figure 5.8: The minimum normal stresses in the three different meshes. NB note the sign

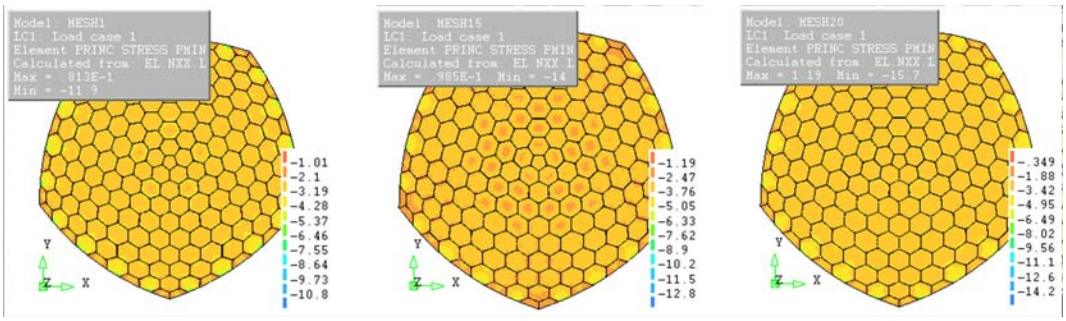

Figure 5.9: The minimum normal stresses in the three different meshes. NB note the sign

5.3 Higher order elements

It is shown that the mesh refinement to MESH20 is sufficient to attain acceptable results for the stresses. However, since the number of elements rises the calculation time also increases. Therefore the possibility of using higher order elements becomes interesting too. The number of elements will become one fourth of the previous number. At the same time the number of nodes, which actually largely defines the calculation time, is lowered

with a factor $\frac{8}{9}$, see Figure 5.10. This might not seem like a large decrease, but since there will be thousands of elements calculated it will actually significantly save calculation time, especially when calculating a large number of buckling modes.

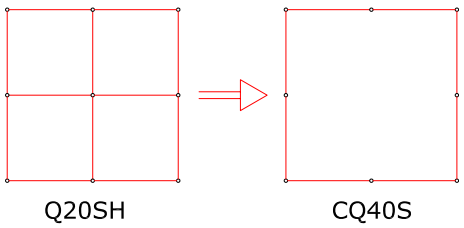

Figure 5.10: The result of changing from a first order (Q20SH) to a second order element (CQ40S): $n_{elements} * \frac{1}{4}$; $n_{nodes} * \frac{8}{9}$.

The second positive point in using the higher order is the interpolation of the results between the integration points will now be a second order polynomial instead of a straight line. This way the accuracy of the model will be the same or better than the finer mesh with first order elements. It is therefore decided to use the higher order elements in the main model.

To show that the model with the higher order elements yields approximately the same results as the models that have been discussed before, Figure 5.11 gives the deflections under self weight.

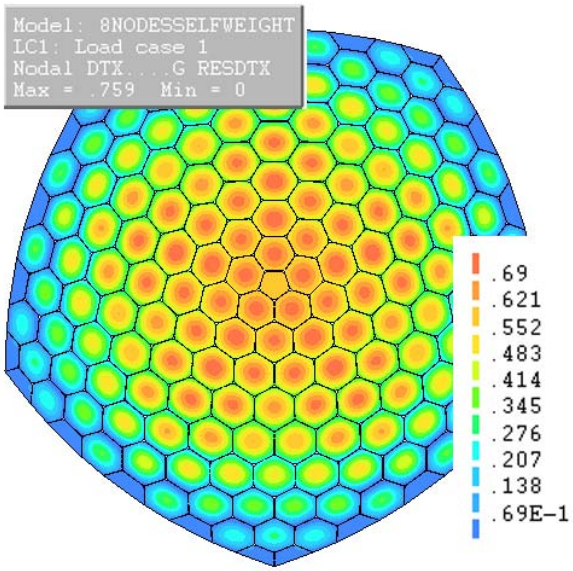

Figure 5.11: The deflections in the model using the 8-node element.

Chapter 6

Linear stability analysis

Introduction

The model has now been defined and tested, see Chapter 5. This means that the stability analysis can be carried out. To summarize the most important aspects of this model:

- the load will be the total load as found in Paragraph D.3: $p_{total} = 1,98 * 10^{-3} N/mm^2$.
- the elements used are the 8-node CQ40S elements, see Paragraph 5.3.
- the material properties are as follows:
  - glass: $E = 7 * 10^{10} Pa$
  - joint: $E = 0,1 * 10^{9} Pa$

6.1 Mode 1

The first buckling mode in the model is shown in Figure 6.1. It shows that apparently local buckling of the glass panels is governing. The buckling factor is actually fairly low at around 2.62. This is therefore the safety factor on buckling stability for the structure for buckling mode 1.

There are three important notions that have to be considered when looking at this first buckling mode.

The first notion is whether it is actually likely that a glass panel buckles. Glass is a very strong and stiff material, but the panels are also very thin. It will be interesting to test a single panel to see what the buckling factor will be under the same load. The behaviour of the singe panel is addressed in Chapter 9. It should be noted that the research in Chapter 9 is also related to the non-linear buckling analysis in Chapter 8.

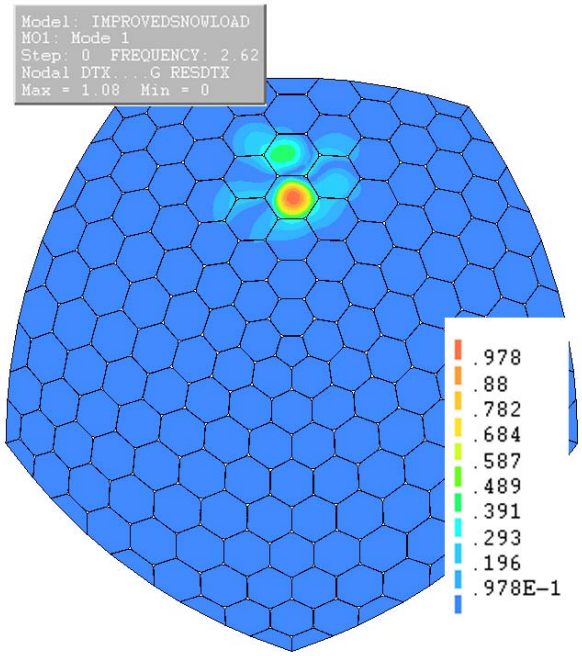

Figure 6.1: The first buckling mode of the shell.

The second notion is whether local buckling of a facet is actually a problem for the shell structure. The shell as a whole will remain stable until the shell will buckle as a system. This means that a large number of buckling modes will need to be investigated to find a buckling mode where not just single glass plates buckle, but a larger part of the shell.

The third notion is that only a linear buckling analysis has been carried out, which does not take into account the imperfections in the structure. An important indicator of the imperfection sensitivity of a shell structure is the spread of the eigen modes. When the eigen modes are close together they can have a large influence on each other. Small deviations of the structure could then lead to a possible combination of eigen modes, resulting in a much lower buckling factor. These issues will be addressed in Paragraph 6.2.

6.2 Governing buckling mode

When looking through the first 50 eigen modes, the first mode where local buckling of the system occurs is mode no. 41, shown in Figure 6.2. This mode shows that overall buckling of the shell is not a governing buckling mode. The more worrying aspect of this buckling mode is that the buckling factor is only 2.9, which is a difference of about

10% with the first buckling mode. Over forty buckling modes are found within a 10% range of the buckling factor, which leads to the suspicion that the dome is sensitive to imperfections. The actual buckling value might therefore be a great deal lower than this 2.9.

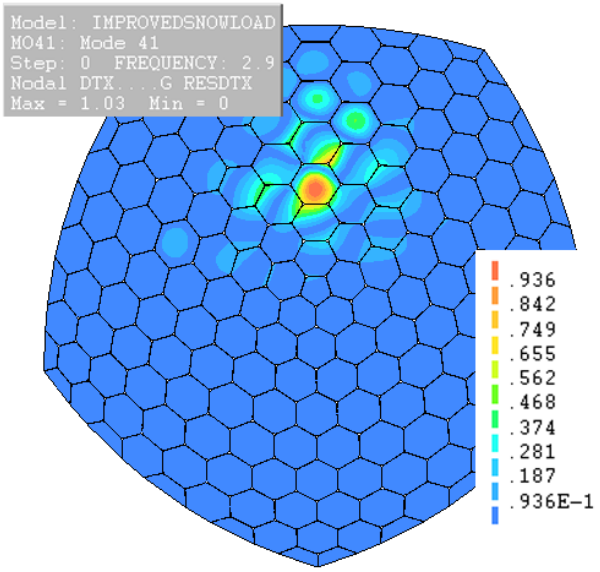

Figure 6.2: Buckling mode 41, showing local buckling of the structural system.

The buckling modes 48 to 50, see Figure 6.3 show very similar buckling modes. The buckling factor is the same here for every buckling mode, which is logical because the buckling modes are actually the same. The radial symmetry of the structure creates a number of 'different' buckling modes in a symmetrical way. This means that a number of modes are actually not real modes and that it is not fair to say that there are 50 modes within a 10% range of the buckling factor. It will therefore be investigated how many truly different buckling modes are found in the first 10% range of the buckling factor.

6.3 Different buckling modes

Similar buckling modes arise from the symmetry of the shell structure and should not all be considered. At least the following groups can be made:

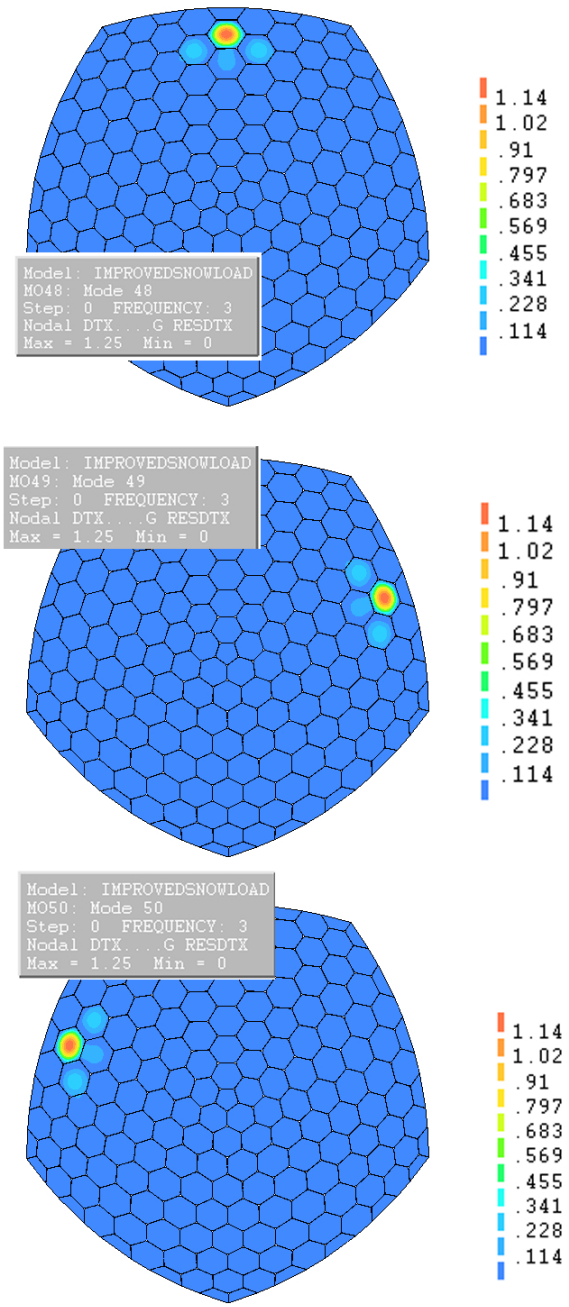

Figure 6.3: Buckling modes 48 to 50 showing local buckling; note the same buckling factor and shape of the buckling modes.

Group no.	Buckling modes	buckling factor
1	1	2.62
2	2	2.63
3	3-4	2.68
4	5	2.75
5	6-10	2.77
6	11	2.78
7	12-16	2.8
8	17	2.8
9	18	2.8
10	19	2.8

Some of these groups are clearly five-fold and following from the symmetry of the structure, like groups 5 and 7. Other groups are very similar in buckling factor but slightly different in buckling shape, like groups 8-12. If the buckling modes are considered this way, still a large number of different buckling modes are found within a 10% range of the buckling factor. This still leads to the suspicion that the shell is sensitive to imperfections which means that a imperfection analysis will be necessary to incorporate this effect. The currently found buckling factor of approximately 2.9 (mode 41) might not be enough as a safety factor for buckling when imperfections are not accounted for.

Chapter 7

Implications of the FEM method

Introduction

The classical theories of plates and shells are usually applied for thin structure while neglecting two aspects:

1. neglecting the non-linear effects of finite deformations: the influence of a changing geometry during a progressive loading
2. The Love-Kirchhoff approximation, which neglects transverse strains and stresses

For the facets in the facetted dome the second simplification is suitable, since the span to thickness ratio is very high. Diana does, however, take the shear deformations into account, more on this can be found in Paragraph 7.2.1.

The first simplification might no longer be valid when considering the buckling behaviour of the plate. In this behaviour the deformations of the plate will be significant and the non-linear effects should be at least considered. The elements in Diana use the linear approximation as proposed in the theory for thin shells. This means that it should be checked whether large differences arise in the results by neglecting the non-linear part. In Paragraph 7.1 it is shown that the influence of the linearization is very small in the model of the facetted dome structure.

Another implication that arises from using a finite element approach is problems with shear and membrane locking. These problems will be explained and addressed in Paragraph 7.2.

7.1 Large deflections

In the theory of thin plates and shells it is assumed that the deflections are small compared to the thickness of the element. Usually the non-linear effects become significant in shells

when the deflections are larger than the thickness of the structure (Donnell 1976). In the case of the facetted dome the largest deformations are found at the point of failure through buckling.

The maximum deformation is found at node 11462, where a resulting total deflection is found of $\approx 37,3mm$. This deflection is more than two times the thickness of the glass panels. The sensitivity of the facetted glass dome does, however, not necessary comply with the rule. The span to thickness ratio is very large ($1500/16 \approx 94$) and therefore a deflection that is equal to the thickness of the glass still results in a very small rotational angle. This angle is the most important factor in the approximation. Figure 7.1 shows the schematic approximation of the strain of a bar in 1d.

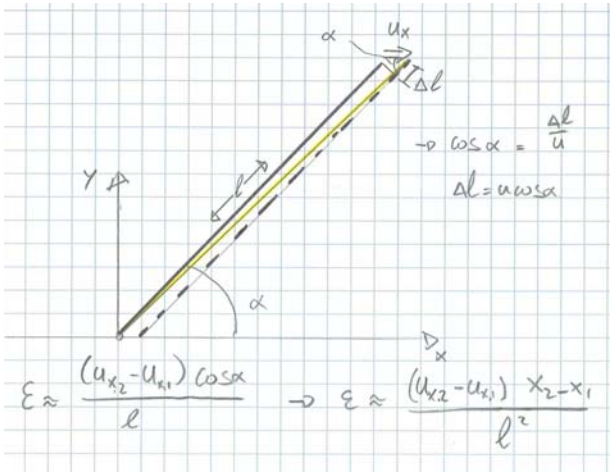

Figure 7.1: The linear approximation of the strain in a bar.

This approximation can be extended to 3d, yielding the following result:

$$\varepsilon_{approx} = (u_{x,2} - u_{x,1})\frac{x_2 - x_1}{l^2} + (u_{y,2} - u_{y,1})\frac{y_2 - y_1}{l^2} + (u_{z,2} - u_{z,1})\frac{z_2 - z_1}{l^2} \tag{7.1}$$

The real strain in the bar (in 3d) is given by the following Equation:

$$\varepsilon = \frac{\sqrt{(x_2 + u_{x,2} - x_1 - u_{y,1})^2 + (y_2 + u_{y,2} - x_1 - u_{y,1})^2 + (z_2 + u_{z,2} - z_1 - u_{z,1})^2} - l}{l} \tag{7.2}$$

With Equations 7.1 and 7.2 the difference between the approximate and real strain can be calculated by using the deflections found in the Diana model. One edge of a finite element will be chosen near the maximum deflection. By comparing the results of the two Equations the influence of a large deflection on the resulting strain can be estimated. The

following coordinates are found:

Node	x	y	z
11462	2110	686	-204
11434	2171	705	-216

The following deformations are found:

Node	dx	dy	dz
11462	-3.78	-1.24	-37.3
11434	-3.77	-1.23	-37.2

The equations have been solved in 3d in Maple and the result is that the difference between the approximation and the exact solution is only 1%. This means that even when the displacements are relatively large, the influence of the non-linear part of the solution of the strains is still rather small. The approximation is therefore considered valid.

7.2 Shear and membrane locking

Introduction

In the description of shell elements in finite element modelling two characteristics are very troublesome: membrane and shear locking. These two phenomena will be discussed in this Paragraph, together with their influence on the results of the model. This discussion will be followed by the implications on the model itself.

7.2.1 Shear locking

Shear locking is the effect that large transverse shear resistance is found in elements, even though the transverse shear should actually vanish. The cause is an incapability of many shell elements to represent deformations where the transverse shear should disappear. The shear stiffness, however, is often significantly larger than the bending stiffness. This leads to the shear stiffness to take up a large deal of the energy exerted on the structure by external loads. The deflections and strains that are predicted by the model will now be much smaller than in reality. This is why it is called ‘shear locking’ (Belytschko, Liu & Moran 2000). The shear locking issue is also mentioned in the DIANA manual. In relation to the flat shell (Mindlin) elements the following is stated:

> *In the Mindlin-Reissner plate theory the transverse displacements and rotations of the mid surface normals are independent and obtained by employing*

> *an isoparametric interpolation respectively from the translations and rotations in the nodes. This technique includes transverse shear deformation. Elements implemented according to this theory are simply called 'Mindlin plate elements'. In their standard form these elements are sensitive for shear locking which results in a excessively stiff behaviour. To overcome this difficulty for the linear and quadratic elements, Diana modifies the transverse shear strain field. (de Witte 2007)*

In the DIANA manual the following is stated about shear locking of curved shell elements:

> *Especially for applications where transverse shear deformations are of importance, you should be aware that shear locking might occur. This possibly leads to inaccurate results for the shear forces. In general it is then advised to use quadrilateral shell elements rather than triangular elements. (de Witte 2007)*

These two remarks show that the shear locking effect is considered in the DIANA models. At the same time DIANA takes the shear deformations into account in its calculation, which should lead to more reliable results. This aspect will be tested in the next Paragraph. The facets in the dome are very slender and therefore have very low transverse shear stiffness. Transverse shear therefore plays a very minor role in the behaviour of the structure and it fulfils the criteria for the Love-Kirchhoff simplifications very well.

Shear locking is not so much a problem of convergence, but of slow convergence. Therefore it is a problem that can be very well tested by refining the finite element mesh. Figure 7.3 shows the deflection at a load factor of 3.65 for a mesh that is twice as fine as the previously used mesh. The difference with the results in the original mesh, see Figure 7.2 is not visible. Therefore the possible effects due to shear locking are not likely to be large.

NB the increase in calculation time for the finer mesh is so significant that the calculation was stopped at a load factor of 3.65.

7.2.2 Membrane locking

Membrane locking is again a typical finite element problem related to shell elements. The term refers to the inability of the shell finite elements to represent in-extensional deformation of the shell. Shells can generally bend without stretching, which is the so-called in-extensional deformation. The membrane stiffness of a shell is, on the other hand, very high. When the finite element does not have the ability to bend without stretching, the energy of the deformation will be incorrectly transferred to the membrane stiffness. This

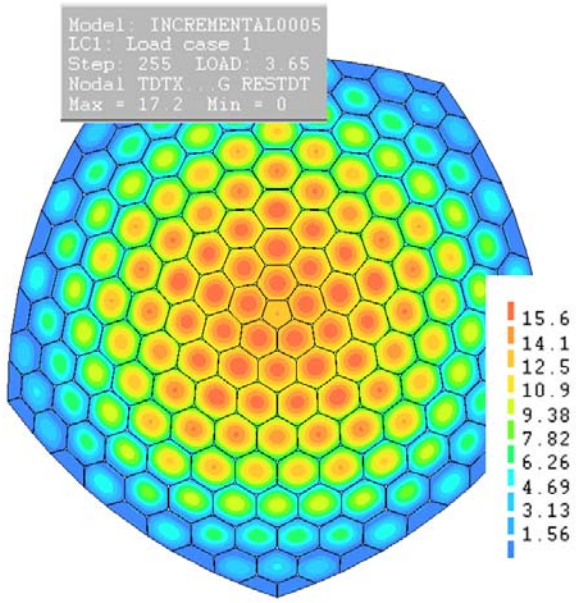

Figure 7.2: The results for the dome with the original mesh; max. deflection at $\lambda = 3.65$*:17.2mm.*

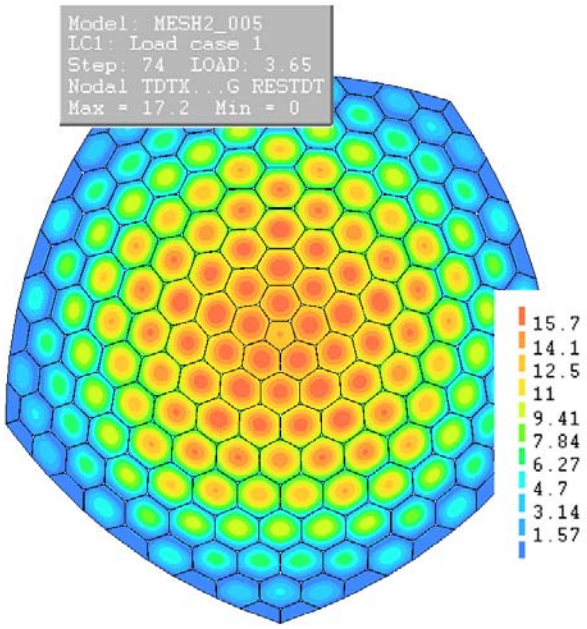

Figure 7.3: The results for the dome with a finer (2x) mesh; max. deflection at $\lambda = 3.65$*:17.2mm*

will lead to an under prediction of the stresses and deformations. In buckling analysis the membrane locking is an especially important phenomenon, since many buckling modes are (nearly) in-extensional.

To test the capability of Diana to take the in-extensional deformations into account, a large part of the supports of the shell is removed. Then small concentrated loads are placed on the now cantilevering dome. The result of removing the supports is that the shell will now no longer be sufficiently supported as a shell structure. In order to resist the forces, the dome will need to develop bending stresses in its thin skin, while membrane stresses hardly develop. This behaviour involves large deformation, the so-called in-extensional deformations.

Figure 7.4 shows the remaining supports of the dome and the locations where the dome is loaded by small concentrated forces. In total the vertical load is two times 6N. The deformed shape of the dome is visible in Figure 7.5. The shape already implies that the dome has developed bending stresses and this can be verified by checking the normal and bending stresses in the structure, see Figures 7.6 and 7.7. The diagrams show that the bending stresses are approximately a factor ten higher than the normal stresses in the structure. This leads to the conclusion that the model does develop inextensional deformations and that membrane locking will not be a large problem.

The considered facetted dome will always be sufficiently supported to retain shell action. Small differences in settlements or imperfections in the shell can, however, still lead to a limited influence of in-extensional deformations. It is shown that the model will take these deformations into account for a large part.

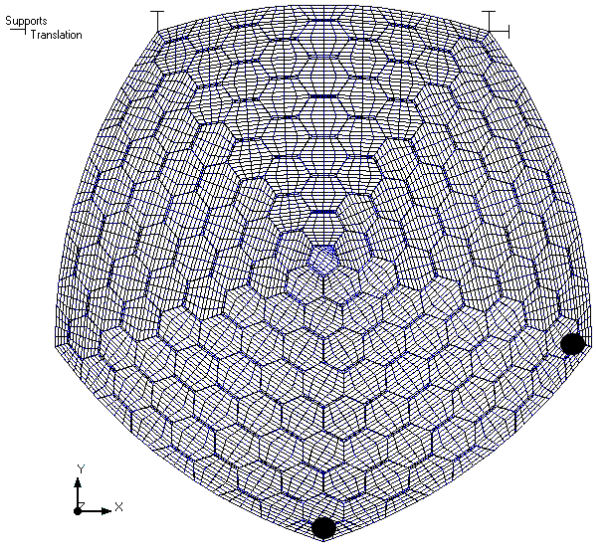

Figure 7.4: The dome with the remaining supports and the location of the concentrated loads (6N each).

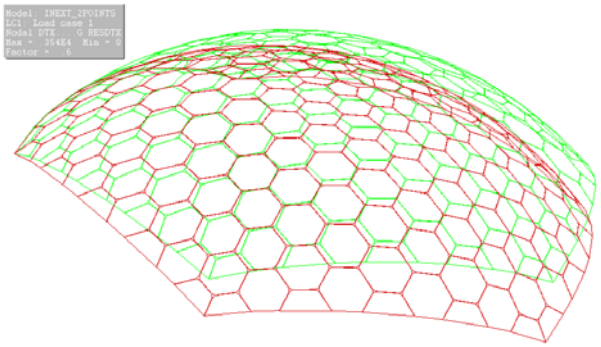

Figure 7.5: The deformed shape (red) of the dome with reduced support conditions.

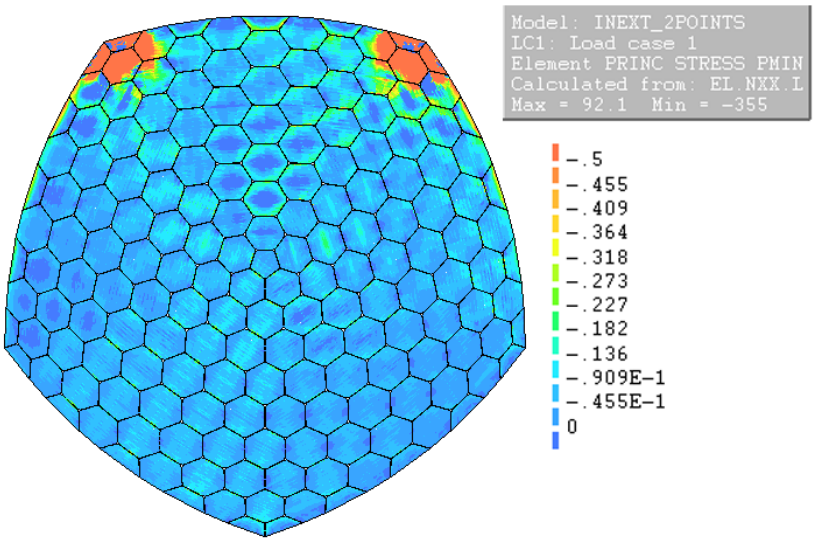

Figure 7.6: The compressive normal (membrane) stresses in the structure with reduced support conditions; only the range $0 \geq n_2 \leq -0.5$ *is shown to reduce the influence of the peaks around the supports on the diagram.*

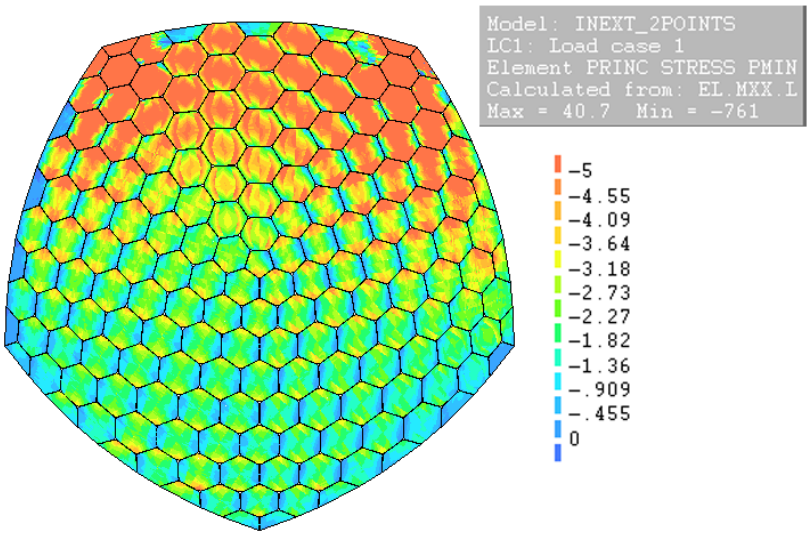

Figure 7.7: The negative bending stresses in the structure with reduced support conditions; only the range $0 \geq m_2 \leq -5$ *is shown to reduce the influence of the peaks around the supports on the diagram.*

7.3 Benchmark problems

Introduction

In the validation of finite element methods and their elements a large number of different benchmark tests have been developed over the years. For shell elements two simple tests are carried out in this paragraph. The first test, see Paragraph 7.3.1, is to see the behaviour of the elements in a shear loading condition. By loading a cantilever plate with a shear force on its outer edge the reaction of the elements to shear forces is tested. The results from the shear benchmark show that the elements react correctly in shear.

The second benchmark problem, see Paragraph 7.3.2, tests the bending behaviour of the elements. A cantilever plate is loaded by a bending moment at its outer edge which should finally result in a curled up shell. The results from the benchmark, however, show that the used shell elements in DIANA cannot reproduce this deformation path. The deformations remain correct until they become larger than approximately 50x the thickness of the plate. The influence of this deviation needs to be tested by using a different FEM program. At the same time it is plausible that the influence is fairly small, since the order of magnitude of the displacements in the dome is much smaller than 50x the thickness of the glass, see Chapters 8 and 10.

7.3.1 Benchmark problem 1: Cantilever loaded with end shear force

In their paper Sze et al. (Sze, Liu & Lo 2004) mention the benchmark problem of a cantilever loaded with a shear force at the tip, see Figure 7.8. This model is recreated in DIANA with the same characteristics. The Poisson's ratio (ν), however, has to be non-equal to zero and is therefore set to an extremely low value: $\nu = 1 * 10^{-6}$. For the DIANA model the CQ40S (8-node) shell elements are used.

The results from the calculation are shown in Table 7.3.1 and Figure 7.9. It is visible that DIANA has no difficulties recreating the solutions found by Sze et al. (Sze et al. 2004). The deviations between the results are maximally a couple of percent and the elements are therefore considered accurate.

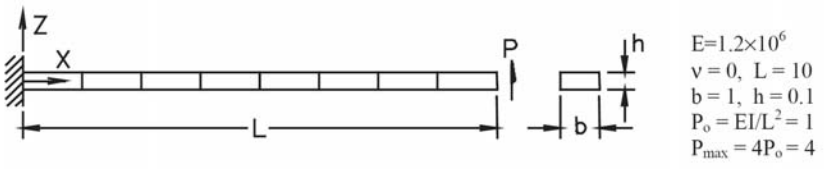

Figure 7.8: The benchmark model as used by Sze et al. (Sze et al. 2004)

Figure 7.9 shows the differences between DIANA and the exact solution in a graph.

Table 7.1: Horizontal and vertical tip deflection for the cantilever loaded with end shear force

	Example		DIANA	
P/P_{max}	δx	δz	δx	δz
0.05	0.026	0.633	0.026	0.663
0.10	0.103	1.309	0.103	1.31
0.15	0.224	1.992	0.223	1.92
0.20	0.381	2.493	0.376	2.48
0.25	0.563	3.015	0.555	3.00
0.30	0.763	3.488	0.75	3.46
0.35	0.971	3.912	0.955	3.89
0.40	1.184	4.292	1.16	4.26
0.45	1.396	4.637	1.37	4.60
0.50	1.604	4.933	1.58	4.9
0.55	1.807	5.202	1.78	5.17
0.60	2.002	5.444	1.97	5.42
0.65	2.190	5.660	2.16	5.63
0.70	2.370	5.855	2.34	5.83
0.75	2.541	6.031	2.51	6.01
0.80	2.705	6.190	2.67	6.17
0.85	2.861	6.335	2.83	6.32
0.90	3.010	6.467	2.98	6.45
0.95	3.151	6.588	3.12	6.57
1.00	3.286	6.698	3.26	6.68

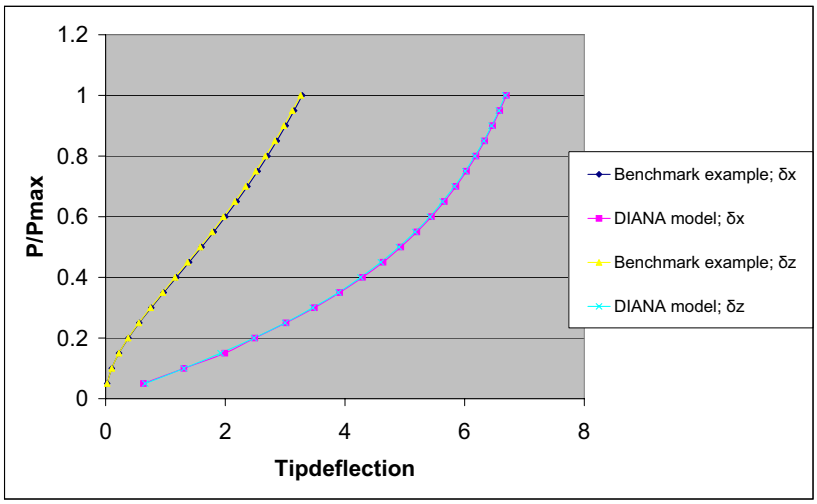

Figure 7.9: The differences between DIANA and the exact solution for the shear benchmark

7.3.2 Benchmark problem 2: cantilever loaded by an end bending moment

The second benchmark problem that is used in this research is a cantilever loaded by a bending moment at the tip. The problem is again taken from (Sze et al. 2004) and is shown in Figure 7.10. The model is recreated in DIANA using the CQ40S (8-node) shell elements.

The results from the calculation are shown in Table 7.3.2 and Figure 7.11. It is visible that DIANA has trouble with recreating the solution found by Sze et al. As long as the deflections are fairly small the model is quite accurate, but when the deflections become larger than 5mm the results start deviating strongly. The magnitude of the deflections is at that time approximately 50x the thickness of the glass. After a load of 0.25 times the initial load the solution starts to diverge and DIANA is unable to find a solution any longer. In the paper by Sze et al. (Sze et al. 2004) the final solution leads to a curled up structure when the load reaches the maximum, see Figure 7.12. This leads to the conclusion that DIANA does not fulfil this bending benchmark.

The implications for the model of the facetted shell are, however, expected to be small. The maximum displacements when the shell starts buckling are in the order of magnitude of 2-3 times the thickness of the glass. The bending model only starts deviating from the benchmark when the vertical displacements become larger than approximately 50x the thickness. The large difference between these displacements makes it plausible that the results yielded by DIANA can be trusted.

The difference likely arises from the fact that DIANA neglects part of the solution for the shell elements by linearisation of the solution. This approximation is based on the Kirchhoff-Love shell theory which is only valid when deformations are small and the elements can be considered thin. This behaviour is also seen in the results in for the benchmark problem; when deflections are relatively small the solutions are the same. As the deflections become very large and the plate is supposed to curl, DIANA has much trouble to follow the right deformation path.

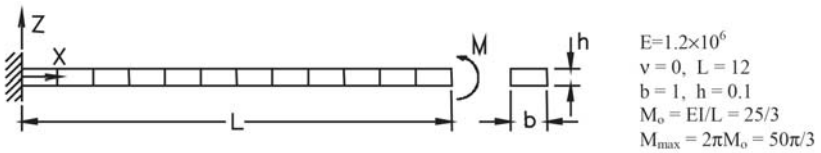

Figure 7.10: The benchmark model as used by Sze et al. (Sze et al. 2004)

Figure 7.11 shows the differences between DIANA and the exact solution in a graph.

Table 7.2: Horizontal and vertical tip deflection for the cantilever loaded with end bending moment

	Exact		DIANA	
M/M_{max}	δx	δz	δx	δz
0.05	0.196	1.870	0.189	1.84
0.10	0.774	3.648	0.793	3.71
0.15	1.699	5.248	1.72	5.32
0.20	2.918	6.598	3.33	7.04
0.25	4.361	7.639	6.48	8.84
0.30	5.945	8.338	*no convergence*	

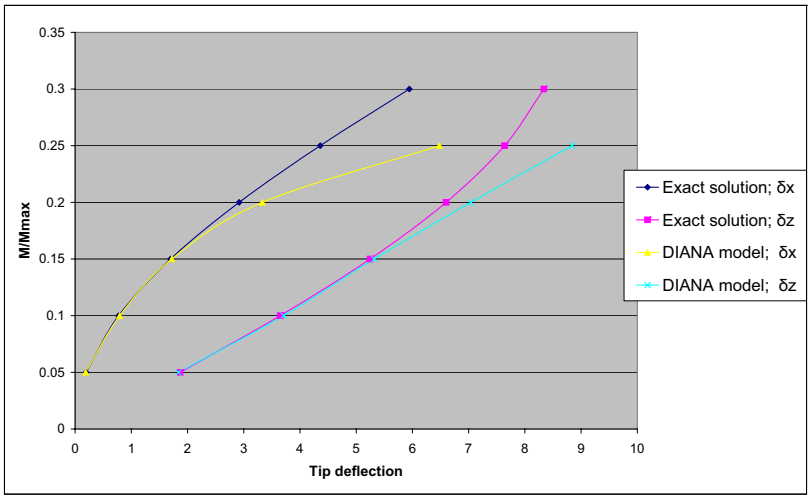

Figure 7.11: The differences between DIANA and the exact solution for the bending benchmark

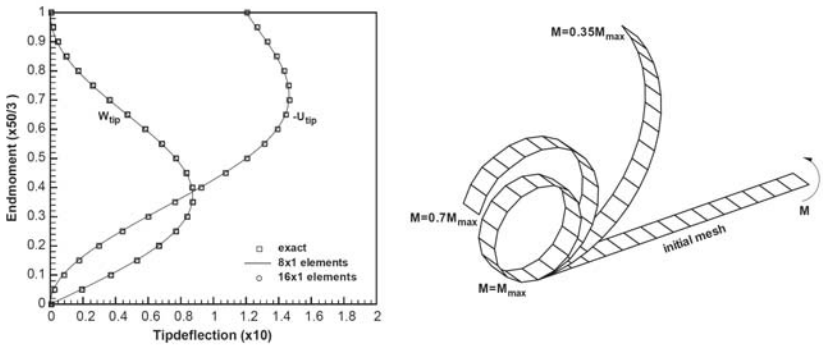

Figure 7.12: The deformation and tip deflections found by Sze et al. (Sze et al. 2004)

7.4 Discussion

From the results of the mesh refinement test, see Paragraph 7.2.1, it can be concluded that the elements that are used in DIANA do not have large problems with shear locking. The shear benchmark test also confirms this and shows that the expected deformation path is also found by DIANA. This leads to the conclusion that shear locking is at least not significant in the current mesh and model.

When the shell is sufficiently supported, in-extensional deformations are not an important factor. A test where a large part of the supports were removed showed that bending stresses do develop in the shell and that small loads result in very large deformations. The shell therefore is in-extensionally deformed. The in-extensional deformations are therefore taken into account, but it is not clear if the in-extensional deformations are fully developed. For sufficiently supported shell conditions the model can be considered valid since the in-extensional deformations are of minor importance. However, local buckling can still be an inextensional mechanism, so some reservation should be pertained. A confirmation of the results by a different FEM-programme will remain important.

Calculations to estimate the error made in the model by neglecting the non-linear terms in the shell equations, see Paragraph 7.1, have shown that the error in the strains is very small. Even though the shell deflects more than twice its thickness, the large span to thickness ratio is the likely cause that the non-linear terms remain small and can be neglected. The bending benchmark test showed the true influence of neglecting the non-linear terms of the solution. The DIANA model could not follow the true deformation path which is not surprising since it is largely created by the non-linear terms in the shell solution. The deviations only start, however, when the deformations become larger than approximately 50x the thickness of the plate. The deformations when the shell buckles in the model are only in the order of 2-3x the thickness of the shell. It is therefore plausible that the problems are not significant for this model.

In this Chapter known problems related to finite element methods have been investigated and their influence has been estimated. It has been made reasonable that the model of the facetted shell is valid for the current load conditions and geometry. To be absolutely sure, however, it will be necessary to test the facetted shell also in a different finite element program. Shell buckling is a sensitive phenomenon and there might be unexpected effects in the behaviour of the dome.

Chapter 8

Non-linear analysis

Introduction

For more insight in the buckling behaviour of the dome it is necessary to perform a geometrically non-linear (buckling) analysis of the dome. The relation between a force vector and displacement vector will no longer be linear, which is for instance the case in plastic behaviour. Since buckling refers to large displacements and deformations, plastic behaviour is inherent to the mechanism. In a nonlinear analysis the load will be stepwise increased to find the first load in which buckling will occur. By adjusting the deflections in each step and taking into account their influence on the next step, the calculation will be more precise than a pure linear analysis. The result will be a lower bound solution for the buckling factor.

8.1 Nonlinear analysis in Diana

In Diana a so-called 'incremental-iterative' procedure is used. The incremental procedure refers to the stepwise increasing of the load. Every step the deformations are calculated and the result is used to define the loads for the next step. This way the dependency of the loads on the deformations is taken into account. However, an incremental procedure results in inaccurate solutions for the nonlinear analysis, unless the step size is chosen very small. Therefore an iterative process is introduced, which reduces the errors significantly. The result is an implicit procedure where the step size can be much larger than in the explicit procedure (without iterations). The basic iteration procedure is shown in Figure 8.1. The extra step that is taken is the determination of the displacement increment Δu by iterative increments δu until an equilibrium, with a prescribed tolerance, is reached between the internal and external loads. (de Witte 2007)

For the iteration a number of different iteration schemes can be chosen. The result

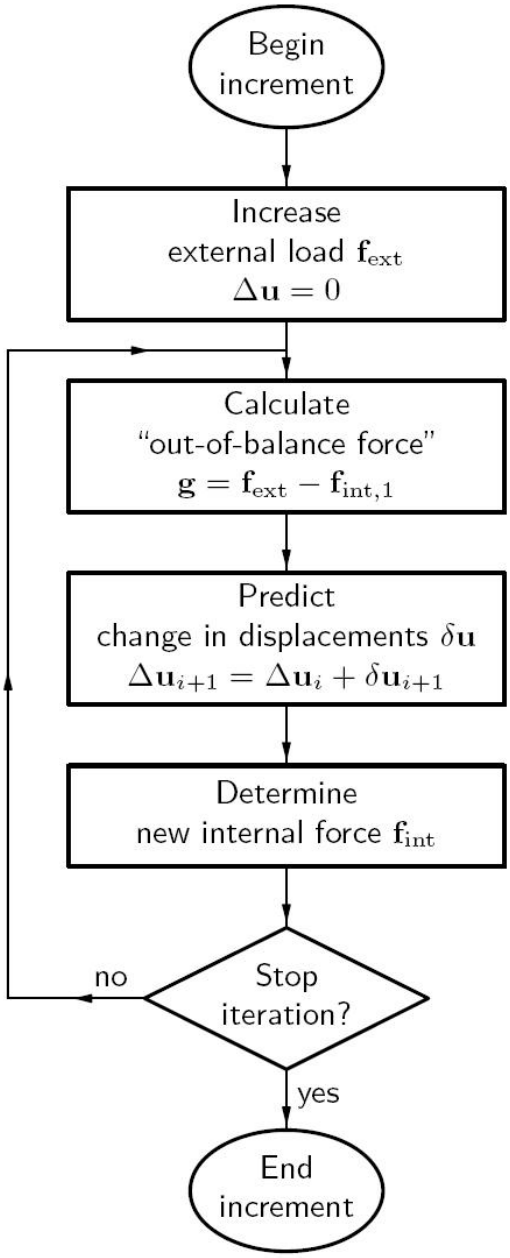

Figure 8.1: The iteration procedure followed by Diana in a incremental-iterative procedure.

of all iteration schemes, however, is the same. The only difference lies in the speed of convergence.

In Diana there are three different iteration schemes are available, Newton Raphson, Quasi-Newton and Constant Stiffness method. There are also variations of these methods available by combining them with either a line search or continuation method. In this

research the Newton-Raphson method will be used.

Newton-Raphson method; the has two subclasses, the regular and the modified Newton-Raphson method. Both methods use a direct approach to determine the displacement increment δu using a stiffness matrix K, see Equation 8.1. This stiffness matrix is the linearised form of the relation between the force vector and the displacement vector.

$$\delta u_i = K_i^{-1} g_i \tag{8.1}$$

g_i in this Equation refers to the out-of-balance vector at the start of iteration i.

In the Newton-Raphson method the stiffness matrix K_i represents the tangential stiffness of the structure:

$$K_i = \frac{\theta g}{\theta \Delta u} \tag{8.2}$$

The regular Newton-Raphson method determines the stiffness matrix every time at every iteration. The prediction of the displacement increment is therefore always based on the last known or predicted situation. This is shown in Figure 8.2.

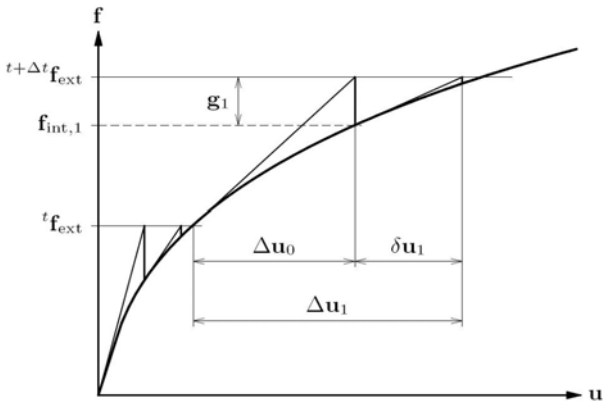

Figure 8.2: Iterations in the regular Newton-Raphson method.

.

This means that every iteration in the Newton-Raphson method is very time consuming, because of the decomposition of the matrix. The number of necessary iteration is relatively low, however.
The Modified Newton-Raphson method, Figure 8.3 only calculates the stiffness matrix at the start of each increment. This means that the iterations will be much quicker than in the Regular Newton-Raphson method. The number of necessary iterations, however is higher. An advantage of the Modified Newton-Raphson method is that it can sometimes

still converge where the Regular method does not converge anymore. The reason for this is the use of the relatively smaller iteration steps.

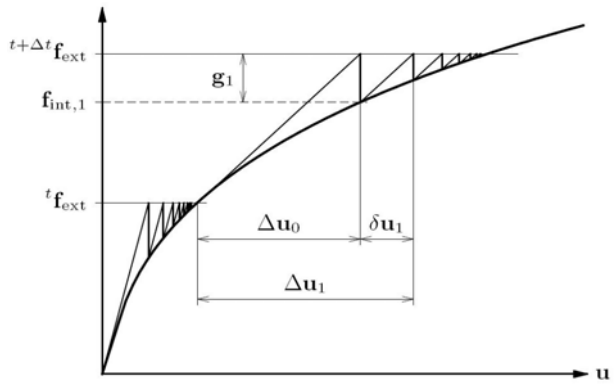

Figure 8.3: Iterations in the Modified Newton-Raphson method.

.

8.2 Results of the non-linear analysis

Analyzing the dome with a stepped load leads to a surprising result: the buckling load that the dome can resist is higher than the buckling load following from the linear analysis. Usually in shell analysis the linear calculation provides a lower bound solution.

Figure 8.4 shows the results of the first analysis with a step size of 0,5*total load. This total load is, as was done in the linear calculation, the combination of the self weight and the snow load on the structure including safety factors. This means that the resulting buckling factor can again be considered as an additional safety factor on the buckling behaviour.

The buckling factor that is found in the first calculation is 6,5. This is almost two-and-a-half times the factor found in the linear analysis ($\lambda_{linear} \approx 2,8$).

In Figure 8.4 it is very hard to see any discrepancies in the deformation. There is no real buckling shape visible; only the normal deformed shape due to a vertical load is visible. A likely cause is that the total deformations due to the vertical load are much larger than the deformations caused by the buckling effect.

A way to get insight in the behaviour of the dome at the buckling point is to make a plot of the deformations vs. the load factor in a buckling location. However, since all facets are very much alike it is hard to define which location is actually decisive. A good indication is the node with the maximum displacement, which can be found by Diana. The location of this node is made visible in Figure 8.5.

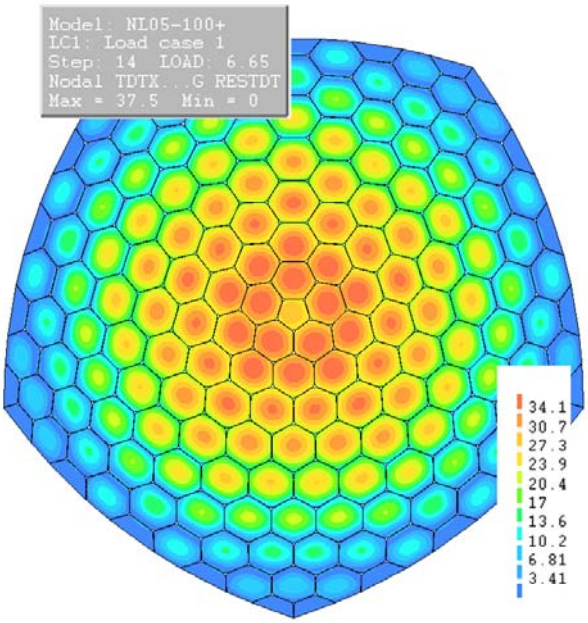

Figure 8.4: The result of the non-linear calculation with step size 0,5; the buckling pattern is not visible due to the large step size.

.

Figure 8.6 shows the displacement of this node against the load factor. It is visible that the step size is too large to find the expected flattening of the graph at the buckling point. It can even be seen that the deformations are still almost radial symmetric, since the same result can also be found for other nodes. A smaller step size will therefore be chosen to see if the buckling point can be defined with more accuracy.

8.2.1 Small step size

Since the flattening point of the graph is difficult to define a very small load step size of 0,005 is chosen. This load step does lead to the desired result which is shown in Figure 8.7. The graph flattens at a total load factor of 6.64 and the result is now slightly different from the result in symmetry nodes, see for instance node 6359 in Figure 8.8. This node is the radial symmetry node located clockwise one-fifth further on the dome.

This result shows that a definitive failure point is found. It should be noted, though, that for the perfect geometry that has been analyzed now the failure does not necessarily take place at node 11462. Due to the symmetry the failure can just as well take place in any of the five symmetry points. The node depends on small deviations in the calculation and solving of the matrices in the FE-program.

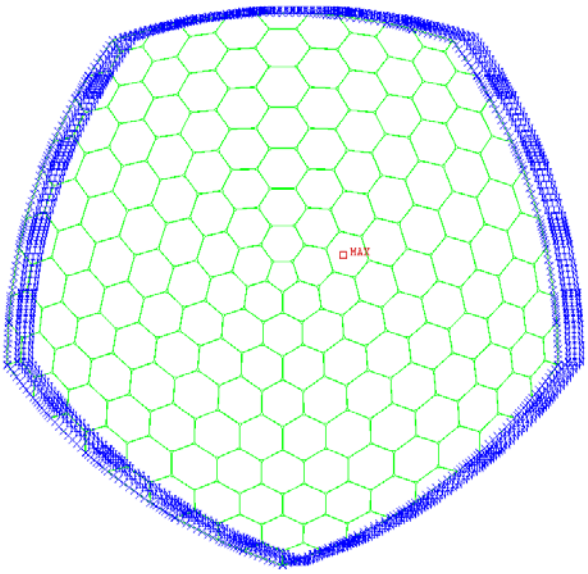

Figure 8.5: The location of the node with the maximum deflection (node 11462).

.

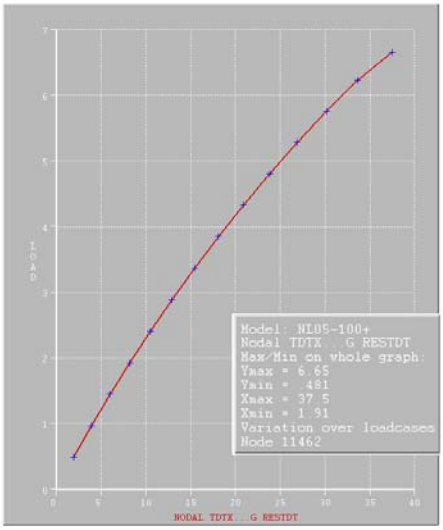

Figure 8.6: The displacement of node 11462 vs. the load factor; step size 0,5.

.

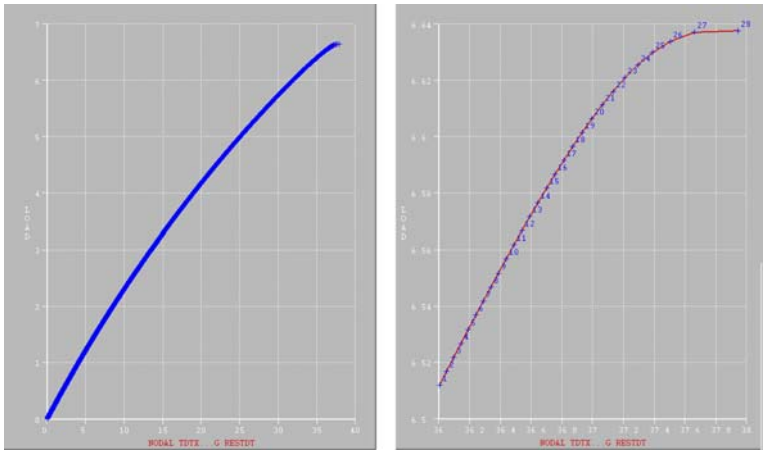

Figure 8.7: The displacement of node 11462 vs. the load factor; right is a detail of the top of the graph; step size 0,005.

.

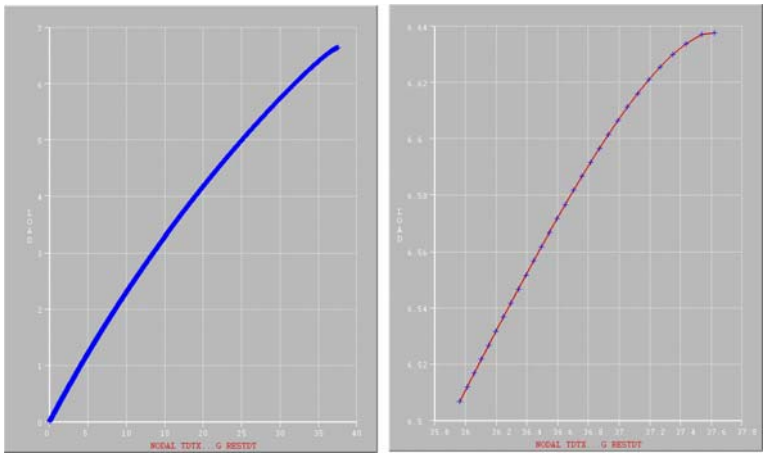

Figure 8.8: The displacement of node 6359 vs. the load factor; right is a detail of the top of the graph; step size 0,005.

.

8.3 Shape of the buckling mode

As mentioned in the previous Paragraph, the shape of the buckling is very difficult to distinguish due to the accumulative overall deformations. When the incremental deformations are plotted, however, the buckling shape can be made visible. In Figures 8.9 to 8.13 a number of incremental deformed shapes are given. When viewing these Figures it is especially important to note the magnitude of the load step in combination with the resulting incremental deformations. In the Figure 8.9, which is at 96,2% of the buckling load, there is hardly any asymmetric deformation visible. Figure 8.10 still shows a large influence of the incremental load (≈ 0.005)over the entire dome. The order of magnitude of the deformation is the same. The deformations tend to become more and more asymmetric and in the last three steps the order of magnitude of the deformation starts rising. Figure 8.13 is the final step and shows large deformations ($u_{max} = 0.142mm$) with a very small incremental load ($\Delta\lambda = \frac{6.64-6.62}{5} = 0.004$). This in combination with the fact that there is no longer any influence of this incremental load on the deformations outside the buckling shape shows that the buckling shape has actually been found.

NB all deformations in the Figures 8.9 to 8.13 are absolute displacements.

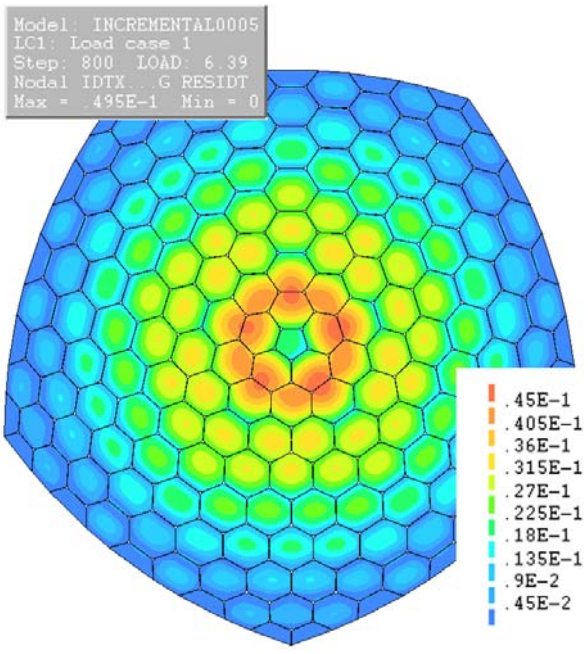

Figure 8.9: Incremental displacements step 800 (≈96,2%); $\Delta\lambda \approx 0.005$ $\delta u_{max} = 0.0495mm$.

.

Figure 8.14 shows the deformed shape of the incremental load step 850. It is visible that the facets start rotating and that the deformation are especially large in the connec-

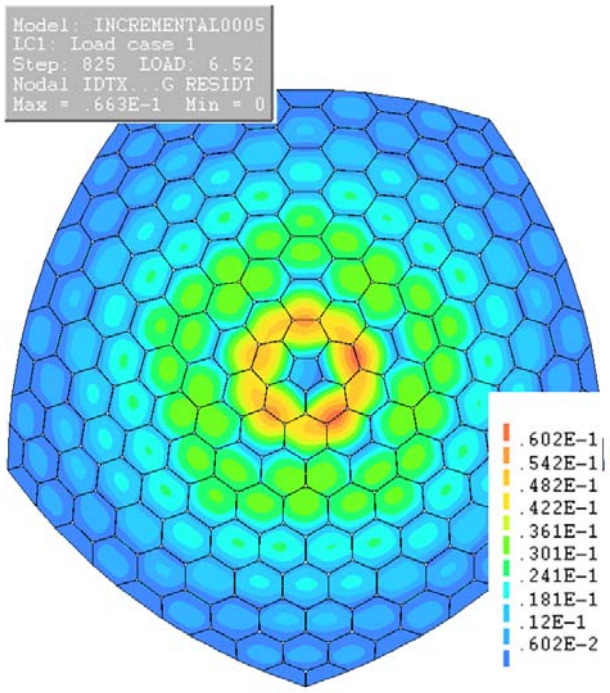

Figure 8.10: Incremental displacements step 825 (≈98,1%); $\Delta\lambda \approx 0.005$ $\delta u_{max} = 0.0663mm.$

.

tions. The buckling is caused by the fact that the fairly flexible connections can not resist the loads any longer.

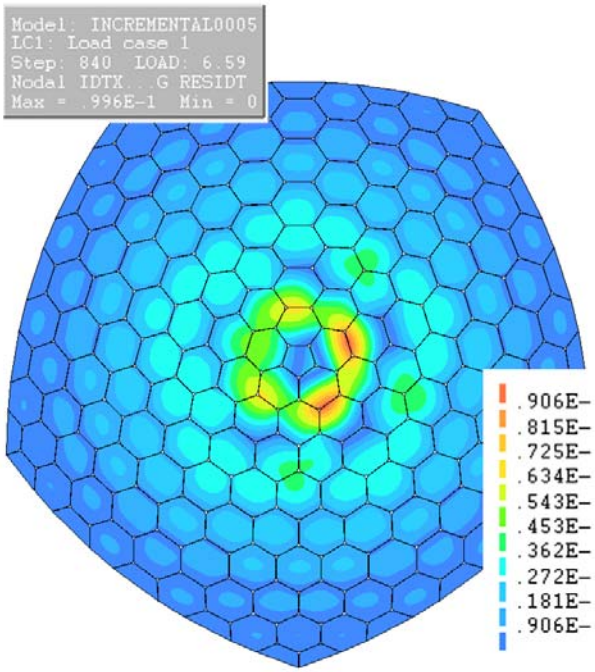

Figure 8.11: Incremental displacements step 840 (≈99,2%); $\Delta\lambda \approx 0.005$ $\delta u_{max} = 0.0996mm.$

.

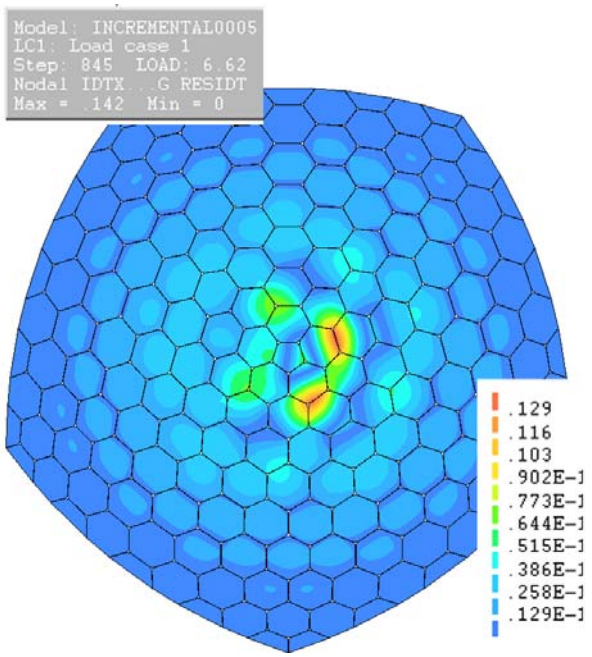

Figure 8.12: Incremental displacements step 845 (≈99,7%); $\Delta\lambda \approx 0.005$ $\delta u_{max} = 0.142.$

.

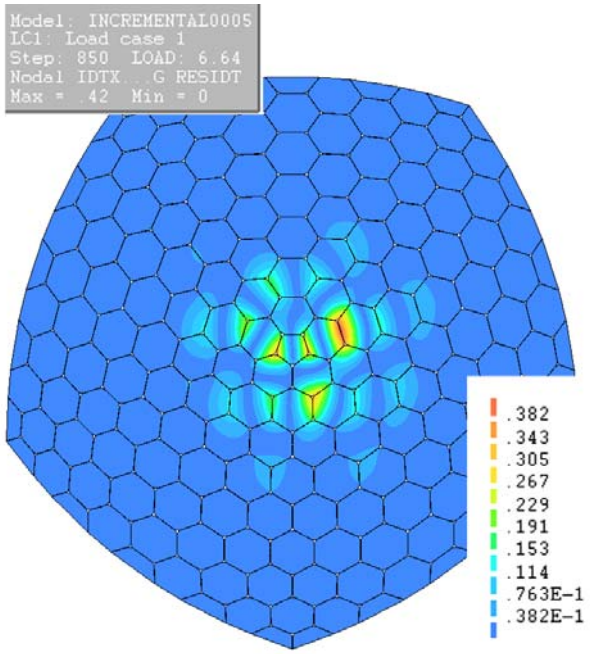

Figure 8.13: Incremental displacements step 850 (100%); $\Delta\lambda \approx 0.004$ $\delta u_{max} = 0.42$.

.

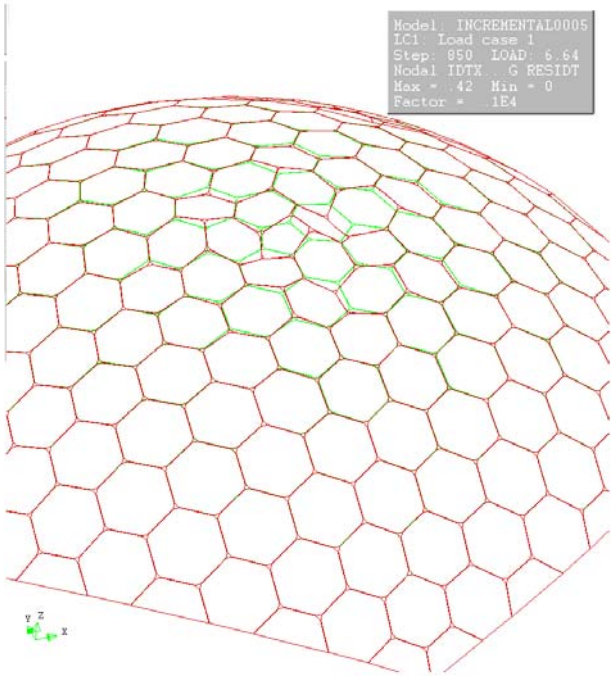

Figure 8.14: The deformed shape (red) at buckling of the dome structure.

.

8.4 Checking the stresses in the dome at buckling

Due to the large deformations in the dome, it might no longer be true that the dome can cope with the introduced stresses. To have a safe stress criterion, the Rankine criterion is used which requires that the stress in every principle direction is not larger than the maximum allowable stress. The Rankine criterion is often used for brittle materials. For glass it is important to note that the compressive stress is not taken into account since glass usually does not fail due to compressive stresses. Either the tensile stress or instability is the reason for failure. Furthermore, only two main directions are taken into account since the material is very thin and no large shear stresses are present. There will only be local shear stress concentrations at a small number of joints, but these have no influence on the buckling behaviour of the structure. Figure 8.15 shows the principle stresses in the dome at the bottom side of the elements. Figure 8.16 shows the 2-dimensional principle stresses at the top side of the elements.

It is visible that the largest tensile stresses can be found at the centres of the facets, which can be easily explained by the bending of the facets. The tensile stresses at the top side of the elements do not reach the values that are found at the bottom side and are therefore disregarded. The maximum tensile stress that can be taken up by the glass is approximately $66N/mm^2$, since a combination of self weight and semi-long term load is considered (see Paragraph A.5). The resulting test is therefore as follows:

$$\begin{array}{l} \frac{\sigma_1}{f_{m,t,u,d}} \leq 1 \\ \frac{52N/mm^2}{66N/mm^2} = 0.79 \end{array} \tag{8.3}$$

The glass will therefore not yet break at the strains caused by the buckling load until the structure fails due to buckling. The buckling factor for the perfect geometry is, with the current material and geometry specifications, therefore equal to the value from the non-linear analysis: $\lambda = 6,64$.

8.5 Discussion

The most interesting first result of the non-linear calculation is that the buckling factor is higher than the one found in the linear calculation. With smooth spherical shell structures this would not be the case; the non-linear calculation will actually yield much lower results, (Samuelson & Eggwertz 1992). This effect is a result of the very high sensitivity to imperfections of a spherical shell. A perfect geometry would yield the same result for the smooth shell. Since the facetted glass dome has a structural behaviour that is, in very crude perspective, quite similar to that of a spherical shell, it was expected that

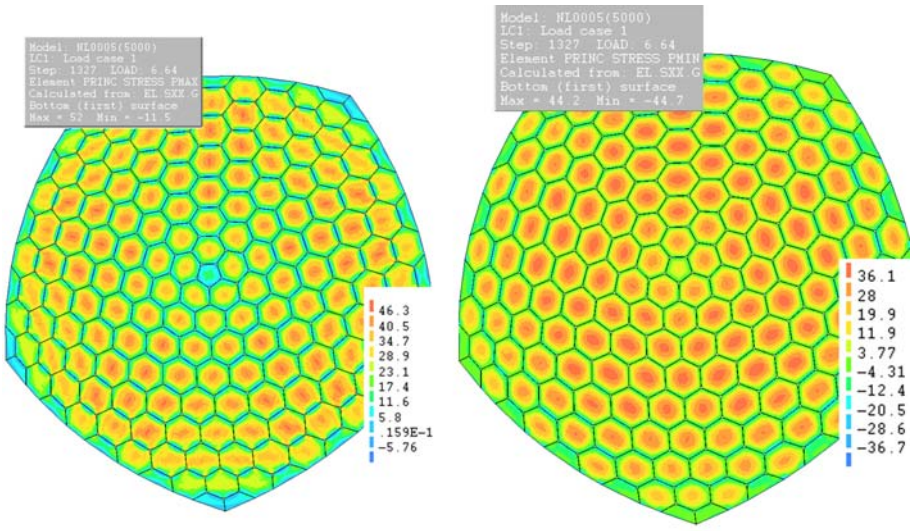

Figure 8.15: The 2-dimensional principle stresses at the bottom side of the elements.

.

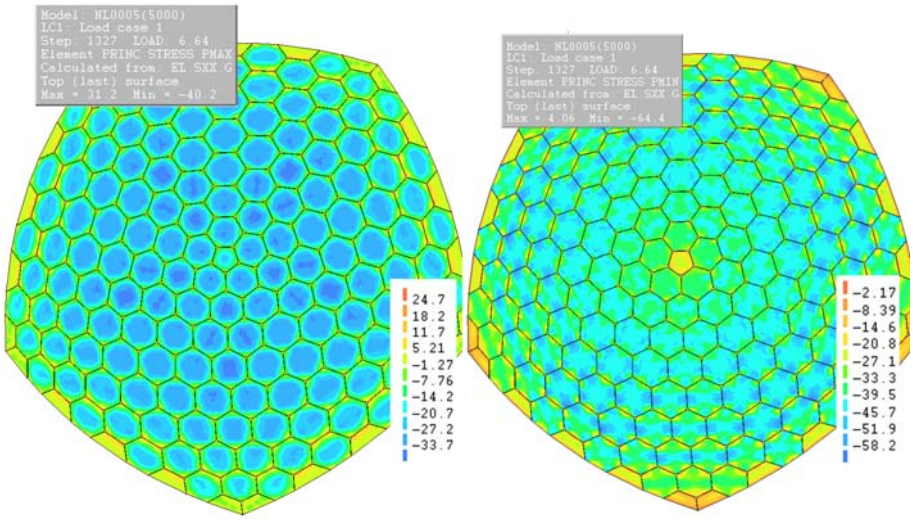

Figure 8.16: The 2-dimensional principle stresses at the top side of the elements.

.

the non-linear calculation would yield the same or a lower buckling factor than the linear analysis.

The increased buckling resistance can be explained by the post-buckling behaviour of single facets. The linear calculation showed that the first buckling modes of the dome are highly dependent on the buckling of single facets. This means that the non-linear behaviour of single plates will probably also highly influence the buckling behaviour of the

full dome. The single facets are investigated in Chapter 9. The results from this analysis indeed show a post-buckling path where aditional load can be carried without failure of the facet. If this behaviour is projected to the facets in the dome, it explains the fact that the buckling factor is significantly higher than the linear calculation revealed.

The effect of imperfections on the non-linear buckling behaviour of the dome will be investigated in Chapter 10. Chapter 9 looks into the post-buckling behaviour of a single facet and the related redistribution of stresses within a single facet.

Chapter 9

Buckling behaviour of a single plate

Introduction

The non-linear analysis of the full dome results in a higher buckling value than the one found in the linear (elastic) calculation. The first buckling modes of the linear calculation, see Chapter 6, were all to a great extent influenced by the buckling of facets independently. This leads to the suspicion that a second order stiffening effect takes place in the facets after linear buckling. By investigating the buckling behaviour of a single facet more insight will be gained in the effects that arise in the facet after buckling. It is the hypothesis that a stiffening effect occurs by redistribution of the forces to the outside of the plate.

The investigation is started in Paragraph 9.1 with a linear elastic analysis of the behaviour of the facet. This is both interesting to gain more insight as well as to validate the model. The non-linear analysis is described in Paragraph 9.2.

The results of the analyses show that there is indeed a second-order stiffening effect in the facets. Due to their shape and supports there is an in-plane redistribtution of forces possible. The facets redistribute the forces away from the centre of the plate and start acting like stiff frames. This results in a higher failure load than according to the elastic theory.

9.1 Linear elastic buckling of a single plate

For the analysis of the single plate a model will be made resembling a simply supported plate. The support conditions need to represent the rotational joint stiffness; however, since the stiffness of the joint is low compared to the stiffness of the plates, free rotation will be a good first estimation. There will be two loads on the plate; first the plate will be loaded in plane to represent the membrane forces resulting from the shell behaviour of the dome. Secondly the out of plane load due to dead weight and snow will be applied.

9.1.1 Only in plane forces

For the simply supported hexagonal plate an equation can be derived for the theoretical in-plane buckling load. In this case a hexagonal plate with a diameter of 1500mm will be considered. This diameter is approximately the same as the average facet in the dome. The following Equation is taken from (Young & Budynas 2001) (see also Figure 9.1):

$$\sigma' = K\frac{Et^2}{a^2(1-\nu^2)} \tag{9.1}$$

Where,

- σ' =critical unit compressive stress;
- $K = 0,597$ for a hexagonal plate;
- $E =$ Young's modulus $= 70 * 10^3 MPa$;
- $t =$ thickness of the plate $= 16mm$;
- $a =$ length of a side $\approx 750mm$;
- $\nu =$ Poisson's Ratio $= 0.2$;

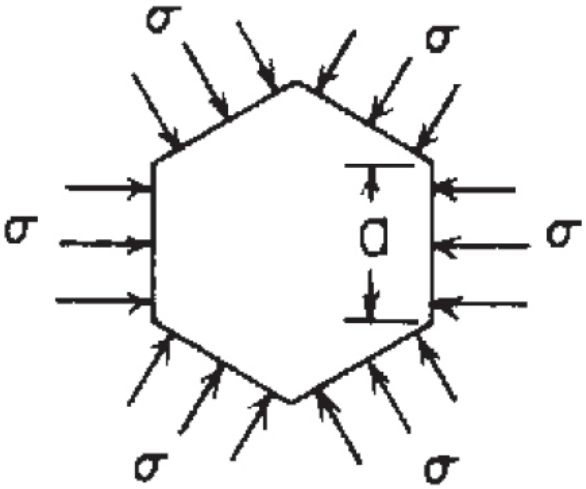

Figure 9.1: Scheme of a polygon plate under uniform compression on all edges, from (Young & Budynas 2001).

This leads to a theoretical buckling load of $\sigma' \approx 19,8 N/mm^2$.

In DIANA a similar model will be created and calculated. The model will be a glass hexagonal which is supported vertically along all edges, letting all rotations free. Since the loads are applied on the edges of the plate, see also Figure 9.1, it will not be possible to horizontally support the plate along the edges. Otherwise the forces would not be introduced into the plate, but will be transferred immediately to the supports. The plate will therefore be fixed horizontally in two points as is shown in Figure 9.2. One point will be fixed in x- AND y-direction; the other is used to prevent rotation and is only supported in y-direction.

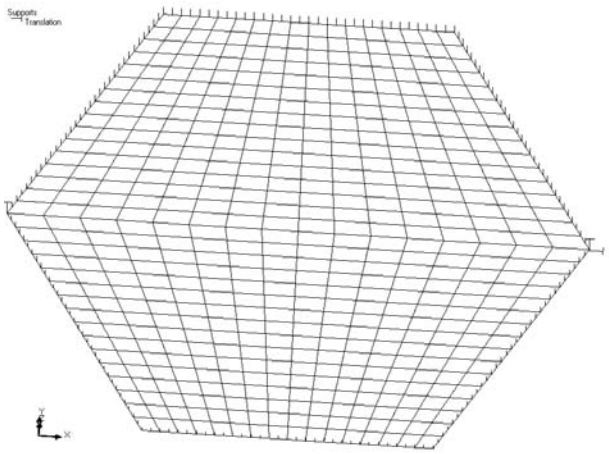

Figure 9.2: Support conditions of the facet.

The loads are all applied perpendicular to the edges of the glass facet. For the edges under an angle with the main axes the load is replaced by two forces parallel to the axis which represent the same resulting force perpendicular to the edge. The desired load on every edge is $1N/mm^2 = 16N/mm$ (t=16mm). For the edges under an angle with the axes this means $\sigma_x = +/-8N/mm$ and $\sigma_y = +/-13,86N/mm$ (the angle with the x-axis is 60^o). For the loading scheme see Figure 9.3.

The result of this calculation is elastic buckling factor of 19,1. This result is reasonably close to the theoretical result to accept it as a fair model. The difference in the result is likely to be caused by the slightly different support conditions. Stresses will concentrate locally around the support, but the overall stress distribution is still uniform and in accordance with the theoretical plate loaded on all edges.

9.1.2 In-plane and out-of-plane forces

By introducing out-of-plane forces to the plate, the theoretical first order linear buckling load does not change since only the normal stresses are considered. However, a second

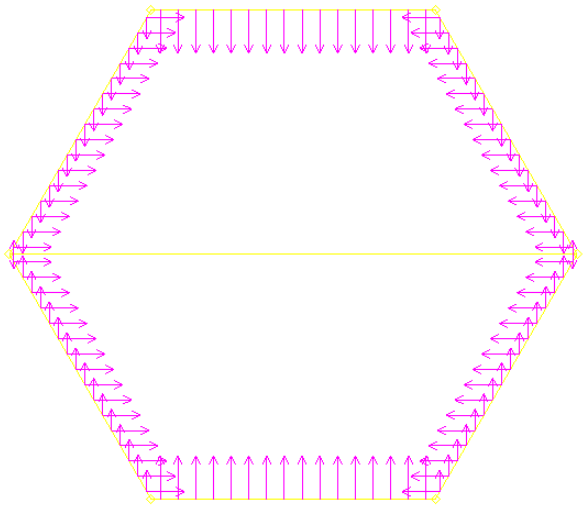

Figure 9.3: The in-plane loads applied to the plate

order calculation, taking into account the initial deformation caused by the out-of-plane loads, will result in a much lower buckling factor. As an out-of-plane load the same loads as applied to the dome are considered: the self weight of the structure and a snow load. Referring to Appendix D, this results in a total load of: $1,44 * 10^{-3} N/mm^2$ (snow, sector 1) $+0,433 * 10^{-3} N/mm^2$ (self weight) $\approx 1,87 * 10^{-3} N/mm^2$.

The result of the linear calculation is mostly interesting because it shows the effect of incorporating the second order effect from the out-of-plane loads. The result is that the elastic buckling factor drops from 19,1 to 7,7.

9.2 Non-linear analysis of a single plate

To be able to see if a stiffening effect arises in the plate, it is necessary to do a non-linear analysis. The same model for the plate will be used and it will be loaded by both in-plane and out-of-plane forces. The results are shown in Figure 9.4 to 9.6.It is shown that there is a transformation from fairly uniformly distributed stresses to a concentration of higher stresses along the edges of the plate.

It is difficult to see the influence because there are stress concentrations in the corners of the facets. To reduce these stress concentrations the vertical support will be turned into a spring support with a high stiffness. Making the infinite stiffness finite will lead to a great reduction in the stress concentration (McGee et al. 2005) and because the spring stiffness will be chosen very high ($\approx 1 * 10^3 N/mm^2$) the influence on the overall behaviour of the facet is negligible. This results in Figures 9.7 to 9.9. Be careful to note the scale

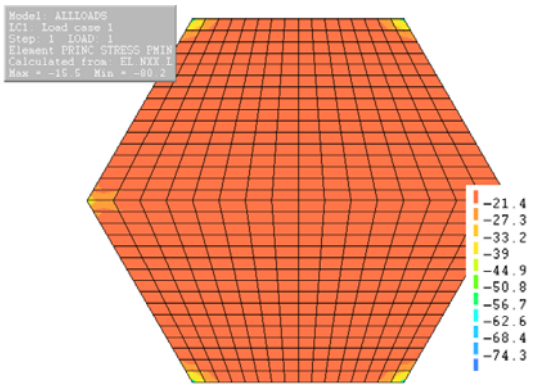

Figure 9.4: The normal stresses (N/mm) in the facet at load factor $\lambda = 1$.

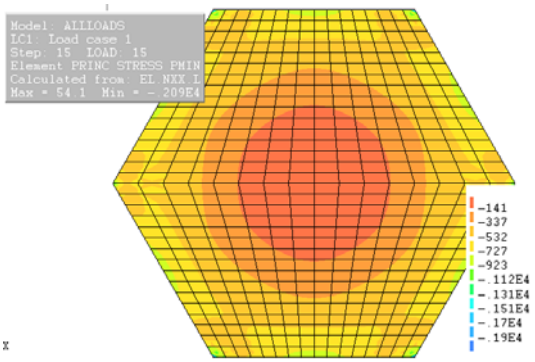

Figure 9.5: The normal stresses (N/mm) in the facet at load factor $\lambda = 15$.

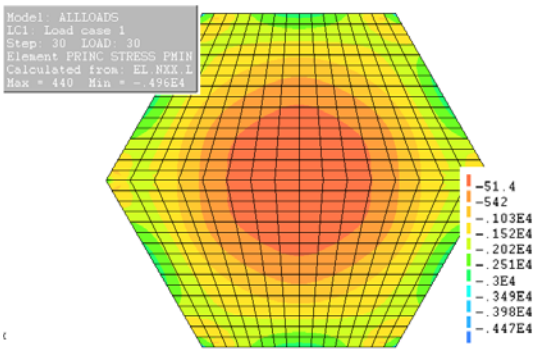

Figure 9.6: The normal stresses (N/mm) in the facet at load factor $\lambda = 30$.

division at the bottom right of each Figure.

The calculations on the model do not diverge when using thirty steps of 1 times the load. This means that no buckling of the plate appears to take place before applying more

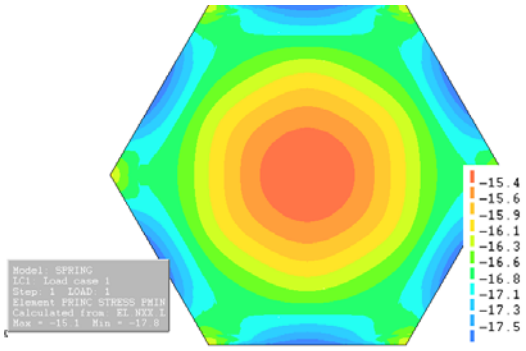

Figure 9.7: The normal stresses (N/mm) in the facet supported by springs at load factor $\lambda = 1$.

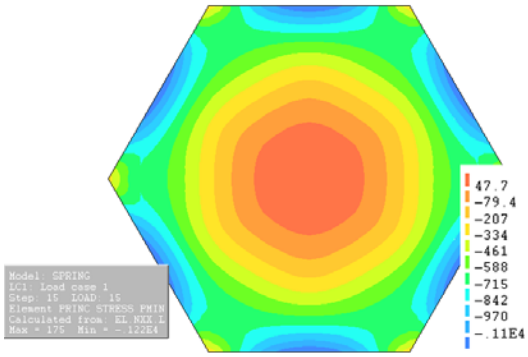

Figure 9.8: The normal stresses (N/mm) in the facet supported by springs at load factor $\lambda = 15$.

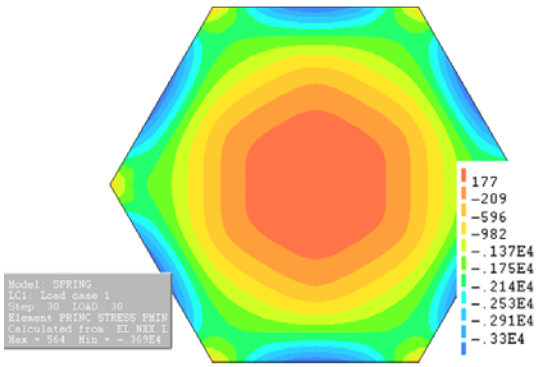

Figure 9.9: The normal stresses (N/mm) in the facet supported by springs at load factor $\lambda = 30$.

than 30 times the load. This is a big difference with the linear elastic calculation, where the results showed buckling of the panel at approximately 8 times the load, see Paragraph

9.1.2.

The reason for this result lies in the effects that take place inside the panel. Since the panel is statically undetermined, it can redistribute its internal stresses to other places within the system. In this case this means that for the in-plane normal forces the plate starts acting like a hexagonal frame with stiff corners. This can be illustrated very well by some of the 'plate' structures designed by Ture Wester, see for instance Figure 9.10. The deflections and stresses in the centre of the plate will therefore no longer increase due to the in-plane normal forces. The centre of the panel will, however, have a decreased resistance against deflection after the forming of the stiff frame. Therefore the out-of-plane load will cause an increasing deflection of the centre of the panel.

At the same time the stiffness will be increased in the panel as the deflections increase due to the membrane stiffness of the panel. This is very well visible in Figure 9.11. In this Figure the curve representing solely the out-of-plane load becomes steeper, revealing a stiffening effect. The second curve, representing a combination of in- and out-of-plane loads, the 'struggle' between the two effects is visible and the curve changes curature direction two times.

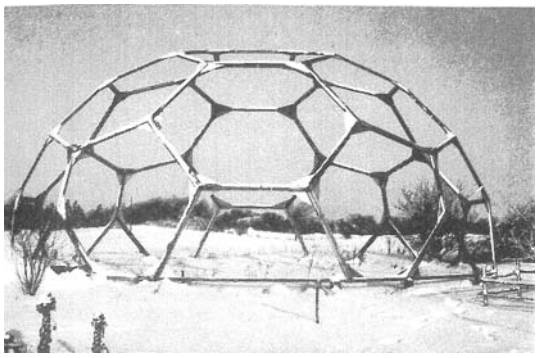

Figure 9.10: A plate structure built up from stiff hexagonal frames (Wester 1990)

In Figure 9.11 it is visible that the direction of the curve seems to shift around a load factor of 7,5. Interestingly, the linear elastic buckling factor that was found for the combination of in- and out-of-plane loading was 7,7. Therefore this area of the load factor could be the location where stiffening occurs for the first time. Figure 9.12 shows this area using much smaller load steps. However, it is very hard to discover the stiffening effect. The reason for this is that the out-of-plane load is fairly high and a dominant factor in the vertical displacement, see also Figure 9.11.

In order to show both the stiffening effect and the influence of the out-of-plane load the reader is referred to Figure 9.13. Here the deflections are plotted against the load factor for a number of different load conditions. The load conditions are as follows:

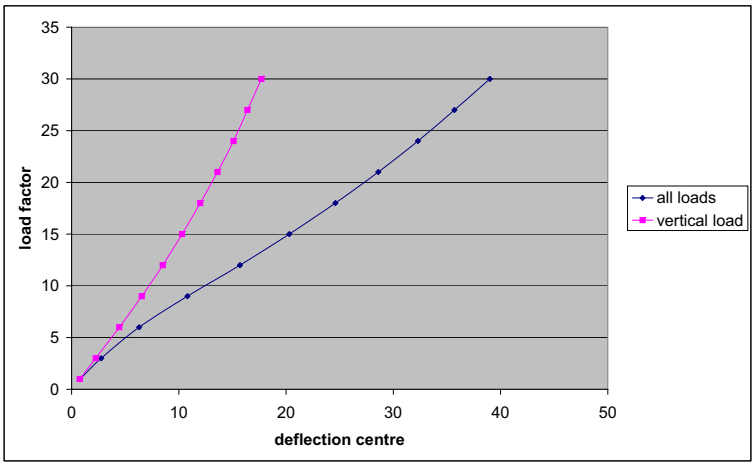

Figure 9.11: The difference in deflections between the out-of-plane loads and the combination of out- and in-plane loads.

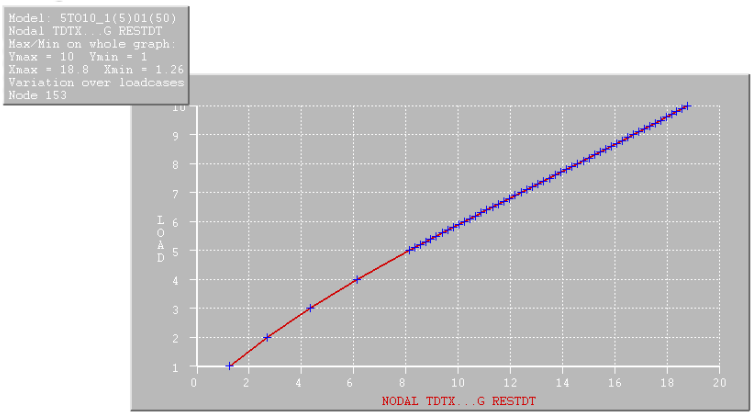

Figure 9.12: The deflections vs. the load factor for a load factor between 5 and 10.

- 'low out-of-plane load' refers to a load condition where the in-plane load is combined with a out-of-plane load that is a factor 100 lower than the combination of snow load and self weight.
- 'full load' refers to the normal load condition where a combination of out-of-plane loads, snow and self weight, and in-plane loads, membrane forces, is applied.
- 'theoretical buckling' refers to the linear elastic buckling load for a simply supported hexagonal plate ($\lambda = 19,8$) see also Paragraph 9.1.1.

In Figure 9.13 it is visible that the bend in the graph of the buckling factor of the plate moves in the direction of the theoretical value when the out-of-plane load is decreased. It

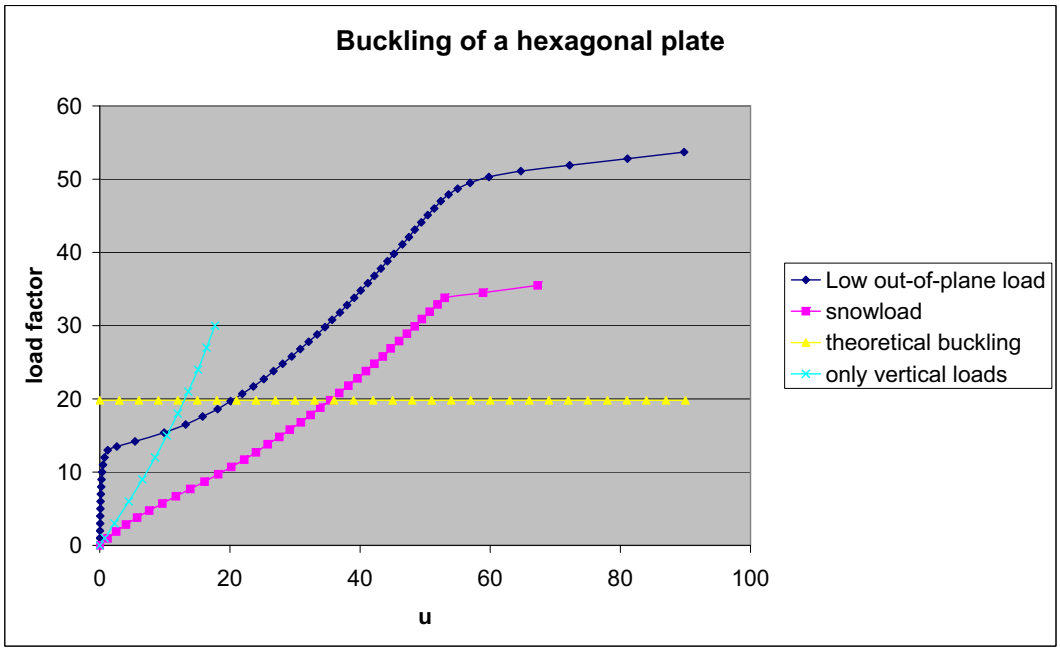

Figure 9.13: The deflections vs. the load factor for different load conditions.

is impossible to exactly find the theoretical value, since an imperfection (in this case the out-of-plane load) is needed in the stepped analysis in order to make the plate buckle. In reality it is of course also impossible to have no out-of-plane load.

9.3 Changing the dimensions of the facets

The theoretical influence of a change in the facet size can be derived from the analysis of a single plate. The findings in this chapter show that the dome is highly dependent on the local effects in and around single facets. This means that a decrease in the diameter of the facets leads to:

1. A smaller influence of the out-of-plane loads
2. A shorter buckling length in the facet
3. The in-plane loads will remain largely the same,since they arise from the shell action in the dome

The first and second item lead to a higher buckling factor for the facets themselves. Because the in-plane forces remain approximately the same, however, the global buckling of the dome will be hardly influenced by decreasing the size of the facets. This leads to the

conclusion that the dome will behave more and more as a smooth shell structure when the facet size is decreased. This is of course logical, since the dome *is* becoming smoother. A more interesting conclusion is that it will be possible to find a geometry where decreasing the facets no longer has a significant effect on the buckling behaviour of the dome. This point will be the point where the global buckling of the dome will be governing over the local buckling of the facets.

Increasing the size of the facets will in theory have a deteriorating effect on the stability of the dome. The local buckling of the facets will become strongly governing and the dome will loose the advantages of its shape. It will even be possible to find a theoretical facet size where it will no longer be possible to increase the glass thickness in order to improve the stiffness of the facets. This will be when the self-weight of the glass is the cause of buckling of the facets.

However, both effects are also countered by the effect in the joints. The joint is very important in the behaviour of the dome, see also Chapter 12, and therefore a larger number of joints will also decrease the stiffness of the structure. In this light it is important to realise that the most important deformation in the joint is due to both the in-plane normal stresses and the out-of plane shear stresses. The out-of-plane shear stresses will decrease but the normal stresses will remain more or less the same. Therefore it is hard to predict the influence of changing the dimensions of the facets since it for great deal depends on the properties of the joint. It will be interesting to look at this aspect in further studies.

9.4 Discussion

In this chapter the behaviour of a single facet has been analyzed in order to find an explanation for the fact that the dome is stronger in a stepped analysis than it was in the linear analysis, where normally in shell analysis the linear calculation yields a coarse upper-bound solution. A stiffening effect is found in the behaviour of the facets, which shows that it is plausible that the facets in the dome do not fail at their linear buckling capacity.

The lower buckling modes of the dome are governed by local buckling of facets. This makes the behaviour of the separate facets an important factor in the buckling of the structure. By stiffening and allowing an increased load on top of the theoretical buckling load the facets directly increase the buckling factor of the full dome.

It can therefore be concluded that the post-buckling behaviour in the facets is a good explanation for an increase of the buckling load of the dome in the non-linear analysis.

Another conclusion that can be drawn from the results for the single plate is that the facets do not show failure around the buckling factor of the dome ($\lambda \approx 6,64$). It is therefore unlikely that the buckling behaviour of the dome is governed by the failure of the facets themselves, but a different mechanism will occur. This result was also found

in Paragraph 8.3. The shape of the buckling mode shows a rotation of facets instead of a failure of the facets themselves. Joint failure is therefore likely to be the governing factor.

Chapter 10

Imperfection sensitivity

Introduction

Imperfections are an important factor in the stability behaviour of shell structures, see for instance the work of Koiter (Koiter 1945) or (Koiter 1967). The facetted dome, however, has a structural behaviour that is highly dependent on the local behaviour of the facets and joints. This behaviour is of course also related to the size of the facets, since using smaller facets results in a smaller influence of the out-of-plane forces on the local effects in the facets. Large imperfections will always be introduced in a dome structure like this, for instance deviations in the material, in construction or due to unequal settlements. Therefore it will be necessary to assess the impact of an imperfect geometry of the structure. The magnitude of the imperfections is much larger than usually needs to be considered for smooth shell structures, because during construction deviations in the order of magnitude of the thickness of the shell need to be considered.

Three different imperfection patterns are chosen to be investigated. The first one is simply displacing a vertex between three facets. The second imperfection pattern is larger and will consist of the displacement of an entire joint. The last pattern will be based on the buckling pattern found in the non-linear analysis.

10.1 Displacement of one vertice

During construction it is possible that, due to construction inaccuracies, the location of a single vertex is different from its original location. To test the impact of such a geometric imperfection the dome will be tested with an imperfect geometry. The order of the displacements will be 1-2cm, which is related to the thickness of the glass elements ($\approx$16mm).

First the imperfection pattern needs to be adopted and applied to the dome. The pattern

will be based on pulling down a vertex between a number of plates. The location will be chosen based on the governing nodes from the non-linear calculation. There are a number of nodes that are important and these nodes are shown in Figure 10.1. Note that due to the radial symmetry the governing nodes can be found on every one-fifth section of the dome, though the buckling behaviour itself eventually happens a-symmetrically

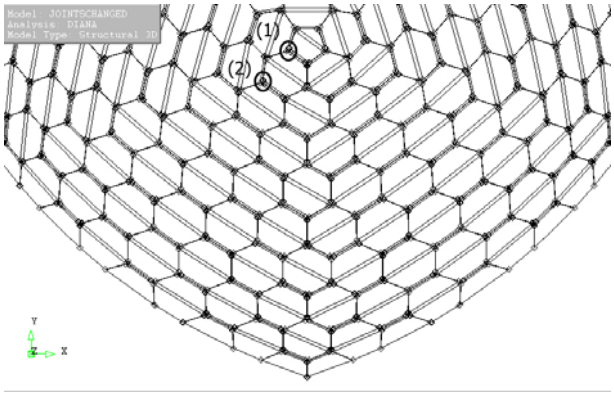

Figure 10.1: (1) and (2) are the important nodes in the dome, with regard to the non-linear buckling pattern.

The displacement of the node is created by changing its location in the original geometry of the dome. The vertex itself will be given the maximum displacement and the adjoining vertices will be given half of the displacement, to make the transition to the rest of the geometry smoother. Figures 10.2 and 10.3 show this graphically. Since every node in the model consists of a triangular shaped hole, all three points at every displaced vertex will be given the same displacement.

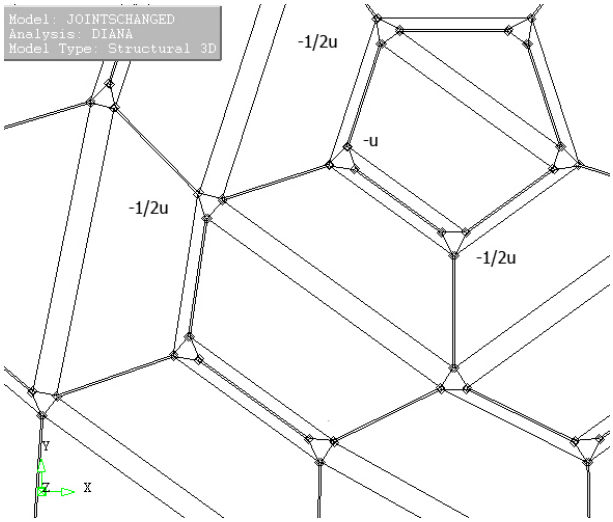

Figure 10.2: Zoomed in on the dome; corner of the pentagon: one vertex will be displaced maximally, while three vertices will be displaced half way. In every vertex six points will be displaced equally.

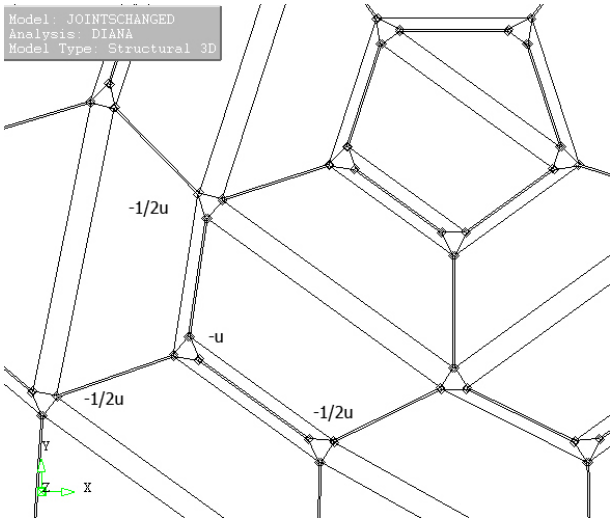

Figure 10.3: Zoomed in on the dome; corner of the first hegagon: one node will be displaced maximally, while three nodes will be displaced half way. In every node six points will be displaced equally.

10.1.1 Node 1: Corner of the pentagon

The first vertex to be pulled down is the corner of the pentagon, see Figure 10.2. The displacement of the node is -20mm vertically and therefore the displacement of the three adjoining vertices is -10mm vertically.

The non linear buckling calculation is carried out with the same method as for the perfect dome structure. The result is shown in Figure 10.4 and 10.5.

The result shows that the buckling behaviour of the dome is strongly dependent on the discontinuity that is created. The buckling factor is almost halved, from 6.64 to 3.40 and the buckling pattern is located at the displaced node. This behaviour is in itself not very surprising when one considers the magnitude of the imperfection compared to the previously found maximum deflections in the dome. The perfect dome had a maximum absolute displacement of a node of approximately 36mm at buckling. When a vertex is then given a displacement of 20mm this must have a strong influence on the structural behaviour.

When considering the load-displacement curve in Figure 10.4 it is visible that the graph is much less steep than in the perfect dome (see Figure 8.7) and that the bend in the curve is much less sharp. The steepness of the curve is a measure for the stiffness of the structure at this location. This means that the stiffness is locally greatly reduced by displacing a node. The reduced stiffness can be explained by the second order effects of the in-plane stresses. The direction of the in-plane forces will need to change at the imperfection and will give a component perpendicular to the joint, pushing it down.

The chosen magnitude of the imperfection is perhaps large compared to the deflections of the perfect dome, but deviations in construction can definitely have this magnitude. At the same time it might be possible that a more smooth imperfection, which is a more likely case during construction, will have a much smaller impact.

10.1.2 Node 2: Corner of the first hexagon

The second vertex to be pulled down is the corner of the first hexagon, see Figure 10.3. The displacement of the vertex is -20mm vertically and the displacement of the three adjoining vertices is -10mm vertically.

The non linear buckling calculation is carried out with the same method as for the perfect dome structure. The result is shown in Figure 10.6. Again the impact of moving the vertex is significant. The influence is in the same order of magnitude and reduces the buckling factor to 3.69. The reduced local stiffness effect found when pulling down a node of the pentagon can also be seen here.

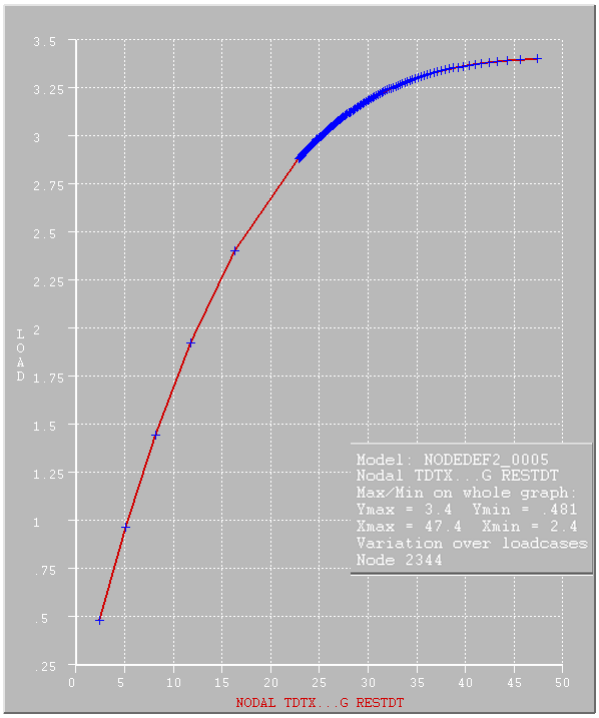

Figure 10.4: The resulting load-deformation diagram of the governing node when one corner of the pentagon is initially displaced. $\lambda \approx 51\%$

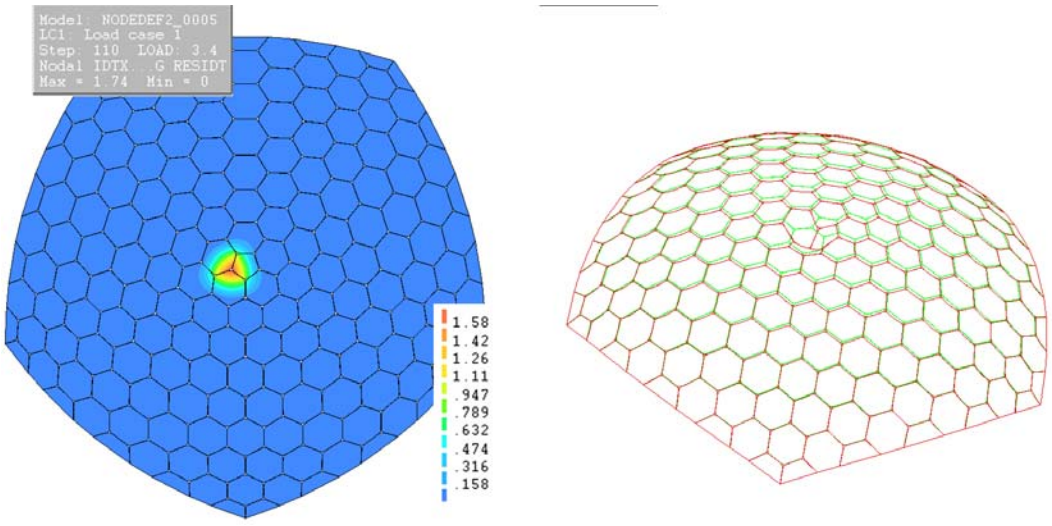

Figure 10.5: The resulting buckling shape when one corner of the pentagon is initially displaced. NB the deformed shape (red) shows the total sum of the deflections, the contour plot only the last incremental deflection

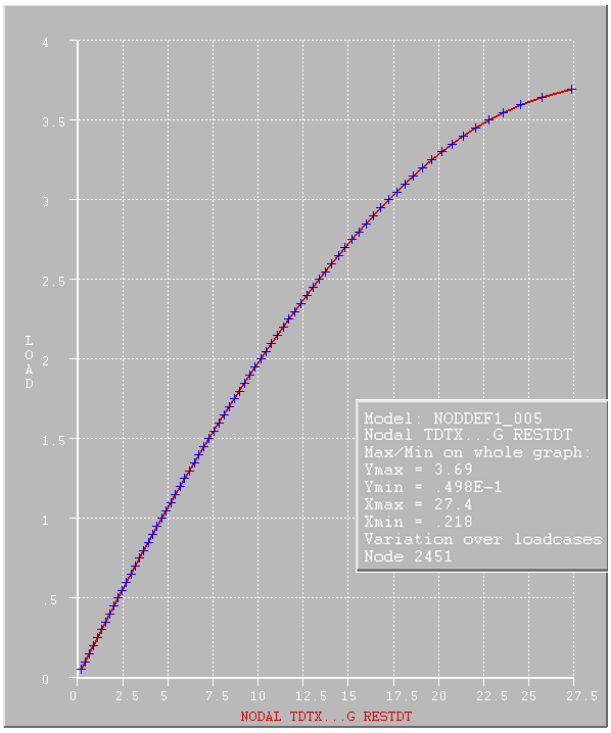

Figure 10.6: The resulting load-deformation diagram when one corner of the first hexagon is initially displaced. $\lambda \approx 56\%$

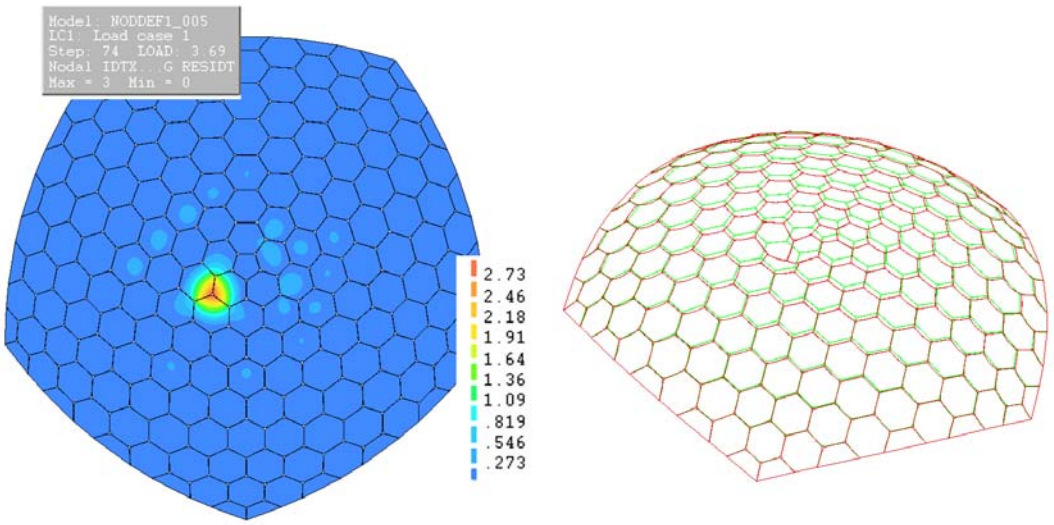

Figure 10.7: The resulting buckling shape when one corner of the hexagon is initially displaced. NB the deformed shape shows the total sum of the deflections, the contour plot only the last incremental deflection

10.2 Displacement of an entire joint

A miss-alignment of an entire joint is also a possibility during construction. The impact of such an imperfection in the dome should therefore be investigated. The order of magnitude of such a miss-alignment can again be around 10-20mm, corresponding to the thickness of the glass facets. An even stronger but nevertheless thinkable imperfection would be that the opposing joint on the facet is miss-aligned in the opposite direction. Therefore two opposing joints will be moved in opposite directions.

According to the buckling mode for the perfect dome that was revealed by the non-linear analysis the joint shown in Figure 10.8 is chosen. The imperfection is created by giving the points in the model that are related to the joint a maximum displacement. Then the adjoining points will be given half that deflection to smooth out the transition, see Figure 10.9. This is physically impossible for the glass to follow, but the analysis will give a good indication of the impact of a dislocated joint.

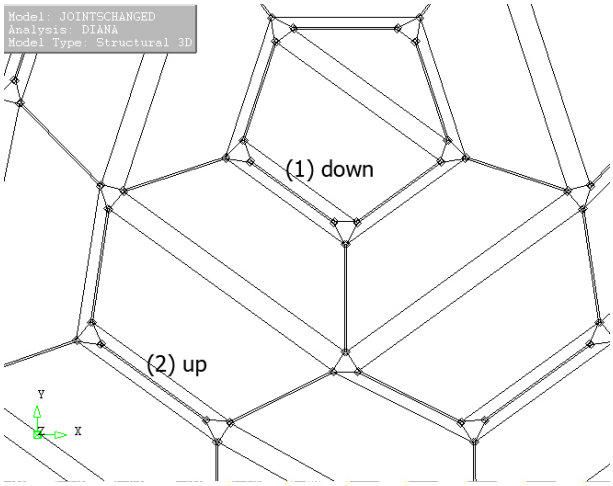

Figure 10.8: The important joints in the dome, with regard to the non-linear buckling pattern; (1) is moved down, (2) is moved up.

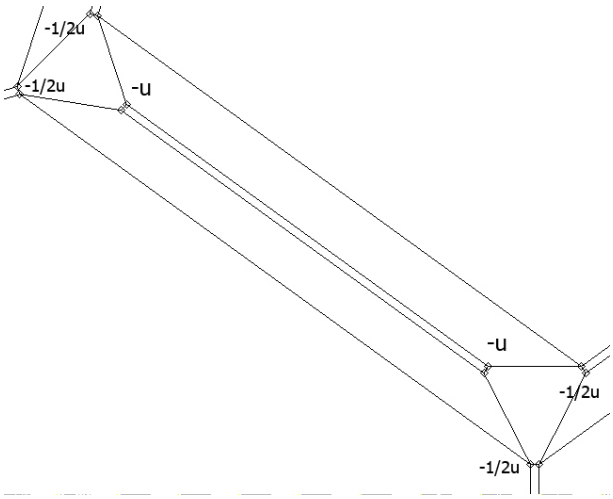

Figure 10.9: Zoomed in on the dome; the four points of each joint will get the maximum deformation; the eight adjoining points in the vertices get half.

The non-linear buckling analysis is carried out with the same settings as before. The result is shown in Figures 10.10 and 10.11.

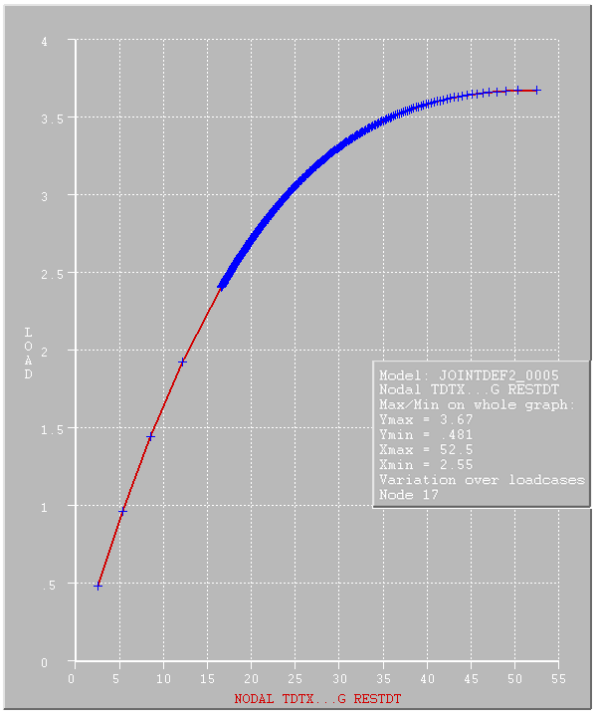

Figure 10.10: The resulting load displacement diagram for a displaced joint. $\lambda \approx 55\%$

The analysis shows that the displacement of the joint lowers the buckling factor of the dome significantly. The new found buckling factor is 3.67 ($\approx 51\%$), which is approximately the same as found when displacing a node in the dome. The stiffness is decreased locally, which is visible in the deformation pattern (Figure 10.11) and the load-displacement diagram (Figure 10.10).

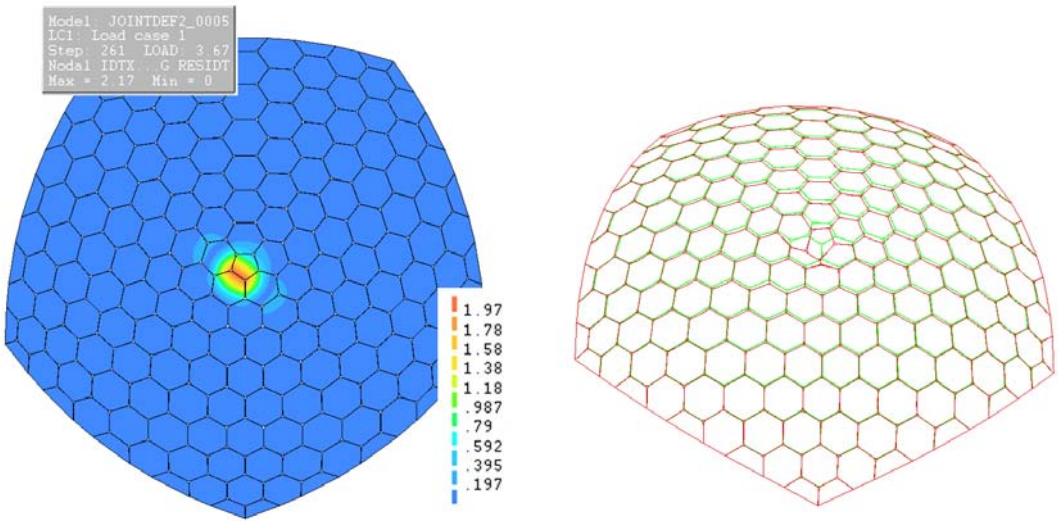

Figure 10.11: The resulting buckling shape initially displacing the named joints. NB the deformed shape shows the total sum of the deflections, the contour plot only the last incremental deflection

10.3 Buckling shape as imperfection pattern

Creating an imperfection that is related to the shape of the (first) buckling mode is theoretically the worst imperfection that can be induced on a structure, since the structure will be pushed into its failure mode. Therefore the last imperfection investigation is related to the buckling shape that is found in the non-linear analysis.

10.3.1 Development of the imperfection pattern

The imperfection pattern will be based on the buckling mode that is found by the non-linear analysis. The deformed shape of the structure at collapse is, however, not suitable because the buckling shape is largely shrouded by the large deflections in the facets. The shape of the buckling mode was discovered by looking at the incremental displacements that were caused by the subsequent load steps, see Paragraph 8.3. By using the incremental displacements of the final load step, the buckling shape can be introduced to the dome.

The maximum deformation in the last, very small, load step is only 0,461mm. Since this is not a realistic imperfection, all displacements will need to be scaled up. The desired order of magnitude is still 10-20mm and therefore a factor between 20 and 50 will need to be applied to the displacements. After that the displacements (in 3d) are added to the original location of the nodes. The result is a deformed structure that has the same, though magnified, shape as the buckling mode.

10.3.2 maximum dislocation 10mm

The first experiment is carried out with a maximum deformation of approximately 10mm. This means a scale factor of 20 on the node displacements. The result is shown in Figure 10.12. The final buckling shape is shown in Figure 10.13.

The buckling factor is significantly lower and it is obvious that the imperfection pattern has greatly influenced the buckling shape. The results show that the buckling factor drops significantly to approximately 63% of the original value (6.64 vs. 4.18). The buckling shape, however, has changed. In the analysis of the perfectly shaped structure the buckling took place at two main locations, which is shown in Figure 8.12. In the buckling mode of the imperfect dome only one of these locations is rediscovered, see Figure 10.13.

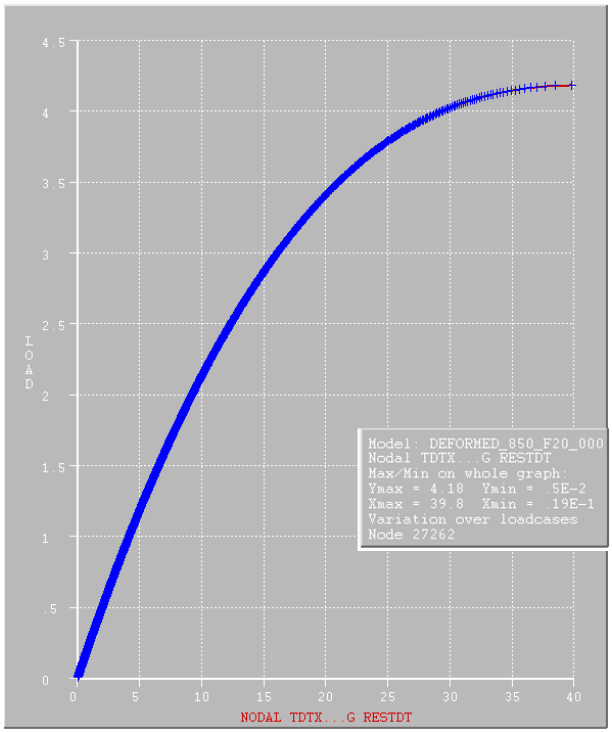

Figure 10.12: Load-deformation diagram for the governing node in the imperfect dome; imperfection magnitude of 10mm. $\lambda \approx 63\%$

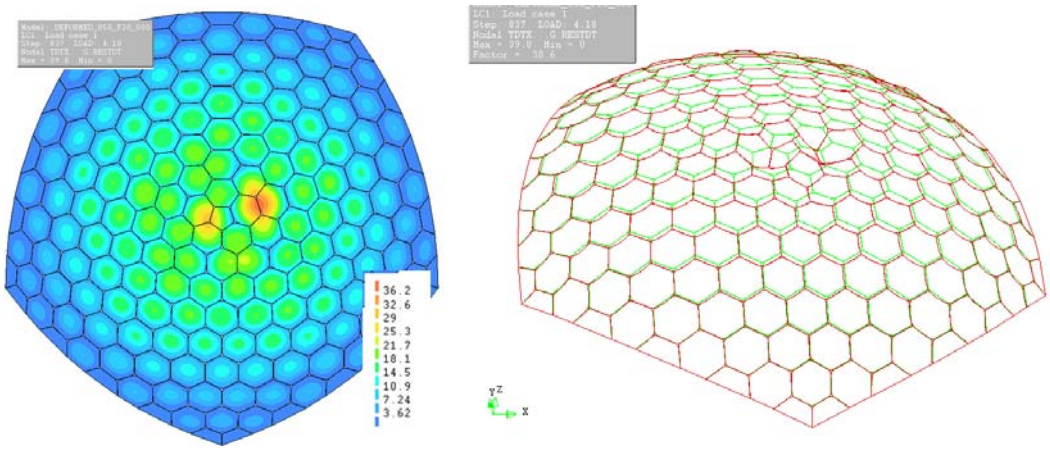

Figure 10.13: The resulting buckling shape using the buckling pattern as imperfection pattern ($d_{max} \approx 10mm$)

10.3.3 maximum dislocation 20mm

The second experiment is carried out with a maximum deformation of approximately 20mm. This means a scale factor of 50 on the node displacements. The result is shown in Figure 10.12. The final buckling shape is shown in Figure 10.13.

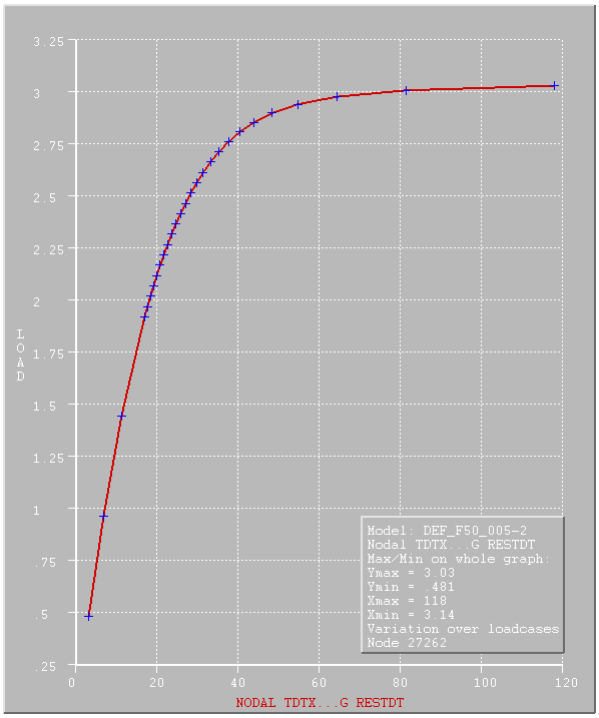

Figure 10.14: Load-deformation diagram for the governing node in the imperfect dome; imperfection magnitude of 20mm. $\lambda \approx 46\%$

The resulting buckling factor is now approximately 3. This means a lowering of the buckling factor to approximately 46% of its original value. The buckling factor that results from the calculation with larger imperfections is, as can be expected, lower. The value is, however, not linearly lower. The initial displacements have been a factor 2.5 larger, while the lowering of the buckling factor has a factor $\frac{6.64-3}{6.64-4.2} = 1.49$. This means that doubling the size of the imperfection does not necessarily mean a doubling of the decrease in the buckling factor. This is important for the sensitivity of the dome to large imperfections. If a smaller imperfection is assumed than actually found in the built structure, this is not necessarily immediately significant since a large imperfection will already have been assumed.

W.T. Koiter (Koiter 1945) drew up a number of laws on buckling of shells and imperfection sensitivity that describe this behaviour, see also Appendix B.3.3. The facetted shell structure can also be related to Koiter's laws. Two significant laws are:

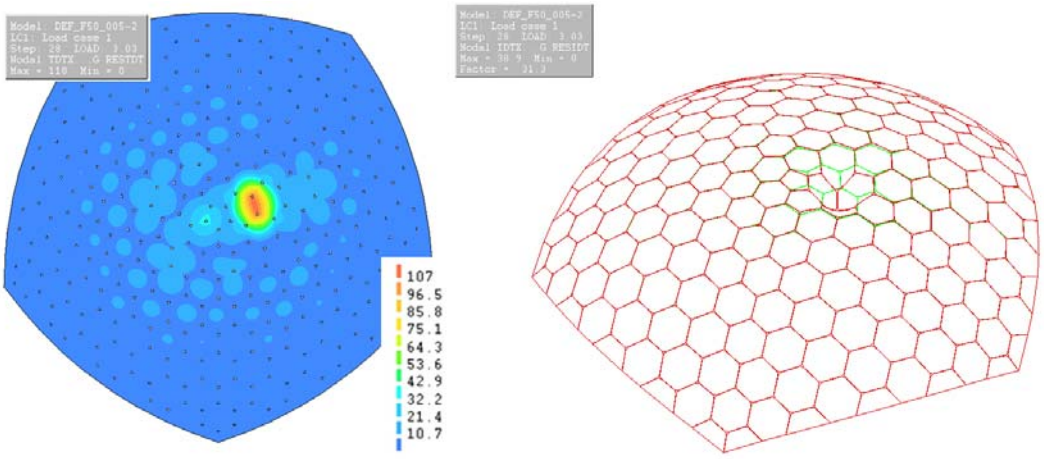

Figure 10.15: The resulting buckling shape using the buckling pattern as imperfection pattern ($d_{max} \approx 20mm$). NB the deformed shape shows the total sum of the deflections, the contour plot only the last incremental deflection

- the $\frac{1}{2}$-power law, Equation 10.1, where w_0 is the amplitude of the imperfection. ρ and c_1 are factors related to the imperfection shape and the given structure respectively.

- the $\frac{2}{3}$-power law, Equation 10.2, where w_0 is the amplitude of the imperfection. ρ and c_2 are factors related to the imperfection shape and the given structure respectively.

$$\frac{\lambda}{\lambda_{cr}} = 1 - 2(w_0 \rho c_1)^{\frac{1}{2}} \tag{10.1}$$

The $\frac{1}{2}$-power law states that the sensitivity to small imperfections is very large, but that the λ_{cr} does not drop linearly with the amplitude of the imperfection. This is also observed in the investigation into the imperfection sensitivity of the facetted dome.

$$\frac{\lambda}{\lambda_{cr}} = 1 - 3(w_0 \frac{1}{2} * \rho * \sqrt{c_2})^{\frac{2}{3}} \tag{10.2}$$

Three values have been found for the relation between the magnitude of the imperfection and the load factor, see Table 10.3.3. These results from the imperfection analysis can be fitted against both of Koiter's laws. It shows that the behaviour of the structure fits best with Koiter's $\frac{1}{2}$-power law, see Figure 10.16. However, because there are only a limited number of points used and the fit is especially difficult in the top part of the graph, it is difficult to draw a definitive conclusion.

Table 10.1: Relation between the buckling factor and the magnitude of the imperfection for the facetted shell

λ	equivalent	magnitude imperfection
6.64	1	0
4.2	0.63	1
3.0	0.45	2.5

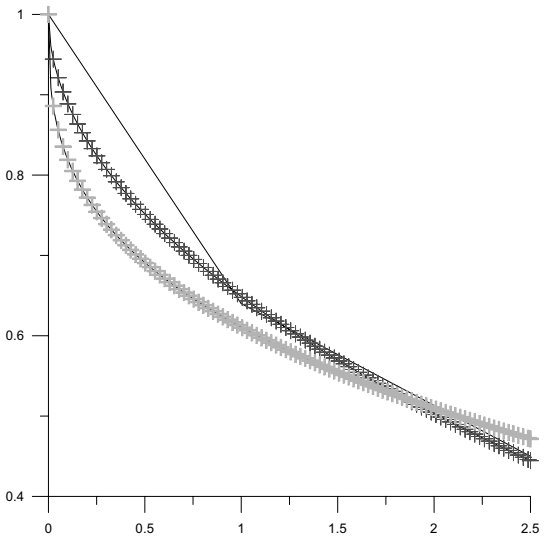

Figure 10.16: The behaviour of the facetted structure fitted with Koiter's $\frac{1}{2}$-power law (black) and $\frac{2}{3}$-power law (grey). It is shown that Koiter's $\frac{1}{2}$-power law has the best fit.

10.3.4 Checking the stresses in the governing imperfection pattern

In order to see whether the dome fails by stresses before buckling, a simple stress calculation is carried out for the results of the governing imperfection pattern. The calculation will be carried out according to the Rankine criterion, which has also been applied in Paragraph 8.4. Introducing the original buckling pattern from the perfect dome as an imperfection turned out to be the governing imperfection pattern and the corresponding stresses are visible in Figure 10.17. Only the stresses in the bottom of the glass are plotted since the tensile stresses are governing for the glass structure. It is immediately visible that at buckling the stresses have very high peaks around the introduced imperefctions. These can be ascribed to the very large displacements, and therefore strains, introduced in the structure at buckling. When the previous load steps are investigated it turns out that the stresses are under control again at a buckling factor of 2.94, see Figures 10.14 and 10.18. The maximum peak in the tensile stress is $58.3 N/mm^2$, while the opposite principle stress is negative at the given location. Since the compressive strength is usually

not considered governing in glass, the test will be as follows:

$$\frac{\sigma_1}{f_{m,t,u,d}} \leq 1$$
$$\frac{58.3N/mm^2}{66N/mm^2} = 0.88 \tag{10.3}$$

The glass therefore fulfills the stress criterion at a load factor of 2.94. The true λ-value should therefore be considered at 2.94 which is a decrease of 56% compared to the perfect dome.

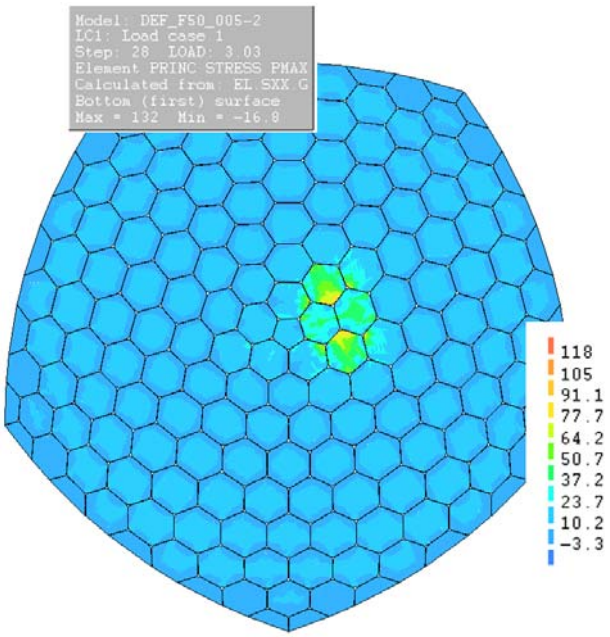

Figure 10.17: The 2-dimensional principle stress P1 in the dome at $\lambda = 3.03$; The extreme stresses are very (too) high due to the large strains at buckling.

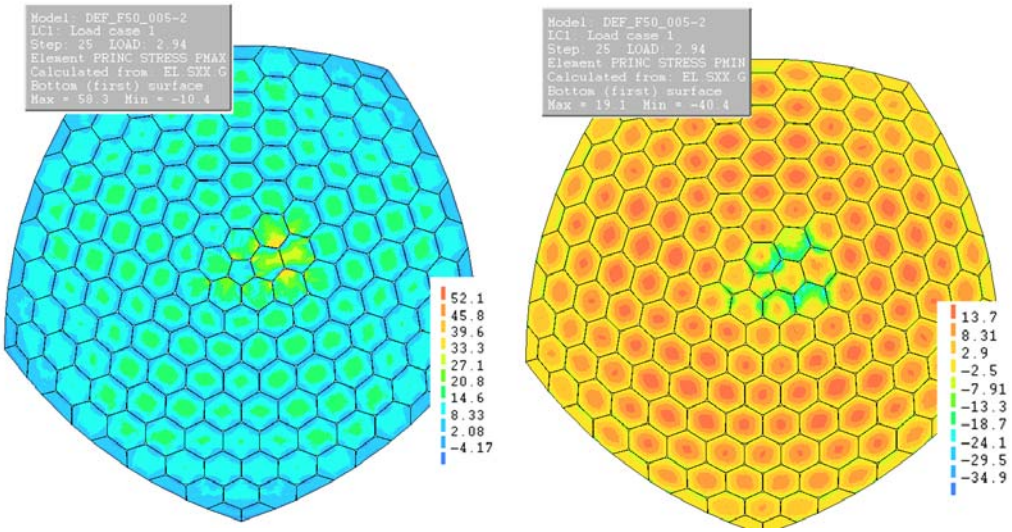

Figure 10.18: The 2-dimensional principle stresses in the dome at $\lambda = 2.94$; The extreme stresses are reduced and are under control.

10.4 Reflection on the construction of a facetted dome

The investigation into the stability of a facetted shell structure has revealed an imperfection sensitivity that requires a high degree of precision during construction. At the same time the structure consists of a large number of elements which makes it a challenge to reach this precision. Furthermore the joint has a large influence on the construction of the dome. This section tries to give some solution directions to solve the construction problems.

10.4.1 On-site assembly and erection

If on site erection and assembly is taken as a starting point, the structure needs to be built in a way that ensures stability during each construction step. At the same time the tolerances need to be met. One way to achieve a precise construction is to fully support every element in the structure during construction. This, however, requires a very large supporting structure with very low tolerances. Therefore it will be interesting to design a phase construction which does not need a large amount of scaffolding.

Bottom up

Figure 10.19 shows three possible stages in the construction of the dome. The most important thing to realise is that the dome is constructed ring-wise. This means that the structure can be stabilised by the original supports at the edge of the structure in combination with a support along the inner edge. The result is a very limited amount of scaffolding.

There is, however, one catch. The structure is probably not stiff enough to span from the lower edge to the outer without large deflections. These deflections are unfavourable for the final geometry and therefore every joint line or facet should be supported, leading to a large amount of scaffolding.

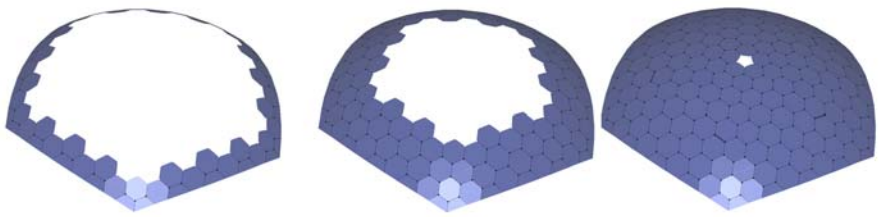

Figure 10.19: A possible phased in-situ construction method; the structure is built bottom up by rings.

A solution to prevent the large deflections is to stiffen the structure itself. If the joints (temporarily) have a very high bending stiffness the structure will require much fewer supports. The stresses in the structure will need to be considered carefully.

Some possibilities to temporarily increase the stiffness of the structure are:

- Placing braces from glass plate to glass plate, which are connected to the glass by for instance vacuum grippers. The braces need to fix the angle between the glass plates and provide stiffness against rotations.
- Stiffening the vertices; since there will be no permanent structural joint in the corners of the facets, the vertices can be used to temporarily fix the angles between the facets. It will need to be investigated whether this is possible without introducing high stresses in the glass due to the clamping of the corners.

Figure 10.20 shows an example of a vacuum gripper which can be used to stabilise glass panels. In the case of building a structure it might, however, be suitable to use more simple methods like gluing. A large system of vacuum grippers is likely to be fairly expensive.

*Figure 10.20: Grippers, left a pump driven gripper with stabilisation (2008*a*); right a manual gripper (2008*b*)*

Top down

The structure can also be built from the top down. This means that the structure already acts like a dome from the very beginning, see Figure 10.21.

The main advantage of this structural method is that the structure is already stiff as a shell structure during all construction phases. At all times the outer edge needs to be supported and new elements need to be added on this edge. The difficulties of this method

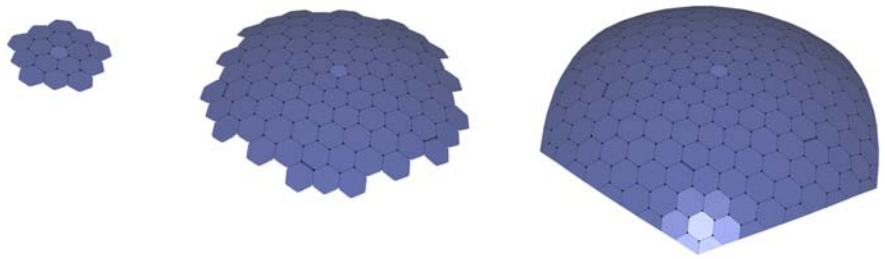

Figure 10.21: A possible phased in-situ construction method; the structure is built top down.

are that the structure needs to be lifted up at every construction step and that the plates are added onto the supported edge. The last challenge can be solved by supporting the outer plates instead of their edges. This will, however, introduce auxiliary stresses in the plates.

The advantage of this method is that hardly any extra stiffening is necessary in the structure since it will be stable as a dome structure.

10.4.2 Pre-fabrication of elements

Besides fully constructing the structure on-site it might also be a possibility to pre-fabricate parts of the structure and assemble them on-site. Especially the radial symmetry of the structure can then be used to re-use scaffolding and other support structures. The difficulty with pre-fabricating parts of the structure is that the elements themselves are stable, but not as stiff as they will be when the dome is fully installed. This might lead to problems with the tolerances in the structure. Again the parts can be stiffened using the same methods as mentioned in Paragraph 10.4.1.

If a sufficient stiffness can be reached within parts consisting of a small number of glass facets, it is a good option to combine pre-fabrication with the top-down method mentioned in the previous paragraph. Figure 10.22 shows some possible stages within such a construction process. When a full ring is closed again at the bottom of the structure it will again start acting as a dome.

The advantage of pre-fabricating large parts of the structure is that many of the joints will be created in a controlled environment and a high quality can be reached. However, at the same time it will always be necessary to create a large number of joints on site. This could make it less interesting to create joints off-site.

10.4.3 Discussion

In this paragraph construction phasing and methods have been shortly assessed. The most interesting construction method is a top-down method which ensures the structure to be

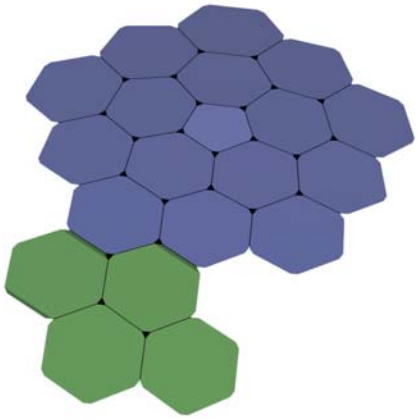

Figure 10.22: A possible phased in-situ construction method; the structure is built top down using larger pre-fabricated parts.

a shell at all times. Furthermore, only a limited amount of scaffolding will be necessary. The largest challenge will remain to place the facets correctly compared to each other.

Pre-fabrication is less interesting for this structure, since the joint will always need to be designed for on-site installation. Perhaps pre-fabrication can give a construction time advantage.

10.5 Discussion

Smooth dome structures are highly sensitive to very small imperfections. The facetted dome was, however, thought to have a much higher resistance against imperfections, due to the fact that the kinks in the dome are imperfections in themselves. There is an important aspect in the facetted shells; consider the magnitude of the imperfections compared to the maximum deflections in the dome at failure: during construction deviations in the order of magnitude of the thickness of the dome can be expected. This means the imperfections in the dome are very large. The maximum deflections of the dome are approximately 2-2.5 times the thickness of the structure, so the imperfection is almost half of the total final deflection at failure. The result is that the dome is very sensitive to the imperfections that need to be incorporated in the design.

From the three different patterns that have been considered, dislocating a node, dislocating a joint and introducing the first buckling pattern, the governing one is the introduction of the buckling pattern. When a maximum dislocation of 20mm is applied, the buckling factor is lowered by an impressive 56%. The chance that such an imperfection pattern is precisely built is of course very small, but still needs to be taken into account.

More realistic imperfections are the dislocation of a node or a joint. These can occur easily, for instance if during construction not everything fits as it should, a panel is slightly larger, a joint is not fixed precise enough, etc. When analyzing these imperfections it is directly obvious that the final failure occurs around the imperfection. The displacement of the element attracts secondary stresses and creates a large dent in the dome. At failure the buckling factor is lowered by almost 50% when dislocating a corner of the top pentagon. The impact of dislocating a corner is therefore not that different from using the buckling pattern. At the same time it should be noted that the dislocation of a node or joint will in reality be more smooth than modelled here. The result is therefore a lower-bound.

As an overview Figure 10.23 shows the load-deformation diagrams for the different imperfection patterns and the perfect dome. It shows that there is an initial difference in stiffness but that the imperfect structures are within a relatively small range. This is a comforting thought because when a more influential imperfection pattern *does* exist it is not likely to differ a lot from the already investigated imperfection patterns.

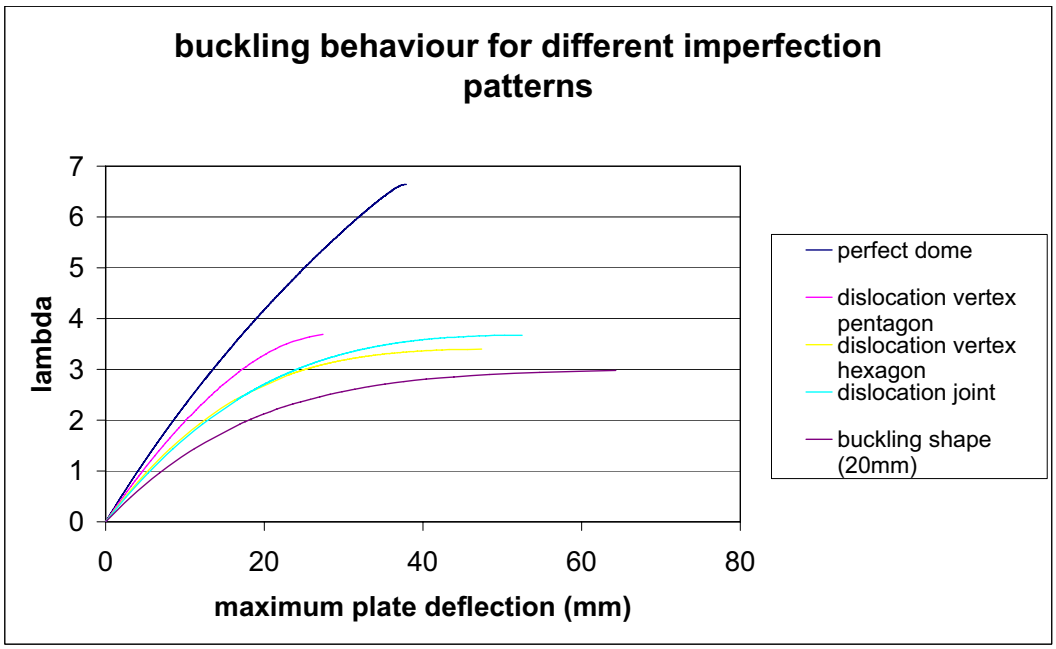

Figure 10.23: A graph comparing the load-deformation diagrams for the different buckling patterns with the perfect dome.

It can be concluded that realistic construction imperfections have such magnitude that they have a very large influence on the behaviour of the structure. Aside from over-designing the structure to cope with the large imperfections, the construction process needs to be designed and supervised very well. It might be very interesting to design the joints between the panels in a way that they prevent large dislocations during construction.

To make sure the geometry is correct the location of all nodes can be continuously checked during construction, by using specialized measuring equipment.

The sensitivity to imperfections also has another consequence. The prediction of the failure load of shell structures by using computer models is very difficult. Literature shows that the difference between physical models and finite element models can be large. The reason for this difference lies largely in the imperfections in the structure. Because the occurence and influence of imperfections are difficult to model correctly the failure load can be over-estimated. The very large imperfections that have been induced on the facetted structure in this chapter do, however, give trust in the solution. Still it is important to do tests on physical models to verify the results.

Chapter 11

Influence of the stiffness of the laminated glass

Introduction

In the previous models calculations have been made with 16mm thick glass panels. This 16mm is equal to two times 8mm glass, however when two glass panels are laminated together this does not necessarily imply that the result is similar to a 16mm thick panel of glass. As already stated in Chapter A, laminated glass acts differently under long term and short term loads. The difference is caused by the creeping of the foil that connects the two glass panels. This means that for a long term load, like the self weight of the structure, the cooperation between the panels is negligible. For the long term loads a reduction in stiffness is therefore necessary.

Short term loads can be considered in different classes. Wind is a load case which has a very short term character and creep effects will not play a role at all. Snow, on the other hand, can have a longer load duration and creep can start playing a significant role in very harsh winters.

An important factor to consider in this case is that creep in the PVB-foil is highly influenced by the temperature: a low temperature results in a limited creep behaviour. Figure 11.1 shows the influence of temperature on the creep behaviour of the PVB interlayer between two glass panels (Krüger 1998). When the snowload is on the dome, the temperature of the structure will be around 0^o Celsius. This means that the creep effect will be limited both due to the load duration as well as the temperature. Furthermore, when the structure is warmed up due to the temperature inside the structure, the snow might melt and have no significant impact at all. To be on the safe side, however, it is thought necessary to take full creep behaviour into account for the snow load, see Paragraph 11.2.

To get insight whether it will be interesting to more thoroughly investigate the creep

behaviour of the laminated glass also a case is investigated where creep is disregarded for the snow load. See Paragraph 11.3. It is concluded that it is interesting to consider a more detailed assessment of the creep behaviour when it is desired to increase the stability of the dome.

NB all values in this chapter are compared to the result of the dome with perfect geometry as considered in Chapter 8. Also the joint stiffness from that dome is considered.

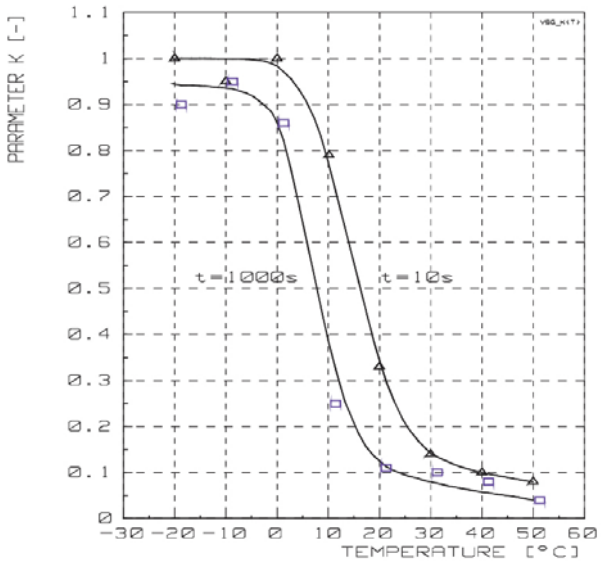

Figure 11.1: The influence of temperature on the creep behaviour of the PVB interlayer (Krüger 1998)

11.1 Defining the stiffness

In practice for laminated glass often a effective thickness is used to take the effect of creep into account. It is also possible to define an effective E-modulus. The difference between the two methods lies in the accuracy of the results. When the bending stiffness is considered dominant, both methods will take this stiffness as a starting point.

The classical plate theory gives the following relationship for the bending stiffness of a plate. This means that the thickness is represented to the third power in the stiffness.

$$D = \frac{Et^3}{12(1-\nu^2)} \tag{11.1}$$

Effective thickness; For the effective thickness method therefore Equation 11.2 is used (prEN13474 2 2000).

$$h_{ef} = \sqrt[3]{\Sigma_i h_i^3} \tag{11.2}$$

For the facetted shell the effective thickness would now become:

$$h_{ef} = \sqrt[3]{2 * 8^3} = 10.1mm \tag{11.3}$$

This is significantly lower than the orignal thickness of 16mm.

The thickness method, however, does not have the possibility to incorporate an increased cooperation between the glass layers as is desired in Paragraph 11.3. Therefore it has been chosen to also use an equivalent E-modulus.

Equivalent E-modulus; Using the same relationship for the stiffness of a plate an equivalent E-modulus can be derived, see Equation 11.4.

$$\begin{aligned} E_{equivalent} &= c_E * E_{glass} \\ c_E &= \frac{\Sigma t^3}{t^3_{equivalent}} \end{aligned} \tag{11.4}$$

The effective E-modulus for the facetted glass dome wil now be:

$$\begin{aligned} c_E &= \frac{\Sigma t^3}{t^3_{effective}} = \frac{2*(8)^3}{16^3} = \frac{1}{4} \\ E_{effective} &= \tfrac{1}{4} * 70 * 10^3 MPa = 17,5 * 10^3 MPa \end{aligned} \tag{11.5}$$

The result is that taking into account the creep effect of the PVB foil gives a significantly lower E-modulus. For glass $E_{equivalent} = 0.25 * 70 * 10^6 N/mm^2 = 17,5 * 10^6 N/mm^2$.

It is clear that both methods yield the same result for the bending stiffness of the material. The difference therefore lies in the resulting normal and shear stiffness of the material. Since the thickness is only linearly represented in both the shear and normal stiffness, the influence of changing the E-modulus is different from changing the thickness of the material.

The effective thickness method has a higher accuracy in defining the normal and shear stiffness. This can be proven by comparing teh normal stiffnes, which is linearly dependent on $E * t$, for all three cases. The normal stiffness should remain the same. The effective thickness method yields $E * 10,16mm$ and the effective E-modulus yields $\frac{E*16mm}{4} = 4 * E$. The original model would have yielded $E * 16mm$. It is obvious that the effective thickness method gives a better result.

It is important to note though that the bending stiffness is the dominant factor in the behaviour of the glass facets. Therefore using the different methods will not yield very

different results. This is shown in Paragraph 11.2.

11.2 Influence on the results of the non-linear analysis

A non-linear analysis is carried out on the dome, making use of the effective thickness. The results show that the buckling factor decreases with approximately 36% to $\lambda = 4,25$. See Figure 11.2. However, seen the very symmetrical deformation pattern of the structure the buckling effect is not visible. The deformations have at the same time increased to fairly high levels ($u_{max} \approx 47mm$).

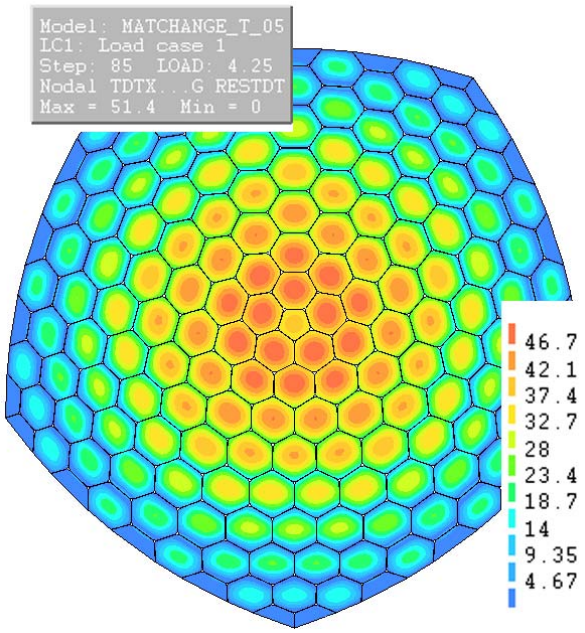

Figure 11.2: The buckling factor ($\approx 4,25 \approx 64\%$) due to the reduced thickness ($t_{equivalent} = 10.1mm$).

The same calculation is now carried out using the effective E-modulus. The results, see Figure 11.3, show that the difference with the effective thickness method is indeed fairly small. The buckling factor is slightly lower, 4.1 vs. 4.25, and the deformations are a bit larger. This makes it clear that the influence of the normal and shear stiffness of the glass on the buckling load is small. However, the increase in deflections is significant. This is probably a result of the reduced normal stiffness compared to the effective thickness method. Apparently the dome reacts strongly to the reduced membrane effect in the plates, see also Paragraph 9.2.

The value of the maximum load factor has now changed from 6,64 to 4,1 when the glass stiffness is reduced by neglecting the cooperation between the glass layers. This

means that the load factor has dropped to approximately 60% while the E-modulus has reduced to 25%. The reduction in load factor is therefore smaller than the reduction in E-modulus.

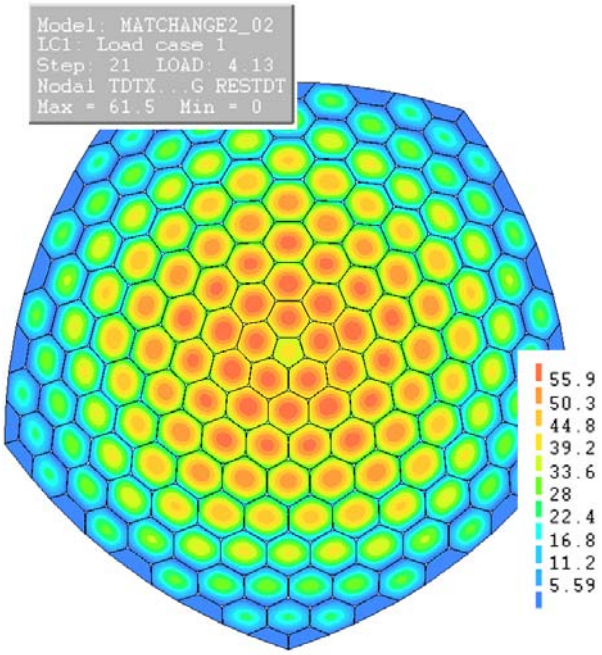

Figure 11.3: The buckling factor ($\approx 4,1 \approx 62\%$) due to the reduced E-modulus ($E_{equivalent} = 17,5 * 10^6 N/mm^2$).

11.3 Neglecting creep for snow load

As mentioned in the introduction, the cooperation between the glass layers can for a combination of reasons be considered much larger than assumed before. This also holds for snow load. To see the influence of this simplification a simple model wil be used for the situation that full cooperation between the glass layers is considered. For this calculation the effective E-modulus method will be used.

When deflections are considered, both the E-modulus (and so its reciproke $\frac{1}{E}$) and the load are linearly represented. When the glass is four times less stiff for the self weight (considering no cooperation), see Equation 11.5, the factor for the effective E-modulus can be estimated by:

$$
\begin{aligned}
E_{effective} &= c_E * E_{glass} \\
\frac{1}{c_E} &= \frac{4*p_{self\ weight}*1*p_{snow}}{p_{self\ weight}+p_{snow}} \\
\frac{1}{c_E} &= \frac{4*0.433*1*1.44}{0.433+1.44} \\
c_E &= 0.59
\end{aligned}
\tag{11.6}
$$

The result is a significantly higher E-modulus than when considering no cooperation. The stiffness of the glass is now: $E_{effective} = 0.59 * 70 * 10^6 N/mm^2 = 41,4 * 10^6 N/mm^2$.

A non-linear analysis is carried out on the dome, making use of the lower E-modulus. The results show that the buckling factor decreases to approximately 90% to $\lambda = 5,72$. See Figure 11.4.

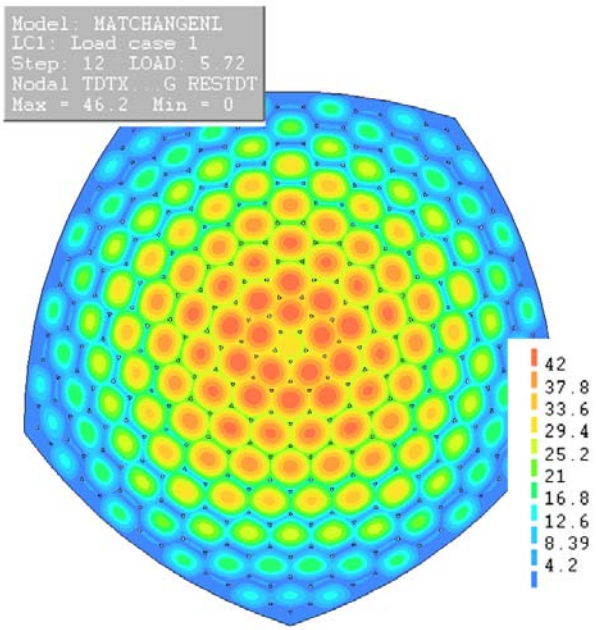

Figure 11.4: The buckling factor ($\approx 5,72 \approx 90\%$) due to the reduced E-modulus ($E_{equivalent} = 41,4 * 10^6 N/mm^2$).

11.4 Discussion

The comparison of the two methods of defining an effective stiffness for the glass when creep is considered confirms the expectation that bending is the dominant behaviour in

the glass facets. The results do show a significant difference in the deformations which proves that the normal and shear stiffness do play a role. Both methods are, however, a safe approximation since the normal and shear stiffness are being under estimated.

The most interesting thing about considering or not considering creep for the snow load is not so much which one to use when designing the glass facetted structure. The approach where full cooperation is considered for the snow load is an approximation that is on the unsafe side and is therefore unsuitable. Comparing the two approaches does, however, show how interesting it would be to further investigate the creep behaviour of laminated glass when a higher stiffness is required.

Figure 11.5 shows a plot of the different load factors λ versus the E-modulus of the laminated glass facets. The three scenarios are considered:

1. No cooperation for both self weight and snow load
2. No cooperation for self weight and full cooperation for snow load
3. Full cooperation for both self weight and snow load

It is clear that the influence of an increase of the stiffness of the laminated glass is especially effective in the lower range of the stiffness. Between $E = 17,5 * 10^6 N/mm^2$ and $E = 41,4 * 10^6 N/mm^2$ there is, however, much to gain by increasing the stiffness of the laminated glass. A more thorough research into the creep behaviour of the foil interlayer can therefore be interesting when more stiffness is required.

Another good option to increase the cooperation between the glass panels is to use Glass Sentry Plus (GSP) foil instead of PVB foil as an interlayer, as is also recommended in Appendix A. The higher stiffness and better creep behaviour will garantuee an increased cooperation between the glass layers and so a higher E-modulus for the laminated glass.

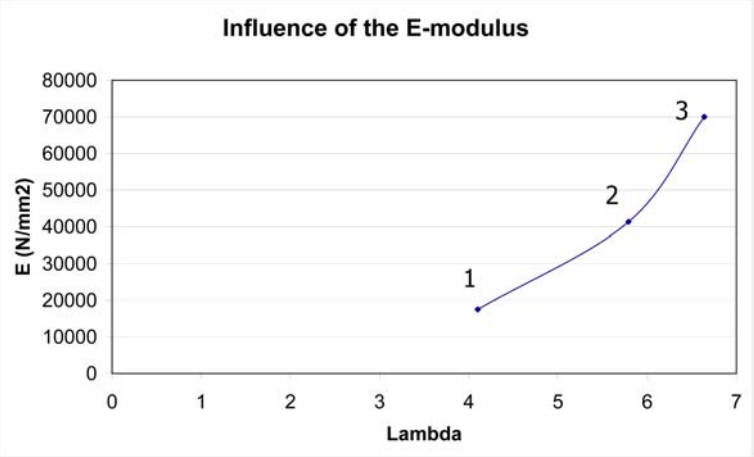

Figure 11.5: The influence of the glass stiffness; the true behaviour of the material due to creep lies between scenarios 1 and 2.

Chapter 12

Influence of the joint properties

Introduction

The non-linear analysis of the buckling stability of the dome revealed that in the chosen joint model, shell elements with a width of 10mm and a thickness of 10mm as well, the joints are decisive in the final buckling modes. The true joint configuration, however, differs from the model. This has been discussed in Chapter 4. Since the influence of the joint stiffness turns out to be very large this is investigated in more detail in this chapter.

The influence and configuration of the joint have also been investigated by Anne Bagger in her research (Bagger n.d.). The joint stiffness depends on the configuration and the materials in the joint. A range of stiffnesses is defined and this range is investigated in this chapter. The starting point is the bending stiffness of the material. The thickness of the joint and the stiffness of the joint material are scaled to make the normal and bending stiffness of the modelled joint fit the designed joint.

After a first investigation with the values resulting from the analysis of the designed joint it turned out that the current joint configuration does not comply with the necessary stiffness requirements. Therefore the influence of the normal/shear and bending stiffness are investigated seperately, see Paragraphs 12.3 and 12.4. This led to the conclusion that especially the normal and out-of-plane stiffness of the joint need to be improved in order to create a working structure. Recommendations for improving the stiffness of the currently designed joint can be found in Paragraph 12.7.

To conclude the investigations in this chapter the behaviour of the structure is compared to a smooth dome and a facetted structure with ‘glass’ joints in Paragraph 12.8.

12.1 Defining the properties for the joint

Introduction

As already stated in Paragraph 4.3.5, the modelled joint in the FEM-program differs from the joint type that is likely to be chosen. Figure 12.1 show the lay-out of this joint in a test sample; between the glass and the aluminium strips four neoprene strips are placed.

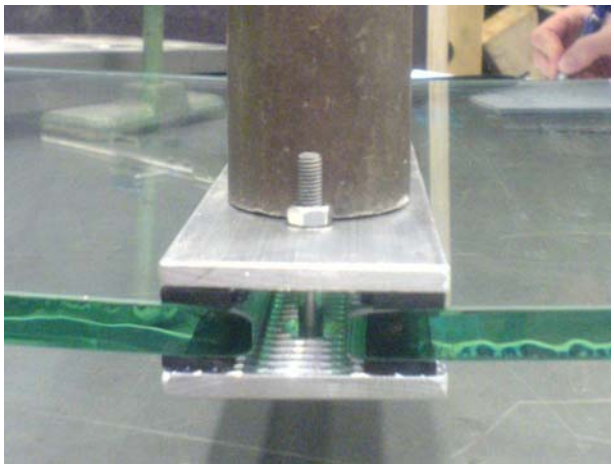

Figure 12.1: A test sample of the designed joint.

Figure 12.2 shows the way the joint has been modelled in Diana.

The thickness of the joint and Young's modulus of the joint material can be controlled in the model. This gives enough control to recreate the bending stiffness of the designed joint as well as to create a corresponding normal stiffness. The shear stiffnesses of the modelled joint cannot be de-coupled from the normal stiffnesses, due to the geometry of the modelled joint.

In this paragraph the necessary range in thickness and joint material stiffness is defined. The results are then implemented in Paragaph 12.2.

12.1.1 Resulting stiffness for the designed joint

In Appendix H the Young's modulus of the neoprene in the joint has been defined and now the resulting stiffness of the joint can be determined using Equations H.12, H.13, H.16 and H.18 in Appendix H.

Table 12.1.1 gives an overview of all the value ranges for the different stiffnesses of the designed joint. These resulting stiffnesses need to be translated to the model.

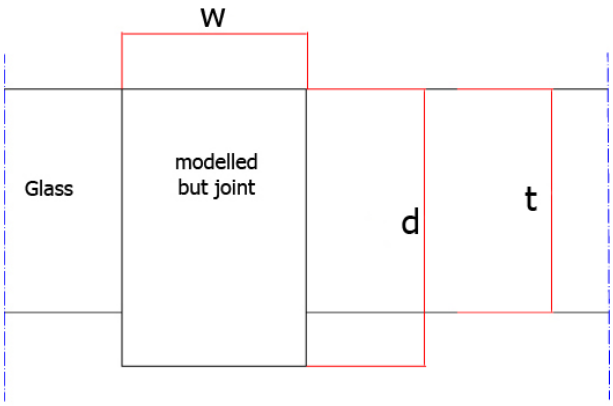

Figure 12.2: The joint configuration within the Diana model.

Table 12.1: The value ranges for the different stiffnesses of the designed joint.

Variable	Value range
k_m	$\in [525;15,2^*10^3]N$
k_n	$\in [4,3;31]N/mm^2$
$k_{s,oop}$	$\in [0,43;12,4]N/mm^2$
$k_{s,ip}$	$\in [4,3;31]N/mm^3$

In comparison, the original stiffness values that were incorporated in the *model* were based on w=10mm, d=10mm and E=100N/mm^2. This leads to $k_m = 1,67 * 10^3 N$ and $k_n = 200N/mm^2$, see also Paragraph 12.1.2. This means that the bending stiffness was already well within the range of the designed joint, even being on the fairly low side. The normal stiffness and the out-of-plane shear stiffness, however, has been severely overestimated. The influence of this over-estimation can be found by applying realistic combinations of normal and bending stiffnesses.

When considering the pre-mentioned Equations for the stiffnesses of the modelled joint it is important to note that when the normal stiffness is altered in the modelled joint, also the shear stiffnesses are altered. This means that in the current model of the joint it is impossible to disconnect the normal and the shear stiffness. Small deviations can be made by deviating the Poisson's ratio for the modelled material, however, Diana only accepts 'realistic' values for the Poisson's ratio. This means that the value can only lie between 0 and 0,5. The shear stiffness will therefore only be considered in combination with the normal stiffness. The relation between bending and normal stiffness is easily defined and therefore it has been chosen to take the normal stiffness as a starting point.

12.1.2 Translating the properties to values for the model

Both the normal and the bending stiffness need to be de-coupled and translated to the model correctly. This can be done by defining a variable that is equal to the ratio between the bending stiffness and the axial stiffness of the joint:

$$\begin{aligned} \beta &= \frac{k_{m,model}}{k_{n,model}} = \frac{\frac{d^3}{6w} * E}{\frac{2d}{w} * E} \\ \beta &= \frac{1}{12} * d^2 \end{aligned} \tag{12.1}$$

$$\beta = \frac{k_{m,model}}{k_{n,model}} = \frac{k_{m,design}}{k_{n,design}}$$

This means that the ratio is only dependent on the thickness and the Young's modulus of the joint material in the model. Since the stiffnesses of the designed joint are known (estimated, see table 12.1.1), the necessary depth and stiffness of the joint in the model can be defined. For the pre-mentioned extreme stiffnesses the following values for the depth and stiffness are obtained:

Minimum: $d = 38,1mm$ and $E_j = 0,57MPa$
Maximum: $d = 76,4mm$ and $E_j = 2,05MPa$

The resulting stiffnesses of the modelled joint are given in Table 12.1.2 and compared to the joint stiffnesses according to the designed joint.

Table 12.2: Comparison of the resulting extreme joint stiffnesses for the modelled and designed joint.

	Model soft	Design soft	Model stiff	Design stiff
$k_m[N]$	525	525	15,2*10^3	15,2*10^3
$k_n[N/mm^2]$	4,3	4,3	31,3	31,3
$k_{s,oop}[N/mm^2]$	1,45	0,43	12,4	12,4
$k_{s,ip}[N/mms]$	1,45	4,3	12,4	31,3

From Table 12.1.2 it can be read that even though the normal and bending stiffness are now corrected, the shear stiffnesses are still incorrect. The out-of-plane stiffness of the joint is interesting, since it is too low at the 'stiff' model and too high at the 'soft' model. This difference can be explained by the strong influence of the thickness of the neoprene strips in the joint. This effect is much stronger than the changes in depth of the modelled joint. The in-plane stiffness is much higher in the model than in the designed joint, especially when the stiffness increases. This can again be ascribed to the large influence of the thickness of the neoprene strips.

12.2 Applying the joint properties to the model

In this paragraph the two extreme combinations of depth and E-modulus are modelled. Furthermore a more realistic value will be chosen based on reasonable properties for the different elements of the joint.

NB due to a small calculation error the used E_j and d in this Paragraph are different from the calculation in the previous Paragraph. The result is that the stiffnesses are slightly higher. Because the results are mainly used to get an impression on the behaviour of the structure the values have not been adjusted. The calculation with the correct values would not yield very different results, especially seen the extreme results.

12.2.1 Combination 1: d=30,12mm and Ej=1,15MPa

The first combination of d and E_j represents the lowest stiffness that is expected from the joint, see Paragraph 12.1.2. The result of the analysis can be found in Figure 12.3. It turns out that the buckling factor becomes very low with the current properties of the joint. The dramatic drop in overall stiffness of the structure can be ascribed to the reduced stiffness: a decrease in bending stiffness, a decrease in normal stiffness and a decrease in shear stiffness of the joint. Their values are respectively, $k_m = 525$; $k_n = 6,9$; while the originally modelled joint had the following properties: $k_m = 1667$; $k_n = 200$;. It is clear that the difference is extremely large.

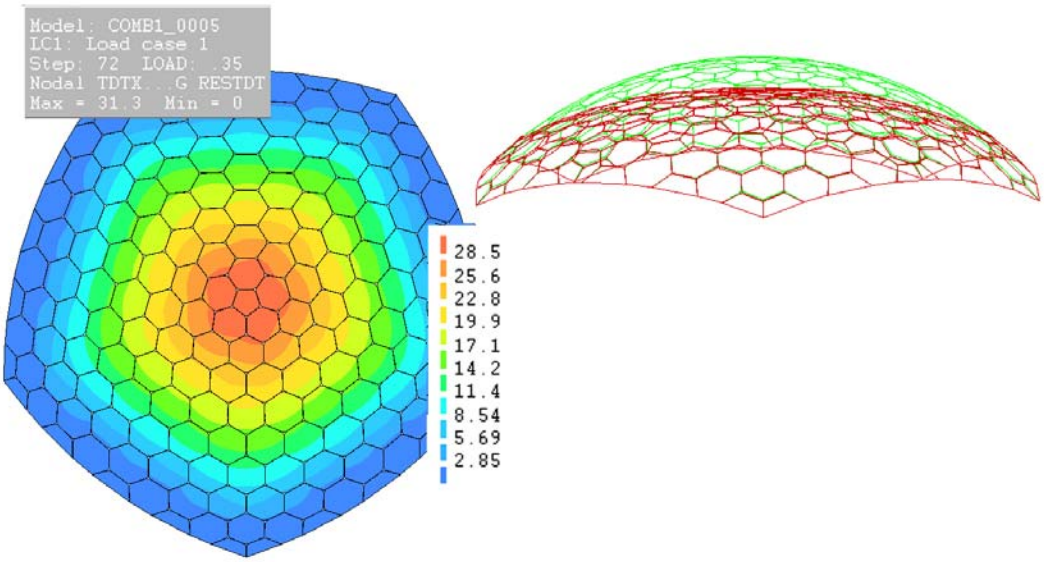

Figure 12.3: The results for combination 1: $d = 30,12mm$ and $E_j = 1,15MPa$

12.2.2 Combination 2: d=73,9mm and Ej=2,26MPa

The second combination of d and E_j represents the highest stiffness that is expected from the joint, see Paragraph 12.1.2. The result of the analysis can be found in Figure 12.4. It is clear that the buckling factor is still dramatically low ($\approx 1,7$). It should again be noted that DIANA has trouble finding a real buckling effect, due to the large displacements that are found in the model.

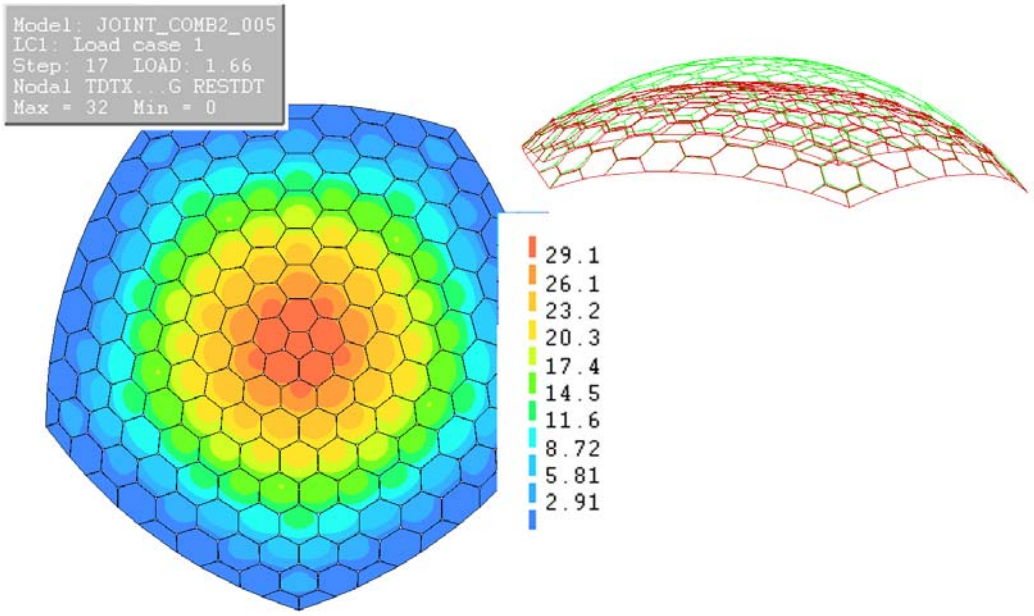

Figure 12.4: The results for combination 2: $d = 73,9mm$ and $E_j = 2,26MPa$

It is clear that the lower buckling factor can no longer be ascribed to a low bending stiffness of the joint. This time the bending stiffness of the joint is actually much higher than in the first models (15kN vs 1,7kN). Therefore it must be true that the influence of the normal and/or shear stiffness of the joint has a large impact on the stiffness of the dome as a whole.

12.2.3 'Realistic' combination: d=35mm and Ej=3,74MPa

When considering the different material properties of the elements in the joint, like thickness of the neoprene strips, width of the aluminum strips, etc. it is tried to find a practicaly realistic combination. This combination is arbitrarly chosen as follows:

- $E_0 = 5MPa$
- $w = 10mm$

- $h = 3mm$
- $t = 16mm$

This results in the following properties for the joint in the model:

- $k_m \approx 2kN$
- $k_n \approx 11,1N/mm^2$
- $d = 36.5mm$
- $E_j = 2,43MPa$

The result of the calculation is given in Figure 12.5. It is shown that the dome does not fulfil the stability conditions, since the deflections become too large and the lambda value too low. Again the result can only be ascribed to the decreased normal and shear stiffness of the joint, since the bending stiffness is of the same magnitude as in the original models (2kN vs 1,7kN).

NB also in this calculation the E_j and d are incorrect. The correct values that result from the chosen properties are: $d = 46,2mm$ and $E_j = 1,20N/mm^2$. Again the influence on the results will not be very large and still a good impression is achieved.

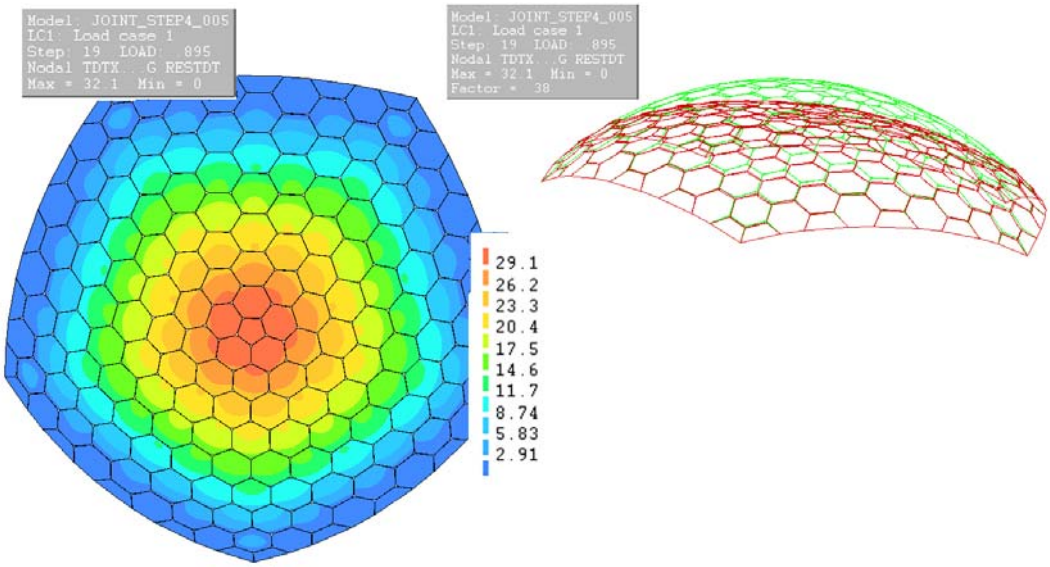

Figure 12.5: The results for combination 3: $d = 36,5mm$ and $E_j = 2,43MPa$

12.3 Investigation into the influence of the normal and shear stiffness of the joint

In Paragraph 12.2 it has been shown that the stability of the dome is not just sensitive to the bending stiffness of the joint, but also to the normal and shear stiffness of the joint. Therefore it will be investigated up to what level the stiffness needs to be improved to create a stable structure. The research is done by again using Equation 12.1. In this case, however, the modelled joint is taken as a starting point to create new ratios between k_m and k_n. The bending stiffness k_m will be kept at the original value, which is a realistic value, and the normal stiffness k_n will be changed. Using three intermediate steps, k_n will be changed from the original value to a realistic value with a comparable bending stiffness. At the same time the shear stiffness of the joint will change because it has a similar relation with the thickness of the joint, see Equation H.16 which holds for the modelled joint. In the current geometry of the modelled joint it is impossible to decouple the normal and shear stiffness of the joint, so it is necessary to look at their combined influence.

Table 12.3: Properties for the modelled joint when increasing the normal stiffness

	k_m (N)	k_n (N/mm^2)	$k_{s,ip}$ (N/mm^3)	$k_{s,oop}$ (N/mm^2)	d (mm)	E_j (MPa)
Original model	1667	200	67,1	67,1	10	100
Model I	1700	150	50,3	50,3	11,66	64,3
Model II	1700	100	33,5	33,5	14,28	35,01
Model III	1700	50	16,8	16,8	20,2	12,4
'Realistic' joint	2000	17,8	6,0	6,0	36,5	2,43

The results of the three models are given in Figures 12.6 to 12.8.

The results of the calculations show that indeed the stiffness of the dome as a whole increases when the normal and shear stiffness are increased. When the normal stiffness is plotted against the lambda value for the five cases that have been investigated, see Figure 12.9, it becomes visible that in a large part of this interval the influence of the normal and shear stiffness of the joint is almost linear. When the stiffness becomes very low, however, the influence increases and the drop in the stiffness of the total dome decreases more quickly. In the higher stiffness region a similar but opposite effect seems to take place.

The results of the investigation show that it is indeed interesting to increase the normal and shear stiffness of the joint. By increasing the normal stiffness to a value of approximately $100N/mm^2$ and increasing the shear stiffness accordingly a lambda of 4.2 can already be reached for a dome with a perfect geometry. If it is possible to further increase

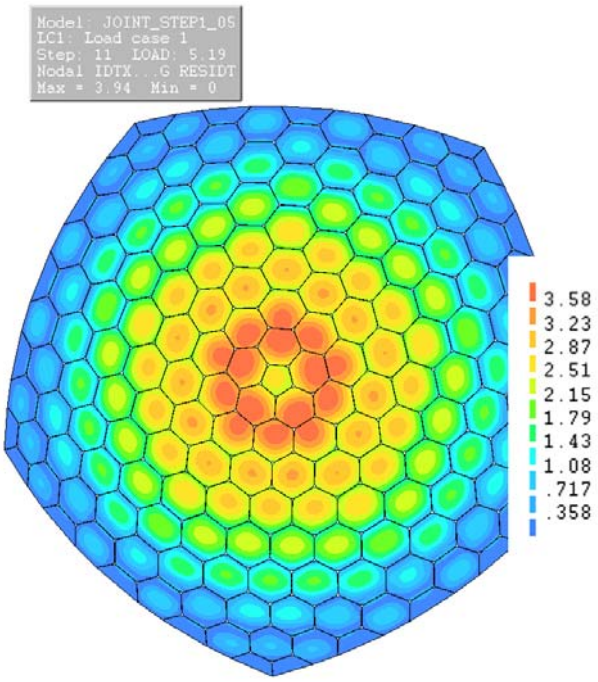

Figure 12.6: The results of Model I (last incremental deformation is shown).

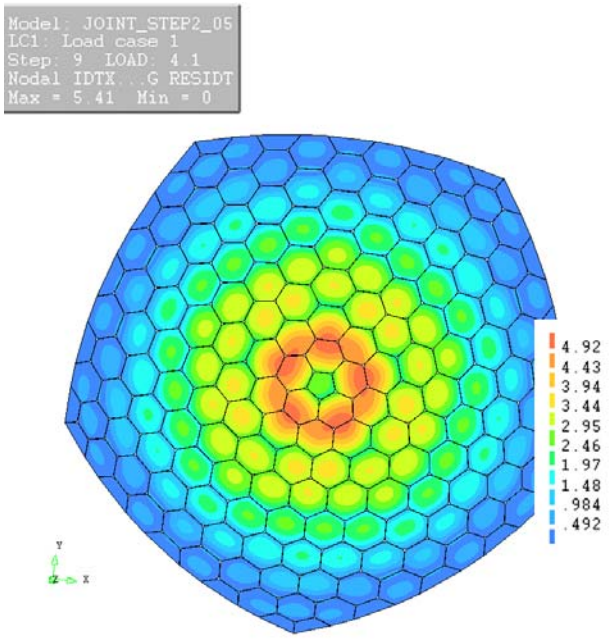

Figure 12.7: The results of Model II (last incremental deformation is shown).

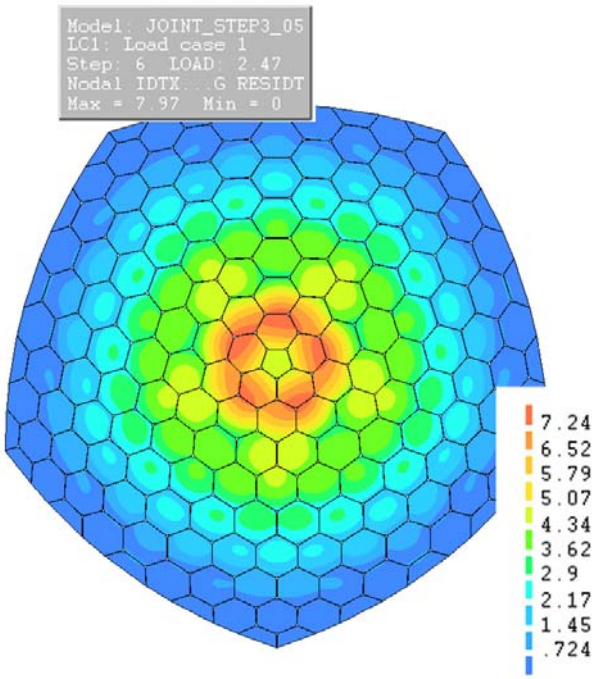

Figure 12.8: The results of Model III (last incremental deformation is shown).

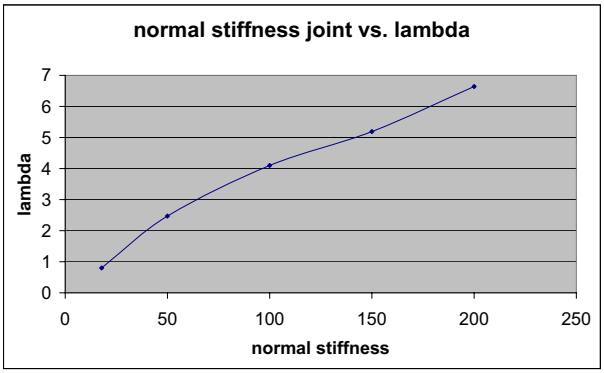

Figure 12.9: The normal stiffness of the joint plotted against the resulting lambda value (k_m 1700N).

the normal stiffness of the joint the effect becomes stronger.

For further investigation it would be very interesting to create a different model for the joint in which it is possible to de-couple the normal and shear stiffnesses. This way it will be possible to see the influence of the different stiffnesses seperately.

12.4 Investigation into the influence of the bending stiffness

Besides investigating the influence of the normal and shear stiffness it is also interesting to look at the influence of the bending stiffness. To achieve this the bending stiffness will be kept the same for different values of the normal stiffness. Also the combination has been made with a varying normal stiffness. In total twenty-one combinations have been tested of which the results are shown in Table 12.4.

Table 12.4: Tested models in varying the bending stiffness

k_m	k_n	$k_{s,oop}$	$k_{s,ip}$	λ
250	50	16,8	16,8	1,9
	100	25,2	25,2	3,3
	150	50,3	50,3	4,1
500	50	16,8	16,8	2,0
	100	25,2	25,2	3,5
	150	50,3	50,3	4,9
1700	50	16,8	16,8	2,47
	100	25,2	25,2	4,1
	150	50,3	50,3	5,2
5000	50	16,8	16,8	2,29
	100	25,2	25,2	4,27
	150	50,3	50,3	5,78
7500	50	16,8	16,8	2,32
	100	25,2	25,2	4,31
	150	50,3	50,3	5,84
10000	50	16,8	16,8	2,34
	100	25,2	25,2	4,33
	150	50,3	50,3	5,86
15000	50	16,8	16,8	2,34
	100	25,2	25,2	4,34
	150	50,3	50,3	5,87

The striking conclusion that can be drawn from this graph is that from a certain level, the bending stiffness of the joint apparently has very little influence on the stability of the dome. Therefore the most improvement can be achieved by increasing the normal and shear stiffness of the joint. At low levels for the bending stiffness the behaviour becomes less predictable, since different effects seem to take place at the different normal stiffnesses. This region is, however, less interesting since the neccessary bending stiffness can easily be obtained.

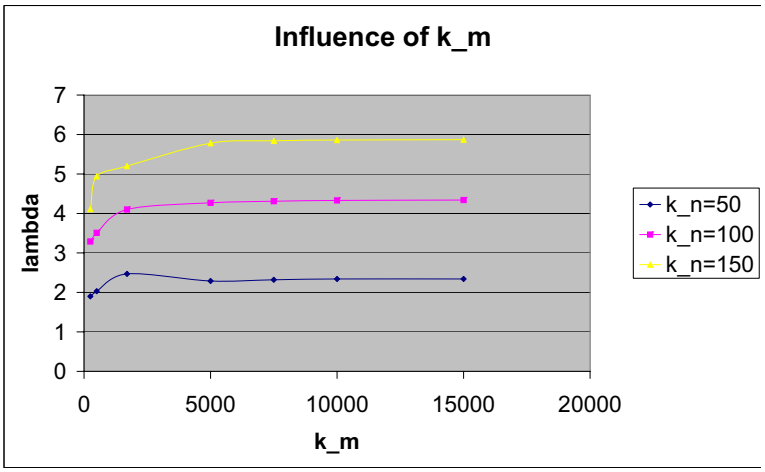

Figure 12.10: The influence of increasing the bending stiffness of the joint for different normal stiffnesses.

12.5 Explanation for the importance of the normal and out-of-plane shear stiffness

The result that the bending stiffness is hardly an issue for the stability of the dome and the normal and out-of-plane shear stiffness have such an impact can be explained by the behaviour of the joint in the model.

The model with $k_m = 1700$ and $k_n = 50$ is considered. The deformations are magnified to a factor 50 and zoomed in on two areas of the dome; one of the bottom corners and the top of the dome, see Figure 12.11. It is visible that the glass facets slide over each other and that the joint is deformed strongly by both shear and normal strains. The mechanism for this behaviour is shown in Figure 12.12. When the joint behaves in this way it is logical that the normal and out-of-plane shear stiffness are decisive for the behaviour of the total dome. It should be noted that when the deformations are considered on a 1x magnification the glass facets do not cross over each other.

The lack of influence of the bending stiffness in the higher regions is also explained by this behaviour, since only shear and normal strains are enough to allow deformations. The increase of bending stiffness will, however, change the stresses in the joint. When the joint restrains the facets for bending it will develop higher bending stresses, following from the clamping of the glass facets. This behaviour is described by Anne Bagger (Bagger n.d.).

When the bending stiffness is dropped severely, the stability of the dome is also lowered, see Figure 12.10. A possible explanation is that the rotation of the glass plates at their 'supports' is increased, see Figure 12.13. Due to this increased rotation angle ω between the plates is enlarged. This effect encourages the plates to move over each other

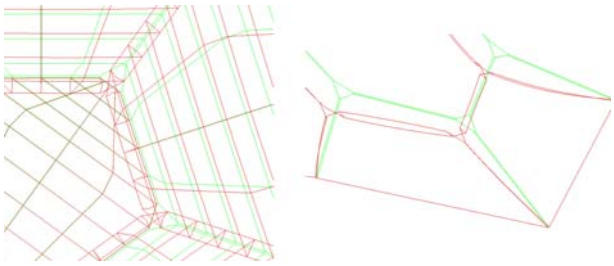

Figure 12.11: Zoomed in on the dome with magnified (50x) deformations (in red); left: top of the dome, right: bottom corner of the dome. Notice the glass facets sliding over each other. NB at scale 1:1 the facets do not slide over each other

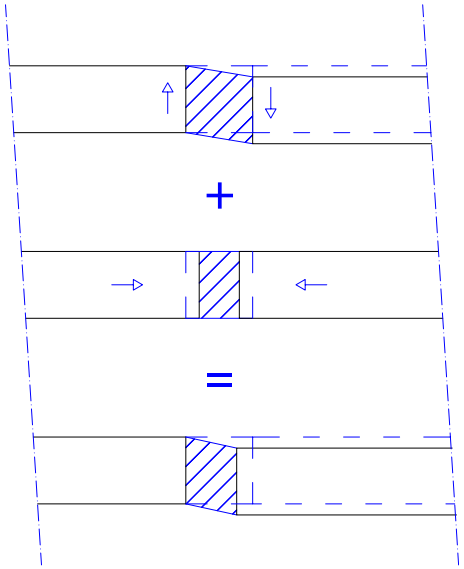

Figure 12.12: The deformation behaviour of the joint.

and therefore the increases combined shear and normal strains.

12.6 Advised properties for the joint

From Figures 12.9 and 12.10 the stiffness requirements for the joint can be derived. It is visible that the bending stiffness is not vital. However a certain bending stiffness is necessary to create a good joint. Therefore it is advised not to let the bending stiffness fall below 5kN. This is a fairly high value, but it can be easily created with the clamping joint proposal.

The shear and normal stiffness are a different story. Both stiffnesses are vital in the behaviour of the joint and the higher they are the better the behaviour of the structure. For

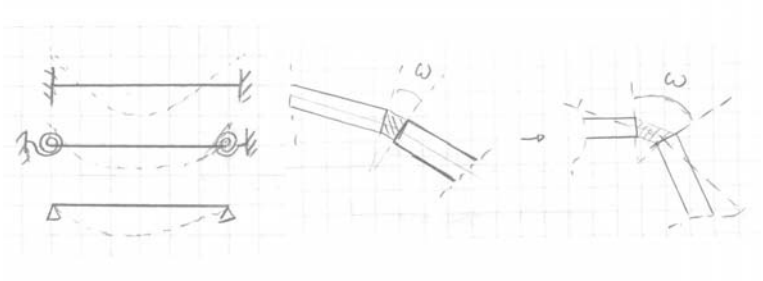

Figure 12.13: Left: influence of the rotation stiffness on the deflection of the glass plates; right: influence of the plate rotation on the deformation of the joint.

the model the shear stiffness is directly coupled with the normal stiffness. In reality this is not necessarily true and therefore it is difficult to see the seperate influence. Therefore it will be interesting to develop a new model where the stiffnesses can be considered seperately. The order of magnitude of the shear stiffness is, however, quite good already.

Figure 12.9 shows that when the joint normal stiffness is around $100N/mm^2$ the load factor starts reaching acceptable values. A value of at least around 4 is necessary for the load factor, since amongst others imperfections have not yet been incorporated in the dome. The corresponding (out-of-plane) shear stiffness is aproximately $25N/mm^2$. This should be kept as a guide line.

The forces that are exerted on the joint in the ultimate limit state are as follows:

Table 12.5: Estimation of forces on the joint in the ultimate limite state

N_x	$\approx$	$-1,6N/mm^2$
N_y	$\approx$	$-0,8N/mm^2$
N_{xy}	$\approx$	$0N/mm^2$
Q_x	$\approx$	$-0,01N/mm^2$
Q_y	$\approx$	$-0,01N/mm^2$

Some other important factors that should be kept in mind when designing or adjusting the current joint design are mentioned:

- Tolerances; the reasons to design for tolerances are two-fold; first, all parts of the structure that are made will have deviations in their geometry. This holds for the glass facets, but also for the joints themselves. Secondly, the erection of the structure will result in in-accuracies and therefore deviations from the orginal designed structure. This means that fitting issues will arise when no tolerances are taken into account.

- Water tightness; the structure will have a separating and a load bearing function at the same time. This means that the water tightness, and perhaps even the insulation, needs to be incorporated in the joint itself. Special care should also be taken in the vertices, where the joint is supposed to have no stiffness. A soft kit butt joint will structurally be a good solution, but aging and fatigue can cause leakage problems.

- Visibility; The transparancy of the structure was one of the starting points in the research of a facetted glass dome. Therefore the visibility and dimensions of the joint should be very important design criteria. In the end it should be considered if it is not more feasible to create a steel frame structure with the glass facets only *stabilizing* the openings instead of fulfilling the full load bearing function. The current design of the joint is still considered slender, refer also to the remarks made in Paragraph 4.3.5.

12.7 Proposition to increase the joint stiffness

Since the current configuration of the joint does not seem to comply with the necessary stiffness to create a stable dome, the design of the joint needs to be changed. The important stiffnesses that need to be improved are the normal stiffness and the out-of plane shear stiffness. In the current geometry the stiffness of the joint is not sufficient.

There are two principles to change the properties of the joint; improving the current design or designing an entirely new joint. In the following both possibilities are discussed and directions to find solutions are given.

There is of course an important note to consider when increasing the stiffness of the joint. The stiffer joint will also attract more stresses to the joint area and local failure should be well considered. Local stress concentrations might affect both the glass as the materials in the joint.

12.7.1 Improving the current design of the joint;

The first possibility to improve the current design is to increase the pre-stressing force exerted on the neoprene by the aluminium strips. The increased force will stiffen the neoprene strips, which are important factors in both the normal as the out-of-plane shear stiffness of the joint. However, this effect is only limited and not likely to be enough to gain the desired stiffness. Furthermore the effect is very hard to predict or analyse because of the non-linear behaviour of the neoprene due to relaxation and creep.

Changing the properties of the designed joint is another fairly small adjustment and can be easily tested. Especially choosing thinner neoprene strips has a large impact on

the resulting normal and shear stiffness of the joint. Tests have shown that it is probably possible to choose a neoprene strip of 1mm. This results in a fairly high normal and out-of-plane stiffness for the joint: $k_n = 94N/mm^2$ and $k_{s,oop} = 257N/mm^2$. These high values are largely created by the increased stiffness of the joint because it is enclosed, see Paragraph H.1.4. It should be investigated whether this increased stiffness is not getting unrealistically large.

If the result is accepted a second problem arises: if the bending and normal stiffness are coupled, the shear stiffness is much different from the calculated value for the designed joint ($257N/mm^2$ vs. $16,8N/mm^2$). This means that the behaviour of the modelled joint is much different from the designed joint, because the stiffness ratios deviate too much.

At the same time the width-thickness ratio of the elements is becoming much distorted. This can give accuracy problems in the results of the finite element model because of large numerical differences in the matrix calculation. The impact of this inaccuracy is expected not to be very large but should definitely be considered.

If these remarks are also disregarded, the resulting load factor is 4.53, see Figure 12.14. This is comparable to the models in Paragraph 12.3, since the values for the normal and shear stiffness are comparable to Model II in Table 12.3.

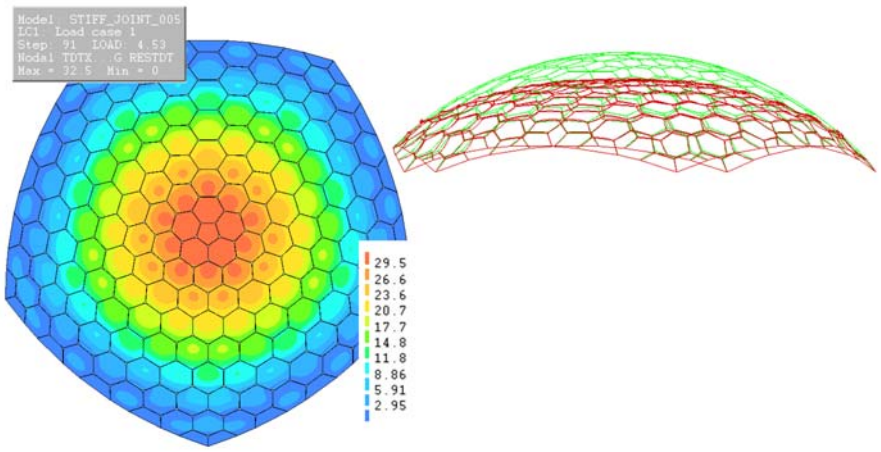

Figure 12.14: Resulting load factor when the joint stiffness is increased due to thinner neoprene strips; $k_n \approx 94N/mm^2$, $k_{s,oop} \approx 257N/mm^2$.

When the first two options do not yield enough stiffness there is another fairly easy way to increase the normal and shear stiffness of the joint. By filling the opening between the glass plates with a rubber-like material, the glass panels will be able to directly transfer their normal stresses between each other, see Figure 12.15. In the old configuration the normal stiffness depended on the shear stiffness of the neoprene strips. At the same time

the in-plane shear stiffness will be slightly increased since the shear deformation of the joint will be countered by the resistance in the rubber filling, see Figure 12.16. This effect will, however, not be very large.

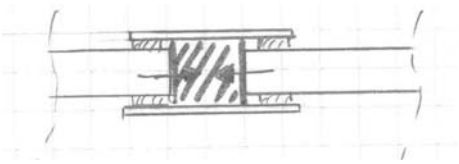

Figure 12.15: Transferring the normal forces from plate to plate.

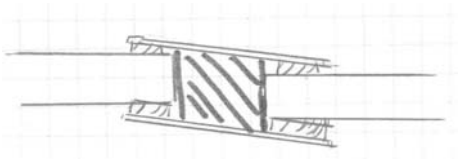

Figure 12.16: The (small) increase in shear stiffness of the joint when filling the joint, due to the limited shear stiffness of the filling.

Filling the opening between the glass panels is not easy with a solid material like neoprene. There has to be contact between the two plates through the filling material; when tolerances are taken into account a solid fill material will need to be available in a range of thicknesses, even when the neoprene can be pressed into place. A good alternative would be a solidifying material which behaves like a rubber after solidification. Good options that have already been used in glass structures are POM and Hilti-hit glues.

An important aspect that should be considered when applying an improved version of the currently designed joint is the angle between the facets. This angle is preferably incorporated in the aluminium strips in the joint. Otherwise the panels will in principle want to be in the same line. Forcing the panels to make an angle with each other will introduce auxiliary stresses in the glass, the joint or both.

12.7.2 Guidelines for designing a new joint

The current joint design has been made with as most important guideline the bending stiffness of the joint. The bending stiffness could not be too high to prevent high stresses in the joint area. However, research by Anne Bagger (Bagger n.d.) showed that the influence of the bending stiffness on the stress distribution is not very high. Some bending stiffness can therefore easily be allowed in the joint. The new starting point for the joint should

therefore not be the bending stiffness, but the normal and shear stiffness. More on this is mentioned in Paragraph 12.6. The forces that are exerted on the joint in the ultimate limit state are

Some interesting ideas for a new joint design can be thought up, for instance:

- gluing elements onto the glass and making the connection between those elements, like in the glass dome in Delft, see Paragraph 2.2. Water tightness might be an issue here, as well as the permanent structural us of glue.
- creating a full rubber (H-)profile that holds both glass panels and at the same time creates the normal stiffness. Tolerance might be an issue here.
- grooves can be created in the edges of the glass panels. This might open up new possibilities for creating a better connection between a joint material and the glass. It is important to investigate the weakening of the glass due to the grinding of the grooves.
- with current techniques it is also possible to laminate elements into a three layer glass laminate. This could lead to a very clean connection with a nicely distributed stress distribution.

12.8 Comparison to a smooth dome

Introduction

There are two reasons why it is interesting to compare the facetted dome structure with a smooth dome structure. First it is interesting what the actual influence of the kinks in the structure are. To make this comparison a facetted structure is modelled in which all joints have been given the same properties as the (glass) facets.

The second investigation is to see the influence of the 'imperfection' that is induced on the facetted structure by the (weak) joints. The joints cause a reasonable deformation of the shape of the structure. Comparing the results of a smooth glass dome with the facetted variant gives a limited insight in this behaviour.

12.8.1 Buckling of a smooth dome of glass

For an estimation of the behaviour of a smooth glass dome a model of half a sphere is used. This model is obtained from B. Peerdeman, Master student at the Delft University of Technology. This model has been created for a Master's thesis on concrete shell structures. For the glass dome only the geometry of the structure has been used.

The model is, as mentioned, half a sphere and had slightly different properties than the main geometry of the facetted shell. The most important difference is the fact that the facetted structure is not based on half a sphere, but only a cap. This leads to a different structural behaviour as well as a different span. Therefore the model has been adjusted to resemble the span and curvature of the facetted dome. This procedure is described in Appendix I.

The loads that are applied are taken from Appendix D. However, the snow load is simplified to a uniform load over the entire structure. The total surface load is therefore $1.76 N/mm^2$, see Appendix]I.
Two different models of the smooth dome will be tested. The first will be a dome structure with a perfect geometry, the second will be given an imperfection at a sensitive location.

1. A perfect dome; the results of analysing a perfect dome structure are expected to be significantly higher than any result seen before in this investigation. The result also shows this. see Figure 12.17. An impressive loadfactor of 61,8 is found.

The deformation pattern that is found is typical for a thin shell structure loaded by a vertical load and supported on hinges. At the top of the dome ripples form. The bottom edge of the structure buckles and the structure fails in a global buckling mode.

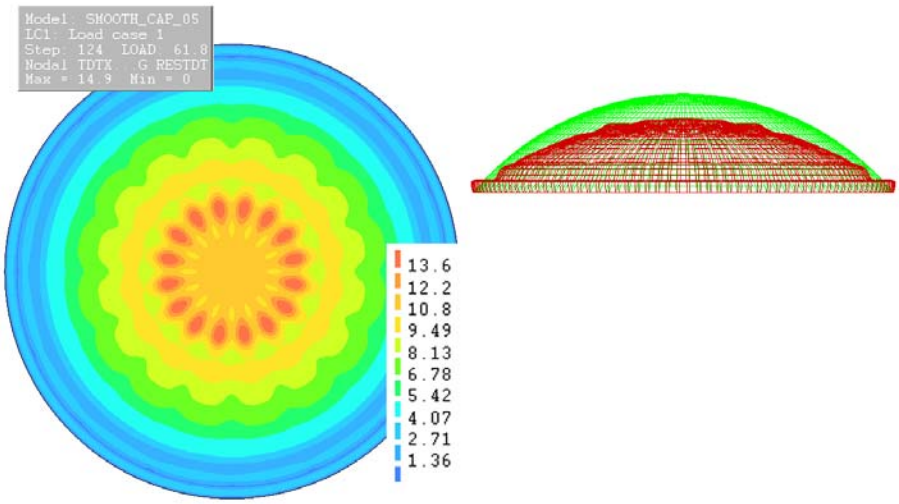

Figure 12.17: The result of the buckling calculation for a smooth glass dome with a perfect geometry.

2. An imperfect dome; in the geometry of the shell top point in the dome is displaced vertically -20mm, see Figure 12.18. The result is a dent-shaped imperfection in the dome at the top. The reason this imperfection is chosen is because this is comparable to a dome

that can deform like the facetted structure with soft joints. The result a buckling factor of 48, see Figure 12.19.

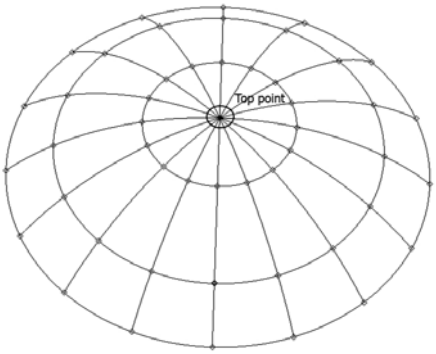

Figure 12.18: Top point in the geometry of the smooth dome is dislocated.

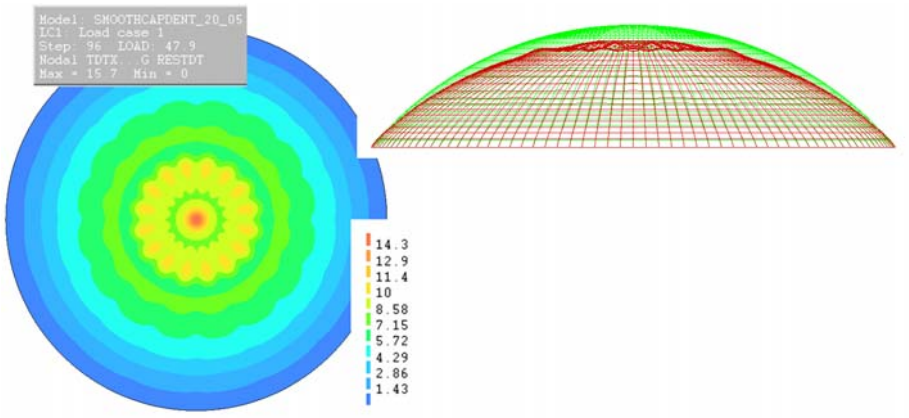

Figure 12.19: The result of the buckling calculation for a smooth glass dome with an imperfect geometry.

12.8.2 Buckling of a dome with 'Glass' joints

The model with the stiff 'glass' joints will have joints with not only the same material properties as the glass facets, but also the same thickness. It is likely that the dome will be much stronger than the dome with the more flexible joints. But at the same time a different buckling pattern is expected, a pattern that is more related to the buckling pattern of the smooth dome that was discussed in the previous paragraph.

Figure 12.20 shows the buckling shape of the dome with glass joints. The buckling factor is an astonishing 57.1. This result is very close to the buckling factor of the smooth

dome. The buckling pattern is made visible by taking the incremental deformations of the last load step. It is interesting to see that the top facet moves up during the last load step and a rippling deformation pattern is created. This buckling pattern is similar to the ripples found in the top of the smooth structure. Interesting to note is also that the bucklnig at the bottom of the edge of the dome is not noticable in the facetted structure. This might be explained by the curved edges at the bottom of the facetted structure. The curves can perhaps generate more sideways stiffness in the plane. The deformation pattern is very much dominated by the local deformation of the flat facets. Due to the fact that the out of-plane forces first need to be transferred to the edges by bending, see Figure 12.21, the deformation are very large compared to the smooth dome.

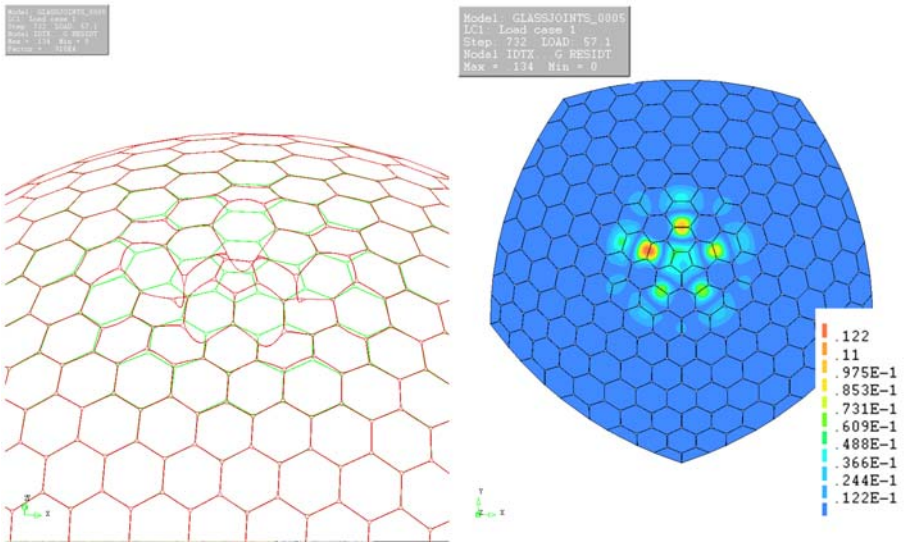

Figure 12.20: The buckling shape of the dome with 'glass' joints.

12.8.3 Comparison smooth and facetted dome with 'glass' joints

The most important fact that can be concluded from this analysis is that the kinks in the geometry certainly have an influence on the buckling behaviour of the dome, but that it is rather small. The final buckling shape is comparable to the buckling shape found in the smooth dome, aside from the deformations at the bottom edge.

The differences with the facetted dome are very well visible when the total deformations, see Figure 12.21, are considered. Because the facets are flat, they are forced to transfer the out-of-plane loads by bending in the facet. This results locally in much larger deformations than in the smooth dome. This behaviour, apparently, hardly influences the buckling load. However, in this perfect geometry the stresses in the facets could be governing before buckling.

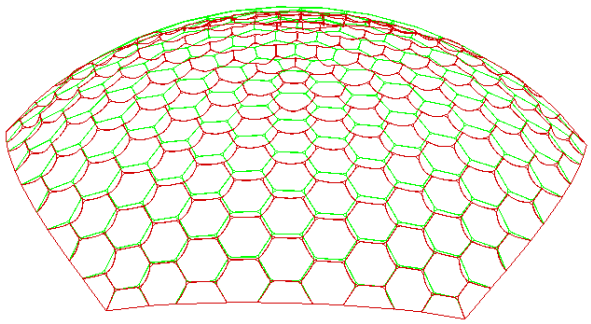

Figure 12.21: The exagerated (20x) total deformation of the facetted dome with 'glass' joints; note that local deformation of the facets is very strong.

12.8.4 Comparison smooth and facetted dome with 'soft' joints

If the behaviour of the smooth dome is compared with the facetted shell structure with flexible joints, see Chapters 8 and 10, it is visible that the deformation behaviour is much different. The facetted shell will not visibly develop the ripples in the top of the dome, but the whole structure will deform relatively smoothly. When the dome buckles, however, the rippling effect does arise, manifesting itself like a rotation of facets, see Chapter 8. The soft joints clearly influence this behaviour. The buckling factor is therefore significantly lower than that of the imperfect smooth dome from Paragraph 12.8.2.

Figure 12.22 shows the load deformation curves for a number of different situations, the smooth dome, the facetted dome with glass joints and the facetted dome with soft joints.

The most important conclusion that can be drawn from this analysis is that it is difficult to compare the behaviour of the facetted structure. Especially when realistic joints are incorporated the influence of the joints themselves become very important. The stiffness of the joint is then a much more important factor than the general shell shape which could be compared to the smooth structure.

12.9 Discussion

The investigation of the stiffness of the joints and its influence on the overall stability and behaviour of the structure yields an alarming result; the current design of the joint is not capable of generating the necessary stiffness. During the preliminary study into the behaviour of the structure the properties of the designed joint were not yet known and therefore an assumption for the stiffness of the joint had to be made. Since it was

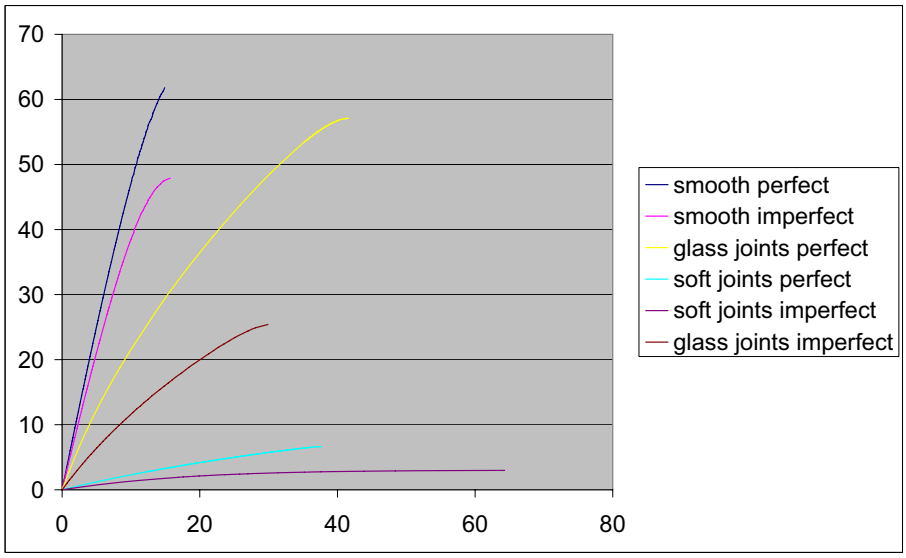

Figure 12.22: A comparison of the three considered dome structures; a smooth glass dome, a facetted glass dome with glass joints and a facetted glass dome with soft joints ($k_m = 1,67kN$ and $k_n = 200N/mm^2$).

expected that the bending stiffness of the joint would be the most important, a realistic estimation of the bending stiffness was used to choose the stiffness of the joint material. However, this unwittingly led to a severe over-estimation of the normal and in-plane shear stiffness of the joint. An investigation into the properties of the designed joint resulted in a re-definition of the joint material and thickness in the model, which had more realistic values. The new joint was, however, not capable of supporting the dome.

The comparison of the influence of the bending stiffness on the one hand and the normal and in-plane shear stiffness on the other hand showed that the bending stiffness actually does not influence the stability of the dome in a great deal. Also the out-of-plane stiffness of the joint did not seem to strongly influence the stability either. The combination of shear and normal stiffness turned out to be decisive. This behaviour is explained by the deformation mechanism inside the joint, where shear and normal strains play an important role, see Figure 12.12.

The joint therefore needs to be improved or re-designed. Recommendations are made to improve the joint, for instance by filling it with a neoprene or similar material. This would result in the possibility for the glass plates to directly transfer normal forces and it will increase the out-of-plane shear resistance of the joint.

Chapter 13

Failure of a single facet in the dome

Introduction

Glass is still considered an almost magical material when it comes to structural use. Building structures where structural glass is a vital part of the main load bearing structure is regarded as risky and needs to be substantiated very well. When designing an overhead glass structure this is even more eminent. The case of the glass facetted dome has a combination of three factors that will make people ask for an increased argumentation of the safety of the structure: glass is used for the main load bearing structure, (structural) glass is installed over head and the structural system is an innovative and seldom used principle.

The first question a person will therefore ask is: What if..? What if a glass facet breaks? This question is of course very valid and is definitely one of the most important questions the structural engineer will need to answer. In this chapter this challenge is taken up and it is shown that the safety of the dome can be ensured during the failure of a facet. The precautions that need to be taken to ensure the safety, like the demands on the joints and the glass, are also discussed.

NB it is very important to note that the buckling factors found in this chapter relate to a different, much lower, load condition than all other analyses in this research. The results should therefore only be interpreted as a safety factor for collapse in case of the failure of one facet.

13.1 Loads during an emergency

In the Building Codes the safety factors for accidental state are different than for the ultimate limit state. When there is a visible failure like the breaking of a facet, the building will be evacuated and the structure will be repaired. Furthermore it is unlikely that the

combination of the absolute maximum loads will coincide with the breakage of a panel. Therefore it is actually valid to remove the safety factors for the structure. For the variable loads a ψ-factor is introduced to lower the value of the non-dominant variable loads even more, since the maximum variable load cmobination does not likely coincide with the accidental situation.

In Figures 13.1 and 13.2 two tables from the European codes (*Eurocode - Basis of structural design* 2002) are shown. Figure 13.1 shows which ψ-factors should be used in accidental load cases and Figure 13.2 shows the value of the ψ-factors for the different load cases.

Table A1.3 - Design values of actions for use in accidental and seismic combinations of actions

Design situation	Permanent actions		Leading accidental or seismic action	Accompanying variable actions (**)	
	Unfavourable	Favourable		Main (if any)	Others
Accidental (*) (Eq. 6.11a/b)	$G_{kj,sup}$	$G_{kj,inf}$	A_d	ψ_{11} or $\psi_{21}Q_{k1}$	$\psi_{2,i}\ Q_{k,i}$
Seismic (Eq. 6.12a/b)	$G_{kj,sup}$	$G_{kj,inf}$	$\gamma_I A_{Ek}$ or A_{Ed}		$\psi_{2,i}\ Q_{k,i}$

(*) In the case of accidental design situations, the main variable action may be taken with its frequent or, as in seismic combinations of actions, its quasi-permanent values. The choice will be in the National annex, depending on the accidental action under consideration. See also EN 1991-1-2.

(**) Variable actions are those considered in Table A1.1.

*Figure 13.1: psi-factors to be used in accidental load cases (*Eurocode - Basis of structural design *2002)*

Table A1.1 - Recommended values of ψ factors for buildings

Action	ψ_0	ψ_1	ψ_2
Imposed loads in buildings, category (see EN 1991-1-1)			
Category A : domestic, residential areas	0,7	0,5	0,3
Category B : office areas	0,7	0,5	0,3
Category C : congregation areas	0,7	0,7	0,6
Category D : shopping areas	0,7	0,7	0,6
Category E : storage areas	1,0	0,9	0,8
Category F : traffic area, vehicle weight ≤ 30kN	0,7	0,7	0,6
Category G : traffic area, 30kN < vehicle weight ≤ 160kN	0,7	0,5	0,3
Category H : roofs	0	0	0
Snow loads on buildings (see EN 1991-1-3)*			
Finland, Iceland, Norway, Sweden	0,70	0,50	0,20
Remainder of CEN Member States, for sites located at altitude H > 1000 m a.s.l.	0,70	0,50	0,20
Remainder of CEN Member States, for sites located at altitude H ≤ 1000 m a.s.l.	0,50	0,20	0
Wind loads on buildings (see EN 1991-1-4)	0,6	0,2	0
Temperature (non-fire) in buildings (see EN 1991-1-5)	0,6	0,5	0
NOTE The ψ values may be set by the National annex. * For countries not mentioned below, see relevant local conditions.			

*Figure 13.2: Values of the ψ-factors for different load cases (*Eurocode - Basis of structural design *2002)*

The two load cases that are considered here are snow-load and self weight. For the

self weight of course no ψ-factor can be taken into account since the load will always be the same. For the accidental situation the total load factor may be set to 1,0.

NB $G_{kj,inf}$ refers to the lower value for the permanent action and $G_{kj,sup}$ refers to the upper value for the permanent action. This is not an issue in this case since the self weight is precise.

Figure 13.1 shows that either $\psi_{1,1}$ or $\psi_{2,1}$ should be applied to non-dominant variable loads. To be on the safe side and since it is the only variable load that is considered it is wise to choose to apply $\psi_{1,1}$. Figure 13.2 then gives for the Danish situation CEN-member, altitude $\leq$ 1000m) that $\psi_1 = 0,2$. In this case, however, the snow load is the only variable load considered and therefore automatically the dominant variable load. A reduction will therefore not be allowed.

The total loads will therefore be: (also refer to Appendix D)

Self weight structure	$p_{g,d}$	$= 1,0 * (0,394 + 0,098) * 10^{-3} N/mm^2 = 0,492 * 10^{-3} N/mm^2$
Snow top facet	$p_{g,d,top}$	$= 1,0 * 0,960 * 10^{-3} N/mm^2$
Snow sector 1	$p_{g,d,1}$	$= 1,0 * 0,946 * 10^{-3} N/mm^2$
Snow sector 2	$p_{g,d,2}$	$= 1,0 * 0,896 * 10^{-3} N/mm^2$
Snow sector 3	$p_{g,d,3}$	$= 1,0 * 0,814 * 10^{-3} N/mm^2$
Snow sector 4	$p_{g,d,4}$	$= 1,0 * 0,679 * 10^{-3} N/mm^2$

13.2 Description of the behaviour when a glass panel breaks

The glass that is used for the facetted dome is laminated glass. The first reason for this choice is that when one glass pane breaks, there will be no pieces falling down because the lamination foil will keep the parts together. An additional effect of the combination of glass layers is that the panel will have a remaining stiffness when a glass layer breaks. If necessary this stiffness can be taken into account when calculating the structure.

It is not sure that all glass layers break at the same time due to an outside impact. However, when all layers of the glass panel break a sagging effect similar to a cloth will occur if toughened glass is used. This needs to be prevented at all time. Strengthened glass will break in larger pieces and will have a remaining stiffness for a short period of time during which the building can be vacated. Therefore a combination of strengthened and toughened glass is advised for overhead glass structures. The implication of this choice is that the strength of the total glass panel is equal to a combination of a toughened and a strengthened glass layer, not two toughened glass layers.

It is also worth mentioning that on the outside of the structure a protective layer of 4mm glass is applied. Therefore, when the dome is struck by an outside blast this panel will be damaged first, with a large chance that both structural panels will survive without being damaged. This effect, however, will not be taken into account when assessing the

Figure 13.3: Breaking of a laminated glass pane; the glass remains together.

safety of the dome.

The structural behaviour that will be taken into account in the model when a facet breaks is that it loses all its stiffness. This is, as explained above, not the exact behaviour of the structure but it represents a coarse but safe approximation.

Because the facet in reality does not totally break and will remain in place, it is important to note that the deflections of this single facet will increase greatly. The joints must therefore be able to cope with the larger rotations of the edges of the glass panel and prevent it to fall out.

13.3 Modelling the failure of a single panel

The loads and the behaviour that are to be modelled have now been defined and the model can be adjusted. The only question remaining is which panel is the governing when failing. Since the integrity of the system depends on every single facet it actually does not really matter which facet is taken out. The magnitude of the stresses is, however, decisive for the buckling stability of the dome. Therefore a facet is chosen where the highest compressive stresses occur in the normal loading situation. Figure 13.4 shows the stresses in the dome in the ultimate limit state. It is visible that the stresses are fairly uniformly distributed for the normal stresses, but the bending stresses are considerably higher in the larger facets four facets from the top pentagon (indicated with an * in Figure 13.4). Therefore one of these facets will be removed from the structure.

13.4 Analysing the new structure

The model is now analyzed in Diana with the same settings as previously used for the non-linear analysis of the full dome. It should be noted, though, that the load is much

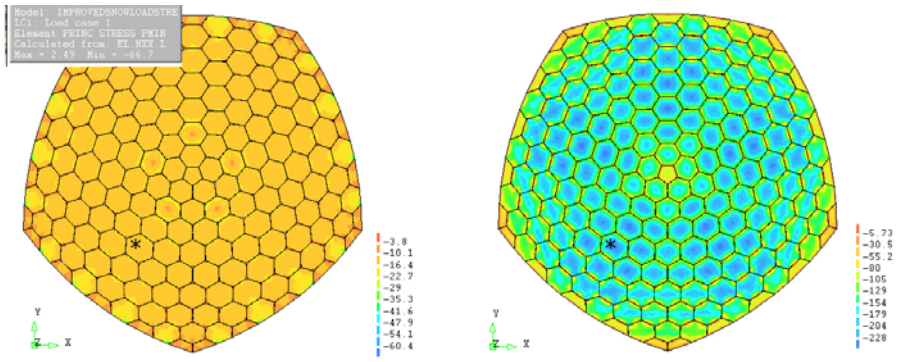

*Figure 13.4: The compressive stresses in the dome; left, normal stresses, right bending stresses; the * indicates the facet with the largest (bending) stresses.*

lower and that the buckling factors found in this analysis should not be compared directly to the buckling factors found in other analyses in this research.

A load step size of approximately 0.5 is used to find the failure load of the structure. The load step is adjusted with a line search method to fairly accurately find the buckling factor even though large load steps are used. The result is shown in the load deflection curve in Figure 13.5. The curve shows that a peak in the curve is reached at load step 8. After this peak the displacement of the node is very large with a decreasing load. This is clearly a form of buckling. Figure 13.6 shows the final total deformations in the structure at failure for load step 8. The safety factor on failure in the model is 3.63.

The result shows that the dome still has a safety factor of 3.63 for buckling when one facet is removed. This is more than enough, especially considering that imperfections will play a minor role since the loss of a single facet is a dominant imperfection in itself.

NB in Chapter 10 a lower load factor than 3.63 was found for an imperfect dome. The reader is, however, reminded that the load conditions for the two models are different. however, even though the two should not be directly compared, it can still be said that the loss of a single facet has quite some impact as an imperfection compared to the patterns used in Chapter 10.

13.5 Implications for the detailing of the structure

As mentioned in Paragraphs 13.2 and A.4, it needs to be prevented for the glass facets to get very large deflections when the glass breaks. Therefore a combination of toughened and strengthened glass is proposed. This results in the same material stiffness but in a lower material strength. This should be correctly investigated when the strength of the dome is checked. Even though the glass panel will not lose all its stiffness when a panel breaks, the deflections will still increase greatly. The rotations at the joints will then

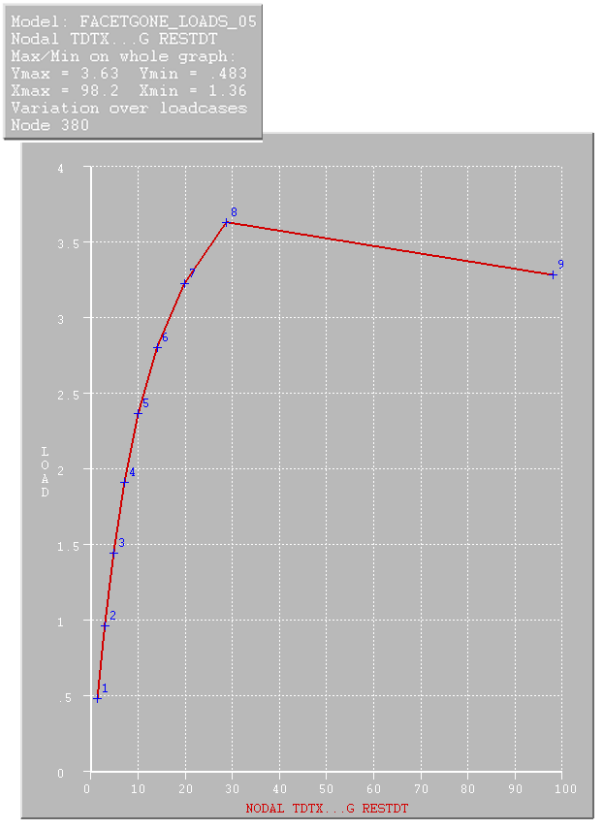

Figure 13.5: The load-deformation diagram for a critical node; especially note the peak at load step 8.

also become much larger. This should not be a problem for the joints, since the joint is designed to cope with rotations and the angle between panels. At the same time a tensile stress will develop in the joints around the broken facet. This is a result from the fact that the lack of stiffness will prevent the facet to transfer the in-plane compressive stresses from the shell action. However, the tensile forces are only developed locally from the self-weight and out-of-plane load on the facet. These tensile forces will be small compared to the tensile stresses that already have to be taken up in the joints. Furthermore, in the current design of the joint the resistance of the joint against pulling forces is equal to the resistance against pushing forces.

A very important aspect is also the replacement of the facet. Since the dome will need to be used also after the calamity, repairing the dome should be possible. In the current proposed design of the joint removing and replacing the joints should not be a problem. A possibility could for instance be to glue the lower parts of the joints to the remaining glass panels and then place the new glass panel on top of them, see Figure 13.7. Hereafter the joints can be closed from the top and the clamping can be achieved. Of course the

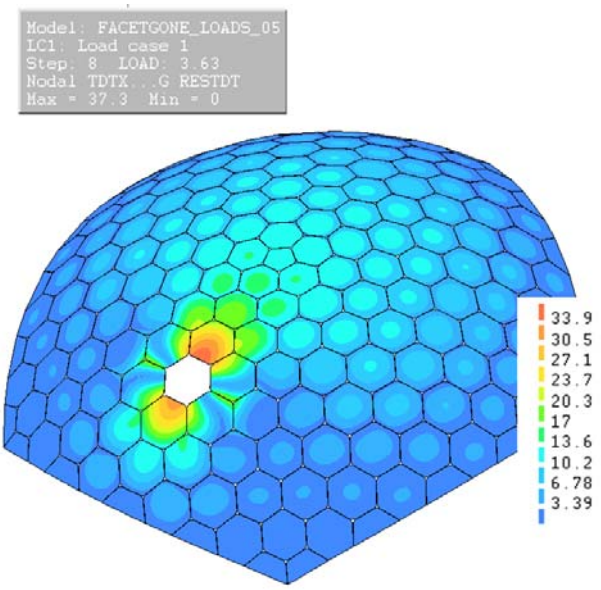

Figure 13.6: The result of the non-linear analysis with one facet removed entirely; step size≈0.5

glass panel needs to be supported until the joint is finished. Combinations with placing only a number of joints before fixing the facet are also possible. In fact the process will eventually be the same as placing the last facet when constructing the dome.

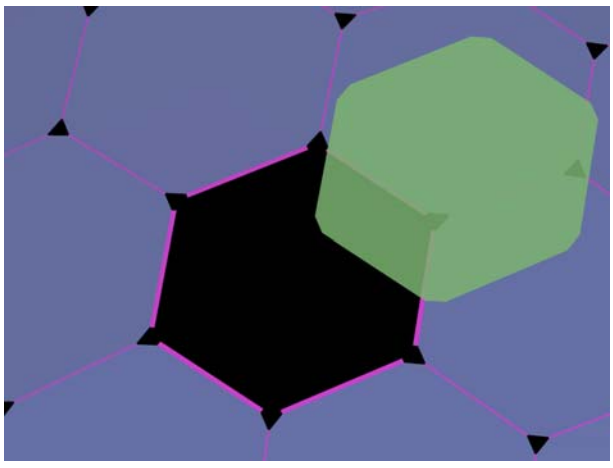

Figure 13.7: Possibility for replacing a facet; the lower part of the joint is glued in place and the glass facet is placed on top. Afterwards the top part of the joint is placed and the clamp tightened. NB the width of the joints is exagerated for a clearer image.

Just placing the facet will, however, not be enough. To make sure the facet fully joins the structural system it can not be placed in a deformed structure. Therefore it will be necessary to lift at least the facets surrounding the hole into a stress-less, their original, position. After placing the facet in the right position, the dome can be released again. The entire dome will react to this lifting and it should be checked to make sure no stress-peaks or unexpected problems arise. The integrity of the dome is likely to make sure that the stresses are redistributed and no real problems are expected.

13.6 Discussion

There will be no problems with the safety of the dome when one critical glass panel breaks. The strength of the dome is of course severely decreased and it needs to be evacuated when the calamity happens. If it is made sure that the glass panel is replaced and the structural behaviour of the dome is fully restored, the dome can be used safely again afterwards.

Chapter 14

Conclusions and recommendations

14.1 Conclusion

The research has shown that structural principle of a facetted glass dome which is safe and stable look very promising. The structural principle works as it should and sufficiently high safety factors are found even when considering strong imperfections.

It is interesting to see that the buckling behaviour of the facetted structure is strongly influenced by the geometrical properties of the facets themselves. Due to the possibility of the facets to redistribute forces in their plane the facets start acting as stiff frames when the load becomes larger. The plates are therefore not governing for the behaviour, but the joints are. This was an important reason to investigate the behaviour of the joint in more detail.

The investigation of the joint and the preliminary design for the execution of the joint lead to an alarming result: the current joint design is not capable of supporting the structure. Initially the bending stiffness and the reduction of peak stresses were thought to be the most important aspects of the joint. This were the main considerations when designing the joint. The investigation, however, led to the conclusion that not the peak stresses but the buckling load is governing, which is strongly influenced by the normal and out-of-plane shear stiffness of the joint. Therefore, it will be necessary to re-evaluate the joint design and create a design with a higher normal and shear stiffness.

The imperfection sensitivity of the structure is an important issue. The total safety factor shows a significant reduction of approximately 55%. As imperfection shape the buckling shape of the perfect geometry is used with an amplitude of 20mm. This is the shape of the first failure mode of the structure, which makes it a very unfavourable imperfection shape. Therefore it represents an upper boundary. Perhaps a thorough investigation of the construction process can lead to smaller imperfections, but it is advised not to take this issue lightly.

When considering the material of the glass facets it turns out that, as could be expected, decreasing the E-modulus influences the overall stiffness of the dome significantly. However, the reduction is not proportionally corresponding to the overall stiffness. When the glass is relatively stiff, the influence of a small stiffness reduction of the glas on the overall stability is much smaller than when the original glass stiffness is already relatively low.

For the structure it means that it is interesting to investigate the creep behaviour of the interlayer between the glass layers in the laminated glass. It is recommended to use a fairly stiff interlayer, like Sentry Glass Plus, which has a relatively low creep. This will greatly enhance the cooperation between the glass layers and therefore the stiffness of the dome structure.

The robustness of the structure has been investigated by removing a critical facet from the structure. The structure responds to this omission by redistributing the forces around the opening. Since the loss of a facet is an incidental load case, the load has been reduced. The damaged structure is still able to withstand over 3,5 times the representative load by dead weight and snow. This shows that the structure is sufficiently robust when losing a single facet.

Replacing the facet and re-establishing the flow of forces in the dome should not pose large problems. The procedure to replace a facet does not need to be very different from placing the last facet during construction. Howevr, in order to re-install the original flow of forces it will be neccessary to compensate the deflections of the structure. This might induce peak stresses in the structure.

To conclude this research it is important to state that even though the structure is at this time not yet ready to be built and more research is still necessary, important steps in the direction of realizing a facetted glass dome have been made. Considering the experience with shell structures and their sensitivity it is advisable to check the current result with a physical model or a second FEM-programme.

The results of the investigation show that the combination of laminated float glass with the principle of a plate structure is a very promising concept for the future.

14.2 Recommendations

In this paragraph a number of recommendations for further analysis are proposed. The recommendations reflect important aspects that have been identified, but not yet analysed in this project.

14.2.1 Joint design

As has been established in the investigation into the stiffness of the joint, see Chapter 12, the current joint design does not fulfil the demands. Therefore the joint design needs to be adjusted or a new design needs to be developed.

The important aspects for the joint will be an increased normal and out-of-plane stiffness. Recommendations for improving the joint are given, but it is not yet investigated whether it will be possible to create the necessary stiffness using these recommendations.

At the same time it should be noted that a stiffer joint will attract higher stress levels. It should be carefully investigated what the influence of the increased local stresses around the joint will be.

14.2.2 Influence of the finite element programme

As the investigation in Chapter 7 showed, DIANA can not entirely follow all realistic deformations when the deformations become very large. This is caused by the fact that no non-linear terms are taken into account in the calculation of the deformations. Since the deformations in the current models of the glass facetted dome are relatively small the influence of this simplification is also small. To be sure about the correctness of the results it is strongly recommended to also test the structure in another finite element program which for instance takes some of the non-linear term into account.

Also the possible problems with shear and membrane locking have not been ruled out entirely. Their occurrence is unlikely and their influence is therefore not expected to be large. By testing the structure in different finite element programmes this can be ruled out more decisively.

Another good way to check the behaviour of the model compared to the real structure is to create a physical (scale) model. If the scale model is correctly built it will give a realistic insight in the behaviour of the dome.

14.2.3 Imperfections

In Chapter 10 it is shown that imperfections have a significant impact on the stability of the structure. In this research the magnitude of the imperfections is estimated in the order of the glass thickness. This seems like a plausible but somewhat high estimation. The imperfection sensitivity does show that it is eminent to analyse the future construction method and the accuracy it encompasses. This way the expected imperfections can be incorporated into the analysis of the structure.

14.2.4 The construction process

The manner of erecting a glass facetted dome is a very important factor in designing the structure itself. The dome of course needs to be stable during the entire construction period. A possibility is to support the entire structure on a secondary structure, like scaffolding. This will result in a large temporary structure which needs a very high degree of precision. To prevent such a costly structure it will be interesting to investigate a (partly) unsupported structure during a sequence of construction phases. A short discussion on this subject can be found in Paragraph 10.4. Furthermore, it will be important to assess if the necessary accuracy can be reached when the structure is not supported at all times. The deformations will be fairly large when the structure is not completed yet, see also Chapter 13. These deformations might interfere with creating the desired geometry of the structure.

14.2.5 Support conditions

In the models in this Master's thesis the support conditions for the dome structure have been idealised. The structure is supported in vertical direction and all rotations are allowed. This might not be achievable in a real structure. The impact will be that introducing restraints at the edges will lead to increased local stresses. The influence on the stability of the structure might also be significant.

Added to this is the possibility of settlement differences. A settlement difference can induce auxiliary stresses in the dome and decrease the load bearing capacity.

14.2.6 Load conditions

In this research only symmetric load cases have been investigated. Asymmetric loads like wind may result in a different decisive load condition for stability. This will need to be investigated before a structure like this can be built.

Furthermore, it should be investigated how the structure reacts to dynamic load cases. A slender structure like this might be very sensitive to wind induced vibrations. When the structure is built in a seismic zone, dynamic loads will be even more important.

14.2.7 Parameter studies

A number of parameter studies are recommended which can help a designer to understand the influence of changes to the design.

Thickness of the glass

The thickness of the glass is a parameter that can be easily changed. A logical thought is that the stiffness of the dome decreases significantly when reducing the thickness of the glass. This was also shown in Chapter 11. It was, however, also visible that the influence of the glass stiffness is not proportionally corresponding with the stiffness of the dome. It will be interesting to identify conditions where increasing the thickness of the glass has little influence. Under these conditions it might be more important to look at other design parameters to influence the stiffness of the structure.

Dimensions of the facets

The dimensions of the facets have been arbitrarily chosen in this investigation. In reality the choice for a certain dimension of a facet depends on a number of aspects, like economy, structural use and aesthetics. It will be very helpful for a designer to have more information on the influence of the dimensions of the facets. This research should of course not be limited to solely structural aspects.

Span of the dome

When considering alternatives for spanning a space it is important to know what the capabilities of the different alternatives are. To be able to make this consideration the possibilities of the glass facetted dome needs to be investigated. Not only the maximum span is of interest, but especially the relationship between aesthetics, (structural) span and economics is interesting to a designer.

Geometry of the structure

(Glass) facetted structures are not just possible as a dome structure, but also variant shapes can be created, see for instance the work of Henrik Almegaard (Almegaard 2003). Also different geometric patterns can be investigated, see Ture Wester (Wester 1990); as long as all vertices are three-way, the structure will behave as a plate structure. These geometry changes should be investigated as separate designs. The lessons from the more straight forward dome will, however, be useful for starting a new design as well.

For a parameter study it will be a good idea to look at the influence of making a higher or a lower cut in the sphere when defining the dome. This is fairly easy to obtain and will give insight in the possible behaviour of deviating geometries as well as in the behaviour of the dome.

14.3 Important notes about the modelling and its implications

Aside from earlier mentioned aspects of the design, a number of important aspects about the model that is used will be high-lighted in this paragraph. Their influence needs to be considered when using and judging the model.

- The finite element mesh in the model is fairly coarse because it is intended to investigate the overall behaviour of the structure. For detailed stress analyses it will be necessary to use a different model or to (locally) refine the model.
- The vertices have been cut off to triangles in this model. In reality the glass facets will stretch to the vertices and a closure has to be made to attain water tightness. The influence of this approach will need to be assessed in a more detailed stress analysis. For the overall (stability) behaviour it is not expected to have a significant influence.
- The behaviour of the joint is simplified in the model. This might need to be corrected in a future study.
- As already mentioned in paragraph 14.2.2, the current DIANA-model does not fully comply with the true results for large deformations. It should be investigated in more detail whether this influences the results.

Appendix A

Glass

Introduction

Since the invention of glass over 5000 years ago it has always been a mysterious and awe-inspiring material. Through the ages it has developed from an opaque, but with rather beautiful properties when coloured and polished, into a high tech material shielding persons from the influences of the sun and rain and allowing us to see clearly.

In this chapter the properties of glass through the ages will be discussed, ending with a focus on the structural possibilities and uses of glass nowadays.

Starting with Paragraph A.1 the earliest history of glass will be discussed leading up to modern production processes. Next, Paragraph A.2 will discuss the current production processes into more depth, including the restrictions the different production processes will place on glass elements. The different ways of treating and strengthening glass will be considered in Paragraphs A.3 and A.4. Paragraph A.5 will then go into the properties of the material glass itself. Finally conclusions will be drawn from the preceding Paragraphs in Paragraph A.6.

A.1 The history of glass

Glass is as old as the earth itself, found in the form of obsidian. Obsidian is a volcanic glass which is formed when lava solidifies in a very short period of time. When lava solidifies this quickly the molecules can't crystals and will be orientated as in a liquid. This state is characteristic for glass. Obsidian is opaque and comes in different colours depending on the pollution in the material.

The first man-made glass is dated back to around 3000 B.C. in Mesopotamia, approximately the current Iraq (see Figure A.2). In these times the glass was merely used as small coloured beads for decoration. It took another thousand years before it became possible

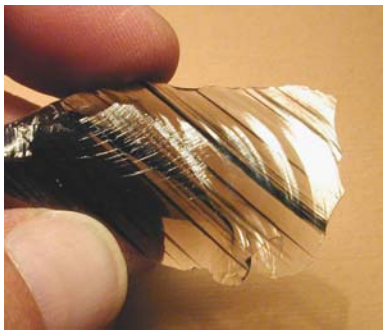

*Figure A.1: A piece of the oldest glass in the world; obsidian. (2007*d*)*

to create hollow glass objects. These objects were still opaque, but very colourful.

*Figure A.2: Mesopotamia, the probable birth place of the first man-made glass. (2007*e*)*

Around 50 B.C. a giant step was made in the development of glass: the glass blowing process. Using a short steel rod with a diameter of 10mm a glowing ball of glass was blown up to form hollow glass vases and glasses. This process made it possible to produce glass objects much quicker than ever before and glass became available to a much larger part of society. The glass blowing process is still used today.

The Romans were the first to develop glass panels to cover window openings. In the ruins of Pompeii glass panels have been found measuring up to 0,5 by 0,7m which is an extraordinary large size for the time. After the decline of the Roman Empire, however, much of the knowledge was lost and it took until the 11th century before there were any new developments on the production of glass panels. Different techniques based on the glass blowing process were developed, like cylinder glass, crown glass or cast glass. All methods remained, however, very laborious. Different mechanical systems were later

developed, but in 1952 the float glass principle was invented by Sir Alastair Pilkington of the Pilkington Brothers Company. This process made it possible to produce large quantities of very high quality glass.

A.2 Modern production of glass

After the invention of the float glass process the world was taken quickly by this new industrial process. Nowadays, almost six decades later, the process is still used as the main production method for glass panels in the world. The principle of the process has hardly changed since its introduction and can now create glass panels with a thickness varying between 0.4mm to 25mm. The most common thickness is, however, 4mm.

The process is shown in Figure A.3 and starts with creating molten glass and (continuously) pouring this onto a shallow bath of molten tin. The molten glass will float on the tin, which is obviously where the process got its name, and spreads out under gravity to form a level surface. The solidifying ribbon of glass is drawn off from the bath and the thickness of the glass can be controlled by adjusting the draw speed. The glass will then be cooled down in a controlled way (annealing) and the finished product will have polished surface with virtually parallel surfaces.

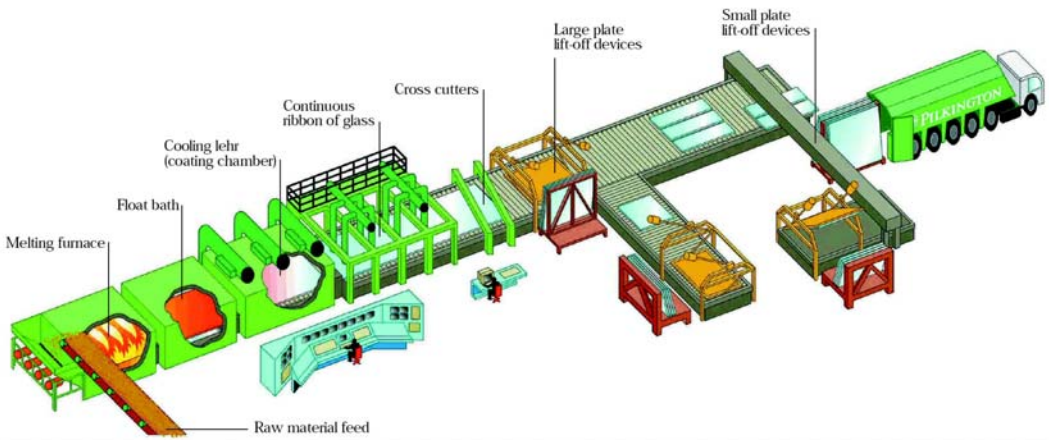

Figure A.3: The float glass production process. (2007f)

A float plant usually operates 24/7 for up to 15 years and can produce about 6000 kilometres of glass per year. The inherent problem with the process is, however, that large losses are created when the plant has to switch to a different glass thickness, colour or type. A small calculation example shows this clearly; when a glass plant is producing 1150m glass per hour and it has to change its thickness from 4mm to 5mm, this will take

about 45 minutes. The almost 900 metres of glass produced during these 45 minutes will need to be considered as lost. It will of course be recycled.

Changing of the composition of the glass, for instance to change the colour of the glass, can take up to four days. It is obvious that a loss of about 300.000m2 of glass (1000m/hour, 3m wide) is not acceptable and changes of glass composition are therefore very rare. Coloured float glass is therefore only produced in a limited range of colours. Even more extreme is the fact that the different colours of glass are nowadays in different parts of the world, for instance green glass coming from Germany and grey and bronze-coloured glass from the British Pilkington factories.

The maximum width of float glass is 3m, while the length is theoretically infinite. This implies that the maximum diagonal of the glass facets can be three metres. However, to be able to efficiently produce pentagonal and hexagonal plates the maximum dimensions are probably smaller. An example is given in Figure A.4. This subdivision leads to an effective width of less than 1,7 metres.

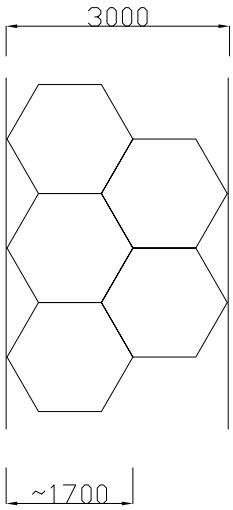

Figure A.4: Subdivision of a strip of float glass from a plant.

Also the structural behaviour of the plates is important, since the plates will need to transfer their own loads by bending to the rest of the structure. However, in the research of T.V. Isgreen (Isgreen 2007) plates with a width of 2 metres were modelled. This dimension proved not to be a problem for the bending stresses in the plates.

A.3 Toughened glass

Introduction

To counteract the vulnerability of glass for tensile stresses, a number of techniques have been developed to introduce compressive stress in normal float glass. This creates the possibility to introduce higher stresses in the glass. In this paragraph a number of the most common techniques will be discussed.

Many bus stops are clad with the so-called toughened glass. As everybody probably knows, it breaks into hundreds of small fragments when the glass is broken. These small fragments are light weight and have relatively blunt edges. This has the advantage that it is safer than the large fragments developing when a normal glass pane breaks.

There are a number of different processes to create toughened glass. The most common is thermal toughening, but also a chemical toughening is possible.

A.3.1 Thermal toughening

A thermally toughened glass pane is produced by first heating the glass to a temperature of 650 degrees Celsius and then cooling the glass down at the surface by using air cannons. The outside will now cool down much quicker than the inside of the glass, leading to tensile stresses in the outer layer. However, when the inside of the glass cools down subsequently, the stress distribution will change again and a compressive stress will remain in the outer layers and a tensile stress in the inside of the glass. The resulting (parabolic) stress distribution is shown in Figure A.5.

An important aspect of thermally toughened glass is that it starts warping due to the internal stresses. This has consequences for the laminating (gluing) of this type of glass. When nickel-sulphur (NiS) enclosures are present in the glass, the glass can suddenly break when exposed to high temperatures. The glass therefore needs to be checked for these enclosures after the toughening process.

As already mentioned, toughened glass breaks instantaneously over the entire surface, leading to small, blunt shards. The cause is that when a crack propagates in the tensile area of the glass, the strain energy that is collected in the glass will suddenly be released. This is also a reason that toughened glass can not be cut, so every plate needs to be prepared to size and with all necessary holes before toughening.

When the cooling process is slowed down, less stresses will arise in the glass. The result is so-called thermally *strengthened* glass (or semi-toughened), which breaks in much larger pieces than toughened glass. When the glass is used in laminated glass, the bonding and residual strength will be much higher. The maximum stress levels that can be allowed are of course lower than in toughened glass.

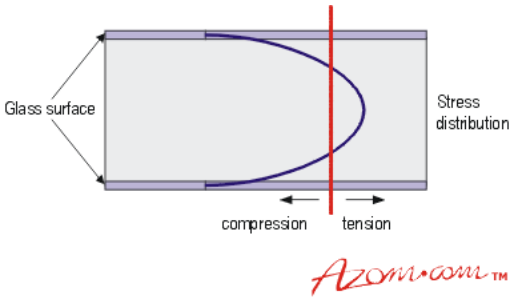

Figure A.5: The stress distribution within an unloaded thermally toughened glass pane (2007g).

A.3.2 Chemically toughened glass

The process of chemically toughening is very expensive and is most commonly used to toughen thin glass. The principle is based on replacing the sodium ions with the larger potassium ions by submersing the glass in a bath containing a potassium salt at 450 degrees Celsius. When the sodium ions in the glass are replaced by the potassium ions, the potassium will wedge into the openings left by the smaller sodium ions. The glass will therefore be very evenly toughened, without any warping effects. Due to the high costs it is not often used in structural applications.

A.4 Laminating glass

Introduction

There are two main reasons to laminate glass for structural applications. The first is to reach sufficient thickness for the structural element, because glass can only be produced in set thicknesses. The second reason is to increase the safety of the glass, where for instance one glass pane/layer can fail without failure of the total structure. Another very important safety aspect is holding the glass together when one layer breaks.

In general laminated glass is regarded as two or more layers of glass interconnected by a foil. It is, however, also possible to glue laminate glass panes. Both types of lamination will be shortly addressed here. In lamination both float glass and toughened glass can be used. The glass can of course still break, but when it does the inter layer will serve as a bridging material between the cracks. This means the structural capabilities of the glass still partly remain, while at the same time it is warning that replacement is necessary.

When laminated glass is produced in a good quality, it will have the appearance of a solid pane. The edges of the glass can, in the case of float glass, be sanded and polished afterwards in order to make the different layers almost invisible.

A.4.1 Laminating with foils

When glass is laminated using a foil, the glass panes are 'glued' together under a high pressure and temperature in an autoclave. These autoclaves generally can handle maximum dimensions of 2,5 by 3,6m. When larger pieces are demanded glues need to be used instead of foils. An often used foil is Poly Vinyl Butyral (PVB) foil. It was originally developed for the car industry and it is produced by stacking a number of layers of glass with PVB foil in between. For structural purposes the PVB foil has some specific characteristics to take into account:

1. the material has high creep behaviour, especially when loaded in shear, see Figure A.6

2. the softening temperature lies around 55 degrees Celsius, so **within** the use temperature

3. the foil can not take up long term loads due to creep, so the plates will not cooperate for the long term loads

Especially due to the low softening temperature this material is not suitably for over head applications, since the foil will not be able to keep the glass together when one of the panes fails.

Research has led to a new type of foil, a so-called ionoplast interlayer, currently marketed by the firm Dupont under the name SentryGlass Plus. This foil has been originally developed for storm (tornado) and burglary proof glazing and has as advantages that the softening temperature lies around 75 degrees Celsius (van Heusden 2005) and it has a much greater stiffness than PVB foil, see Figure A.6. The foil therefore has much less creep problems as well as the capability to transfer greater loads.

Also, compared to PVB, there will be little deflection and a good hysteresis (self healing capability) after the development of the first cracks. The main characteristics for the structural use of SentryGlass Plus foil:

1. low creep behaviour

2. the softening temperature lies around 75 degrees Celsius, which is outside the use temperature

3. the material is relatively stiff

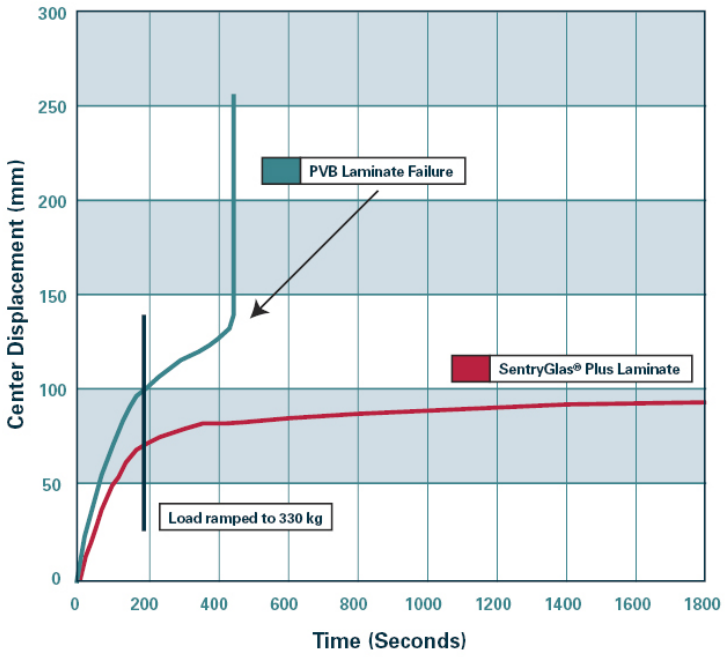

Figure A.6: Creep behaviour of different laminates. (du Pont de Nemours & Company 2005).

When toughened glass (see Paragraph A.3) is used the glass will break into a large amount of small fragments. This means that even though the foil can keep the glass layers together, the stiffness of the plates will be gone. The plate will start hanging through like a cloth. To prevent this behaviour, often a combination of toughened and strengthed glass is often used. The larger fragments of the strengthened glass will then be able to maintain some stiffness for a short period fo time.

A.4.2 Glue laminating

The greatest structural advantages of using glues for laminated glass panes are the very low creep and the high stiffness of the connection. However, this also creates the greatest weakness of the method. Since the connection between the panes is so strong that so much energy will come free when a layer breaks, a large chance exists that both panes will fail and large pieces of glass will fall down. This will need to be addressed in the design by an extra safety factor.

Another danger in the use of glue is that the laminating process is carried out manually which can lead to the enclosure of small particles, possibly causing cracks in the glass.

Finally it is worth mentioning that it is not necessary to use an autoclave for producing glue laminated glass. The size of the glass elements can therefore be much larger.

A.4.3 Conclusions

A number of aspects are important for the glass used in a facetted glass dome, of which the following are considered the most important:

- Dimensions of the facets
- safety (overhead use)
- low creep (loads are for a great deal in plane)

ad. 1 The dimensions of the facets have an absolute maximum of 3m in diameter. This would mean that an autoclave is not possible. However, the facets will need to transfer bending stresses to and the division of the 3m wide strip of float glass is therefore advisable. This will lead to dimensions of up to 1,6m (see Paragraph A.2). It will therefore be no problem to use an autoclave.

ad. 2 The safety aspect is very negative when using glue lamination, since the failure of one pane in the lamination can lead to the failure of the other panes as well. This is unacceptable for overhead use, especially structural use. PVB foil lamination is also not suitable for over head use, since the softening temperature of the foil is too low. This can be solved by using Sentry Glass Plus foil.

ad. 3 The glue laminates are the stiffest and have the least creep. PVB foil, on the other hand has quite bad properties considering creep. The Sentry Glass Plus foil has a good creep behaviour on the long term.

Based on these three aspects it is thought that Sentry Glass Plus is the most suitable type of laminated glass to use in a facetted glass shell structure.

A.5 Structural properties of glass

Introduction

There are a number of material properties that are important for the design of a facetted glass shell structure. The properties of glass will therefore be dealt with in this paragraph. First the strength of glass will be discussed, to know the maximum stresses that can be allowed. Hereafter the other material properties are shown and their influence discussed.

A.5.1 The structural strength of glass

The allowable stresses in glass are for a great deal dependent on the condition of the glass surface. Theoretical values for the tensile strength of glass are much higher than the actual stresses at which failure occurs. This is because theoretical values are mostly based on the chemical bonding between the molecules, while microscopically small cracks are not accounted for. The propagation of cracks in glass is very quick and a sudden failure will occur when the stresses are too large, because the material has almost no deformation capacity before failure. Figure A.7 shows the influence of damages on glass, translated from (van Heusden 2005). It is important to also consider aging and damaging of the glass due to for instance small particles in the air. Especially glass exposed to the elements outside will be damaged by combinations of wind and dust etc. This will lead to an increase in the presence of very small scratches on the surface of the glass and consequently a decrease in the structural strength of the glass. A suitable solution to prevent this damage is to use a sacrificial glass layer ($\tilde{4}$mm) which does not fulfil a structural function.

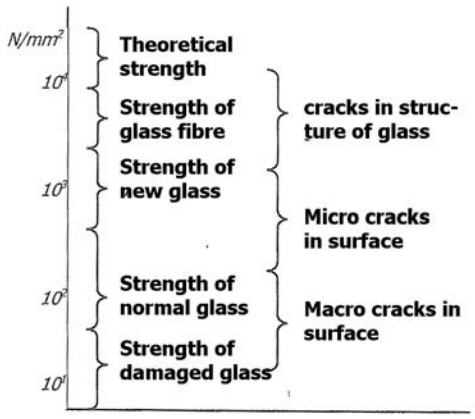

Figure A.7: Influence of damages on the tensile strength of glass (van Heusden 2005)

The bending tensile strength of glass is described in the Dutch codes (NEN2608-2 2007). It is proposed to use the following method from these codes to estimate the bending tensile strength of glass:

Normal float glass:

$$f_{m,t,u,d} = \frac{f_{g,k} * k_b * k_e * k_{mod}}{\gamma_m} \tag{A.1}$$

Thermally hardened glass:

$$f_{m,t,u,d} = \frac{f_{g,k} * k_b * k_e * k_{mod}}{\gamma_m} + \frac{f_{b,u} - f_{g,k}}{\gamma_v} \tag{A.2}$$

The values found for the bending strength are suitable for glass loaded out of plane. This is mostly the case for the bending stresses in the glass panes in the facetted shell. The in plane stresses are expected to be low and mostly in compression. An important factor is k_{mod}, which takes into account the duration of the loads. The value for the bending tensile strength is therefore subdivided in four categories:

1. self weight (≈50 years)
2. self weight + momentane value loads middle long term (≈1 month)
3. self weight + extreme values loads middle long term (≈2 days)
4. self weight + extreme values loads short term (≈5 seconds)

With the values for the different coefficients found in (NEN2608-2 2007), for this application the bending tensile strength is as follows:

For normal float glass:

1. $f_{m,t,u,d} = 7,25N/mm^2$
2. $f_{m,t,u,d} = 11N/mm^2$
3. $f_{m,t,u,d} = 13N/mm^2$
4. $f_{m,t,u,d} = 25N/mm^2$

For thermally strengthened glass:

1. $f_{m,t,u,d} = 25,1N/mm^2$
2. $f_{m,t,u,d} = 28,9N/mm^2$
3. $f_{m,t,u,d} = 30,9N/mm^2$
4. $f_{m,t,u,d} = 42,9N/mm^2$

For thermally toughened glass:

1. $f_{m,t,u,d} = 60,8N/mm^2$
2. $f_{m,t,u,d} = 64,6N/mm^2$
3. $f_{m,t,u,d} = 66,6N/mm^2$
4. $f_{m,t,u,d} = 78,6N/mm^2$

NB the numbers refer to the load duration

The compressive strength of glass has not been investigated in much extent yet. Usually the compressive strength is not the governing factor in the failure of a glass structure. Glass structures usually fail due to reaching the maximum tensile stress or instability. This is also expected for the facetted glass dome. The compressive strength of glass will therefore not be investigated any further at this time.

A.5.2 Other properties of glass

In the European building codes (NEN-EN572-1 2004) an overview is given of the properties of glass. The properties refer to basic soda lime silicate glass products, which is the most commonly used type of glass for float glass. Figure A.8 gives an overview of the properties of glass.

Table 1 — General characteristic values

Characteristic	Symbol	Numerical value and unit
Density (at 18 °C)	ρ	2 500 kg/m^3
Hardness (Knoop)	$HK_{0,1/20}$	6Gpa
Young's modulus (modulus of elasticity)	E	7×10^{10} Pa
Poisson's ratio	μ	0,2
Characteristic bending strength	$f_{g,k}$	45 x 10^6 Pa [a]
Specific heat capacity	C	$0{,}72 \times 10^3$ J/(kg·K)
Average coefficient of linear expansion between 20 °C and 300 °C	α	9×10^{-6} K^{-1}
Resistance against temperature differential and sudden temperature change		40 K [b]
Thermal conductivity	λ	1 W/(m·K)
Mean refractive index to visible radiation (380 nm to 780 nm)	N	1,5
Emissivity (corrected)	ϵ	0,837

[a] The characteristic bending strength shall be used in conjunction with the design method given in prEN 13474.

[b] Generally accepted value that is influenced by edge quality and glass type.

Figure A.8: Properties of soda lime silicate glass (NEN-EN572-1 2004).

For this thesis especially the density and the Young's modulus are of interest.

A.6 Discussion

In the facetted glass dome the choice of glass is highly dependent on the resulting stresses. It will be necessary to use laminated glass, at least for safety issues. The recommended type of lamination is the Dupont Sentry Glass Plus foil or alike. The low creep and high stiffness in a large range of temperatures are necessary to be building a safe over-head glass structure.

An often used safety measure is to have an extra outer layer of glass added to the glass panes. This outer layer will have no structural function but will make sure that the structural glass will not be damaged by wear due to a combination of wind and particles in the air. The thickness of the layer can be around 4mm, resulting in an extra dead load of about $10kN/m^2$. This dead load should be accounted for in stress models.

If normal float glass is strong enough to deal with the bending stresses in the dome, it should be used since it is the cheapest glass Also the fact that it breaks in larger pieces is better for the bonding when one of the layers breaks. If the stresses become higher it will be possible to use toughened glass, however, more attention should be paid to the strength of the panels after failure of one layer. A combination of thermally strengthened glass and toughened glass is also an option. When both panels break the bonding in the thermally strengthened glass will be higher than when two toughened glass panels would have been used.

Appendix B

Theory of smooth shells

Introduction

In this chapter the theory of smooth shells will be discussed. The focus will lie on understanding the structural behaviour of the shells in order to better understand the characteristics of a facetted shell with approximately the same shape. Because a dome shape is chosen for the facetted shell structure, the theories on shells of revolution is at the heart of this chapter.

Paragraph B.1 will deal with the membrane theory for shells of revolution. Next the bending theory for such shells is discussed in Paragraph B.2. With these two Paragraphs a good idea is developed about the behaviour of domes under different load conditions. The subject of this thesis focuses on the stability behaviour of a facetted dome. That is why Paragraph B.3 will deal with the buckling behaviour of smooth domes. Finally Paragraph B.4 will discuss the basics of the finite element method for shell structures.

B.1 The membrane theory for shells of revolution

The membrane theory assumes, as the name already states, that only in-plane membrane forces are present in the shell to achieve equilibrium. The membrane theory holds for load cases where the loads are distributed over vast areas of the shell, such as water pressure in a vessel or wind loads. It is important to note the four basic assumptions that are made to comply with the membrane theory ((Gibson 1965)):

1. the shell is homogeneous and isotropic
2. the thickness of the shell is small compared to its radius of curvature
3. the bending strains are negligible and only strains in the middle surface are considered

4. the deflection of the shell due to the applied loads is small

When assumptions are taken into account, the schematic representation of a infinitesimal part of the shell is shown in Figure B.1. This part needs to be in equilibrium, which gives three equations for the equilibrium (Jawaad 1994):

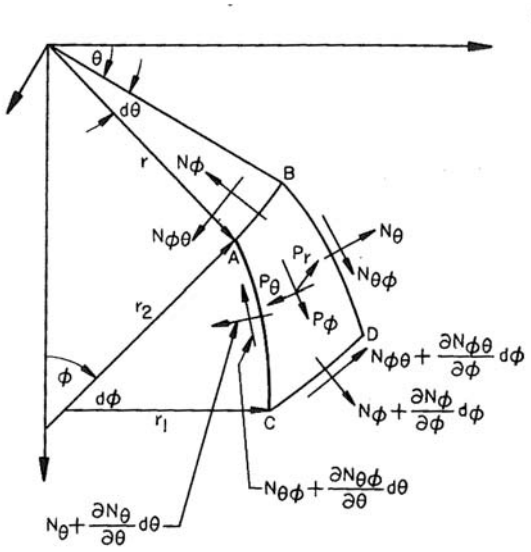

Figure B.1: An infinitesimal part of a shell with all forces considered in the membrane theory, from (Jawaad 1994).

1. The summation of forces parallel to the tangent at the meridian:

$$\frac{\delta(r*N_{\phi})}{\delta\phi} - r_1 * \frac{\delta N_{\theta\phi}}{\delta\theta} - r_1 * N_{\theta} cos(\phi) + p_{\phi} r r_1 = 0 \tag{B.1}$$

2. The summation of the forces in the direction of the parallel circles:

$$\frac{\delta(r*N_{\phi\theta})}{\delta\phi} - r_1 * \frac{\delta N_{\theta}}{\delta\theta} - r_1 * N_{\theta\phi} cos(\phi) + p_{\theta} r r_1 = 0 \tag{B.2}$$

3. The summation of the forces perpendicular to the middle surface:

$$N_{\theta} r_1 sin\phi + N_{\theta} r - p_r r r_1 = 0 \tag{B.3}$$

With the three equilibrium equations, it is possible to solve the resulting stresses by using the boundary conditions of the shell.

A special load case is an axisymmetrical load, for instance dead weight, snow loads, which makes the Equations more simple for two reasons. The first reason is that all derivatives to θ become zero, since the loads and forces are independent of θ when all forces and deformations are symmetric around the axis. The second simplification comes forth from the fact that Equation B.2 describes the torsion around the axis of the shell. Since deformation *around* the axis is zero due to the axisymmetric load, this equation can be disregarded. With some rewriting the following two formulas are derived (Timoshenko & Woinowsky-Krieger 1959):

$$\frac{N_\phi}{r_1} + \frac{N_\theta}{r_2} = -Z \tag{B.4}$$

and

$$2\pi r N_\phi sin(\phi) + R = 0 \tag{B.5}$$

With these two formulas it becomes possible to derive the stress distribution in a spherical shell loaded only by its own weight (Timoshenko & Woinowsky-Krieger 1959); the load is called q and the radius of the sphere is a, which gives $r_0 = asin(\phi)$, so:

$$R = 2\pi \int_0^\phi a^2 q sin(\phi) d\phi = 2\pi a^2 q(1 - cos\phi) \tag{B.6}$$

Equations B.4 and B.5 now lead to the following membrane forces:

$$\begin{array}{rcll} N_\phi & = & -\frac{aq(1-cos\phi)}{sin^2\phi} & = \frac{aq}{1+cos\phi} \\ N_\theta & = & aq\left(\frac{1}{1+cos\phi} - cos\phi\right) & \end{array} \tag{B.7}$$

Two interesting and useful results can be derived from Equation B.7. Firstly, that the forces along the meridian (N_ϕ) are always compressive and increases when the angle ϕ increases. This is what was expected and is would be good for a facetted glass dome, since compression is preferred. The second result is that the hoop forces (N_θ) are negative (compressive) for small values of ϕ but will change sign at the zero-point of the Equation. This means that when the angle ϕ becomes larger than $51^o50'$, the hoop forces will become tensile forces. This is also very interesting when trying to limit the tensile forces in a dome, like it is desired in the facetted glass dome too.

The stresses in the FEM-model can be compared to the stresses found in this analysis. It is, however, important to realize that these formulas are a good approximation of the actual stresses in the shell when it is supported in such a way that the meridonial stresses can be taken up by the support directly, see Figure B.2a. Usually, however, the supports

are more like shown in Figure B.2b, for instance when a supporting ring is used. These support conditions will introduce bending stresses in the shell near the supports. Bending stresses can also occur in areas with a low or negative curvature. A description of theses stresses will be given in Paragraph B.2.

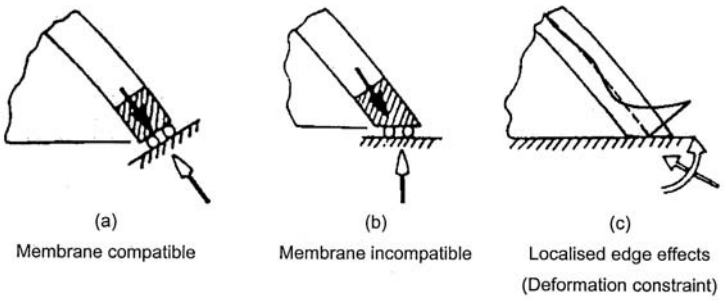

Figure B.2: Schematic support conditions for a shell, from (Hoefakker & Blaauwendraad 2005).

B.2 Bending theory for shells of revolution

The bending theory for shells of revolution, as discussed here, will give description of the bending stresses arising in the shell due to support conditions. When the bending moments are also considered the infinitesimal part of the shell will be represented by Figure B.3.

Defining the exact bending stresses is, however, a long and cumbersome process analyzing a set of differential equations. This evaluation is not thought important for this research, since the analyses will be done by using FEM software. There is, however, an interesting concept called the influence length. The influence length can be used to determine over what area the edge disturbances will occur. The solution of the differential equations often has the form (Hoogenboom 2005):

$$f = e^{-\beta x} sin(\beta x)$$

or (B.8)

$$f = e^{-\beta x} cos(\beta x)$$

f stands for either a bending moment, a displacement, a shear force or a membrane force. A plot of such a function is given in Figure B.4. It can be mathematically proven that when $\beta x > \pi$ the value of f is less that 5% of its maximum. The influence length is

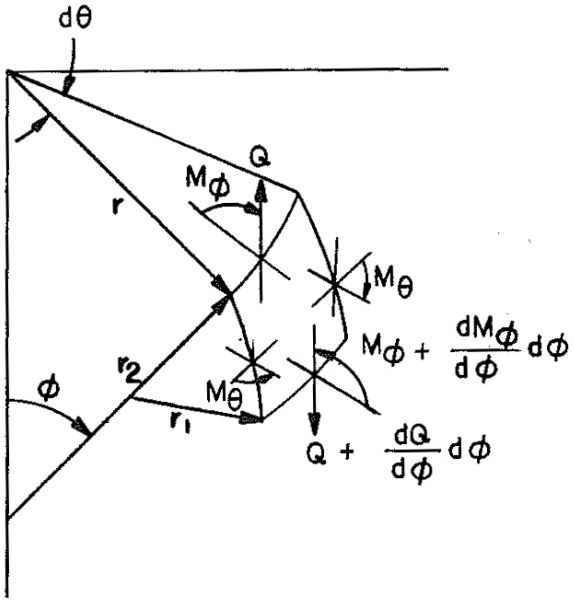

Figure B.3: An infinitesimal part of a shell with all forces considered in the bending theory, from (Jawaad 1994).

therefore defined as:

$$l_i = \frac{\pi}{\beta} \tag{B.9}$$

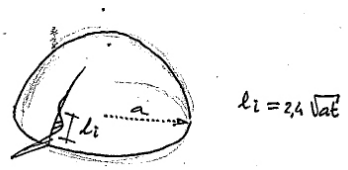

Figure B.4: The influence length for a spherical shell, from (Hoogenboom 2005).

For the elementary shells the influence lengths are determined. The influence length for a spherical shell is:

$$l_i = 2{,}4\sqrt{rh} \tag{B.10}$$

Where, r is the radius of the shell and h is the thickness of the shell.

The influence length can be used to judge whether the locations of the bending moments in the FEM-model are in congruence with expectations.

B.3 Buckling behaviour of spherical shell structures

The buckling behaviour of shells has been researched by many different researchers and many theories have been developed. However, it is has always been very difficult to find a satisfying theory because the buckling is highly dependent on small deviations from the perfect shell. Deviations that can (*will*) arise due to the construction process of the shell, like residual stresses, differences in the shape, temperature differences etc. Theoretical values are therefore highly over-estimating the practical buckling capacity of the shell structures. The imperfections not only give a much lower value than theoretically possible, but experiments also often show a large scatter, see Figure B.5. This Paragraph will try to give an overview of the difficulties in dealing with shell buckling and a way to handle the design of shells for buckling.

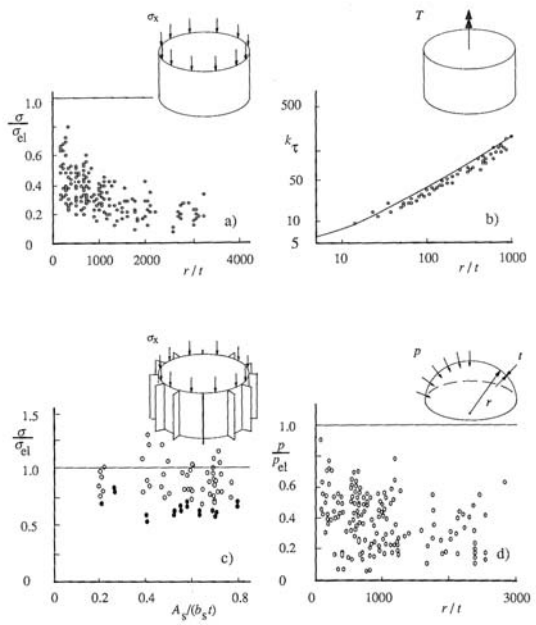

Figure B.5: Comparison between theory and test results (Samuelson & Eggwertz 1992). a.cylinder under axial load; b. cylinder subjected to torque (Brush & Almroth 1975); c. stiffened cylinder under axial load (Singer 1982); d. spherical shell under external pressure (Kollar 1982).

B.3.1 Local and global buckling

There are two main forms of buckling that can be defined for shells, referred to as global or snap-through buckling and local buckling, see Figure B.6. When global buckling occurs, the shell buckles inward as a whole due to the external loads. In local buckling only

a small part of the shell buckles inward. Buckling especially happens in the parts of the shell where curvatures are low. This is why stiffening the shell by increasing the curvature is very effective, though it is difficult to create large spans combined with high curvature.

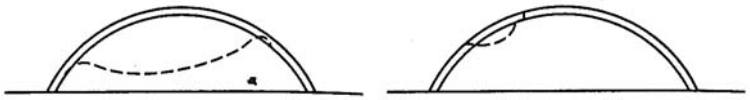

Figure B.6: Local and global buckling of a shell, from (Schodek 2004).

B.3.2 Differential equation for shell buckling

The structural behaviour of shells including large displacements is described by an eight order differential equation (Hoefakker & Blaauwendraad 2005)

$$\frac{Et^3}{12(1-\nu^2)}\nabla^2\nabla^2\nabla^2\nabla^2 * u_z + E*t*\Gamma^2 * u_z = \nabla^2\nabla^2 p_z - n_x x * u_{z,xx} - 2*n_{xy}*u_{z,xy} - n_{yy}*u_{z,yy} \tag{B.11}$$

where u_z is the displacement perpendicular to the shell surface, p_z is the loading perpendicular to the surface. Γ^2 and ∇^2 are operators.

$$\begin{aligned} \nabla^2 &= \frac{\partial^2()}{\partial x^2} + \frac{\partial^2()}{\partial y^2} \\ \Gamma^2 &= k_x * \frac{\partial^2()}{\partial y^2} - 2*k_{xy}\frac{\partial^2()}{\partial x * \partial y} + k_y * \frac{\partial^2()}{\partial x^2} \end{aligned} \tag{B.12}$$

The x and y direction often are not linear but are plotted on the surface of the shell. The differential equation can be solved analytically for elementary shell shapes and elementary loading. For a spherical shell the solution is given in Equation B.13.

$$\begin{array}{ll} \text{Critical loading } p_{cr}[N/m^2] & \text{Critical membrane force } n_{cr}[N/m] \\ \frac{2}{\sqrt{3(1-\nu^2)}} * \frac{Et^2}{a} & \frac{-1}{\sqrt{3(1-\nu^2)}} * \frac{Et^2}{a} \end{array} \tag{B.13}$$

E is Young's modulus, ν is Poisson's ratio, t is the shell thickness and a is the radius of the middle surface of the shell.

B.3.3 Imperfection sensitivity

Certain groups of shell structures are highly sensitive to imperfections, because the polynomial expansion of the potential energy expression contains a cubic term:

$$\Pi = a_0 + a_1 q + a_2 q^2 + a_3 q^3 + a_4 q^4 + ... \tag{B.14}$$

Here, $q =$ amplitude of the dominant buckling mode associated with the critical load, and coefficients a_0, a_1, etc. are dependent on the load as well as the magnitude of the imperfections. In structures that are insensitive to imperfections, like columns and plates, the cubic term is zero. In shells, however, it is not absent and can be particularly large. This is why non-linear analysis is necessary for the stability of shell structures. The elementary shell structures that are sensitive to imperfections are:

- open cylinders, axially loaded;
- hyperboloid, axially loaded;
- closed cylinder, loaded in all directions;
- sphere
- dome

It is important to realize that a *geometrically* perfect shell is still not free of imperfections. Imperfections can also be caused by small load deviations or misalignments, creep, etc.

The non-linearity behaviour is the most important cause for the imperfection sensitivity of shell structures. It appears to be a consequence of the act that many different buckling loads exist of which the critical load lies very close. The consequence is that an interaction between the buckling modes will arise causing the critical load to drop dramatically.

Koiter's laws; Prof. W.T. Koiter was a Dutch Professor, who wrote his dissertation during WWII and published it, in Dutch (Koiter 1945), right after the war. His dissertations contained a revolutionary theory on initial post-buckling behaviour of structures. The English translation (Koiter 1967), however, was only published in 1967, after which it became famous for explaining the significant differences between critical loads and experimental maximum loads. The equilibrium path of a perfect system, which results from the condition $\frac{\delta \Pi}{\delta q}$, can be described by:

$$\frac{\lambda}{\lambda_{cr}} = 1 - c_1 q - c_2 q^2 \tag{B.15}$$

in which q again stands for the amplitude of the buckling mode of the critical state. $q = 0$ at the critical state and c_1 and c_2 are characteristic of the given structure. λ and λ_{cr}

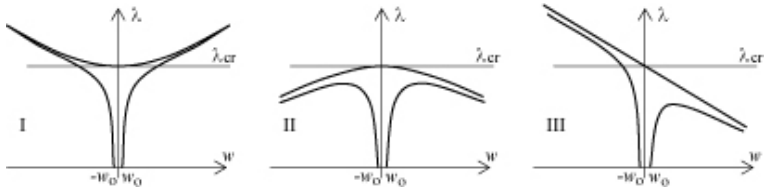

Figure B.7: Basic types of post buckling behaviour (Koiter 1945).

represent load parameters. Three types of behaviour can be identified, depending on the values for c_1 an c_2, which are shown in Figure B.7.

As can be seen in Figure B.7, type I structures are insensitive to imperfections, while type II and type III are. Type III behaviour is the most imperfection sensitive and can be described by Equation 10.1, in which ρ is a coefficient depending on the imperfection shape. Figure B.8 shows the Koiter laws that ahve been derived from the behaviour. Equation B.16 is Koiter's half-power law. This is the typical imperfection sensitivity behaviour for, amongst others, the spherical shell. Equation B.17 is Koiter's third-power law which gives the imperfection sensitivity for less sensitive (shell) structures.

$$\frac{\lambda_{max}}{\lambda_{cr}} = 1 - 2(q_0 \rho c_1)^{\frac{1}{2}} \tag{B.16}$$

$$\frac{\lambda}{\lambda_{cr}} = 1 - 3(w_0 \frac{1}{2} * \rho * \sqrt{c_2})^{\frac{2}{3}} \tag{B.17}$$

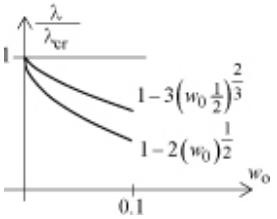

Figure B.8: Maximum load as a function of the imperfection amplitude (w_0=q_0) (Koiter 1945).

Figure B.8 clearly shows the large influence of the amplitude of the buckling mode on the ratio between the maximum load and the (theoretical) critical load. This means that the shell structure is very sensitive to imperfections.

Design principle for buckling of shell structures; to be able to take the problems of the imperfections and deviations from the theoretical critical loads into account, often a

procedure is used in which a safe estimation of the load carrying behaviour of the shell is used. This procedure is as follows (Samuelson & Eggwertz 1992):

1. determine the theoretical critical buckling stress is computed with the classical theory
2. define an empirical factor η representing the influence of small initial deformations, load disturbances etc.
3. define α being a reduction factor representing the manufacturing process, tolerances etc.
4. now calculate the buckling resistance for the elastic shell with:

$$\sigma_u = \sigma_{el,reduced} = \alpha\eta\sigma_{el} \quad \text{if,} \quad \alpha\eta\sigma_{el} < \tfrac{1}{3}\sigma_y \tag{B.18}$$

5. When test results show a large scatter or when there are not enough tests performed to form basis for design, an extra safety factor of 0,75 is recommended
6. When $\alpha\eta\sigma_{el} < \frac{1}{3}\sigma_y$, the buckling takes place in the elastic-plastic region. In this case an extra variable factoe ω_s is introduced, which is a function of the slenderness ratio λ_s according to:

$$\lambda_s = \sqrt{\frac{\sigma_y}{\sigma el, reduced}} \tag{B.19}$$

B.4 Finite element methods for the buckling of thin shells

This Paragraph is based on (Hoogenboom 2005).

Buckling analysis by using FEM is possible with current software. The software can compute the critical loads and the normal modes that are associated with the different buckling forces. The high sensitivity to buckling that is associated with spherical shells is important to take into account after the FEM analysis has been carried out, as also has been stated in Paragraph B.3.

Meshing; The size of the mesh used for the FEM analysis can be judged by using the influence length. In a linear approximation of a variable it will be necessary to use at least 6 elements in a length l_i to achieve some accuracy, see Figure B.9. It should be noted though that a greater accuracy is of course reached when using smaller elements or a higher degree approximation.

Finite elements for a shell are not accurate when deviating too much from a square. If the aspect ratio is considered as the length over the width of the element, it should be

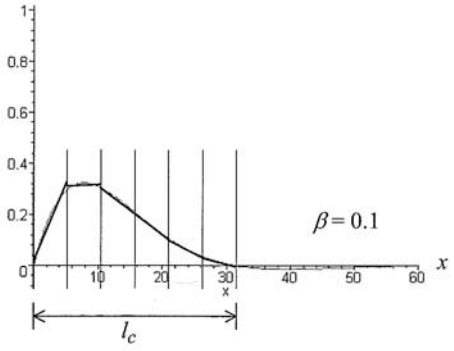

Figure B.9: Accuracy with different numbers of elements for the influence length (Hoogenboom 2005).

smaller than two for most elements. Combining this with the length that was approximated with the influence length of the shell, this gives an approximation for the width of the element along the edge of the shell.

More on meshing the facetted dome will be investigated while using the finite element programme. The meshing will likely need to be varied in order to achieve correct results.

Analysis; The buckling analysis can be carried out either linearly or non-linearly. The non-linear method gives a better approximation of the critical load in combination with imperfections. In such an analysis the load is applied in small increments, after which the displacements are computed. The analysis involves equilibrium iterations path following methods and termination criteria, which makes the analysis very complicated and cumbersome.

For the analysis of the facetted shell structure it will be started to use a linear analysis. It is expected that this analysis will lead to a sufficiently precise approximation of the behaviour of the structure. Because the facetted shell has a large 'imperfections' caused by the facetted shape and the connections, the influence of additional small imperfections are expected not to significantly influence the buckling behaviour of the structure.

Appendix C

Geometry of the shell structure

C.1 Introduction

In order to design an efficient glass facetted dome structure a number of geometrical theories are can be used. Structural dualism, which has already been mentioned a number of times in this thesis, is one of the most important ones and will serve as a basis for this research.

First, however, Paragraph C.2 will go into the theories on geodesic domes and spheres. The geodesic dome is a triangulated structure with a very high efficiency, which makes it likely that its dual will be highly efficient as a plate structure.

Paragraph C.3 will deal with the development of the concept of structural duality between plate and lattice structure (Wester 1984). This will eventually lead up to Paragraph C.4 which handles the duality of geodesic structures.

C.2 Geodesic spheres and domes

C.2.1 Introduction

Geodesic domes and spheres are structures that are based on a network of struts, together approaching the shape of a smooth sphere. A geodesic structure is called a geodesic sphere when it is completed into a full sphere. In all other (chamfered) forms it is a dome, see Figure C.1.

The term 'geodesic' refers to the fact that the network of struts is arranged on great circles, also called 'geodesics'. Because the geodesics intersect each other they form triangular shapes which are not only structurally stable in themselves, but can also distribute the stresses over the total sphere. It is so efficient that it will actually become proportionally stronger when its size increases and the geodesic dome has the highest ratio of enclosed volume to weight.

*Figure C.1: The geodesic dome biosphere, built for the 1967 EXPO in Montreal, Canada. The dome represents 75% of a full sphere. (2007*h*)*

C.2.2 History

The father of the geodesic dome is Buckminster Fuller. The eccentric inventor in many different fields had his greatest success in developing and building his geodesic domes. The first dome that could in fact be considered a geodesic dome was, however, already built in Jena, Germany right after the First World War. Engineer Walter Bauersfeld of the Zeiss Optical Works had the idea to build a large sphere in which he could place projectors showing the stars and planets of the universe, while at the same time accommodating a large number of spectators. This revolutionary idea, seen the fact that before all such planetary domes were mechanical systems, lead to the necessity to design a large and very light spherical structure. Bauersfeld and his team designed a light iron rod framework, based on a highly subdivided icosahedron with great circles; the first geodesic sphere.

In the United States Buckminster Fuller researched the geodesic principle further and commercialized the idea. Where Bauersfeld only built the planetariums, Fuller saw a greater potential in the geodesic dome, admiring its efficiency and geometrical advantages. Fuller had visionary ideas about the future of the planet in which the geodesic sphere played an important role. The floating cities, so-called 'cloud nines' were among some of his most visionary ideas. It is based on the fact that in a well designed geodesic dome with a diameter of 400m the air it encloses is about 1000 times as heavy as the structure enclosing it (2007*i*). This means that by increasing the temperature by merely one degree the sphere would already start to float! This way floating cities could be built, where due to the enormous scale of the structure the weight of the persons and buildings

in it would be negligible compared to the enclosed air. Cities like clouds would dwell the earth.

By acquiring U.S. patents he has for a long time been the only one designing and building such geodesic domes, which therefore quickly became known as 'Fuller domes'. The way the patents were guarded sometimes reminded people of military secrets, for years the only thing people got to see of the geodesic domes were small pictures in magazines like Science and of course the gigantic structures being built all over the North American continent.

C.2.3 Main build-up of geodesic domes

The geodesic dome is based on platonic solids; most commonly on the icosahedron, see Figure C.2, but also octahedra and tetrahedra can be used. The smoothest spheres are, however, conceived by using an icosahedron. The procedure to create a geodesic sphere from an icosahedron is as follows. The simplest geodesic sphere is actually the platonic solid itself, in this case an icosahedron. However, to create a more smooth approximation of a sphere it is needed to subdivide the faces of the icosahedron into smaller triangles. Figure C.2 shows one of the most basic subdivisions of one of the faces. The next step is to project the small triangles onto a sphere. This will lead to an approximation of the shape of the sphere by a regular pattern of triangles. The edges of the triangles will be an approximation of the earlier mentioned 'geodesics' of the sphere. The resulting sphere is shown in Figure C.3.

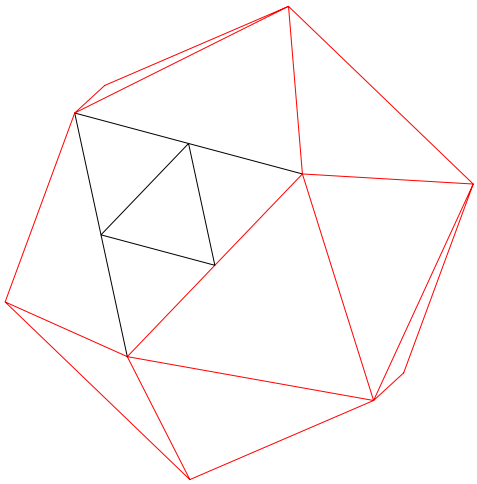

Figure C.2: An icosahedron with one face subdivided.

Figure C.3: The resulting icosphere with the subdivision shown in Figure C.2.

C.2.4 Methods of subdividing the faces of the platonic solids

There are different ways of subdividing the faces of the platonic solids into triangles. Three classes have been defined in literature, namely classes I, II and III. Class I and II are the most commonly used. Class I subdivides the main triangles from face to face, in such a way that the lines are parallel to the edges (0 degrees); class II subdivides the main triangles from face to vertex, giving 90 degree angles with the edges (see Figure C.4).

Class III comprises all other divisions where the angles are neither 0 nor 90 degrees. An example is given in Figure C.4, right. It is clear that class I and II give the neatest subdivision of the sphere. Furthermore the Class III subdivision does not necessarily imply only triangles as result.

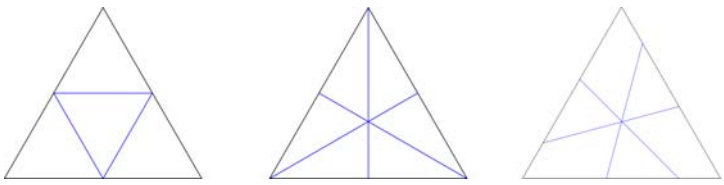

Figure C.4: Subdivision according to class I (left), II and III (right)

Next to classes there is also another factor in subdividing the faces of the solids, namely the so-called frequencies. The frequency of the subdivision refers to the number of times the edge of the face is subdivided. That is why the earlier examples, see Figure C.4 both have frequency two. An example of a higher frequency subdivision is

given in Figure C.5.

Figure C.6 shows an overview of the possibilities to subdivide the faces of the polyhedra (referring only to the more common class I and II).

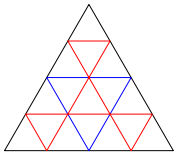

Figure C.5: A frequency 4, class I subdivision.

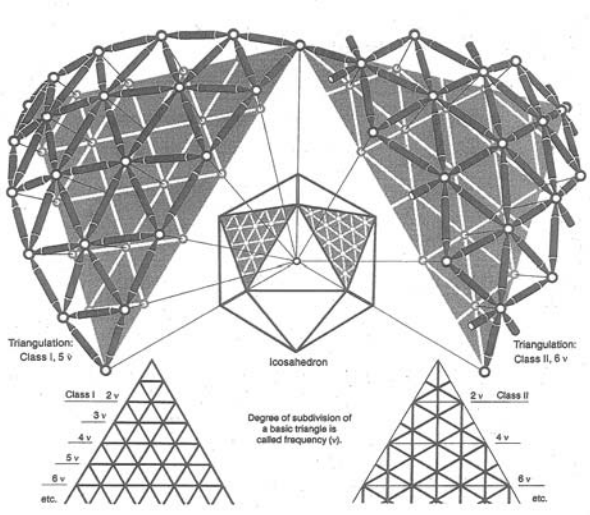

Figure C.6: Subdividing the faces according to class I and II, from (Wester 1984).

C.3 Structural duality between plate and lattice structures

In his book 'Structural order in space, the plate-lattice dualism' (Wester 1984) Ture Wester elaborates on the duality between plate and lattice structures based on platonic

solids. The duality principle shows that plate and lattice structures are dual in their structural behaviour, which is very interesting seen the wide spread experience with lattice structures.

C.3.1 The Platonic polyhedra

The five regular platonic polyhedra are the tetrahedron, the hexahedron (cube), the octahedron, the dodecahedron and the icosahedron, see Figure C.7. The solids were discovered by mathematicians from ancient Greece. They are called regular because the same number of sides meets at each vertex and always at the same angle. Their identical polygons also meet at the same angles at each edge. The properties of the Platonic polyhedra are as follows:

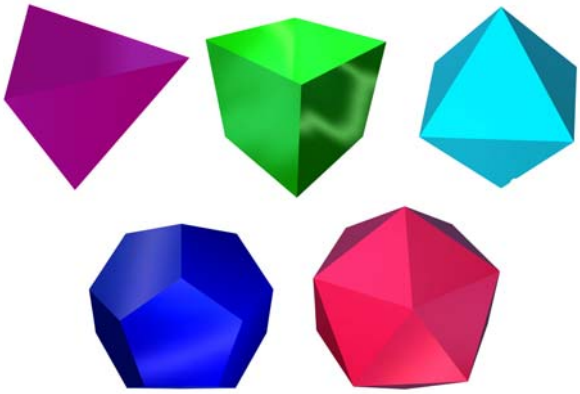

Figure C.7: The five regular platonic solids, from (2007j).

Solid	vertices	edges	faces	sides per face	stable as
Tetrahedron	4	6	4	3	plate/lattice structure (Y/Δ)
Hexahedron	8	12	6	4	plate structure (Y)
Octahedron	6	12	8	3	lattice structure(Δ)
Dodecahedron	20	30	12	5	plate structure (Y)
Icosahedron	12	30	20	3	lattice structure (Δ)

Table C.1: Properties of the five Platonic polyhedra.

The five Platonic polyhedra are the only possible regular polyhedra. They can be subdivided in two groups, which have extreme geometrical characteristics. The first group has faces that are built from the least possible edges, thus forming triangles. The second group has vertices that have the least possible adjacent edges called three-way vertices (Wester 1984). The tetrahedron is a special polyhedron, since it complies with both characteristics. This is why it is called the Platonic master solid.

When structurally analysing the Platonic polyhedra it is found that all polyhedra with triangular faces are stable when the edges are constructed as bars which are joined in the vertices. This leads to the well known and common lattice structures. When, however, the polyhedra with the three-way vertices are considered, they turn out to be stable when they are built up from thin plates that are hinged connected. This means stable plate structures are found. Table C.3.1 also shows this property of the Platonic solids.

C.3.2 Duality and the platonic polyhedra

The structural behaviour of the two systems is opposite. A lattice structure concentrates all forces in the edges and nodes in the form of normal forces, while a plate structure transfers the forces through plate-action in the planes of the facets and distributed stresses in the joints between the facets. This opposite behaviour is called the structural duality between plate and lattice structures. The implication of this duality is also that every lattice structure has its own unique dual, being a plate structure.

The dual of a lattice structure can be found in a fairly easy way. By connecting the centre of each triangle formed by the bars of the lattice structure, a new geometry is found. This geometry is the dual of the lattice structure.

When creating the duals for the five Platonic polyhedra, two interesting facts arise. First is that the tetrahedron, earlier already mentioned being the 'Platonic master solid', can not only be both a lattice and a plate structure, but is also its own dual.

The second fact is that the four remaining polyhedra are each others duals. Meaning that the dual for the octahedron (Δ) is the hexagon (cube; Y) and the dual for the icosahedron (Δ) is the dodecahedron (Y). This in fact means that the five Platonic polyhedra can actually be considered as being only three fundamentally different polyhedra. This duality is shown in Figure C.8 and can also be expressed symbolically (Wester 1984) as in Equation C.1.

$$\frac{\Delta}{Y} = \frac{tetra}{tetra} = \frac{octa}{hexa} = \frac{icosa}{dodeca} = \frac{lattice}{plate} \tag{C.1}$$

C.4 Geodesic structures and duality

The next step is of course finding the dual of a geodesic dome. Since the plate-lattice dualism still holds, this will lead to highly efficient plate structures.

The starting point for an efficient geodesic dome can be the icosahedron. If the dual form of the geodesic dome needs to be found it will therefore be interesting to start with the dual of the icosahedron: the dodecahedron. There is only one problem when starting with a Y-structure like the dodecahedron; subdividing the planes in smaller planes is fairly difficult. This can be solved by using the same technique of subdivision as in the geodesic

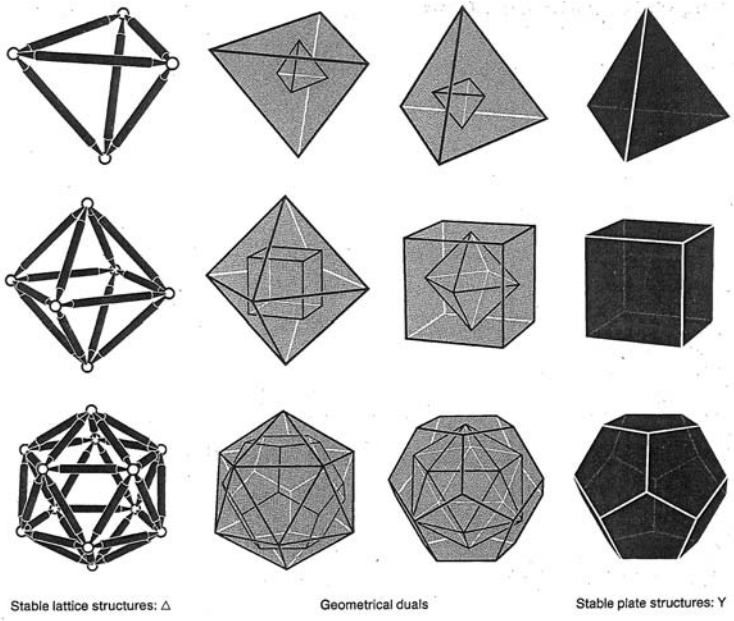

Figure C.8: Duality of the Platonic polyhedra, from (Wester 1984).

(lattice) structures and adding one step: creating the dual. This means that the icosahedron will remain the starting point for the structure and that the dual will be created after the triangulation steps.

The process of subdividing a plate structure, in contrast to the triangulation of lattice structures, is called hexagonation. Figure C.9 ((Wester 1984)) shows the hexagonation of an icosahedron (note: compare this to Figure C.6).

C.5 A facetted glass shell

It seems that the dual of the geodesic dome is an interesting venture point for designing a facetted glass shell structure. The efficient distribution of forces in combination with a straight forward shape makes it possible to truly analyse the effect of the faceting itself.

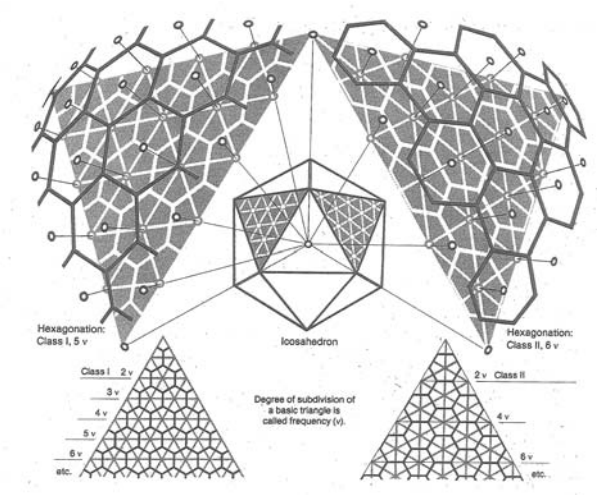

Figure C.9: Hexagonation, from (Wester 1984).

Appendix D

Loads

D.1 Options for modelling the loads

For calculating the maximum load bearing capacity of the shell structure in relation to the stability, different loading conditions can be considered. Three main loading options are:

1. Using a representative load
    - gives a direct value for the maximum load
    - is only useful for symmetrical loads
    - mostly academically interesting
2. Using the self weight
    - yields a factor on the self weight
    - not a useful result
    - only for symmetrical loads
3. Realistic loads
    - results in a safety factor on the loads
    - both symmetrical and a-symmetrical load conditions
    - all loads need to be defined (preferably Danish codes)

The most interesting option is using the realistic loads. It is, however, in early stages also possible to use a representative load. Basing the calculations on a factor on the self weight is less interesting, since this factor can always be found and the real load bearing capacity of the structure is much more important. In iDiana a stability calculation can

only be made for one load case at the same time. This has a result that all the loads should be incorporated in one load case which combines the design loads for both the permanent load and the governing variable load. This load condition will be defined at the end of this Chapter.

D.2 Magnitude of the loads

The loads on the shell structure consist of a number of cases. Of course these cases can be subdivided into permanent and variable loads.

D.2.1 The permanent loads;

the self weight of the structure is the most important permanent load. The self weight depends on the thickness of the glass and the density $\rho = 0,25 * 10^{-5} kg/mm^3$, see also Figure A.8. The uncommon dimension refers to the use of mm in the FEM model, see Paragraph E.6. The weight of the glass facets adds up to:

$$p_{facets} = \rho * t * g = 0,25 * 10^{-5} kg/mm^3 * 16mm * 9,81N/kg = 0,394 * 10^{-3} N/mm^2 \tag{D.1}$$

The weight of the joints will not be incorporated in the model, but the weight of the glass is addressed to the joints as well. This will lead to an increase in the total load, but it is not thought to have a large impact, considering the small surface of the joints. The third element of the permanent loads is a sacrificial glass top layer on the outside of the dome. The common thickness of such a layer is 4mm and therefore has the following weight:

$$p_{extraglass} = \rho * t * g = 0,25 * 10^{-5} kg/mm^3 * 4mm * 9,81N/kg = 0,098 * 10^{-3} N/mm^2 \tag{D.2}$$

D.2.2 The variable loads;

the variable loads can be defined by using national or international standards. Because the shell structure will in first instance be designed for the Danish situation, the Danish standards for loads on building structures should be used: 'DS410; Last påkonstruktioner'. However, since the Eurocodes are very similar to the Danish standards and will be the official codes in the future, it is chosen to take the Eurocodes as a basis for the design. It is important, though, that the Danish situation is still considered.

The two governing loads from this document are the snow load and the wind load. However, for simplicity only a symmetric snow load is considered in this study.

Snow loads; the snow loads can be divided in two categories, first the evenly distributed snow load and secondly the un-evenly distributed snow load. The evenly distributed snow load is as follows:

$$\begin{aligned} &s_k = (0,264Z - 0,002)(1 + \tfrac{A}{256}^2) \\ &A = 0,\ Z = 4,5 \\ &S_k = 1,2kN/m^2 \end{aligned} \tag{D.3}$$

Where, Z is the zone number taken from the EuroCodes (*Eurocode 1: Actions on structures - Part 1-3: General actions - Snow loads* 2003), A is the altitude of the site above sea level.

$$\begin{aligned} &s_k = \mu_1 * C_e * C_t * s_k \\ &\mu_1 = 0,8;\ C_e = 1,0;\ C_t = 1,0 \\ &s_k = 1,2kN/m^2 \\ &s = 0,8 * 1,0 * 1,0 * 1,2 = 0,96kN/m^2 = 0,96 * 10^{-3}N/mm^2 \end{aligned} \tag{D.4}$$

Where μ_1 is a shape factor. For the evenly distributed snow load the shape factor for a cylindrical roof is chosen. C_e is a factor for the exposure of the roof and is set to 1,0 in order to stay on the safe side. C_t is a thermal coefficient which is again chosen on the safe side and set to 1,0.

The shape factor for the un-evenly distributed snow load can not be determined based on the codes, since a cylindrical shell of revolution is not mentioned. Therefore assumptions will have to be made on the asymmetrical snow load. This is left to a future study.

Curved shape; in the codes the snow load is always defined as a load on the projected ground surface, see Figure D.1a. This has consequences for defining the load on the shell. In iDiana the load is defined as a surface load on the facets themselves in the Z-direction, see Figure D.1b. The result is that if the value per surface area as stated in the codes is directly adopted, the total resulting snow load on the dome will be higher, since the surface area of the dome is significantly larger than its ground surface.

The inconsistency between the two load shapes can be solved by calculating the projected length of the facet on the ground surface and factorizing the load accordingly. To approximate this behaviour for the shell structure, a smooth spherical dome is taken as a starting point. By taking the derivative of the arch shape, the angle that the facet makes with the ground surface can be estimated, see Figure D.2.

To simplify the calculations the facetted shell will be subdivided in four ring shaped sectors with each a different snow load, see Figure D.3. The derivative of the dome will

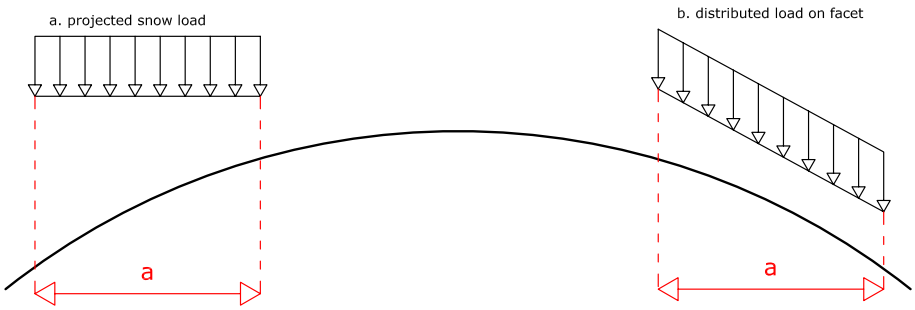

Figure D.1: a. the snow load according to the codes; b. the surface load on the facets.

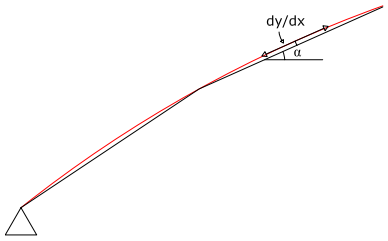

Figure D.2: The angle of the facets compared to the derivative of a smooth dome.

be sought in four locations, after which the necessary factor on the load will be defined.

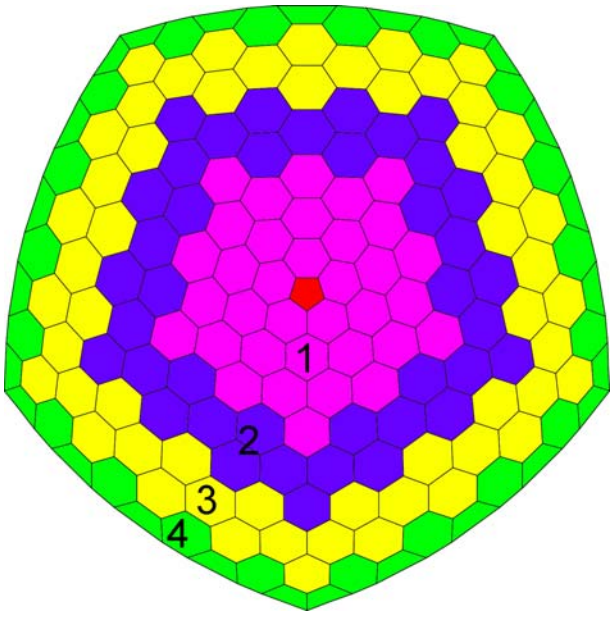

Figure D.3: Subdivision of the dome in four sectors.

The following equations for a circle are used:

$$y = \sqrt{R^2 - x^2}$$
$$\frac{dy}{dx} = \frac{-x}{\sqrt{R^2 - x^2}} \tag{D.5}$$

Where, $R \approx 13m$ (see Chapter 4). The radius of the facetted shell, on the other hand, is approximately 9,2m. When x is chosen at four different locations of the dome the load factors become:

$$\begin{array}{llll} x = \frac{1}{4} * 9,2 & \frac{dy}{dx} \approx 0,18 & \alpha \approx 10^o & cos(10^o) = 0,985 \\ x = \frac{2}{4} * 9,2 & \frac{dy}{dx} \approx 0,38 & \alpha \approx 21^o & cos(21^o) = 0,933 \\ x = \frac{3}{4} * 9,2 & \frac{dy}{dx} \approx 0,62 & \alpha \approx 32^o & cos(32^o) = 0,848 \\ x = 9,2 & \frac{dy}{dx} \approx 1 & \alpha \approx 45^o & cos(45^o) = 0,707 \end{array} \tag{D.6}$$

Applying these load factors to the different sectors leads to the following surface loads:

Sector 1 $0,985 * 0,96 * 10^{-3} N/mm^2 = 0,946 * 10^{-3} N/mm^2$
Sector 2 $0,933 * 0,96 * 10^{-3} N/mm^2 = 0,896 * 10^{-3} N/mm^2$
Sector 3 $0,848 * 0,96 * 10^{-3} N/mm^2 = 0,814 * 10^{-3} N/mm^2$
Sector 4 $0,707 * 0,96 * 10^{-3} N/mm^2 = 0,679 * 10^{-3} N/mm^2$

D.3 Total load for the stability calculation

As already mentioned; only one load case will be considered, the evenly distributed load combination. The load factors will need to be applied before the load can be addressed to the model. The considered load factors are taken from the Eurocodes, NEN-EN1990-2002 (*Eurocode - Basis of structural design* 2002) and shown in Figure D.4.

The total evenly distributed load follows from the following Equation:

$$p_{total} = \gamma_g * p_g + \gamma_q * p_q \tag{D.7}$$

Here p_q will be the variable snowload, since this is governing for the evenly distributed load.

The combination of the loads into one load case will be done in iDiana. The different loads will be:

Table A1.2(A) - Design values of actions (EQU) (Set A)

Persistent and transient design situations	Permanent actions		Leading variable action (*)	Accompanying variable actions	
	Unfavourable	Favourable		Main (if any)	Others
(Eq. 6.10)	$\gamma_{Gj,sup} G_{kj,sup}$	$\gamma_{Gj,inf} G_{kj,inf}$	$\gamma_{Q,1}$ $Q_{k,1}$		$\gamma_{Q,i} \psi_{0,i} Q_{k,i}$

(*) Variable actions are those considered in Table A1.1

NOTE 1 The γ values may be set by the National annex. The recommended set of values for γ are :
$\gamma_{Gj,sup} = 1,10$
$\gamma_{Gj,inf} = 0,90$
$\gamma_{Q,1} = 1,50$ where unfavourable (0 where favourable)
$\gamma_{Q,i} = 1,50$ where unfavourable (0 where favourable)

NOTE 2 In cases where the verification of static equilibrium also involves the resistance of structural members, as an alternative to two separate verifications based on Tables A1.2(A) and A1.2(B), a combined verification, based on Table A1.2(A), may be adopted, if allowed by the National annex, with the following set of recommended values. The recommended values may be altered by the National annex.
$\gamma_{Gj,sup} = 1,35$
$\gamma_{Gj,inf} = 1,15$
$\gamma_{Q,1} = 1,50$ where unfavourable (0 where favourable)
$\gamma_{Q,i} = 1,50$ where unfavourable (0 where favourable)
provided that applying $\gamma_{Gj,inf} = 1,00$ both to the favourable part and to the unfavourable part of permanent actions does not give a more unfavourable effect.

*Figure D.4: Load factors according to NEN-EN1990-2002 (*Eurocode - Basis of structural design *2002)*

Self weight structure	$p_{g,d}$	$= 1,1 * (0,394 + 0,098) * 10^{-3} N/mm^2 = 0,433 * 10^{-3} N/mm^2$
Snow top facet	$p_{g,d,top}$	$= 1,5 * 0,960 * 10^{-3} N/mm^2 = 1,44 * 10^{-3} N/mm^2$
Snow sector 1	$p_{g,d,1}$	$= 1,5 * 0,946 * 10^{-3} N/mm^2 = 1,42 * 10^{-3} N/mm^2$
Snow sector 2	$p_{g,d,2}$	$= 1,5 * 0,896 * 10^{-3} N/mm^2 = 1,34 * 10^{-3} N/mm^2$
Snow sector 3	$p_{g,d,3}$	$= 1,5 * 0,814 * 10^{-3} N/mm^2 = 1,22 * 10^{-3} N/mm^2$
Snow sector 4	$p_{g,d,4}$	$= 1,5 * 0,679 * 10^{-3} N/mm^2 = 1,02 * 10^{-3} N/mm^2$

Appendix E

Modelling the dome in iDiana

Introduction

After the geometry has been drawn in Autocad, it will be exported as a .dxf file to the iDiana pre-processor for Diana. This chapter will describe the different steps and considerations in the process of creating the finite element model.

The main steps in the process

This first Paragraph will define the main steps that are necessary to create a finite element model of the shell in iDiana. These steps will thereafter be discussed in the following Paragraphs.

1. Importing the .dxf-file, Paragraph E.1
2. Flipping some of the surfaces, Paragraph E.2
3. Creating sets, Paragraph E.3
4. Defining and addressing the symmetrical loads, Paragraph E.4
5. Defining and addressing of the element types, Paragraph E.5
6. Defining and addressing of the properties, Paragraph E.6
7. Copying and rotating the structure to create the whole shell, Paragraph E.7
8. Defining and addressing the constraints, Paragraph E.8
9. Mesh generation, Paragraph E.9

NB in Appendix G the inputfile for iDiana is given in which all the steps can be recognised.

E.1 Importing the .dxf-file

The .dxf file consists of a combination of 3d-face elements. When importing these elements into iDiana, these elements will be transformed into a combination of points, lines and surfaces. This is actually exactly what is desired.

E.1.1 Connectivity

When all surfaces need to be connected in iDiana, it is necessary that the points from which the different surfaces are built are the same on the edges. This does not pose a problem in the facets themselves, because all edges of the surfaces share the same points. In the connections between the joints and the facets, however, the surfaces do not use the same points, due to the smaller width of the joints compared to the width of the edge of the facet, see Figure E.1. This can only be solved by defining extra points on the edge of the facet, which can be done by defining subdivision of the surfaces in the facet, see Paragraph E.1.2.

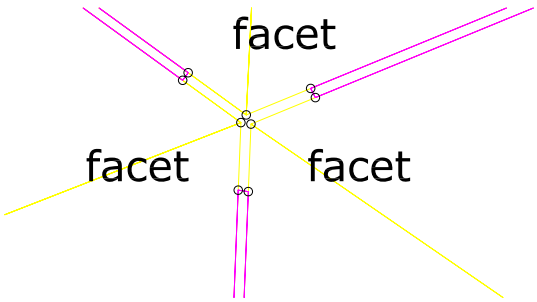

Figure E.1: The connection between facet and joint; no points are shared, so the elements will not be considered connected in iDiana.

E.1.2 Geometry of the facets

When creating the .dxf model of the geometry, it is important to note that iDiana can only read triangular and quadrangular surfaces. This means that it is not possible to model the facets as single surfaces, since the consist of 6 nodes at the corners and also 12 connecting nodes at the locations of the joints. There are a number of possibilities to subdivide the facets into smaller faces, while respecting all the nodes. Two of these options are shown in Figure E.2.

The difficulty with the left hand subdivision is that the elements get a very sharp angle in near the centre of the facet. This will lead to a lower accuracy of the results. The right

hand subdivision is therefore better than the left hand subdivision, but still has some very narrow faces.

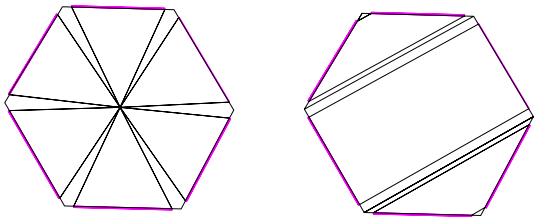

Figure E.2: Two possible subdivisions of the facet into 3d-faces.

When considering the structural behaviour of the plate structure it is shown that the vertices are forceless. This also means that the stresses in the free corners, where there is no joint, will be very low. Therefore the influence of these pieces of glass on the structural behaviour of the shell will be minimal. This especially holds when considering the overall stability behaviour, since local peak stresses are less interesting in this case. If the glass corners are left out, consequently a lower number of nodes will need to be defined for each facet. The facet can in this case be defined by a mere 5 (quadrangular) surfaces instead of the 9 to 12 surfaces with the subdivisions in Figure E.2. A result is the subdivision in Figure E.3. And this is also the subdivision that will be used in the model.

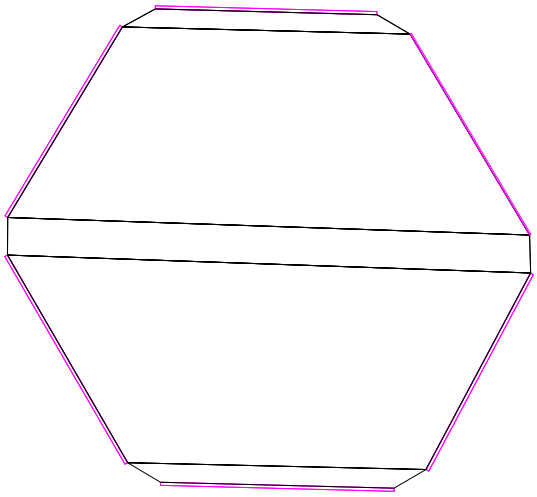

Figure E.3: Subdividing the facets without using the original corners of the hexagon.

E.2 Directions of the surfaces

To be able to use the model as a finite element model, it needs to be checked that all surfaces have the same normal direction. This can be easily checked with the iDiana command 'LABEL GEOMETRY NORMAL'. This will directly show which surfaces have a deviating direction. With a second command the normals of the surfaces can be flipped.

E.3 Creating sets

In order to work with the model more easily it is very useful to define different sets. The greatest advantage is the possibility to address the properties by set. Also for rotating it has advantages, since the elements are rotated by the set. Elements that need not to be rotated will be kept in a separate set.

In this case the joints and the glass facets have different properties, so at least two sets will be created. A third set is added, being the top facet. This is for the rotation, since the top facet will not be rotated.

E.4 Load generation

The loads are defined per load case and later addressed to different elements or sets in the structure. This means that asymmetric loads do not have to be generated separately, but can be addressed to a certain number of elements. The symmetric loads that will be considered are the self weight and a snow load. The stability calculation will be done using the same loads. The symmetric loads on the structure can be addressed to the different elements before rotating and will be rotated along with the one-fifth of the shell, see Paragraph E.7. Possible asymmetric loads will need to be addressed after rotating.

E.5 The elements in the model

There are two types of elements interesting for this model. Firstly, the elements that represent the glass facets in the model and secondly the elements representing the connections between the facets. It is important to note that the element type needs to be defined *before* the material properties can be addressed to the elements.

The glass facets transfer their forces in two ways:

1. local bending due to direct loading perpendicular to the plane

2. membrane action, in order to transfer the loads between the facets

The model will need to be able to deal with both behaviours. Therefore, it will be necessary to use shell elements. A shell element has degrees of freedom for both the translations and rotations that result from the load, with corresponding stresses. The elements can be either of a triangular or a quadrilateral shape. The quadrilateral elements are slightly more complex and give a longer processing time, but also generally yield better results. It is thought that for the stability study it will be better to use the quadrilateral elements.

Three suitable elements can be found in the DIANA element library (de Witte 2007). The difference between the three is the number of integration points along the edge. All three elements are curved shell elements, even though the facets in the model are actually flat slabs. However, the flat shell elements are not suitable for stability calculation (de Witte 2007).

The Q20SH shell element; the simpler of the two elements is the Q20SH shell element. This element has four nodes and acts as an isoparametric curved shell element. Mindlin-Reissner theory is used to analyze the plate bending, (de Witte 2007). The schematic lay out of the element is shown in Figure E.4 and more information on the element can be found in Appendix F.

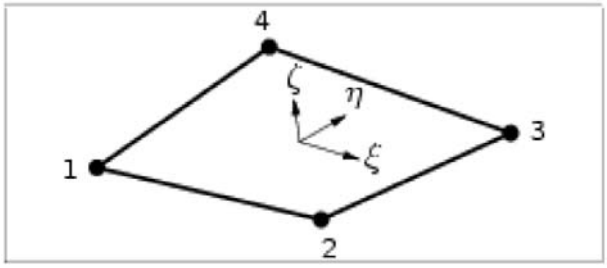

Figure E.4: The Q20SH curved shell element, from (de Witte 2007).

The CQ40S shell element; the second element is the CQ40S shell element. This element has an extra node on each edge, resulting in a total of eight nodes. As with the Q20SH element it behaves as an isoparametric curved shell element. Again, Mindlin-Reissner theory is used to analyze the plate bending (de Witte 2007). The schematic lay out of the element is shown in Figure E.5 and more information on the element can be found in Appendix F.

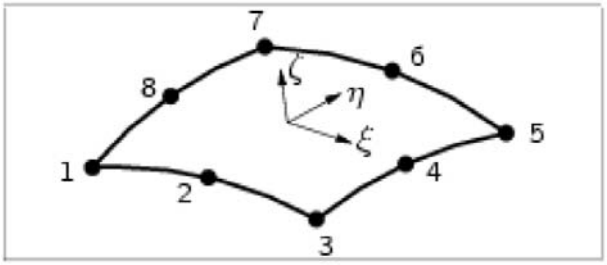

Figure E.5: The CQ40S curved shell element, from (de Witte 2007).

The CQ40S shell element; the second element is the CQ60S shell element. This element also behaves like the Q20SH element but has again an extra node on each edge, resulting in a total of twelve nodes. The schematic lay out of the element is shown in Figure E.5 and more information on the element can be found in Appendix A.

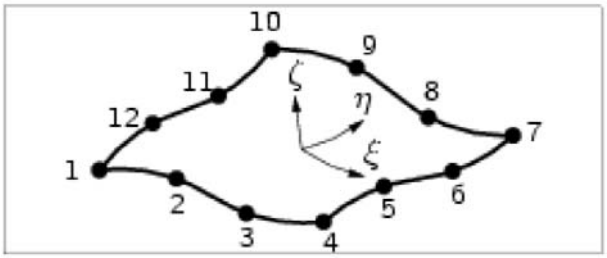

Figure E.6: The CQ60S curved shell element, from (de Witte 2007).

Since the joints will also need to be able to transfer a combination of bending and membrane behaviour, the same elements will be used.

In the start it will be interesting to use the simpler Q20SH element for the model, since it will be quicker to calculate the structure. The lower accuracy of the element might actually not be a problem when assessing the overall stability behaviour. This can easily be tested by applying the CQ40S element for a simple loading condition and look at the differences between the results. If the results show a fairly large difference for the same meshing, the model can be fairly easily changed to the more accurate eight node element.

E.6 Addressing the properties

The material properties are defined in iDiana. Since the program only works with the values, it is important to use the correct dimensions for all properties. The .dxf model

is defined in millimetres and the loads and forces are defined in respectively kilos and Newtons. An interesting notion is the physical quantity of the gravitational acceleration. Since the model is in Newton and kilos, the definition will need to be N/kg and not m/s^2. This appears to be the same, but actually the time step definition differs. Since the 'mm' is used and not the 'm', the time step will change from seconds to $(\frac{s}{\sqrt{1000}})^2$. This has important implications for the eigen frequencies, since the eigen frequencies will now be defined according to this new time step.

The basic assumptions that will be used for the glass facets are the following:

- linear elastic material
- isotropic material
- $E = 7 * 10^{10} Pa = 7 * 10^4 N/mm^2$ (see Figure A.8)
- $\mu = 0,2$ (see Figure A.8)

The joint material will be varied to see the influence of the stiffness of the joint. For the first model, however, the material properties of rubber will be used. This is in accordance with the models in Paragraphs 4.3.4 and 4.3.5.

- linear elastic material
- isotropic material
- $E = 0,1 * 10^9 Pa = 0,1 * 10^3 N/mm^2$ (see Figure A.8)
- $\mu = 0,5$ (see Figure A.8)

E.7 Rotating in Diana

After one fifth of the dome is imported into iDiana and all properties are addressed to this shell part, it will be copied and rotated. When the fully defined shell is rotated all properties will be rotated as well. This will lead to a model of the full shell structure. Connections between overlapping elements will be automatically generated by iDiana, as long as they fulfil the requirement that the nodes on the edges that need to be connected are at the same location. The nodes will not be doubled, but joined. A number of extra points and lines have been defined in the .dxf model to create a centre of rotation. These points will need to be deleted after rotation. To make sure that all joints are merged, the MERGE-command will be given in iDiana after the rotation. The tolerance will be set to 1mm, to make sure that the joints, which have a width of 10mm, will not be merged into one line.

E.8 Constraints

The constraints will be addressed to the different edges *after* the rotation has taken place. This is necessary since the constraint properties are not included in the copy command in iDiana. The constraints will be addressed to all edges at the bottom of the shell structure.

E.9 Meshing

The mesh generation is done by iDiana, dependent on the division of all edges in the model. The division will in the first model be kept very simple and with more or less equal elements. Using this mesh, possible problem areas in the model can be found. In these areas the meshing can then later be adjusted. This Paragraph will discuss the different steps that have been taken to create a suitable meshing for the stability analysis.

E.9.1 Mesh division methods in iDiana

There are three principally different ways to subdivide the surfaces into finite elements:

- Division by element size
- Division by the line
- Division by the surface

Ad. 1
Dividing the mesh by element size is not very suitable for this problem, since the shape and size of the surfaces differs a lot. By choosing an approximate element size iDiana is left to decide on the subdivisions, which will lead to too little control. Almost always when an element size is fed to iDiana, it will lead to a large number of incompatibilities between elements, which means some surfaces will not be subdivided. This effect can be partly repaired by using the command 'automate' for the subdivisions. iDiana will now try to change the subdivisions on the lines in order to create a fitting mesh. Often this will not be enough to remove all problems and the remaining surfaces will need to be adjusted by hand, if even possible. Furthermore, the element size is a very arbitrary factor and changing the size of the average element by a couple of millimetres can have a large effect on the neatness of the first meshing step.
Ad. 2
Using line subdivisions is a more elaborate but very controllable method of creating the mesh elements. The number of subdivisions on a line is the most elementary variable in defining the mesh. By choosing the same line division for every line, however, an uneven

mesh will be created, see Figure E.7. This is of course due to the different sizes of the surfaces in the (.dxf-)model.

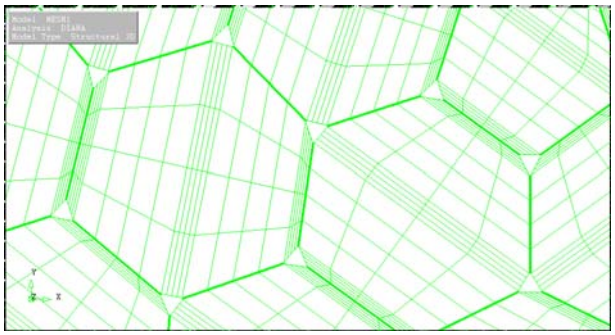

Figure E.7: A mesh generated with the same line division (4) on every line.

Ad. 3
The surface division command in iDiana is in fact an extended version of the line division command. In this case the division of the opposing edges of the surface can be defined separately from each other. For instance when the original line division is 4, the surface division can make the distinction between the two pairs of opposing edges and make them 1-4. Now one edge will then have subdivision 1 and the other subdivision 4. This creates good possibilities to equal out the differences between the larger and smaller surfaces in the model.

The best way to create the mesh in this model is therefore a combination of the line and surface subdivision methods. First a general subdivision will be chosen for all lines, after which the smaller surfaces will get an adjusted subdivision using the surface-routine.

E.9.2 Meshing

The most coarse and direct subdivision thinkable would be having a subdivision of 'one' on every edge. However, since the differences between the different surfaces are significant a first overall line subdivision of 'four' is chosen, see Figure E.7.

Figure E.7 shows that the subdivisions in the smaller surfaces are much finer than the subdivisions in the two larger surfaces in each facet. A good approximation will be to make the smaller surfaces one-to-four instead of four-to-four, see Figure E.8.

The second very fine subdivision arises in the joints. The joint faces are very small compared to the surfaces in the facets. By changing the subdivision in these surfaces to one-four as well, the subdivision is made as coarse as possible without introducing compatibility problems with the adjoining surfaces. It must be noted that the aspect ratio of the elements will still not be optimal. However, it is not expected that this will give

large problems in the overall stability behaviour of the shell structure. For local effects and stress calculation the mesh should be refined locally.

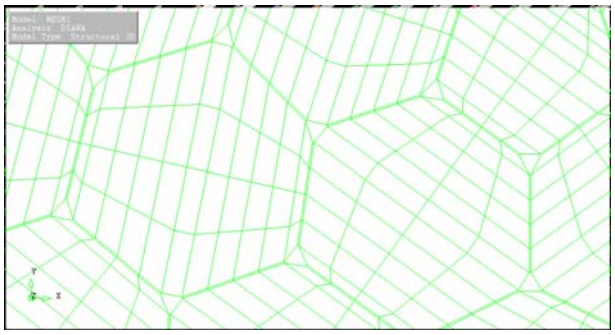

Figure E.8: The new mesh after adjusting the subdivision in the smaller surfaces to one-four.

E.9.3 Mesh refinement

The mesh that has been defined in Paragraph E.9.2 will need to be refined to find acceptable results. To refine the mesh a very useful command is incorporated in iDiana, namely refining the mesh by a factor. This way a finer mesh can be created very quickly, which is also important when choosing a higher order element type, see Paragraph 5.3.

The error in the results of the different mesh refinements can be calculated by comparing the results of the two meshes. The real displacement u can be defined by Equation E.1, the error can then be found using the following Equation E.2. These Equations do imply that the elements are more or less square.

$$\begin{aligned} u &= u_1 + f * l \\ u &= u_2 + f * \frac{l}{f_r} \\ u &= f_r * u_2 - u_1 \end{aligned} \tag{E.1}$$

Where, l is the length of the element, f is a factor depending on the element and f_r is the refinement factor.

$$E = \frac{u - u_2}{u} \tag{E.2}$$

If the error is acceptable, the model does not need to be refined further. For higher order elements the same calculation can be made, however, the length l will now have the same order as the element. This yields the following results:

$$\begin{aligned} O(l^2): \quad & u = \tfrac{4}{3}u_2 - \tfrac{1}{3}u_1 \\ O(l^3): \quad & u = \tfrac{8}{7}u_2 - \tfrac{1}{7}u_1 \end{aligned} \tag{E.3}$$

The effects on the model are investigated in Chapter 5.

E.9.4 Changing the element type

The accuracy of the model can also be increased by using higher order elements with a larger number of integration points. The possibilities have already been mentioned in Paragraph E.5.

Appendix F

Elements from the iDIANA library

The information in this Appendix is directly taken from the iDIANA user manual (de Witte 2007).

Subsections

10.7.2 Q20SH - quadrilateral, 4 nodes

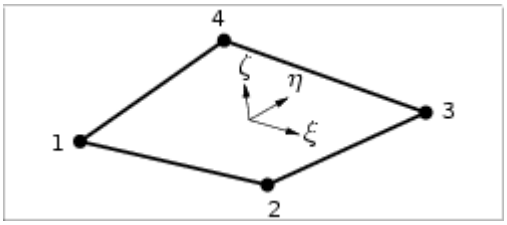

The Q20SH element [Fig.10.15] is a four-node quadrilateral isoparametric curved shell element. It is based on linear interpolation and Gauss integration over the $\xi\ \eta$ element area. The integration in ζ direction (thickness) may be Gauss or Simpson. To avoid shear locking, which results in a excessively stiff behavior, DIANA automatically modifies the transverse shear strain fields. The polynomials for the translations *u* and the rotations ϕ can be expressed as

$$u_i(\xi,\eta) = a_0 + a_1\xi + a_2\eta + a_3\xi\eta$$
$$\phi_i(\xi,\eta) = b_0 + b_1\xi + b_2\eta + b_3\xi\eta$$

Typically, for a rectangular element, these polynomials yield approximately the following strain and stress distribution along the element area in a ζ lamina. The strain ε_{xx}, the curvature κ_{xx}, the moment m_{xx}, the membrane force n_{xx} and the shear force q_{xz} are constant in *x* direction and vary linearly in *y* direction. The strain ε_{yy}, the curvature κ_{yy}, the moment m_{yy}, the membrane force n_{yy} and the shear force q_{yz} are constant in *y* direction and vary linearly in *x* direction. The only possible (and default) integration scheme over the element area is 2 x 2 . [n^{ξ} = 2 , n^{η} = 2] The default in ζ direction (thickness) is 3-point Simpson, [n^{ζ} = 3] 2-point Gauss is a suitable option. Schemes higher than 3-point in ζ direction are only useful in case of nonlinear analysis.

Connectivity (*syntax*)

```
'ELEMEN'
CONNEC
1          5 6          12 13                                                80
          Q20SH      no1n  no2n  no3n  no4n
```

Q20SH
is the element type name, followed by the numbers of the four nodes *no1* to *no4* in sequence from Figure 10.15.

Other input data

Local $\bar{x}$ axis ... §10.1.
Thickness and shape ... §10.3.
Integration schemes ... §10.4.2.
Shear reduction factor ... §10.5.
Point load ... §10.6.1.
Edge load ... §10.6.2.
Face load ... §10.6.3.
Temperature & concentration load ... §10.6.4.
Initial stress ... §10.6.5.

Default (*file*.dat)

```
'ELEMEN'
CONNEC
 14  Q20SH  27 48 15 18
MATERI
 14  1
GEOMET
 14  1
'MATERI'
  1  YOUNG  2.1E6
     POISON 0.2
'GEOMET'
  1  THICK 0.1
```

This input data specifies a Q20SH element between nodes 27, 48, 15 and 18. The element has a Young's modulus E = 2.1 x 10^6 , a Poisson's ratio ν = 0.2 and a uniform thickness of 0.1. By default DIANA assumes an element $\bar{x}$ axis from node 27 to 48, a 2 x 2 x 2 integration scheme and a hyperbolic-parabolic shape.

(*file*.dat)

```
'ELEMEN'
CONNEC
  8  Q20SH  12 9 35 24
MATERI
  8  1
GEOMET
  8  2
DATA
  8  1
'MATERI'
  1  YOUNG  2.1E6
     POISON 0.2
'GEOMET'
  2  XAXIS  0.0 1.0 1.0
```

```
     THICK  0.10 0.15 0.12 0.11
     CYLIN  0. 0. 0.   1. 1. 0.
'DATA'
  1  NINTEG 2 2 3
'LOADS'
CASE 1
ELEMEN
  8  EDGE   KSI1
     FORCE  3.6 -2.4
     DIRELM NORMAL
```

Element 8 is connected to nodes 12, 9, 35 and 24. The element $\bar{x}$ axis points at 45° with the global *YZ* axes. The thickness varies from 0.10 to 0.15 to 0.12 to 0.11 in nodes 12, 9, 35 and 24 respectively. The element is patched on a cylinder with an axis through the origin of the *XYZ* coordinate system and in a direction of 45° with the *X* and *Y* axis. The element has a 2 x 2 x 3 integration scheme. The edge from node 24 to node 12 is loaded with a distributed force perpendicular to the edge and in the element tangent plane. This force varies from 3.6 outward in node 24 to 2.4 inward in node 12.

Subsections

10.7.4 CQ40S - quadrilateral, 8 nodes

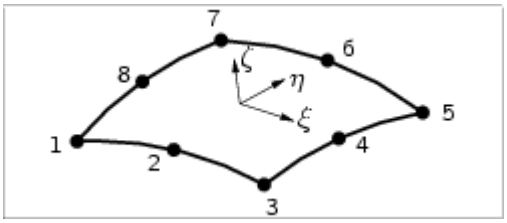

The CQ40S element [Fig.10.17] is an eight-node quadrilateral isoparametric curved shell element. It is based on quadratic interpolation and Gauss integration over the $\xi\ \eta$ element area. The integration in ζ direction (thickness) may be Gauss or Simpson. The polynomials for the translations *u* and the rotations ϕ can be expressed as

$$u_i(\xi,\eta) = a_0 + a_1\xi + a_2\eta + a_3\xi\eta + a_4\xi^2 + a_5\eta^2 + a_6\xi^2\eta + a_7\xi\eta^2$$
$$\phi_i(\xi,\eta) = b_0 + b_1\xi + b_2\eta + b_3\xi\eta + b_4\xi^2 + b_5\eta^2 + b_6\xi^2\eta + b_7\xi\eta^2$$

Typically, for a rectangular element, these polynomials yield approximately the following strain and stress distribution along the element area in a ζ lamina. The strain ε_{xx}, the curvature κ_{xx}, the moment m_{xx}, the membrane force n_{xx} and the shear force q_{xz} vary linearly in *x* direction and quadratically in *y* direction. The strain ε_{yy}, the curvature κ_{yy}, the moment m_{yy}, the membrane force n_{yy} and the shear force q_{yz} vary linearly in *y* direction and quadratically in *x* direction. To avoid membrane and shear locking , the only (and default) is a reduced 2 x 2 [n_{ξ} = 2 , n_{η} = 2] ζ integration scheme over the area. The default in ζ direction (thickness) is 3-point Simpson, [n_{ζ} = 3] 2-point Gauss is a suitable option. Schemes higher than 3-point in ζ direction are only useful in case of nonlinear analysis.

Connectivity (*syntax*)

```
'ELEMEN'
CONNEC
1         5 6         12 13                                                80
          CQ40S      no1_n no2_n ...no8_n
```

CQ40S
is the element type name, followed by the numbers of the eight nodes *no1* to *no8* in sequence from Figure 10.17.

Other input data

Local $\bar{x}$ axis ... §10.1.
Thickness and shape ... §10.3.
Integration schemes ... §10.4.2.
Shear reduction factor ... §10.5.
Point load ... §10.6.1.
Edge load ... §10.6.2.
Face load ... §10.6.3.
Temperature & concentration load ... §10.6.4.
Initial stress ... §10.6.5.

Default (*file*.dat)

```
'ELEMEN'
CONNEC
 14   CQ40S   27 48 15 45 22 36 7 16
MATERI
 14   1
GEOMET
 14   1
'MATERI'
  1   YOUNG   2.1E6
      POISON  0.2
'GEOMET'
  1   THICK   0.1
```

This input data specifies a CQ40S element between the eight nodes, starting with node 27. The element has a Young's modulus E = 2.1 x 10^6 , a Poisson's ratio ν = 0.2 and a uniform thickness of 0.1. By default DIANA assumes an element $\bar{x}$ axis from node 27 to 48, a 2 x 2 x 2 integration scheme and a hyperbolic-parabolic shape.

(*file*.dat)

```
'ELEMEN'
CONNEC
  8   CQ40S   27 48 15 45 22 36 7 16
MATERI
  8   1
GEOMET
  8   2
DATA
  8   1
'MATERI'
  1   YOUNG   2.1E6
      POISON  0.2
'GEOMET'
  2   XAXIS   0.0 1.0 1.0
      THICK   0.10 0.12 0.15 0.13 0.12 0.12 0.10 0.09
```

```
     CYLIN  23. -5. 8.   1. 1. 0.
'DATA'
  1  NINTEG 2 2 3
'LOADS'
CASE 1
ELEMEN
  8  EDGE   KSI1
     FORCE  3.6 -2.4 -7.3
     DIRELM NORMAL
```

The $\bar{x}$ axis of element 8 points at 45° with the global *YZ* axes. The thickness varies from 0.10 in node 27 to 0.12 in node 48 etc. to 0.09 in node 16. The element is patched on a cylindrical shell with the axis through *X* = 23 , *Y* = - 5 and *Z* = 8 and pointing in a direction of 45° with the *X* and *Y* axis. The element has a 2 x 2 x 3 integration scheme. The edge from node 7 to node 27 (with node 16 as mid point) is loaded with a distributed force perpendicular to the edge and in the element tangent plane. This force varies from 3.6 outward in node 7 via 2.4 inward in node 16 to 7.3 inward in node 27.

Subsections

- Other input data

10.7.6 CQ60S - quadrilateral, 12 nodes

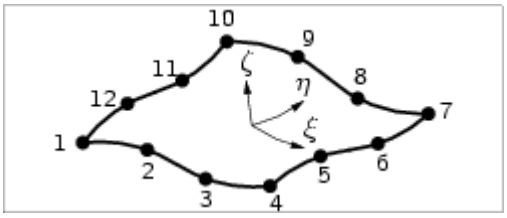

The CQ60S element [Fig.10.19] is an twelve-node quadrilateral isoparametric curved shell element. It is based on third-order interpolation and Gauss integration over the ξ η element area. The integration in ζ direction (thickness) may be Gauss or Simpson. The polynomials for the translations *u* and the rotations ϕ can be expressed as

$$u_i(\xi,\eta) = a_0 + a_1\xi + a_2\eta + a_3\xi\eta + a_4\xi^2 + a_5\eta^2 + a_6\xi^2\eta + a_7\xi\eta^2 \ldots$$
$$\phi_i(\xi,\eta) = b_0 + b_1\xi + b_2\eta + b_3\xi\eta + b_4\xi^2 + b_5\eta^2 + b_6\xi^2\eta + b_7\xi\eta^2 \ldots$$

Typically, for a rectangular element, these polynomials yield approximately the following strain and stress distribution along the element area in a ζ lamina. The strain ε_{xx}, the curvature κ_{xx}, the moment m_{xx}, the membrane force n_{xx} and the shear force q_{xz} vary quadratically in *x* direction and linearly in *y* direction. The strain ε_{yy}, the curvature κ_{yy}, the moment m_{yy}, the membrane force n_{yy} and the shear force q_{yz} vary quadratically in *y* direction and linearly in *x* direction. By default DIANA applies a 3 x 3 [n_{ξ} = 3 , n_{η} = 3] integration scheme over the element area, 2 x 2 is a suitable option. The default in ζ direction (thickness) is 3-point Simpson, [n_{ζ} = 3] 2-point Gauss is a suitable option. Schemes higher than 3-point in ζ direction are only useful in case of nonlinear analysis.

Connectivity (*syntax*)

```
'ELEMEN'
CONNEC
1         5 6         12 13                                                80
          CQ60S      no1n no2n ...no12n
```

CQ60S
is the element type name, followed by the numbers of the twelve nodes *no1* to *no12* in sequence from Figure 10.19.

Other input data

Local $\bar{x}$ axis ... §10.1.
Thickness and shape ... §10.3.
Integration schemes ... §10.4.2.
Shear reduction factor ... §10.5.
Point load ... §10.6.1.
Edge load ... §10.6.2.
Face load ... §10.6.3.
Temperature & concentration load ... §10.6.4.
Initial stress ... §10.6.5.

Examples of input data for the CQ60S element are like those for the CQ40S element [§10.7.4], but the CQ60S element has twelve instead of eight nodes and therefore requires more values for thickness and loading.

Appendix G

input-file iDiana model

In this Appendix a transcript of the input-file is given that transforms the .dxf-model into the full model of the dome. Notable points in the file are the flipping of surfaces, rotating and copying the one-fifth part of the dome and generating the mesh.

NB the transcript has been cleaned up from repetitive commands to improve readability.

```
model
PROPERTY FE-PROG DIANA STRUCT_3D
yes
```

Defining the material and geometric properties of the elements:

```
PROPERTY PHYSICAL FACET GEOMETRY FLATSHEL REGULAR THISOTRO 16 1.5
PROPERTY PHYSICAL JOINT GEOMETRY FLATSHEL REGULAR THISOTRO 10 1.5
PROPERTY MATERIAL GLASS ELASTIC ISOTROP 7E4 0.2
PROPERTY MATERIAL GLASS MASS DENSITY 2.5E-6 0
PROPERTY MATERIAL JOINTMAT ELASTIC ISOTROP 0.1E3 0.4
PROPERTY MATERIAL JOINTMAT MASS DENSITY 0 0
```

Creating different sets for the joints, facets, and the top facet; this way the properties can easily be addresses to the appropriate elements.

```
construct set open joints
CONSTRUCT SET APPEND s1 s2 s3 s4 s5 s6 s7 s8 s9 s10
CONSTRUCT SET APPEND s11 s12 s13 s14 s15 s16 s17 s18 s19 s20
CONSTRUCT SET APPEND s21 s22 s23 s24 s25 s26 s27 s28 s29 s30
CONSTRUCT SET APPEND s31 s32 s33 s34 s35 s36 s37 s38 s39 s40
CONSTRUCT SET APPEND s41 s42 s43 s44 s45 s46 s47 s48 s49 s50
CONSTRUCT SET APPEND s51 s52 s53 s54 s55 s56 s57 s58 s59 s60
CONSTRUCT SET APPEND s61 s62 s63 s64 s65 s66 s67 s68 s69 s70
CONSTRUCT SET APPEND s71 s72 s73 s74 s75 s76 s77 s78 s79 s80
CONSTRUCT SET APPEND s81 s82 s83 s84 s85 s86 s87 s88 s89 s90
CONSTRUCT SET APPEND s91 s92 s93 s94 s95 s96 s97 s98 s99 s100
construct set close
CONSTRUCT SET OPEN TOP
CONSTRUCT SET APPEND S101 S102 S103 S104
VIEW GEOMETRY TOP
CONSTRUCT SET CLOSE
construct set open facets
CONSTRUCT SET APPEND ALL
CONSTRUCT SET REMOVE JOINTS
CONSTRUCT SET REMOVE TOp
Construct SET REMOVE L742 L737
construct set close
```

Flipping a number of surfaces in order to have all normals in the same direction (towards the inside of the dome) and deleting unnecessary elements:

```
Geometry flip s1
…
Geometry flip s200
UTILITY DELETE POINTS P345 P348 P349 P352 P353 P356 P357 P360
yes
```

Creating separate sets to change the mesh division of part of the dome; see Chapter `Modelling the dome in iDIANA':

```
CONSTRUCT SET OPEN LARGE
CONSTRUCT SET APPEND S101
…
CONSTRUCT SET APPEND S177
CONSTRUCT SET CLOSE

CONSTRUCT SET OPEN SMALL
CONSTRUCT SET APPEND ALL
CONSTRUCT SET REMOVE LARGE
CONSTRUCT SET CLOSE
```

```
MESHING DIVISION SURFACE SMALL 1 4
MESHING DIVISION SURFACE S60 4 1
…
MESHING DIVISION SURFACE S250 1 4
```

Assigning the properties to all elements;

```
PROPERTY ATTACH all MATERIAL GLASS
PROPERTY ATTACH JOINTS MATERIAL JOINTMAT
PROPERTY ATTACH all physical facet
PROPERTY ATTACH JOINTS physical JOINT
```

Copying and rotating the one-fifth part of the dome:

```
GEOMETRY COPY FACETS ROTATE P438 P440 72
GEOMETRY COPY FACETS ROTATE P438 P440 144
GEOMETRY COPY FACETS ROTATE P438 P440 216
GEOMETRY COPY FACETS ROTATE P438 P440 288
GEOMETRY COPY joints ROTATE P438 P440 72
GEOMETRY COPY joints ROTATE P438 P440 144
GEOMETRY COPY joints ROTATE P438 P440 216
GEOMETRY COPY joints ROTATE P438 P440 288
UTILITY DELETE POINTS P438 P439 p440
yes
CONSTRUCT MERGE ALL 1
```

Defining the boundary constraints

```
PROPERTY BOUNDARY CONSTRAINT L727 X Y Z
…
PROPERTY BOUNDARY CONSTRAINT L2397 X Y Z
```

Defining the element type

```
MESHING TYPES ALL QU8 Q40s
MESHING DIVISION FACTOR ALL 2
```

Defining sets for the different sectors of the variable load; see Chapter 'Loads';

```
construct set open load1
construct set append s105
…
construct set append s762
construct set close

construct set open load2
construct set append s139
…
construct set append s883
construct set close

construct set open load4
construct set append s252
…
construct set append s801
construct set close

construct set open load3
construct set append facets
construct set append SE1
construct set append SE2
```

```
construct set append SE3
construct set append SE4
construct set remove load1
construct set remove load2
construct set remove load4
construct set close
```

Applying the loads to the structure;

```
PROPERTY LOADS PRESSURE 1 load1 -1.42E-3 Z
PROPERTY LOADS PRESSURE 1 load2 -1.34E-3 Z
PROPERTY LOADS PRESSURE 1 load3 -1.22E-3 Z
PROPERTY LOADS PRESSURE 1 load4 -1.02E-3 Z
PROPERTY LOADS PRESSURE 1 top -1.44E-3 Z
PROPERTY LOADS PRESSURE 1 all -0.541E-3 Z
```

Generating the mesh and saving the model;

```
Meshing Generate
VIEW MESH
SAVE
```

Appendix H

Defining the properties for the joint

Introduction

In this appendix the stiffness properties of the modelled and the proposed joint are defined and related to eachother. The results are used in Chapter 12.

H.1 Defining the properties for the joint

Introduction

As already stated in Paragraph 4.3.5, the modelled joint in the FEM-program differs from the joint type that is likely to be chosen. Figures H.1 and H.2 show the lay-out of this joint.

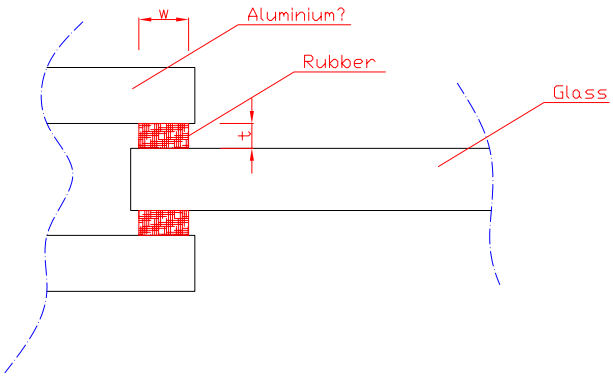

Figure H.1: The joint configuration that is currently designed for use in the glass dome.

Figure H.3 shows the way the joint has been modelled in Diana.

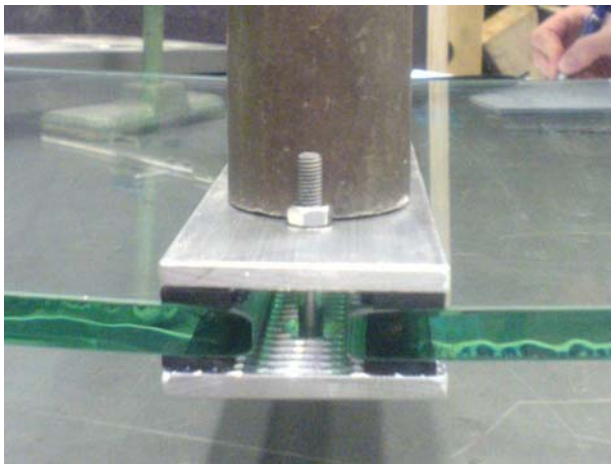

Figure H.2: A test sample of the designed joint.

The thickness of the joint and Young's modulus of the joint material can be controlled in the model. This gives enough control to recreate the bending stiffness of the designed joint as well as to create a corresponding normal stiffness. Both stiffnesses are expected to be important for the behaviour of the dome. In this paragraph the necessary range in thickness and joint material stiffness is defined. The results are then implemented in Paragaph 12.2. For clarity a schematic view of the modelled joint is given in Figure H.4; the different variables are mentioned.

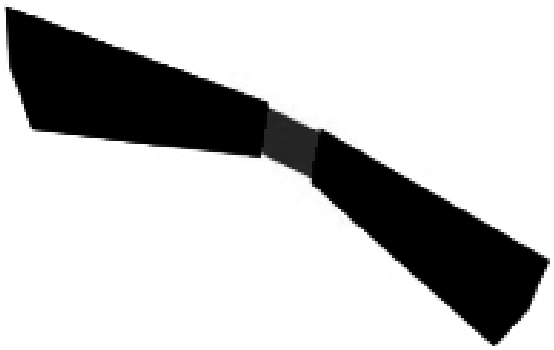

Figure H.3: The (exaggerated) joint configuration within the Diana model.

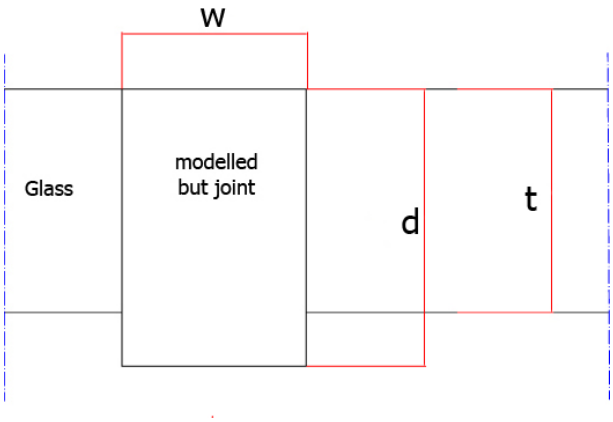

Figure H.4: The applied variables for the modelled joint.

H.1.1 Stiffness of the modelled joint

Bending stiffness

if the joint is modelled as shown in Figure H.5, the bending stiffness of the joint can be derived, see Equation H.1. The joint is a rectangular block of material, where *d* stands for the depth of the joint and *w* for the width.

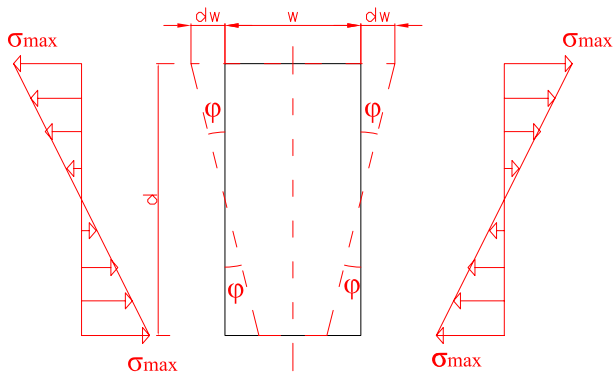

Figure H.5: Modelling of the joint for the derivation of the bending stiffness.

$$
\begin{aligned}
m &= \tfrac{2}{3}d * F_r = \tfrac{2}{3}t * \tfrac{1}{2}t * \tfrac{1}{2}\sigma_{max} \\
\sigma_{max} &= \varepsilon * E = \tfrac{\Delta w}{\frac{1}{2}w} * E \\
\Delta w &= tan(\phi) * \tfrac{1}{2}d \\
m &= \tfrac{1}{6}\tfrac{tan\phi * d^3}{w} * E
\end{aligned}
\tag{H.1}
$$

When small rotations are considered, $tan(\phi) \approx \phi$, which will simplify the Equation for the bending moment. The stiffness coefficient k_m will be defined as follows:

$$
\begin{aligned}
k_m &= \tfrac{m}{tan\phi} = \tfrac{m}{\phi} \\
k_m &= \tfrac{1}{6}\tfrac{d^3}{w} * E
\end{aligned}
\tag{H.2}
$$

This reveals a linear dependency of the bending stiffness on the width of the joint and third power dependency of the bending stiffness on the thickness of the joint.

The normal stiffness of the modelled joint

The normal stiffness can be derived from the model as shown in Figure H.6. Equation H.3 shows the derivation.

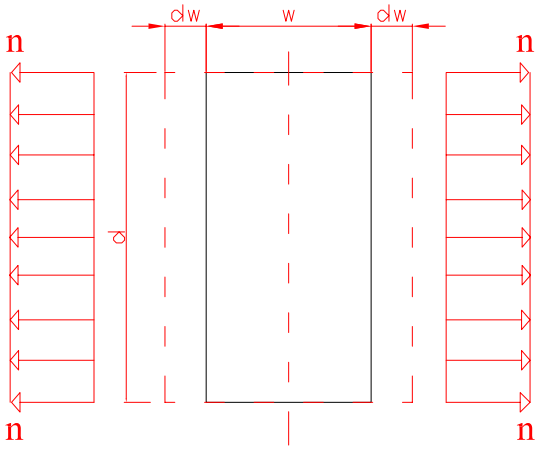

Figure H.6: Modelling of the joint for the derivation of the normal stiffness.

$$
\begin{aligned}
n &= t * \sigma \\
\sigma &= \varepsilon * E = \frac{\Delta w}{\frac{1}{2}w} * E \\
n &= 2 * \frac{\Delta w * d}{w} * E
\end{aligned}
\tag{H.3}
$$

The stiffness coefficient k_n can now be defined as:

$$
\begin{aligned}
k_n &= \frac{n}{\Delta w} \\
k_n &= \frac{2d}{w} * E
\end{aligned}
\tag{H.4}
$$

This reveals a linear dependency of the normal stiffness, both on the width w and the thickness t.

Out-of-plane stiffness of the modelled joint

The out-of-plane shear stiffness of the joint can be derived using Figure H.7. The result is as follows:

NB $\frac{1}{2}w$ is used to be able to compare the deformation behaviour to the designed joint where only half the joint will be considered, see Paragraph H.1.2.

$$
\begin{aligned}
s &= G * \phi \\
\phi &= \frac{\Delta d}{\frac{1}{2}w} \\
s &= 2G * \frac{d * \Delta d}{w}
\end{aligned}
\tag{H.5}
$$

This means that the the out-of-plane shear stiffness $k_{s,oop,mod}$ is equal to:

$$
k_{s,oop,mod} = 2G * \frac{d}{w} \tag{H.6}
$$

In-plane stiffness of the modelled joint

The in-plane shear stiffness of the modelled joint can be derived in the same way as the out-of-plane shear stiffness. The only difference is that the variables are different. The derivation, also see Figure H.8, is as follows:

NB $\frac{1}{2}w$ is used to be able to compare the deformation behaviour to the designed joint where only half the joint will be considered, see Paragraph H.1.2.

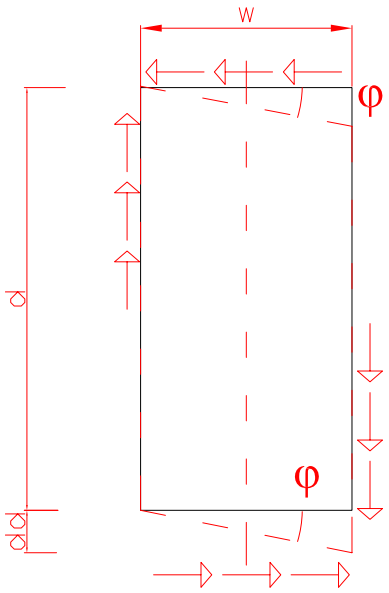

Figure H.7: The mechanism of the out-of-plane shear deformation of the modelled joint.

$$s = G * \phi$$

$$\phi = \frac{\Delta l}{\frac{1}{2}w} \tag{H.7}$$

$$s = 2G * \frac{l * \Delta l * d}{w}$$

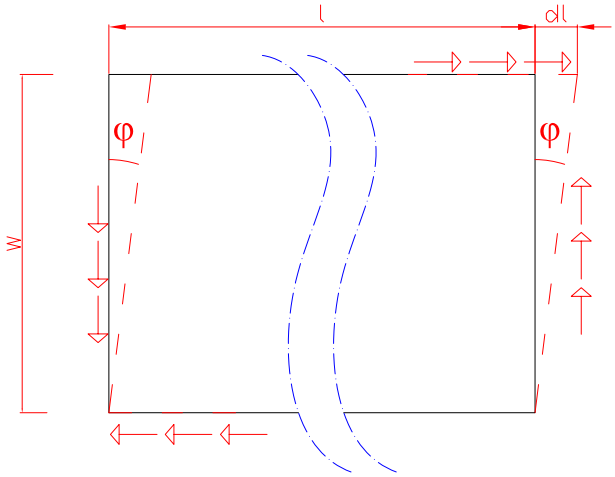

Figure H.8: The mechanism of the in-plane shear deformation of the modelled joint.

The total result for the in-plane shear stiffness of the modelled joint ($k_{s,ip,mod}$) is:

$$k_{s,ip,mod} = sG * \frac{d}{w} \tag{H.8}$$

H.1.2 Stiffness of the designed joint

To compare the influence of the material stiffness of the proposed joint with the used joint stiffness in the FEM model, an analysis of the four stiffnesses will be made for this joint configuration. It should be noted that in reality rubber is not a linear elastic material and will have a slightly deviating behaviour than will be assumed in this Paragraph. The models in this Paragraph are therefore only an approximation to get an idea on the relations and dependencies of the different variables. In this way the models can serve as a coarse estimation of reality to be able to find an order of magnitude for calculations on the influence of the joints on the behaviour of the structure.

The meaning of the variables in the derivations can be found in Figure H.9.

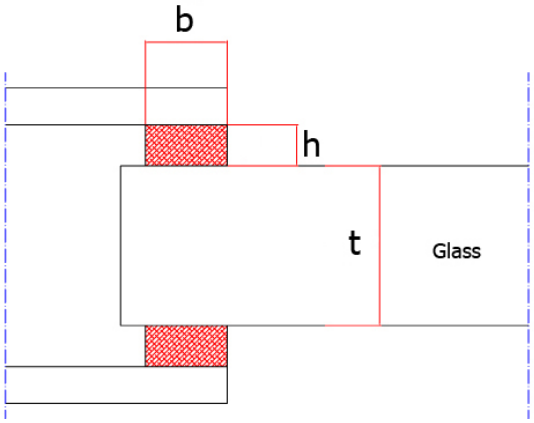

Figure H.9: The applied variables in the designed joint.

Bending stiffness

The designed joint has a completely different geometry than the model, see Figure H.2. The bending stiffness of this joint can be derived with the model shown in Figure H.10. It is not totally clear where the rotation point C will lie when actually creating this joint. This will be dependent on the materials of the joint, which is why the derivation of the bending stiffness is given as a function of the location of the rotation point.

There are two factors of importance in the bending deformation of the joint, the shear deformation in the longitudinal and the latitudinal direction of the rubber. The influence

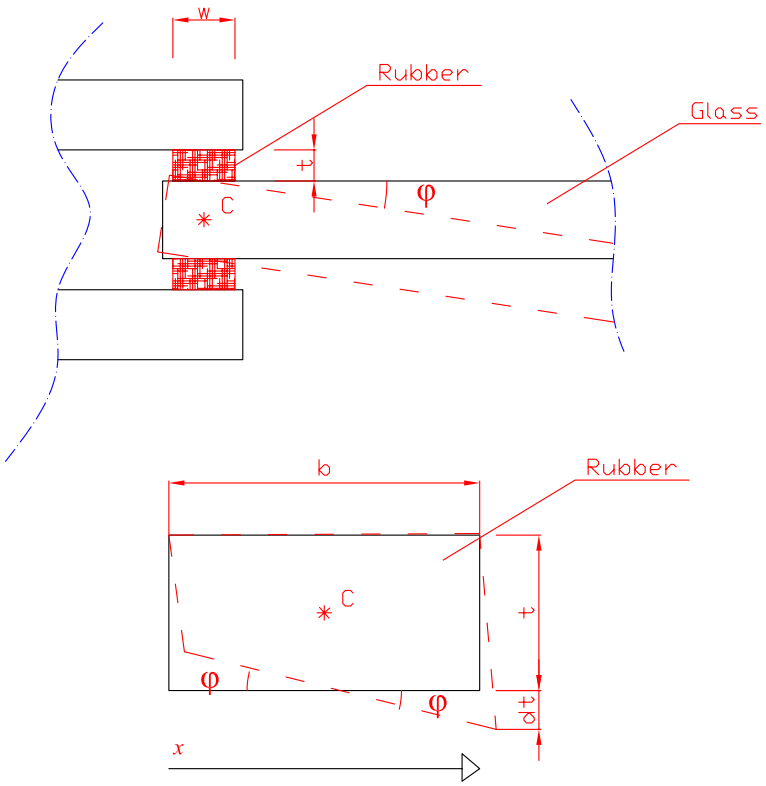

Figure H.10: Modelling of the joint for the derivation of the bending stiffness.

of the two factors can be de-coupled and when the rotation point is chosen at the edge of the glass, the stiffness in the two directions is as follows:

$$\begin{aligned} \varepsilon &= \frac{\phi \frac{1}{2} b}{t} \\ \sigma &= \varepsilon * E \\ \\ \gamma &= \frac{\phi \frac{1}{2} t_{glass}}{t} \\ \tau &\approx \gamma * \frac{1}{3} E \end{aligned} \tag{H.9}$$

The bending moment for the longitudinal part, dependent on the location of the rotation point now becomes:

$$
\begin{aligned}
m &= 2 * (\tfrac{1}{2}x * \sigma_a * \tfrac{2}{3}x + \tfrac{1}{2}(b-x) * \sigma_b * \tfrac{2}{3}(b-x)) \\
m &= 2 * (\tfrac{1}{3}x^2 * \sigma_a + (\tfrac{1}{3}x^2 - \tfrac{1}{3}bx + \tfrac{1}{3}b^2)\sigma_b)
\end{aligned}
$$

$$
\begin{aligned}
\sigma_a &= E * \varepsilon_a = \tfrac{\phi * x}{t} * E \\
\sigma_b &= E * \varepsilon_b = \tfrac{\phi * (b-x)}{t} * E
\end{aligned}
\tag{H.10}
$$

$$
\begin{aligned}
m &= 2 * \tfrac{1}{3}\tfrac{\phi}{t}E * (x^3 - (b-x)^3) \\
m_{bending} &= \tfrac{2}{3}\tfrac{\phi E}{t}(3bx^2 - 3b^2x + b^3)
\end{aligned}
$$

The factor two in the equation refers to the two pieces of rubber in the joint.

The result shows a similar result to the bending stiffness of the modelled joint. It yields a linear dependency on the thickness of the joint and a third power dependency on the width of the joint. The shear part will add an extra rotational stiffness, which is in the same order of magnitude, since the thickness of the glass can not be neglected. It is important to note that the width and thickness have been defined in a slightly different way here and that they are not directly the same as the width and thickness of the modelled joint.

The shear part can be derived similarly. Since it is not as strongly dependent on the width b of the joint it will be considered constant. It has the following value:

$$
\begin{aligned}
m &= \tau * b * t_{glass} \\
\tau &= G * \gamma = G * \tfrac{phi * \frac{1}{2}t}{h} \\
m_{shear} &= G * \tfrac{\phi * b * t^2}{2h}
\end{aligned}
\tag{H.11}
$$

The total bending stiffness is now given by Equation H.12, where the rotation point is chosen at the edge of the rubber.

$$
k_{m,design} = \frac{b^3}{6h}E + \frac{bt^2}{2h}G \tag{H.12}
$$

H.1.3 Normal stiffness of the designed joint

The normal stiffness of the joint actually depends on a shear deformation of two rubber parts. The derivation of this stiffness is therefore similar to the derivation of the shear stiffness of the butt joint. The model is shown in Figure H.11. The result is given in Equation H.13.

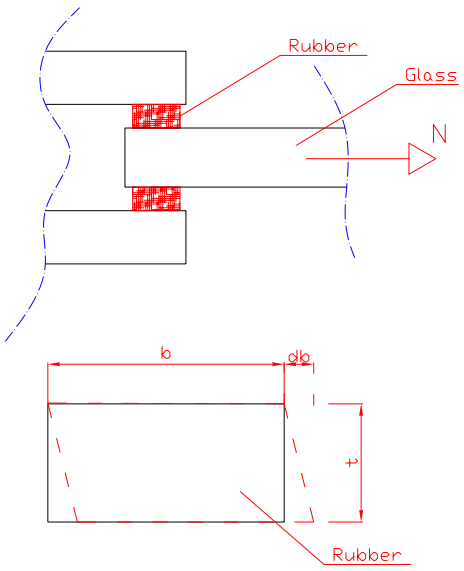

Figure H.11: Modelling of the joint for the derivation of the normal stiffness.

$$s = G * \phi = 2G * \frac{w * \delta w}{t}$$
$$k_n = \frac{s}{\delta w} = 2G * \frac{w}{t} \tag{H.13}$$

Out-of-plane shear stiffness of the designed joint

The out-of-plane shear stiffness of the joint depends on two mechanisms, the local rotation of the joint and the pure shear (compression/tension) in the neoprene layers in the joint.

Figure H.12 shows the mechanism in the joint loaded in shear. The resulting stress and strain in the neoprene layers are also shown. The following holds for the strains and stresses (Bagger n.d.):

$$\Delta h = \phi * \tfrac{1}{2}b = \tfrac{\Delta u}{s} * \tfrac{1}{2}b$$
$$\sigma = \varepsilon * E_n = \tfrac{\Delta u}{s} * \tfrac{1}{2}b * \tfrac{1}{h} * E_n \tag{H.14}$$
$$\tau = \gamma * G_n = \tfrac{Deltau}{s} P \tfrac{1}{2}b * \tfrac{1}{h} * G_n$$
$$m = 2 * \tfrac{1}{6}\sigma b^2 + \tau * b * t = \Delta u * \tfrac{b^3}{6sh} + \tfrac{\Delta u b t^2}{2sh} * G_n$$

From the stresses the connection with the shear force needs to be made to be able to get the shear stiffness from the local rotation of the joint. The mechanism is shown in Figure H.13. This results in:

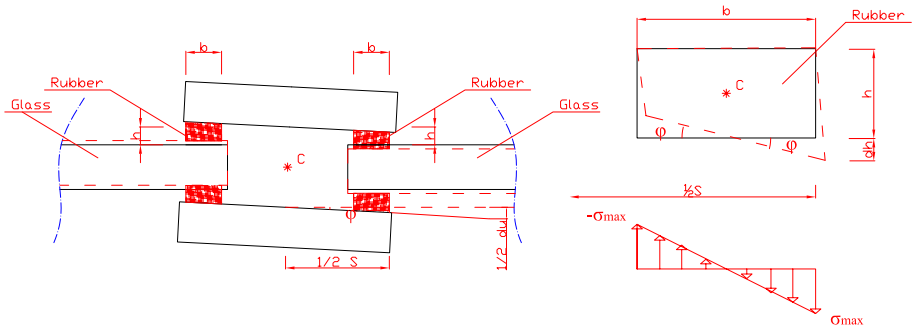

Figure H.12: The mechanism of the shear deformation of the joint by local rotation in the joint.

$$m_{resistance} = \frac{1}{2}Vl$$
$$V = \frac{m_{resistance}2}{l} \tag{H.15}$$

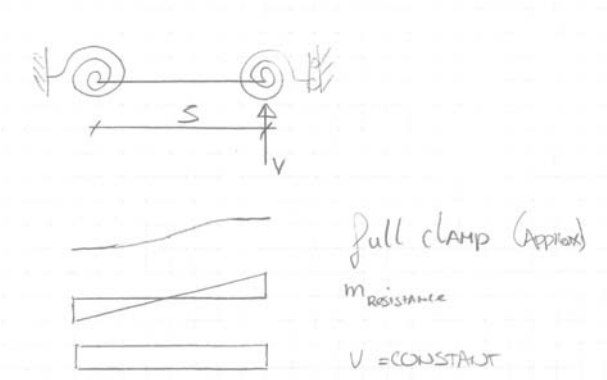

Figure H.13: Scheme of the connection between the bending stresses and the shear stiffness.

The total out-of-plane shear stiffness $k_{s,oop,des}$ of the designed joint can now be estimated as:

$$V = k_v * \Delta u$$
$$k_{s,oop,des} \approx k_{s,rot} = \frac{b^3}{3s^2h} * E_n + \frac{bt^2}{2s^2h}G_n \tag{H.16}$$

In-plane shear stiffness of the designed joint

The in-plane stiffness of the designed joint is more straight-forward to derive, see Figure H.14. The mechanism leads to the folowing derivation per neoprene strip:

$$\begin{aligned} \gamma &= \tfrac{\Delta l}{t} \\ s &= G * \gamma * b = G * \tfrac{\Delta l * b}{t} \\ \\ k_{s,ip,strip} &= G * \tfrac{b}{t} \end{aligned} \tag{H.17}$$

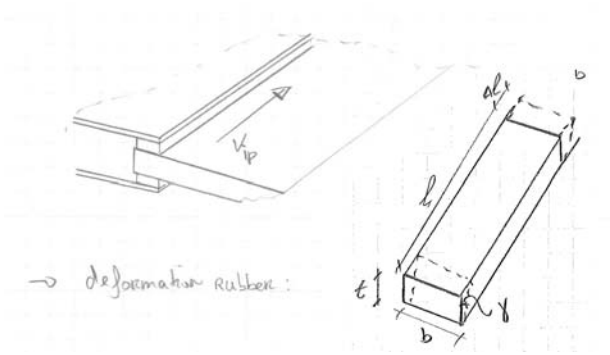

Figure H.14: The mechanism of the in-plane shear deformation of the designed joint.

The in-plane stiffness will be defined per unit length. Since there are two strips at one side of the joint the total in-plane stiffness for the designed joint ($k_{s,ip,des}$) is equal to:

$$k_{s,ip,des} = 2 * G * \frac{b}{t} \tag{H.18}$$

H.1.4 Stiffness of a constrained rubber-like material in compression

In Equations H.12, H.13, H.16 and H.18 the E and G are characteristics of the neoprene strips in the joint. The materials that are currently being investigated by Anne Bagger and Helle Krogsgaard at the DTU are produced by Betech Seals. The important characteristics of the material can be derived from their product catalogue (BetechSeals n.d.). However, because a rubber-like material behaves more stiff when it is partially constrained the E-modulus needs to be defined from a compression model in combination with the hardness of the rubber.

An ideal rubber fibre has a Young's modulus of 3 times the shear modulus G. When such a rubber is put under a compressive stress it will not be compressed but it will yield to the areas where the material is not restrained. This is the reason the stiffness of the material depends on the shape and the loading conditions: the loaded area and the unrestrained area, see Figure H.15.

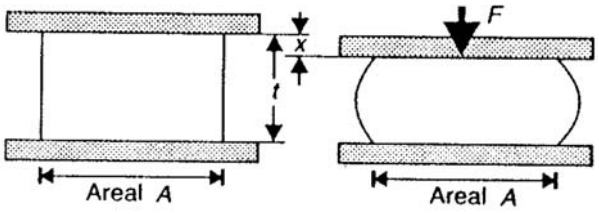

Figure H.15: A partially constrained rubber under compression; the rubber bulges out in the thickness t when loaded in compression, rather than being compacted; from (Hastrup 1992)

For a square piece of rubber one loaded area needs to be taken into account and the entire area that can bend out freely (Hastrup 1992). Equation H.19 then yields the resulting E-modulus.

The variable k is a correction factor that goes to 1 for very ductile materials and to 0,5 for very stiff rubbers. The value for k can be derived from Figure H.16. It should be noted that this formula only holds for deformations up to 10-15%.

Hårdhed H [°IRHD]	Youngs modul E_o [MPa]	Korrektions-faktor k
30	0,92	0,93
35	1,18	0,89
40	1,50	0,85
45	1,80	0,80
50	2,20	0,73
55	3,25	0,64
60	4,45	0,57
65	5,85	0,54
70	7,35	0,53
75	9,40	0,52

Figure H.16: The relationship between the hardness, Young's modulus and correction factor k for rubber-like materials, from (Hastrup 1992).

$$E_c = E_0(1 + 2k * S^2) \tag{H.19}$$

The E_0 can also be estimated with the table in Figure H.16 when the hardness of the material is known in ^{o}IRHD (International Rubber Hardness Degrees). Where an IRHD value of 0 represents a material with a Young's modulus of zero and an IRHD value of

100 represents a material with an infinite Young's modulus.

The hardness of the material is stated in Shore A hardness in the product catalogue of Betech. An exact conversion between Shore A and ^{o}IRHD is difficult since they are derived from different tests and therefore have no true correlation. When comparing test results on the same materials it is shown that for highly elastic materials Shore A and ^{o}IRHD are comparable (2008*c*). From the documentation of Betech Seals (BetechSeals n.d.) the same result is yielded and the hardnesses are stated in Table H.1.4.

Shore A	^{o}IRHD
90	92
80	82
70	73
60	63

Since the hardness of the suitable rubbers lies approximately between 60 ± 5 and 70 ± 5 Shore A, this can be considered equal to a hardness of 55-75^{o}IRHD. Deriving the Young's Modulus from Figure H.16 leads to a E_0 between 3,25 and 9,4MPa. At the same time k can be read from Figure H.16 which yields corresponding values for k between 0,64 and 0,52.

For a block shape S is defined by the ratio between one loaded side and all sides that are free to bend out. In the joint as it is designed now the following then holds (see also Figure H.15):

$$S = \frac{b * l}{2 * h * l} \tag{H.20}$$

Where the areas at the end of the rubber ($b * h$) are neglected since they are very small compared to the longitudinal sides of the rubber. h is the thickness of the rubber and b is the width of the rubber. The thickness of the rubber can vary between 2 and 5mm, the breadth between 10 and 15mm.

Defining E_c is now possible using the previously found values for E_0, k and S in combination with Equation H.19. This leads to the following value range for E_c:

$$E_c \in [7.4 - 146.9 N/mm^2] \tag{H.21}$$

The shear modulus G can be estimated at $\frac{1}{3} * E_0$, because the Poisson's ratio of the material is close to 0,5.

Table H.1.4 gives an overview of all the value ranges for the different properties.

Table H.1: The value ranges for the different joint properties.

Variable	Value range
E_0	$\in [3,25;9,40]MPa$
k	$\in [0,52;0,64]$
b	$\in [10;15]mm$
h	$\in [3;5]mm$

Appendix I

Developing the model of the smooth dome

Introduction; the model of the smooth glass dome has been based on an earlier developed model of a dome structure by B. Peerdeman (Peerdeman 2008). The existing model, however, is half a sphere and needs to be adjusted for use in the study into the glass shell structure.

Development of the correct shape; The original shape of the model is shown in Figure I.1. The facetted glass shell had been cut of with an angle with the vertical of approximately $50{,}5^o$, see Paragraph 4.1.2. In this case almost the same angle ($90^o - 42^o = 48^o$) is acquired when removing bottom four rows of surfaces from the model. The result is shown in Figure I.2. The diameter of the dome is almost the same as the facetted shell at this cut, because both models were based on a sphere with the same diameter. The diameter of the smooth cap will now be 19,2m while the facetted shell has an approximate diameter of 19m, see Paragraph 4.1.2.

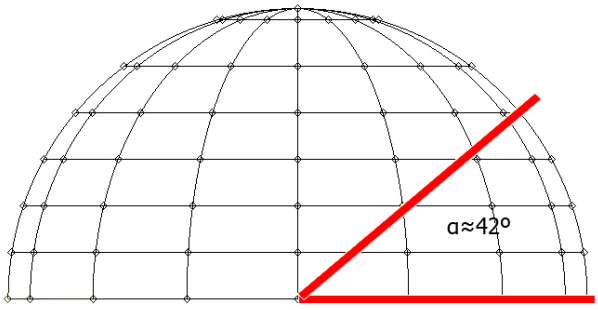

Figure I.1: The original model of the smooth dome (Peerdeman 2008).

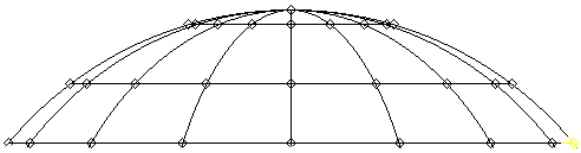

Figure I.2: The resulting shape of the smooth dome structure.

Properties of the dome; The dome will, aside from being smooth, need to have the same geometrical and material properties as the facetted dome. The thickness of the glass is therefore set at 16mm and the E-modulus of the material is the same as glass, $7 * 10^4 N/mm^2$.

The supports of the dome will also need to be the same as the facetted structure. Therefore all edges will be supported in three directions while keeping the rotations free.

Loads; the load conditions will be based on the loads in Appendix D. However, to simplify the load condition a constant load will be applied to the entire dome. The load consists of the self weight of the structure, $0.541 * 10^{-3} N/mm^2$, and the snow load from Sector 3, $1.22 * 10^{-3} N/mm^2$. This leads to a total vertical load of $1.76 * 10^{-3} N/mm^2$.

Bibliography

(2007*a*), World Wide Web; http://www.gooseham-barton.com/Images/gallery/edenproject.jpg.

(2007*b*), World Wide Web; http://en.wikipedia.org/wiki/Image:Biosphere.PNG.

(2007*c*), World Wide Web; biosphere.ec.gc.ca.

(2007*d*), World Wide Web: www.gc.maricopa.edu/earthsci/imagearchive.

(2007*e*), World Wide Web; http://upload.wikimedia.org/wikipedia/commons/8/8b/Lagash.JPG.

(2007*f*), World Wide Web; http://www.pilkington.com/resources/floatplant.jpg.

(2007*g*), World Wide Web; www.azom.com/details.asp?ArticleID=87.

(2007*h*), World Wide Web; http://www.bronstigemangoest.nl/images.

(2007*i*), World Wide Web; http://www.cjfearnley.com/fuller-faq-5.html.

(2007*j*), World Wide Web; www.platonicsolids.info.

(2008*a*), World Wide Web; http://www.PIAB.com.

(2008*b*), World Wide Web; http://new.thomasnet.com/images/large/801/801108.jpg.

(2008*c*), World Wide Web: www.ides.com.

Almegaard, H. (2003), Skalkonstruktioner; Metoder til afklaring af sammenhaengene mellem form, stabilitet, stivhed af understoetninger, PhD thesis, By og Byg Statens Byggeforskningsinstitut.

Almegaard, H. (2004), 'The stringer system - a truss model of membrane shells for analysis and design of boundary conditions', *International Journal of Space Structures* **19**(1), 1–10.

Bagger, A., J. Jönsson & T. Wester (2007*a*), Facetted shell structure of glass. Paper submitted to Glass processing days 2007 (?).

Bagger, A., J. Jönsson & T. Wester (2007*b*), Investigation of stresses in facetted glass shell structures. submitted to IASS.

Bagger, Anne (n.d.), Research into the influence of the joint stiffness in facetted shell structures. working title, part of undergoing PhD. research.

Behling, S. & S. Behling (1999), *Glas Konstruktion und Technologie in der Architektur*, Prestel Verlag.

Belytschko, Ted, WingKam Liu & Brian Moran (2000), *Non linear finite elements for continua and structures*, Wiley.

BetechSeals (n.d.), *Produktkatalog O-ringe; Betech Seals*, Betech Seals, www.betechseals.dk.

Blandini, L. & W. Sobek (2005), The glass dome, *in* 'Glass Processing Days 2005'.

Brush, D.O. & B.O. Almroth (1975), *Buckling of bars, plates and shells.*, McGraw-Hill New York.

Dansk Standard (1998).

de Witte, F.C. (2007), *DIANA Finite Element Analysis; User's Manual*, TNO DIANA BV, P.O. Box 49, 2600AA, Delft, The Netherlands.

Donnell, L.H. (1976), *Beams. plates and shells*, McGraw-Hill Book Company.

du Pont de Nemours, E.I. & Company (2005), Dupont sentry glass plus interlayer; strength characteristics, Technical report, Du Pont de Nemours and Company.

Eurocode 1: Actions on structures-General actions-part 1-4 (2003).

Eurocode 1: Actions on structures - Part 1-3: General actions - Snow loads (2003).

Eurocode - Basis of structural design (2002).

Gibson, J.E. (1965), *Linear elastic theory of thin shells*, Pergamon Press New York.

Hastrup, Kaare (1992), *Plasst og gummi staabi*, Teknisk Forlag.

Hoefakker, J.H. & J. Blaauwendraad (2005), *Theory of Shells*, Delft University of Technology; Faculty of Civil Engineering and Geosciences.

Hoogenboom, P.C.J. (2005), Notes on shells. Hand out for the course CT5143: Stresses in Shells.

Isgreen, T.V. (2007), Fem-modellering af facetterede skaller i glas, Master's thesis, Danmarks Tekniske Universitet; BYG.

Jawaad, M.H. (1994), *Theory and Design of Plate and Shell Structures*, Chapman and Hall, Inc.

Knebel, K., J. Sanchez-Alvarez & S. Zimmerman (2003), 'The structural making of the eden domes', Internet, http://www.mero-tsk.de.

Koiter, W.T. (1945), Over de Stabiliteit van het Elastisch Evenwicht, PhD thesis, Delft University of Technology (former TH Delft).

Koiter, W.T. (1967), Nasa technical translation f10,833, Technical report, NASA.

Kollar, L. (1982), Buckling of complete spherical shells and spherical caps, *in* E.Ramm, ed., 'Buckling of shells, a state of the art colloquium', Vol. I, pp. 5.1–5.25.

Krüger, Gunter (1998), 'Temperature effects on the structural behavior of laminated safety glass', *Otto Graf Journal* **9**, 153–163.

McGee, O.G., J.W. Kim & A.W. Leisa (2005), 'Sharp corner functions for mindlin plates', *Journal of Applied Mechanics* **72**, 1–9.

NEN-EN572-1 (2004), 'Glas voor gebouwen - basisproducten van natronkalkglas - deel 1: Definities en algemene fysische en mechanische eigenschappen'.

NEN2608-2 (2007), 'Glass in building - part 2: Glazed installations non-vertical installed - resistance against selfweight, wind load, snow load and isochore pressure - requirements and determination method'.

Peerdeman, Bart (2008), Stability of concrete shell structures (working title), Master's thesis, Delft University of Technology; fac. of Civil Engineering and Geosciences.

prEN13474 2 (2000), 'Glass in building - design of glass panes - part 2: Design for uniformly distributed loads'.

Samuelson, L. A. & S. Eggwertz, eds (1992), *Shell Stability Handbook*, Elsevier Science Publishers Ltd.

Schodek, D.L. (2004), *Structures*, 4th edn, Prentice Hall of India.

Singer, J. (1982), The status of experimental buckling investigation of shells, *in* E.Ramm, ed., 'Buckling of shells, a state of the art colloquium', Vol. I, pp. 9.1–9.33.

Sze, K.Y., X.H. Liu & S.H. Lo (2004), 'Popular benchmark problems for geometric nonlinear analysis of shells', *Finite elements in analysis and design* **40**, 1551–1569.

Timoshenko, S. & S. Woinowsky-Krieger (1959), *Theory of Plates and Shells*, second edn, McGraw Hill Book Co.

van Heusden, J.F. (2005), Constructief glazen element, Master's thesis, Delft University of Technology; Faculty of Civil Engineering and Geosciences.

Veer, F.A., J. Wurm & G.J. Hobbelman (2003), The design, construction and validation of a structural glass dome, *in* 'Glass Processing Days 2003'.

Wester, T. (1984), *Structural Order in Space the plate-lattice dualism*, Smed Grafik.

Wester, T. (1990), 'A geodesic dome-type base on pure plate action.', *International Journal of Space Structures* **5**(3&4), 155–167.

Young, W.C. & R. Budynas (2001), *Roark's Formulas for Stress and Strain*, 7th edn, McGraw-Hill Professional.

List of Tables

List of Figures